Quantification et dynamique spatio-temporelle des puits de carbone associés aux herbiers à Posidonia oceanica

Briac Monnier

▶ **To cite this version:**

Briac Monnier. Quantification et dynamique spatio-temporelle des puits de carbone associés aux herbiers à Posidonia oceanica. Ecologie, Environnement. Université Pascal Paoli, 2020. Français. NNT : 2020CORT0016 . tel-03545082

HAL Id: tel-03545082
https://theses.hal.science/tel-03545082

Submitted on 27 Jan 2022

HAL is a multi-disciplinary open access archive for the deposit and dissemination of scientific research documents, whether they are published or not. The documents may come from teaching and research institutions in France or abroad, or from public or private research centers.

L'archive ouverte pluridisciplinaire **HAL**, est destinée au dépôt et à la diffusion de documents scientifiques de niveau recherche, publiés ou non, émanant des établissements d'enseignement et de recherche français ou étrangers, des laboratoires publics ou privés.

UNIVERSITE DE CORSE PASCAL PAOLI
ECOLE DOCTORALE ENVIRONNEMENT ET SOCIETE
FRES 3041 – UMR CNRS SPE 6134

Thèse présentée pour l'obtention du grade de

DOCTEUR EN PHYSIOLOGIE ET BIOLOGIE DES ORGANISMES – POPULATIONS – INTERACTIONS
Mention : Biologie des populations et écologie

Soutenue publiquement par

Briac MONNIER

le 16 Décembre 2020

Quantification et dynamique spatio-temporelle des puits de carbone associés aux herbiers à *Posidonia oceanica*

Directeurs :
M. Gérard PERGENT, Pr, Université de Corse, France
M. Miguel Ángel MATEO MÍNGUEZ, Dr-HDR, CEAB-CSIC, Espagne

Rapporteurs :
Mme Sylvie GOBERT, Pr, Université de Liège, Belgique
M. Oscar SERRANO, Dr-HDR, Edith Cowan University, Australie

Jury

Mme Sylvie GOBERT, Pr, Université de Liège, Belgique
M. Oscar SERRANO, Dr-HDR, Edith Cowan University, Australie
M. Jean-François SANTUCCI, Pr, Université de Corse, France
Mme Christine PERGENT-MARTINI, Dr-HDR, Université de Corse, France
M. Philippe CLABAUT, Dr-HDR, France
M. Gérard PERGENT, Pr, Université de Corse, France
M. Miguel Ángel MATEO MÍNGUEZ, Dr-HDR, CEAB-CSIC, Espagne

Invité :
M. Philippe BORNENS, SETEC IN VIVO, France

THESE DE DOCTORAT

UNIVERSITE DE CORSE PASCAL PAOLI
FRES 3041 – UMR CNRS SPE 6134
FACULTÉ DES SCIENCES ET TECHNIQUES
EQUIPE ECOSYSTEMES LITTORAUX

CENTRO DE ESTUDIOS AVANZADOS DE BLANES
CONSEJO SUPERIOR DE INVESTIGACIONES CIENTIFÍCAS – CEAB-CSIC
GROUP OF AQUATIC MACROPHYTE ECOLOGY

Présentée par
M. Briac MONNIER

Pour l'obtention du grade de
Docteur en Physiologie et Biologie des organismes Populations – Interactions

Mention
Biologie des populations et écologie

Quantification et dynamique spatio-temporelle des puits de carbone associés aux herbiers à *Posidonia oceanica*

Soutenue le 16 Décembre 2020 à Corte

Devant le jury composé de :

Mme **Sylvie GOBERT**, Pr, Université de Liège, Rapporteur
M. **Oscar SERRANO**, Dr-HDR, Edith Cowan University, Rapporteur
M. **Jean-François SANTUCCI**, Pr, Université de Corse, Examinateur
Mme **Christine PERGENT-MARTINI**, Dr-HDR, Université de Corse, Examinateur
M. **Philippe CLABAUT**, Dr-HDR, Examinateur
M. **Miguel Ángel MATEO MÍNGUEZ**, Dr-HDR, CEAB-CSIC, Co-directeur de thèse
M. **Gérard PERGENT**, Pr, Université de Corse, Directeur de thèse
M. **Philippe BORNENS**, SETEC IN VIVO, Invité

Préface

Ce doctorat a été réalisé au sein de l'Equipe Ecosystèmes Littoraux (EqEL) grâce à l'obtention d'un contrat doctoral financé par l'Université de Corse Pasquale Paoli.

Ces travaux de recherche ont été menés dans le cadre d'une convention de co-direction de thèse internationale entre l'Equipe Ecosystèmes Littoraux (EqEL) de l'Université de Corse Pasquale Paoli (France) et le 'Centro de Estudios Avanzados de Blanes - Consejo Superior de Investigaciones Científicas' (Espagne).

La direction des travaux de doctorat a été assurée conjointement par le Professeur Gérard Pergent (Université de Corse Pasquale Paoli) et le Docteur – Habilité à Diriger des Recherches – Directeur de Recherche Miguel Ángel Mateo Mínguez (*Centro de Estudios Avanzados de Blanes - Consejo Superior de Investigaciones Científicas*).

Les résultats présentés font partie intégrante de l'Action « CHANGE » de l'Université de Corse Pasquale Paoli (Fédération de Recherche Environnement Société – FRES 3041) et s'inscrivent dans le cadre de différents programmes scientifiques : (i) le programme régional Puits de carbone : Atout du Développement Durable de la Corse face au défi du CHANGEment climatique (PADDUC-CHANGE), (ii) le programme franco-italien Gestion Intégrée des Réseaux Ecologiques à travers les Parcs et les Aires Marines (GIREPAM) et (iii) le programme régional CARBONSINK.

Ces travaux de recherche ont bénéficié du soutien financier de (i) l'Union Européenne (Programme FEDER GIREPAM Interreg – Maritime), (ii) de la Collectivité de Corse (Programme PADDUC-CHANGE), (iii) de l'Office de l'Environnement de la Corse (OEC), (iv) de l'Office Français pour la Biodiversité (OFB) et (v) du GIS Posidonie.

Ces travaux de recherche ont également bénéficié de moyens scientifiques et techniques mis à disposition par (i) l'Ifremer (navire océanographique L'Europe) et Genavir (Groupement pour la Gestion de Navires de Recherche) à travers l'UMS Flotte Océanographique Française.

“I need the sea because it teaches me”

Pablo Neruda

À mes parents et à mon frère

Remerciements

La réalisation d'une thèse est une aventure enrichissante, faite de rencontres, d'échanges mais également d'obstacles, de stress et de moments de doute. Bien que présenté comme étant un travail personnel, ce travail de recherche est le fruit de la collaboration et de la participation de nombreuses personnes. Je tiens donc à remercier l'ensemble des personnes qui ont contribué à la concrétisation de ce travail

Je tiens tout d'abord à remercier l'ensemble des membres du jury d'avoir accepté d'évaluer ce travail et tout particulièrement **Sylvie Gobert** et **Oscar Serrano** d'avoir accepté d'être les rapporteurs de cette thèse. Je remercie également les examinateurs et les membres du comité de suivi de ces travaux pour leurs conseils et les échanges tout au long de ces années.

J'exprime mes plus profonds remerciements à mon directeur de thèse, **Gérard Pergent**, pour m'avoir ouvert les portes de la recherche et de m'avoir accordé sa confiance en acceptant d'encadrer cette thèse. Merci pour vos conseils, votre patience et votre optimisme (pas de problèmes, que des solutions). Merci également d'avoir porté ces travaux depuis le début et d'avoir rendu tout cela possible. Je garderai en mémoire la fabrication artisanale du premier carottier dans lequel nous portions tous nos espoirs et la délivrance après le premier carottage dans la matte à bord de L'Europe ! Que de chemin parcouru…

Je remercie chaleureusement mon co-directeur de thèse, **Miguel Ángel Mateo**, la deuxième personne sans qui ces travaux n'auraient jamais pu voir le jour ! Je vous remercie sincèrement d'avoir accepté d'encadrer ce travail, pour cette collaboration et pour la confiance que vous m'avez accordée. Malgré la distance, vous avez toujours été présent et disponible quand j'en avais besoin. Un grand MERCI pour votre accueil au sein du CEAB et de m'avoir offert l'opportunité de participer à cette inoubliable mission océanographique sur les côtes d'Andalousie ! Un dernier point : promis, je ferais davantage d'efforts en anglais !

Je tiens également à exprimer ma gratitude à **Christine Pergent-Martini** pour son savoir, ses conseils et ses recommandations toujours avisées. Merci pour votre écoute, votre aide et votre appui durant la campagne ! Merci aussi pour le temps précieux que vous avez consacré tout au long de mes années de thèse notamment pour résoudre les problèmes insolubles de la bureaucratie universitaire !

Mes remerciements s'adressent également à **Philippe Clabaut**, le géologue et sédimentologue de l'équipe, pour tes innombrables conseils et surtout pour ton aide à l'interprétation des sonogrammes et à la lecture des séquences sédimentaires durant la mission océanographique. Merci d'avoir contribué à sortir des hangars de l'Ifremer les sondeurs de sédiments et surtout la « Manta » sans qui ces travaux n'auraient très probablement jamais pu voir le jour !

Je remercie **Christian Dayries**, **Laurent Guillon** et **Eric Janaudy** de Costa Verde Loisirs pour leur participation active aussi bien sur l'eau que sous l'eau aux différentes missions terrains. Merci pour votre grande disponibilité et votre perpétuelle bonne humeur. Merci également à **Thierry** et **Yohann Coulon** pour leur grande contribution au développement et aux essais du carottier pneumatique en plein hiver ! Un grand merci pour votre aide sur ce projet.

La collaboration espagnole m'a permis de vivre des moments inoubliables avec notamment la participation à une première campagne océanographique. Pour cela, je tiens à remercier chaleureusement les membres de l'équipe GAME avec qui j'ai partagé ces moments uniques et pour tout ce qui m'ont apporté. Je tiens tout d'abord à remercier **Elena Díaz Almela** pour son accueil, sa gentillesse, son amitié et pour m'avoir fait vivre des moments historiques dans les rues de Barcelone ! Merci également à **Nerea Piñeiro-Juncal**, **Carmen Leiva-Dueñas**, **Anna Sans** qui ont eu la patience de m'initier aux joies de l'analyse sédimentaire et pour toute leur aide. Je remercie également **Candela Marco-Mendez** pour sa bonne humeur et de m'avoir fait découvrir les tapas vegan de Sa Capça. Un grand merci à **Óscar Serrano** et **Paul Lavery** avec qui j'ai beaucoup appris durant la campagne. Je voudrais aussi saluer l'ensemble des participants de la formation « Sizing Blue Carbon ».

Ces travaux de thèse m'ont offert l'opportunité de participer à une seconde campagne océanographique à bord du N/O L'Europe. Je souhaiterais ainsi remercier les membres d'équipage Genavir qui ont permis de mener à bien la mission Carbonsink dans les meilleures conditions : **Arnaud Lemettais**, **Julien Boudet**, **Christopher Blanc**, **Antoine Prohet**, **Xavier Giannini**, **Jean Michel Le Goff**, **Dominique Doigneau**, **Matthieu Jaffry**, **Tony Fait**, **Jean-Baptiste Rohou**. Merci pour tous les bons moments passés à bord et cette soirée de fin de mission inoubliable dans les rues de Por ! Mes remerciements s'adressent également à **Anne Pacault**, **Laure Simplet**, **Emeric Gauthier** et **Yannick Thomas** de l'Ifremer Brest pour leur contribution à l'acquisition des données de sismique-réflexion et leurs conseils avisés pour l'interprétation des données sismiques et acoustiques. Merci aussi à **Matthieu Ghilardi** du CEREGE pour les analyses granulométriques.

Je souhaite remercier mes collègues de l'Université de Corse ; **Emilie Garel** du Département de Géologie, **Jérémie Santini** et **Stéphanie Federici** du Département de Biochimie, **Franck Renucci** et **Marie José Battesti** du Département de Chimie de m'avoir ouvert leur laboratoire et permis d'utiliser une partie de leur matériel. Je remercie l'École Doctorale « Environnement Société » et tout particulièrement **David Moungar** et **Anna Savossiouk** pour leur grande disponibilité au cours de ces années de thèse, **Johanne Albertini** pour son appui administratif, **Antoine Pieri** pour ses nombreux coups de mains et **David Celio** pour ses nombreux dépannages et conseils.

Un grand merci à **Christophe Mori** pour son aide pour les statistiques et pour ton invitation à la sortie carottage à Catamalzi. Merci également à **Antoine Orsini**, pour ce road-trip en 4x4 sur la piste de la Revelatta. Merci aussi à **Thomas Bouchet**, pour son soutien et avec qui j'aurai aimé poursuivre mes travaux de recherche sur les pozzines d'altitude.

Je voulais remercier mes collègues et amis avec qui j'ai passé d'incroyables moments : **Jean-Baptiste Tramoni**, **Christopher (Topher) Castellani**, **Brahim Samba Bomou**, **Vito Ciullo**, **Baptiste Defaye**, **Quentin Godeaux**, **Margaux Dupuy**, **Ibrahim Souleiman**, **Kadar Mohamed Hassan**, **Caroline Torres**, **Cynthia Pérez Carrillo** et bien d'autres. Je souhaite remercier tout spécialement **Natacha (alias Natasha) Villechenaud** qui a toujours été présente pour les pauses café indispensables pour se vider l'esprit et **Guillaume Gerandi** qui m'a soutenu jusqu'au derniers instants !

Un merci également aux deux « Michel » de la STARESO : **Michel Marengo** et **Michèle Leduc** pour leurs encouragements et les petites discussions au café. Je remercie très chaleureusement **Marie Garrido** pour m'avoir donné envie de m'investir en recherche et **Alain Jeudy de Grissac** pour ses nombreux conseils à chacune de ses visites sur le campus cortenais !

Je ne peux pas oublier tous ceux qui ont cohabité dans le bureau de l'Équipe Ecosystèmes Littoraux pendant mes années de thèse, sans vous ce travail aurait été beaucoup plus difficile. Merci à **Audrey Valette-Sansevin** avec qui j'ai partagé les premiers instants de cette aventure, **Emeline Barralon** pour sa bienveillance, son aide et sans qui les missions terrains auraient été ennuyeuses ! Je remercie les stagiaires **Thomas, Pauline, Alban, Alizée, Océanne, Julien, Thomas, Andréa**, **Coraline**, **Nathalie**, pour leur aide et la bonne humeur au laboratoire et notamment **Julie Lapaquellerie** qui a contribué à l'avancement de ce doctorat. Un grand merci à **Fabien Cantaloube** pour son aide précieuse lors des longues journées de tamisage et **Léa Lehmann** qui a eu la lourde tâche de me supporter au cours des derniers mois de cette thèse…

J'exprime ma gratitude et mes profonds remerciements à **Sonia Ternengo** pour ses encouragements et son aide depuis le tout début. Merci d'avoir mis à ma disposition le matériel et les équipements quand cela était nécessaire. Merci pour ta confiance et de m'avoir permis de découvrir le monde de l'enseignement durant toutes ces années. Au-delà de l'aspect professionnel, merci pour ta gentillesse, ton amitié ainsi que pour tous ces bons moments passés en ta compagnie ou avec ta famille, que ça soit autour d'une pizza ou d'un verre.

Votre amitié a rendu ces années si agréables. Pour cela, je tiens à dire un grand merci à mes amis pour leur soutien et tous ces bons souvenirs : **Jean-Philippe** et **Natacha** pour ces moments de vie partagés ainsi qu'**Eva** pour ces innombrables délires que l'on a pu avoir ensemble ! Merci à **Jamila**, **Aude**, **Tristan**, **Micka** (brun), **Micka** (blond) pour ces incalculables parties de jeu en votre compagnie. Merci à mes basques préférés **Mikel** et **Caroline** pour leurs visites en Corse et leur soutien. Merci à **Julien** (mon frère de bide), une des belles rencontres de ces années de thèse. Merci à **Marion** pour ton sens de l'amitié, ta bonne humeur et ta grande gentillesse. Petite dédicace à **Stella**, qui a toujours été là pour moi.

Je voudrais remercier chaleureusement **Imane** pour sa gentillesse et son éternelle bonne humeur ! Tu as toujours été là pour me donner un petit coup de main. Outre le fait de m'avoir supporté durant toutes ces années, tu auras supporté les hauts et les bas d'un couple de doctorants et pour cela, tu mérites amplement mon respect.

Je tiens à remercier ma famille, surtout mes parents **Mireille** et **Michel**, mon frère **Marin** pour leur soutien et leurs encouragements pendant toutes ces années et malgré la distance ! Merci à mes parents de m'avoir rapproché de la nature et de la mer depuis tout petit. D'une manière ou d'une autre, elle a toujours été là. Que ce soit en Bretagne sur les grandes étendues de la Côte d'Émeraude, aux balades sur le littoral du massif des Maures ou de l'Île de Ré, en passant par les nombreuses plongées en apnée pour explorer les fonds sous-marins sur les côtes de Balagne ou de l'Extrême Sud de la Corse. Merci à vous !

Je ne saurais finir ses quelques lignes sans oublier de remercier la personne qui aura passé le plus de temps à m'encourager. **Ouafa**, je ne te remercierai jamais assez pour l'aide et le soutien que tu m'as apporté durant ces années de thèse et surtout au cours des derniers mois. Merci d'avoir traversé avec moi ces bons comme ces mauvais moments et pour tous les sacrifices que tu as dû faire. Merci pour le temps que tu m'as consacré et ta grande contribution à ce travail.

Liste des abréviations

ABA : Traitement Acide-Base-Acide
BCE : Blue Carbon Ecosystems (Ecosystèmes à Carbone Bleu - ECB)
BP : Before Present (Avant le Présent – AP; *i.e.* 1950)
C : Carbone
C_{inorg} : Carbone inorganique
C_{org} : Carbone organique
C.V. : Coefficient de Variation
$CaCO_3$: Carbonate de calcium
CAR : Carbon Accumulation Rate (Taux d'accumulation du carbone)
CCNUCC : Convention cadre des Nations Unies sur les changements climatiques
CE : Common Era (Ere Commune ; *i.e.* ère après l'an 0 du calendrier grégorien)
CH_4 : Méthane
CI : Confidence Interval (Intervalle de confiance - IC)
CO_2 : Dioxyde de carbone
CO_{2e} : Equivalent en dioxyde de carbone
COM : Coarse Organic Matter (Matière organique grossière)
COP : Conférence of the Parties (Conférences des Parties)
DACP : Dark Ages Cold Period
DTM : Digital Terrain Model (Modèle Numérique de Terrain - MNT)
e.g. : *exempli gratia* (par exemple)
ESRI : Environmental Systems Research Institute
GES : Gaz à effet de serre
GIEC : Groupe d'experts Intergouvernemental pour l'Etude du Climat
GIS : Geographic Information System (Système d'Information Géographique - SIG)
GPS : Global Positioning System
H_2O_2 : Péroxyde d'hydrogène
HCl : Acide chlorhydrique
i.e. : *id est* (c'est-à-dire)
LIA : Little Ice Age (Petit Age Glaciaire)
LiDAR : Light Detection and Ranging
LOI : Loss on Ignition (Perte au feu)
MBES : Multibeam Echosounder (Sondeur multifaisceaux)
MSL : Mean Sea Level
MWP : Medieval Warm Period (Optimum Climatique Médiéval)
N : Nombre d'échantillons ou de mesures
N_2O : Protoxyde d'azote
PPB : Production primaire brute
PPN : Production primaire Nette
PVC : Polychlorure de vinyle
r : Coéfficient de corrélation
R/V : Research Vessel (Navire océanographique - N/O)
R^2 : Coéfficient de détermination

RCP : Representative Concentration Pathways (Scénarios d'évolution des teneurs en GES)
RSL : Relative Sea Level
RWP : Roman Warm Period
S.D. : Standard Deviation (Ecart type ; σ)
S.E. : Standard Error (Erreur standard)
SAR : Sediment Accretion Rate (Taux d'accrétion du sédiment)
SCUBA : Self Contained Underwater Breathing Apparatus (Scaphandre autonome)
SOM : Sediment Organic Matter (Matière organique du sédiment)
SSS : Side Scan Sonar (Sonar à Balayage Latéral - SBL)
SST : Sea Surface Temperature (Température de surface de la mer)
TIC : Total Inorganic Carbon (Carbone inorganique totale)
TOC : Total Organic Carbon (Carbone organique totale)
TOM : Total Organic Matter (Matière organique totale)
TWTT : Two-way Travel Time (Temps de parcours aller-retour)
UICN : Union Internationale pour la Conservation de la Nature
UNFCCC : United Nations Framework Convention on Climate Change (voir CCNUCC)
vs : versus
WGS : World Geodetic System (Système géodésique mondial)

Unités

Distance	m : mètre ; mm : millimètre ; cm : centimètre ; km : kilomètre
Superficie	m^2 : mètre carré ; cm^2 ; centimètre carré ; ha : hectare ; km^2 : kilomètre carré
Volume	m^3 : mètre cube ; cm^3 : centimètre cube
Masse	g : gramme ; kg : kilogramme ; t : tonne ; Tg ; Téragramme (10^{12}) ; Pg : Pétagramme (10^{15})
Temps	s : seconde ; ms : milliseconde ; an : année (yr : year)
Vitesse	m s^{-1} : mètre par seconde ; mm an^{-1} (mm yr^{-1}) : millimètre par an
Fréquence	Hz : hertz ; kHz : kilohertz
Température	°C : degrés Celsius

Masses atomiques, masses molaires et ratios

Hydrogène	H	1
Carbone	C	12
Azote	N	14
Oxygène	O	16
Calcium	Ca	40
Dioxyde de carbone	CO_2	44
Carbonate de calcium	$CaCO_3$	100
Ratio dioxyde de carbone / carbone (CO_{2e})	CO_2 / C	3,67
Ratio carbonate de calcium / dioxyde de carbone	$CaCO_3$ / CO_2	2,27

Résumé

Dans le contexte du changement climatique, la nécessité de réduire les concentrations atmosphériques de dioxyde de carbone (CO_2) pour atteindre les objectifs de l'Accord de Paris a récemment accentué l'intérêt pour la quantification de la capacité des écosystèmes côtiers (*i.e.* les herbiers marins, les mangroves et les prés-salés) à séquestrer le carbone communément appelé « Carbone Bleu ». Bien que ces écosystèmes à Carbone Bleu représentent moins de 1 % de la surface des océans, ils sont notamment reconnus pour fixer et séquestrer de grandes quantités de carbone conservées dans leurs sédiments constituant des puits de carbone majeurs en zone côtières. En Méditerranée, l'espèce endémique *Posidonia oceanica* (Linnaeus) Delile constitue de vastes herbiers marins considérés comme (i) des puits de carbone à long terme et (ii) des archives biologiques dues à la formation d'une structure remarquable appelée « matte ». Ces dépôts, composés des tissus très réfractaires de la plante enfouis dans les sédiments, constituent des accumulations de carbone pouvant être préservées pendant des millénaires et atteindre plusieurs mètres d'épaisseur. Afin d'estimer la contribution de ces herbiers à l'atténuation du changement climatique, une estimation des stocks de carbone a été réalisée dans la zone Natura 2000 « Grand Herbier de la Côte Orientale » en Corse (France). Cette approche expérimentale est basée sur l'analyse de plus de 1 380 km de données de sismique-réflexion haute résolution et de 49 carottes sédimentaires (40-365 cm de long) collectées entre 10 et 50 m de profondeur lors de trois campagnes océanographiques à bord du navire « L'Europe » (Ifremer). La cartographie prédictive établie par krigeage ordinaire met en évidence une forte hétérogénéité spatiale des épaisseurs de matte dans le site d'étude. Les épaisseurs des mattes (moyenne : 251,9 ± 0,2 cm) sont significativement plus importantes en eaux peu profondes, près des embouchures des fleuves et lagunes côtières, où une épaisseur de matte atteignant 867 cm a pu être enregistrée. Les datations au ^{14}C révèle la présence des herbiers depuis l'Holocène (7000-9000 ans AP) ainsi qu'une forte variabilité dans l'accrétion de la matte résultant de l'interaction de multiples facteurs biotiques et abiotiques. En se basant sur la surface occupée par ces herbiers et l'épaisseur moyenne relevée, le volume de matte a été estimé à 403,5 ± 49,4 millions de m^3. Les analyses biogéochimiques et sédimentologiques ont montré une forte variation dans l'accumulation et les stocks de carbone organique et inorganique (respectivement C_{org} et C_{inorg}). Ainsi, les stocks de C_{org} et C_{inorg} (moyenne : 327 ± 150 t ha^{-1} et 245 ± 45 t ha^{-1}, respectivement), montrent une très grande variabilité selon la profondeur, la matrice sédimentaire (substrat sableux *vs* rocheux) ou encore l'influence des dépôts sédimentaires (estuaire *vs* mer ouverte). La signature isotopique ($\delta^{13}C$) a permis de révéler une contribution significative des apports allochtones en matière organique (macroalgues et sestons) principalement en milieu estuarien et dans les zones superficielles. Les estimations globales des quantités de carbone stockées sur les premiers 250 cm de matte (épaisseur moyenne au niveau du site) ont été estimées entre 4,5 et 13,2 millions de t C_{org}. En convertissant ces résultats en équivalent CO_2 (CO_{2e}), les quantités ainsi piégées correspondraient à 16,5 et 48,3 millions de t CO_{2e} soit l'équivalent de 9,4 à 27,4 années d'émissions de CO_2 de l'ensemble de la Corse. L'extrapolation des données à l'échelle insulaire démontre que les herbiers auraient stocké l'équivalent de 26,6 à 72,0 années d'émissions de CO_2. De plus, l'une des carottes sédimentaires prélevées a révélée l'existence d'un ancien banc de corail *Cladocora caespitosa* (Scleractinia) enfoui dans la matte. Les analyses ont permis de reconstruire sa dynamique depuis le milieu de l'Holocène (4750 ans) et confirment le rôle joué par la matte comme archive biologique dans l'étude des changements paléo-climatiques et paléo-écologiques survenus en milieu côtier.

Mots-clés : *Posidonia oceanica*, herbiers marins, puits de carbone, Corse, changement climatique.

Abstract

In the context of climate change, the increasing necessity to reduce atmospheric carbon dioxide (CO_2) concentrations to meet the objectives of the Paris Agreement has recently intensified interest in quantifying the capacity of coastal ecosystems (*i.e.* seagrass meadows, mangroves and saltmarshes) to sequestered carbon referred commonly as 'Blue Carbon' (BC). Although these BC ecosystems represent less than 1% of the world's ocean surface, they are particularly effective in the capture and sequestration of high amounts of carbon stored in their sediments constituting thus large carbon sinks in coastal areas. In the Mediterranean Sea, the endemic seagrass species *Posidonia oceanica* (Linnaeus) Delile constitutes extensive meadows considered as (i) long-term carbon sinks and as (ii) valuable archive due to the development of an outstanding structure known as 'matte'. These belowground deposits, composed of high refractory seagrass materials embedded in a sediment matrix, constitute carbon reservoir which can be preserved over millennia and reach several meters thick. In order to estimate the contribution of *P. oceanica* meadows to the climate change mitigation, an estimate of carbon stocks has been conducted in the Natura 2000 area 'Grand Herbier de la Côte Orientale' in Corsica (France, NW Mediterranean). This experimental approach is based on more than 1 380 km of high-resolution seismic reflection data and 49 sediment cores (40-365 cm-long) collected between 10 and 50 m depth during three oceanographic research surveys aboard the vessel 'L'Europe' (Ifremer). The prediction map calculated by data interpolation highlighted a strong spatial heterogeneity of the matte thickness in the study site. The thicknesses of matte deposits (mean: 251.9 ± 0.2 cm), are significantly more important in shallow waters, near lagoon and river estuaries where matte thickness reaching 867 cm have been recorded. Radiocarbon dating reveal the presence of the seagrass meadows since the mid-Holocene period (7000-9000 cal. yr BP) and a high variability in the matte accretion resulting from the interaction of multiple biotic and abiotic factors. Based on the surface occupied by these seagrass meadows and the average thickness of matte, the volume of matte was estimated at 403.5 ± 49.4 million m^3. The sedimentological and biogeochemical analysis performed on matte cores showed a high variation in the accumulation and stocks of organic and inorganic carbon (C_{org} and C_{inorg}, respectively). Thus, C_{org} and C_{inorg} stocks (mean: 327 ± 150 t ha^{-1} and 245 ± 45 t ha^{-1}, respectively), show high variability related to water depth, sedimentary matrix (sandy *vs* rocky substrate) or the depositional environment (open sea *vs* estuary). Isotopic signature ($\delta^{13}C$) allowed to reveal a substantial contribution of allochthonous inputs of organic matter (macroalgae and sestonic sources) mainly in estuarine environment and shallow areas. Overall estimates of the amounts of carbon stored over the first 250 cm of matte (average thickness at site level) were estimated between 4.5 and 13.2 million t C_{org}. By converting these results into CO_2 equivalent (CO_{2e}), the quantities thus trapped would correspond to 16.5 and 48.3 million t CO_{2e}, the equivalent of 9.4 to 27.4 years of CO_2 release from the entire population of Corsica. Extrapolation of data to the regional scale shows that seagrass meadows would have stored the equivalent of 26.6 to 72.0 years of CO_2 release. Additionally, to these results, one of the *P. oceanica* mattes core revealed the unprecedented finding of a dead bank of the coral *Cladocora caespitosa* (Scleractinia) embedded in the matte. The analyses contribute to study its long-term since the mid-Holocene (last 4750 years) and confirm the role played by matte as valuable biological archive for the reconstruction of palaeoclimatic and palaeoecological changes in the coastal environment.

Keywords: *Posidonia oceanica*, seagrass meadows, carbon sink, Corsica, climate change.

Table des matières

Chapitre 1

Introduction générale

1.1. Contexte général : cycle global du carbone et changement climatique

Le système climatique terrestre est défini comme un système complexe d'interactions entre cinq composantes majeures : l'atmosphère, l'hydrosphère, la cryosphère, la biosphère et la lithosphère (Chavaillaz, 2016). L'étude de l'évolution du climat repose sur la connaissance approfondie du système climatique et des multiples interactions existant entre ces composantes. Depuis plusieurs décennies, les simulations futures du climat à l'échelle planétaire reposent sur la prise en compte du cycle global du carbone (Pepin, 2012) et tout particulièrement la teneur en dioxyde de carbone (CO_2) atmosphérique qui représente l'une des principales phases de ce cycle. De manière conceptuelle, le cycle global du carbone du système Terre peut être considéré comme une série de réservoirs reliés par des flux d'échange de carbone. Selon Sundquist (1986), deux domaines distincts peuvent être considérés :

(i) Le domaine dit « rapide », constitué par le carbone présent dans l'atmosphère, l'océan, les sédiments océaniques de surface en partie marine et la biomasse végétale, les sols et les eaux douces en partie terrestre, est caractérisé par un flux d'échange important et un taux de renouvellement des réservoirs [1] relativement rapide (< 10 000 ans) ;

(ii) Le domaine dit « lent » correspond aux réserves de carbone présents dans les roches et les sédiments. Les échanges de ces réservoirs principalement géologiques avec le domaine « rapide » s'effectuent par le biais des émissions volcaniques de CO_2, de l'altération chimique, de l'érosion et de la formation de sédiments sur le fond marin à un taux de renouvellement bien supérieur au précédent domaine (> 10 000 ans).

Au cours de la période Holocène (11 700 ans – période industrielle), le domaine « rapide » était caractérisé par un état stable comme en témoigne les faibles variations du CO_2 atmosphérique enregistrés dans les carottes de glace et ce, malgré les émissions dues au développement des activités anthropiques au cours de ces derniers milliers d'années

[1] Le taux de renouvellement est défini comme la masse du réservoir de carbone divisée par le flux d'échange.

(Pongratz *et al*., 2009). Cependant, depuis le début de la période industrielle[2], la hausse continue des teneurs en gaz à effet de serre (GES) (le protoxyde d'azote (N_2O), le méthane (CH_4) et principalement le dioxyde de carbone (CO_2)) a causé un important déséquilibre du cycle naturel du carbone et par conséquent du système climatique mondial (IPCC, 2013). En effet, un large consensus dans la communauté scientifique a permis d'établir que les activités anthropiques était à l'origine du transfert de grande quantité de carbone du domaine « lent » au domaine « rapide » et au dérèglement du système climatique mondial (Myhre *et al*., 2013). Cette libération de CO_2 dans l'atmosphère résulte principalement des émissions anthropiques provenant (i) de l'utilisation des combustibles fossiles issues des réservoirs géologiques comme source d'énergie (*i.e.* charbon, hydrocarbure et gaz), (ii) du changement de l'affectation des sols (*i.e.* déforestation, agriculture, détérioration d'écosystèmes) et (iii) dans une moindre mesure, par la production de ciment (Rotty, 1983 ; IPCC, 2007 ; Boden *et al*., 2011).

Selon les projections et scénarios des modèles climatiques (RCP2.6 - RCP8.5[3]), établis par le Groupe d'experts Intergouvernemental sur l'Evolution du Climat (GIEC), une hausse continu des teneurs en CO_2 atmosphérique pourrait conduire à des changements globaux ou régionaux majeurs au cours du XXI^{ème} siècle tels que l'augmentation globale des températures (Fig. 1.1.a), une hausse du niveau marin (Fig. 1.1.b), une acidification des océans ou encore des évènements extrêmes plus fréquents (*i.e.* inondations, sécheresses, tempêtes ; IPCC, 2013 ; 2019). Depuis la période industrielle, la concentration moyenne globale en CO_2 a augmenté de plus de 40 % passant ainsi de 278 ppm à plus de 400 ppm ; un niveau que l'atmosphère terrestre n'a pas connu pendant au moins les 800 000 dernières années et peut-être bien plus longtemps (Lüthi *et al*., 2008 ; Fischer *et al*., 2008). À partir des années 2010, le CO_2 est devenu le gaz carboné présentant la plus forte concentration dans l'atmosphère terrestre (Dlugokencky et Tans, 2013) correspondant à une masse de 828 Pg C (Prather *et al*., 2012 ; Joos *et al*., 2013). Parallèlement, entre la période industrielle et le début des années

[2] Période industrielle (*Industrial Era*) : augmentation de l'activité anthropique établie depuis l'année 1750 CE par le Groupe d'experts Intergouvernemental sur l'Evolution du Climat (GIEC) (IPCC, 2013).
[3] Representative Concentration Pathways : scénarios d'évolution des concentrations de GES classés du plus optimiste au plus pessimiste (RCP2.6 ; RCP4.5 ; RCP6.0 ; RCP8.5) et nommés d'après la valeur du forçage radiatif induit à l'horizon 2100.

2010, les émissions de CO_2 provenant des activités humaines ont conduit au rejet total de 555 ± 85 Pg C dans l'atmosphère, soit près de 67 % du CO_2 atmosphérique (IPCC, 2013).

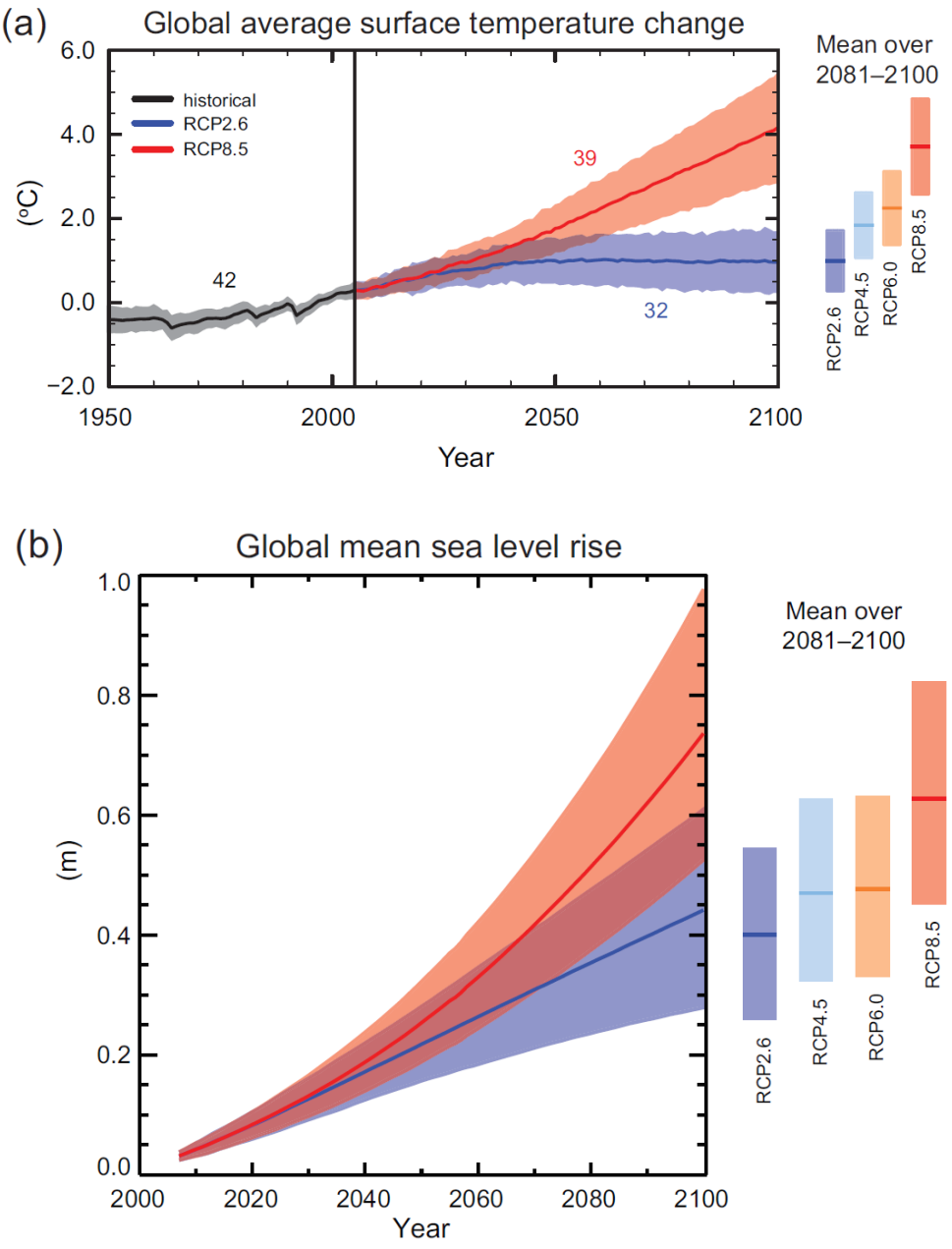

Figure 1.1. Projection de (a) l'évolution de la température annuelle moyenne du globe en surface et (b) l'évolution du niveau moyen des mers par rapport à la période 1986-2005 pour les deux scénarios RCP2.6 et RCP8.5. Adapté d'après IPCC (2013).

Dans un objectif de limitation du réchauffement planétaire à 1,5-2,0 °C par rapport aux niveaux préindustriels, les émissions anthropiques mondiales nettes de CO_2 doivent être

réduites de 25 à 45 % d'ici à 2030 par rapport à leur niveau de 2010 et atteindre 0 % d'ici à 2050-2070 (IPCC, 2019). Pour atteindre cet objectif, la principale stratégie pour réduire les concentrations de CO_2 atmosphérique repose sur la diminution des émissions anthropiques. Dans ce contexte, les Parties signataires de l'Accord de Paris sur le climat faisant suite à la 21ème Conférences des Parties (COP21) de la Convention Cadre des Nations Unies sur les Changements Climatiques (CCNUCC), se sont engagés à limiter le réchauffement climatique à un niveau inférieur à 2°C par rapport aux niveaux préindustriels (UNFCCC, 2016). Outres ces mesures historiques, l'Accord de Paris reconnaît l'importance de la conservation et du renforcement des puits et réservoirs des gaz à effet de serre et encourage les pays à prendre des mesures pour conserver et renforcer ces puits (UNFCCC, 2016). En effet, l'ensemble des Parties signataires ont reconnu pour la première fois le rôle clé des écosystèmes terrestres et marins dans l'absorption des émissions de CO_2 anthropique et dans l'atténuation des effets du changement climatique. Dans ce contexte, l'Union Internationale pour la Conservation de la Nature (UICN) a souligné l'importance des écosystèmes naturels et la nécessité de s'appuyer sur les « Solutions Fondées sur la Nature » afin de relever les défis globaux comme la lutte contre les changements climatiques (UICN, 2016). Ainsi, afin d'évaluer la contribution des écosystèmes à l'atténuation des changements climatiques, l'Accord de Paris encourage les Parties à fournir un rapport national d'inventaire des émissions anthropiques par les sources et des absorptions anthropiques par les puits de gaz à effet de serre, en suivant les méthodes adoptées par le GIEC (UNFCCC, 2016).

En effet, alors que la moitié des émissions de CO_2 reste dans l'atmosphère (240 ± 85 Pg C), le reste du CO_2 est éliminé et stocké dans d'autres réservoirs du cycle du carbone (Fig. 1.2. ; Houghton, 2007 ; IPCC, 2013, 2019). Le cycle global du carbone est un cycle naturel continu basé sur les échanges entre les différents compartiments majeurs du système Terre *(i.e.* principalement biogéosphère – atmosphère) (IPCC, 2001). Les quatre réservoirs majeurs sont l'atmosphère, les océans, les réserves fossiles et les écosystèmes terrestres incluant la végétation et les sols (Fig. 1.2. ; Sarmiento et Gruber, 2002 ; Houghton, 2007). Dans la biosphère, une quantité significative du carbone est séquestrée par les organismes vivants (biomasse) ou stockée dans des réservoirs tels que les sols, les fonds marins ou les roches biogéniques sur des périodes de temps plus ou moins importantes (plusieurs décennies voire millénaires) (Trumper *et al*., 2009).

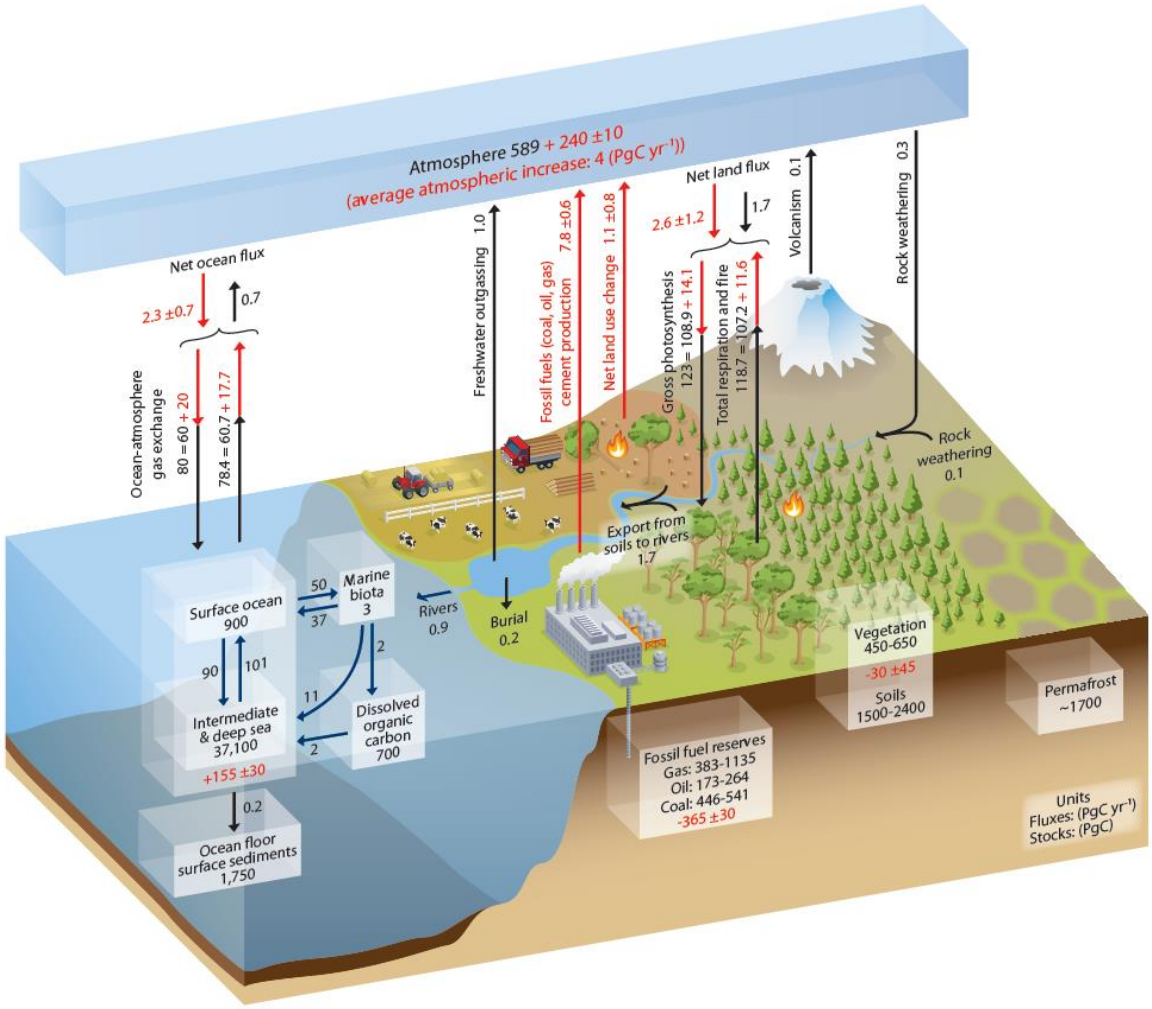

Figure 1.2. Représentation schématique du cycle global du carbone (IPCC, 2013). Les valeurs représentent la quantité de carbone sein de chaque réservoir, aussi appelé « stock de carbone » (en Pg C) et les échanges annuels en carbone (en Pg C an^{-1}). Les valeurs et les flèches en noir indiquent la quantité du réservoir et les échanges. Les valeurs et les flèches en rouges correspondent aux échanges annuels anthropiques moyennés sur la période 2000-2009. La séquestration du CO_2 atmosphérique issue des activités anthropiques par l'océan ('*Net ocean flux*') et les écosystèmes terrestres ('*Net land flux*') sont représentés par les flèches rouges. Les valeurs en rouges dans les réservoirs indiquent les changements liés au carbone anthropique depuis la période industrielle (1750).

Le processus de séquestration conduisant au piégeage du carbone au sein de réservoirs a pour origine des processus physiques, biologiques et chimiques qui agissent à diverses échelles de temps (IPCC, 2013). Ce mécanisme de séquestration dépend

principalement de la forme sous laquelle sera stocké le carbone et du taux de renouvellement de ce stock. Un écosystème est considéré comme étant un puits de carbone dès que celui-ci accumule davantage de carbone qu'il n'en libère (Trumper *et al*., 2009 ; Commissariat général au développement durable, 2019). Néanmoins, en réponse aux changements climatiques ou environnementaux (*e.g.* modification des températures, acidification des océans, élévation du niveau marin) ou à des évolutions dans l'usage des sols (*e.g.* agriculture, déforestation, urbanisation), un écosystème considéré jusqu'alors comme un puits de carbone peut devenir une source si les émissions de carbone sont supérieures à la séquestration (Trumper *et al*., 2009).

Parmi les principaux réservoirs impliqués dans le cycle global du carbone, la biosphère terrestre est reconnue comme l'un des plus importants (IPCC, 2013). La séquestration de carbone au sein de ce puits résulte principalement du processus photosynthétique réalisé par les plantes terrestres (123 ± 8 Pg C an^{-1} ; Beer *et al*., 2010). Cette séquestration du carbone par les écosystèmes est majoritairement réalisée par la biomasse végétale vivante (450-650 Pg C ; Prentice *et al*., 2001) mais aussi par les sols riches en matière organique (1 500-2 400 Pg C ; Batjes, 1996). Selon les estimations, ce puits de carbone communément désigné sous l'appellation « Carbone Vert » (*Green Carbon* en anglais), représente plus de 2 000 Pg C (Nellemann *et al*., 2009). Cependant, bien que la biomasse terrestre et les sols participent à la séquestration de grande quantité de carbone, la longévité de ces puits demeure incertaine (Schlesinger et Lichter, 2001 ; Fourqurean *et al*., 2012). En effet, la reminéralisation du carbone piégé dans les écosystèmes terrestres, issue majoritairement de la déforestation et des changements dans l'usage des sols, est responsable de 8 à 20 % des émissions anthropiques (Forster *et al*., 2007). En comparaison avec d'autres réservoirs du cycle du carbone, le taux de renouvellement du carbone séquestré par ces puits est relativement important, généralement quelques décennies ou siècles au plus (Chambers *et al*., 2001 ; Nellemann *et al*., 2009). Le carbone ainsi séquestré retourne vers l'atmosphère sous la forme de CO_2 ou de CH_4 à travers (i) des processus de respiration et de décomposition de la biomasse morte et (ii) des processus de dégradation (*e.g.* feux de forêts, agriculture ; IPCC, 2013).

Malgré le fait qu'au cours des dernières décennies l'attention portée sur la séquestration ait été focalisée sur les écosystèmes terrestres (les forêts essentiellement), la

capacité de séquestration la plus importante est attribuée aux océans (Nelleman *et al*., 2009 ; Mcleod *et al*., 2011 ; Lovelock et Reef, 2020). En effet, la quantité totale de carbone présent dans les océans de la planète est estimée à 38 000 Pg C, principalement sous forme de carbone inorganique dissous (Fig. 1.2. ; Mcleod *et al*., 2011), soit 50 fois plus que dans l'atmosphère et 18 fois plus que dans la biosphère continentale (Carbone Vert). D'après les estimations du GIEC, près d'un quart des quantités totales de CO_2 émises par les activités anthropiques ont été absorbés par les océans depuis le début de la période industrielle (155 ± 30 Pg C ; Sabine et Feely, 2007 ; IPCC, 2013 ; Ciais *et al*., 2012). Le rôle de l'océan comme zone tampon du système climatique est notamment mis en évidence grâce à l'existence de deux mécanismes majeurs intervenant dans l'absorption du CO_2 atmosphérique : la pompe physico-chimique (*i.e.* transfert à l'interface air-océan) et la pompe biologique (*i.e.* piégeage par le phytoplancton et les micro-organismes photosynthétiques) (Siegenthaler et Sarmiento, 1993 ; Houghton, 2007).

Cependant, alors que le rôle de la végétation des écosystèmes côtiers dans le cycle global du carbone et sa capacité de séquestration du carbone sont reconnus depuis plusieurs décennies (*e.g.* Smith *et al*., 1981), ces écosystèmes ont pendant longtemps été négligés et non pris en considération dans les programmes de réduction des GES (Macreadie *et al*., 2014 ; Duarte *et al*., 2017). Cependant, à la fin des années 2000, deux rapports primordiaux (Laffoley et Grimsditch 2009 ; Nellemann *et al*., 2009) ont permis de souligner l'importance de ces écosystèmes dans l'atténuation des changements climatiques. En effet, sur l'ensemble des quantités de carbone séquestrées annuellement par les organismes photosynthétiques, plus de la moitié (55 %) est capturée par les organismes vivants marins (Arrigo, 2005 ; González, *et al*., 2008 ; Bowler, 2009 ; Simon *et al*., 2009). La majorité du carbone capturé par les organismes marins (45 %) proviendrait uniquement du phytoplancton (Falkowski *et al*., 2004) et le reste (10 %) serait attribué aux puits de carbone associés à la végétation côtière (Nellemann *et al*., 2009). Le carbone ainsi séquestré et stocké par ces écosystèmes est désigné sous le terme de « Carbone Bleu » (Nellemann *et al*., 2009). La publication de ces deux ouvrages a déclenché au cours de la dernière décennie le développement de stratégies d'atténuation du changement climatique basées sur leur protection et restauration, similaires à celles déjà initiée pour les écosystèmes terrestres (*e.g.* programme REDD+) ainsi que de

nombreuses initiatives (*e.g.* The International Blue Carbon Initiative[4]) et études scientifiques visant à quantifier la contribution de ces écosystèmes à « Carbone Bleu » (ECB) à l'atténuation des effets du changement climatique (Alongi, 2018).

1.2. Les écosystèmes côtiers à Carbone Bleu

Les écosystèmes côtiers dominés par les plantes (*i.e.* les mangroves, les prés salés et les herbiers marins) (Fig. 1.3.) offrent de nombreux biens et services profitables aux populations et à la biodiversité contribuant notamment à atténuer les effets du changement climatique. Beaucoup de ces services sont primordiaux en zone côtière pour faire face à ces bouleversements climatiques tels que la protection contre les tempêtes et les cyclones, l'atténuation de l'élévation du niveau marin, la prévention de l'érosion le long du littoral, la qualité des eaux côtières, le recyclage des nutriments, le piégeage des sédiments, la fourniture d'habitats pour de nombreuses espèces marines et la sécurité alimentaire pour de nombreuses communautés côtières à travers le monde (Kennedy, 1984 ; Robertson et Alongi, 1992 ; King et Lester 1995 ; Hogarth, 1999 ; Beck *et al*., 2001 ; Kathiresan et Bingham, 2001 ; Saenger 2002 ; Mumby, 2006 ; Gedan *et al*., 2009 ; Barbier *et al*., 2011 ; Sousa *et al*., 2012 ; Cullen-Unsworth et Unsworth, 2013).

En plus de ces rôles essentiels, ces écosystèmes participent à l'atténuation du changement climatique et au cycle du carbone marin en séquestrant et en stockant d'importantes quantités de carbone de l'atmosphère et des océans (Chmura *et al*., 2003 ; Duarte *et al*., 2005 ; Bouillon *et al*., 2008 ; Duarte *et al*., 2010 ; Kennedy *et al*., 2010 ; Mcleod *et al*., 2011 ; Fourqurean *et al*., 2012 ; Pendleton *et al*., 2012 ; Serrano *et al*., 2012 ; Lavery *et al*., 2013 ; Atwood *et al*., 2017 ; Serrano *et al*., 2019). Ces écosystèmes côtiers, qui représentent moins de 2 % de la surface des océans, stockent 10 à 24 Pg C dans le premier mètre du sol (Duarte *et al*., 2013). Sur la totalité du carbone piégé dans les sédiments marins, 50 % provient de ces écosystèmes côtiers (Duarte *et al*., 2013), l'équivalent de 1 à 2 % des émissions actuelles de CO_2 issues de la combustion des énergies fossiles (Serrano *et al*., 2019).

[4] Programme mondial rassemblant des gouvernements, des instituts de recherche et des organisations visant à atténuer le changement climatique à travers la restauration et l'utilisation durable des écosystèmes côtiers et marins. Plus d'informations sur https://www.thebluecarboninitiative.org/

Ces écosystèmes participent à la fixation à la séquestration du CO_2 atmosphérique, dans la biomasse vivante (feuilles, tiges, branches) et souterraine (racines), dans la biomasse non-vivante ou nécromasse (*e.g*. litière et bois mort) mais surtout dans les sédiments (Howard *et al*., 2014a). En effet, de manière similaire aux écosystèmes terrestres, ce carbone organique (C_{org}) est séquestré à court terme sous forme de biomasse vivante végétale (pendant quelques années à plusieurs décennies) (Howard *et al*., 2017) mais également sur des échelles de temps plus longues (de quelques siècles à plusieurs millénaires) dans les sédiments comme le démontrent les datations au radiocarbone entreprises dans les herbiers marins (Serrano *et al*., 2012), les prés salés (Ward *et al*., 2008) et les mangroves (Filho *et al*., 2006).

Figure 1.3. De gauche à droite, prés salés sur les côtes écossaises constitués de *Blysmus rufus* et *Eleocharis uniglumis* (© Scotland's Nature Agency) ; forêt de mangroves de Lembongan en Indonésie (© Lutz S.) ; herbiers marins à *Posidonia oceanica* en Méditerranée (© Pergent G.).

La séquestration et la préservation du carbone au sein de ces réservoirs résultent de la combinaison de multiples facteurs (Nellemann *et al*., 2009). L'enfouissement de grande quantité de carbone dans les sédiments découle de la haute productivité primaire de ces écosystèmes (Cebrian et Duarte, 1995). Une grande partie de la biomasse stockée dans les sédiments est issue des racines et rhizomes présentant de faibles concentrations en azote et phosphore dans leurs tissus (Duarte *et al*., 1998) et la présence de faibles taux d'oxygène dans les sédiments saturés en eau contribuant ainsi à limiter la décomposition et l'oxydation de la matière organique par l'activité microbienne (Duarte et Cebrian, 1996 ; Middelburg *et al*., 1997a ; Kennedy *et al*., 2010 ; Chapman *et al*., 2013). Cependant, des tissus ligneux (*i.e*. les

tiges) et de la litière (*i.e.* les feuilles) peuvent également être des composants importants du stock C_{org} sédimentaire dans les prés salés (Krauss *et al*., 2018 ; Van de Broek *et al*., 2018). Ainsi, contrairement aux écosystèmes terrestres, la séquestration du carbone dans les sédiments côtiers est jusqu'à 10 à 50 fois plus importante pour des surfaces d'habitats équivalentes (Mcleod *et al*., 2011 ; Duarte *et al*., 2013). L'accumulation du carbone dans les sédiments de la végétation côtière varie entre 18 et 1 713 g C_{org} m^{-2} an^{-1} (Chmura *et al*., 2003 ; Bird *et al*., 2004 ; Duarte *et al*., 2005 ; Kennedy *et al*., 2010) avec des valeurs moyennes établis entre 212 ± 18 et 218 ± 24 g C_{org} m^{-2} an^{-1} pour les prés salés, 163 ± 0 et 761 ± 46 g C_{org} m^{-2} an^{-1} pour les mangroves et 138 ± 38 et 220 ± 20 g C_{org} m^{-2} an^{-1} pour les herbiers marins (Laffoley et Grimsditch, 2009 ; Duarte *et al*., 2013 ; Alongi, 2018). Contrairement aux écosystèmes côtiers, l'accumulation de C_{org} dans les sols des écosystèmes terrestres (*e.g.* forêts) varie entre 0,7 et 13,1 g C_{org} m^{-2} an^{-1} et est estimée en moyenne à 5,1 ± 1,0 g C_{org} m^{-2} an^{-1} pour les forêts tempérées, 4,0 ± 0,5 g C_{org} m^{-2} an^{-1} pour les forêts tropicales et 4,6 ± 2,1 g C_{org} m^{-2} an^{-1} pour les forêts boréales (Schlesinger, 1997 ; Zehetner, 2010 ; Mcleod *et al*., 2011).

La séquestration de matière organique dans les sédiments est aussi renforcée par le piégeage de matières organiques produites par des écosystèmes adjacents (*i.e.* C_{org} allochtone) aussi bien terrestres que marins (Fig. 1.4 ; Kennedy *et al*., 2010). La complexité structurelle de la végétation côtière (*e.g.* système racinaire, végétation dense, canopée) ainsi qu'un grand nombre de facteurs peuvent influencer l'accumulation des particules sédimentaires en suspension et le C_{org} associé (Hendriks *et al*., 2008 ; Serrano *et al*., 2016b ; Howard *et al*., 2017). En effet, la séquestration du C_{org} allochtone peut être influencée par les paramètres physico-chimiques de l'environnement (*e.g.* la salinité, la disponibilité en nutriments, la température, les apports en eaux douces, l'élévation du niveau marin, le type de sédiment), les paramètres biologiques (*e.g*. l'espèce, la compétition interspécifique, l'herbivorie, la bioturbation) et depuis quelques années par le changement climatique (Mcleod *et al*., 2011 ; Serrano *et al*., 2016b ; Mazarrasa *et al*., 2018 ; Macreadie *et al*., 2019 ; Lovelock et Reef, 2020). La proportion de carbone provenant de sources externes varie fortement d'un écosystème côtier à l'autre (Howard *et al*., 2014a). En effet, pour les herbiers marins, une estimation montre qu'environ 50 % du C_{org} stocké dans les sédiments proviendrait de sources allochtones (Kennedy *et al*., 2010). En revanche, le C_{org} séquestré dans les sédiments des mangroves et des prés salés proviendrait essentiellement de la production

primaire de la végétation côtière (Middleton et McKee, 2001), bien que cela puisse varier d'un site à l'autre (Middelburg *et al*., 1997b ; Bouillon *et al*., 2003 ; Adame *et al*., 2012).

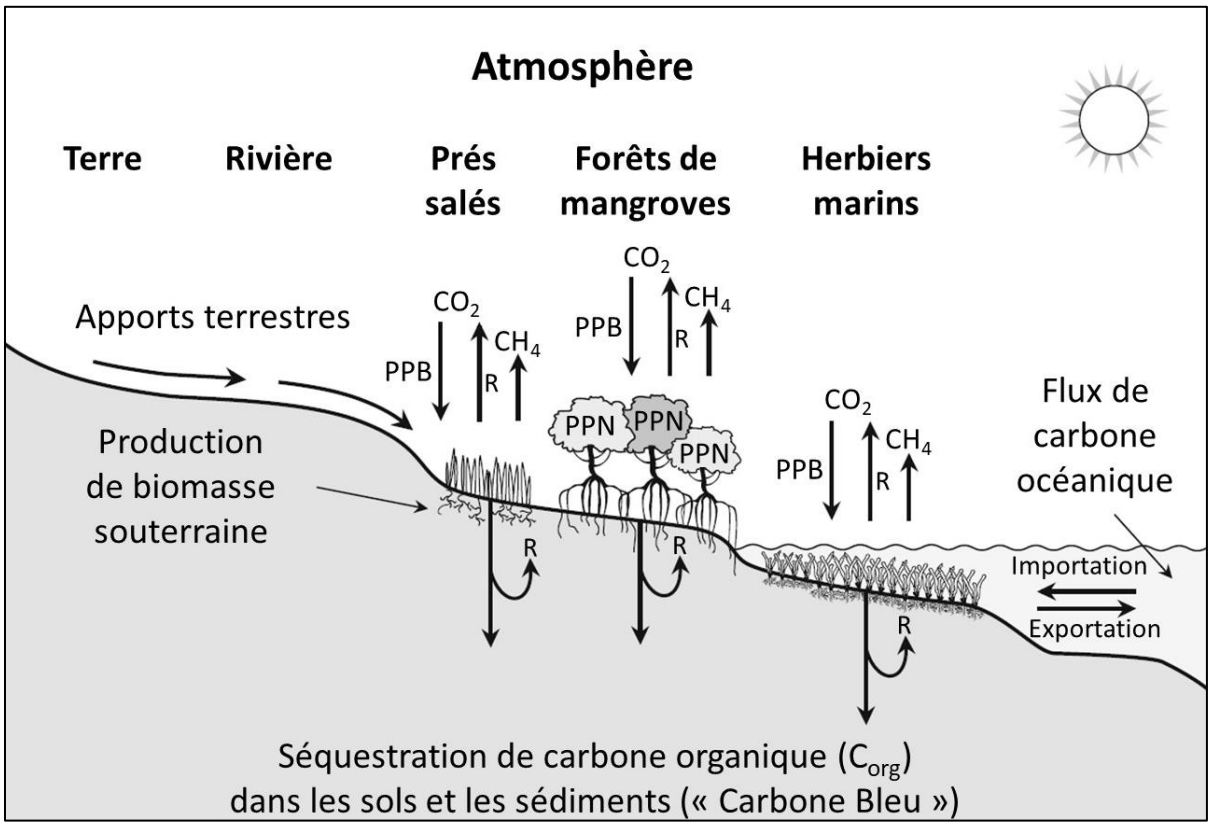

Figure 1.4. Modèle conceptuel du carbone dans les écosystèmes côtiers. PPB : Production Primaire Brut ; PPN : Production Primaire Nette ; R : Respiration. Adapaté et traduit de Alongi (2018).

L'apport régulier de particules sédimentaires organiques ou minérales couplé à la préservation du carbone dans le sol de ces habitats côtiers favorise le développement et l'accrétion des puits de C_{org} au cours du temps (Chmura *et al*., 2003). Les plus impressionnants puits de carbone côtiers sont constitués de dépôts sédimentaires atteignant plus de 10 mètres d'épaisseurs et un âge supérieur à 10 000 ans. Les exemples les plus connus dans la littérature sont les dépôts organiques retrouvés sous les mangroves du Belize (McKee *et al*., 2007), les dépôts tourbeux de 7 mètres d'épaisseurs présents sous les prés salés de Californie (Drexler *et al*., 2011) ou encore les mattes des herbiers à *Posidonia oceanica* en Méditerranée atteignant plus de 4 mètres d'épaisseurs (Lo Iacono *et al*., 2008 ; Serrano *et al*., 2012) voire ponctuellement 14 m (Miković, 1977 *in* Varda, 2015).

L'accent mis sur l'importance des écosystèmes côtiers dans le stockage du carbone a focalisé les efforts sur l'évaluation des teneurs et les modalités de préservation du C_{org} sur de longues périodes de temps. En effet, bien qu'une part importante du matériel enfoui dans les sédiments des écosystèmes côtiers soit issue de la matière organique (C_{org}), le reste est constitué de composés inorganiques silicatés (*i.e.* minéraux) et carbonatés ($CaCO_3$). Plusieurs estimations ont montré que la teneur en C_{inorg} carbonaté pouvait représenter une part importante du carbone enfouie dans les sédiments des écosystèmes côtiers (Kristensen *et al*., 2008 ; Fourqurean *et al*., 2012) voire, dans certains cas, excéder la teneur en C_{org} dans les sédiments des herbiers marins (Mazarrasa *et al*., 2015). Les estimations globales ont notamment montré que les herbiers marins et les mangroves participent à la séquestration d'importantes quantités de carbone inorganique (C_{inorg}), avec respectivement 15 à 62 Tg C_{inorg} an^{-1} et 0,8 Tg C_{inorg} an^{-1} (Mazarrasa *et al*., 2015 ; Saderne *et al*., 2019). Cette séquestration du C_{inorg} ne représente qu'environ 3 % du C_{org} enfouie dans les sédiments des mangroves (Rosentreter *et al*., 2018) et atteint entre 30 et 50 % pour les herbiers marins (Duarte *et al*., 2005 ; Mcleod *et al*., 2011). Les quantités de C_{inorg} ainsi séquestré dans les sédiments sont estimées à 182 ± 94 g C_{inorg} m^{-2} an^{-1} au sein des herbiers marins et 90 ± 43 g C_{inorg} m^{-2} an^{-1} pour les mangroves (Saderne *et al*., 2019). De plus, alors que les prés salés n'abritent pas d'organisme calcaire, la séquestration atteint 100 ± 15 g C_{inorg} m^{-2} an^{-1} dans le Golfe Arabique (Saderne *et al*., 2018) voire 467 ± 99 g C_{inorg} m^{-2} an^{-1} en Pays-Bas (Zwolsman *et al*., 1993), en raison du fort taux d'accrétion sur ce site (1,1 ± 0,3 mm an^{-1}). Ces estimations globales ont également souligné que la présence de C_{inorg} résulte de mécanismes de calcification initiés par les organismes calcaires vivant au sein de ces habitats côtiers (*e.g.* épiphytes, invertébrés benthiques, algues calcifiées, foraminifères) mais surtout du dépôt de C_{inorg} carbonaté allochtone provenant de sources lithologiques ou d'écosystèmes adjacents (*e.g.* récifs coralliens) (Saderne *et al*., 2019). Toutefois, la séquestration des $CaCO_3$ dans les écosystèmes à carbone bleu résulte de l'équilibre entre les apports (*i.e.* autochtone et allochtone) et les pertes (*i.e*. dissolution et exportation). Bien que ces écosystèmes participent significativement à la séquestration du C_{inorg}, pouvant compenser la séquestration du C_{org}, le $CaCO_3$ peut également représenter une source importante d'émission de CO_2. En effet, les processus de calcification (*i.e.* production de 0,6 moles de CO_2 émis par mole de $CaCO_3$ précipité) (Macreadie *et al*., 2017) et de dissolution des $CaCO_3$ liés au métabolisme de la végétation et des organismes associés ainsi que la minéralisation de la matière organique (*i.e.* la libération

d'acides H_2SO_4, HNO_3 ; Mucha *et al*., 2005 ; Haoliang *et al.*, 2007) peut conduire localement à l'émission de CO_2 au sein de ces écosystèmes (Macreadie *et al*., 2017 ; Saderne *et al*., 2019). Malgré ces mécanismes, les estimations globales soulignent que les écosystèmes côtiers jouent aussi un rôle majeur dans la séquestration du $CaCO_3$ et qu'il est fondamental de prendre en considération le C_{inorg} lors de l'évaluation des stocks et flux de carbone au sein de ces puits de carbone.

1.3. Les herbiers à *Posidonia oceanica* : un puits de carbone unique en Méditerranée

1.3.1. *Posidonia oceanica*

Espèce endémique de la mer Méditerranée, *Posidonia oceanica* (Linnaeus) Delile est une Magnoliophyte marine caractéristique de l'étage infralittoral (Molinier et Picard, 1952 ; Boudouresque *et al*., 2012). Cette espèce se développe dans les eaux côtières entre la surface et une quarantaine de mètres de profondeurs où elle constitue de vastes herbiers couvrant une superficie d'environ 1 224 707 ha (Telesca *et al*., 2015), dont 53 735 ha sur le littoral de la Corse (Valette-Sansevin *et al*., 2019). Les herbiers à *Posidonia oceanica* jouent un rôle important (i) au niveau écologique comme source de production de matière végétale et en constituant des lieux de frayère et nurserie ainsi que des habitats pour de nombreuses espèces animales et végétales sessiles ou vagiles (Bellan-Santini *et al*., 1994), (ii) dans les équilibres physiques du système littoral en atténuant l'hydrodynamisme, en piégeant les sédiments et en protégeant les zones littorales de l'érosion (Jeudy de Grissac et Boudouresque, 1985 ; Gacia et Duarte, 2001 ; De Falco *et al*., 2000, 2003) et (iii) en termes économiques par les services et biens qu'ils fournissent (*e.g.* Vassallo *et al*., 2013). Cet écosystème constitue également un puissant intégrateur de la qualité globale des eaux marines et est également utilisé en tant que bioindicateur de l'environnement marin (Pergent-Martini et Pergent, 2000 ; Ferrat *et al.,* 2002 ; Lafabrie *et al.,* 2007 ; Serrano *et al*., 2011).

La plante constitue des tiges rampantes (plagiotropes) ou dressées (orthotropes) nommées rhizomes (Fig. 1.5 ; Caye, 1980). Ces rhizomes portent des racines qui peuvent

atteindre jusqu'à 70 cm de longueur permettant à la plante de se fixer au substrat et ainsi de coloniser tous types de fonds marins (*i.e.* vaseux, sableux et rocheux) (Giraud, 1979 ; Vacchi *et al*., 2017a). Les rhizomes possèdent à leurs extrémités un faisceau de cinq à huit feuilles rubanées (20 à 80 cm de longueur et de 0,8 à 1,1 cm de largeur) (Boudouresque et Meinesz, 1982) ; l'ensemble des feuilles constituant la canopée. Ces faisceaux sont constitués de feuilles (adultes, intermédiaires et juvéniles) qui se forment et se développent selon une forte saisonnalité (Pergent et Pergent-Martini, 1991 ; Alcoverro *et al*., 1995). Les feuilles adultes sont constituées d'un limbe (partie photosynthétique) et d'un pétiole (*i.e.* base) fixé au rhizome. La formation des feuilles à lieu tout au long de l'année avec un maximum à la fin de l'été et en automne (Ott, 1980 ; Pergent et Pergent-Martini, 1991 ; Alcoverro *et al*., 2001).

Figure 1.5. Herbiers à *P. oceanica* et un tombant de matte dans la baie de Sant'Amanza (Corse-du-Sud) (© Monnier B.) et représentation des différents organes de la plante. Adapté de Abadie (2012).

Lors de la chute des feuilles (généralement à la période automnale), le limbe se dissocie tandis que le pétiole resté fixé au rhizome et est alors appelé écaille (Fig. 1.5). Le bilan carbone de la plante montre des valeurs positives en été (en juillet et août) et négatives (de septembre à juin) en raison de la diminution de l'activité photosynthétique, de l'irradiance et d'une turbidité plus importante (Alcoverro *et al*., 2001 ; Mateo *et al*., 2006). Malgré le bilan carbone négatif observé durant une majeur partie de l'année, le maintien de la croissance de *P. oceanica* est largement assuré par la mobilisation des réserves de carbohydrates stockés

durant la période estivale dans la rhizosphère (*i.e.* rhizomes ; Pirc, 1985 ; Alcoverro *et al*., 2001).

1.3.2. La matte des herbiers à *P. oceanica* : un puits de carbone et une paléo-archive

Sur les fonds marins, les herbiers à *P. oceanica* constituent de véritables barrières végétales favorisant la décantation et la sédimentation des particules en suspension dans la colonne d'eau (Boudouresque et Jeudy de Grissac, 1983 ; Jeudy de Grissac et Boudouresque, 1985 ; Gacia et Duarte, 2001). Le piégeage de ces particules (organiques et inorganiques) d'origine allochtone couplé à la sédimentation autochtone (*i.e.* particules et débris d'organismes ayant vécu dans l'herbier, sur les feuilles ou à la base des rhizomes) contribue à l'accumulation d'une grande quantité de sédiment dans les interstices entre les rhizomes et les racines (Meinesz et Boudouresque, 1982 ; Jeudy de Grissac, 1984). Pour résister à un ensevelissement et s'assurer un accès à la lumière, les rhizomes orthotropes mettent en place une croissance verticale estimée en moyenne généralement entre 1 mm an^{-1} et 25 mm an^{-1} (Pergent *et al*., 1995 ; Marbá *et al*., 1996) même si des valeurs supérieures peuvent être observées ponctuellement (77 mm an^{-1} ; Boudouresque *et al*., 1984).

Le lacis constitué de rhizomes et de racines vivants et morts associés au sédiment biogénique et silicoclastique qui comble les interstices forme un ensemble complexe hautement organique et résistant appelé « matte » (Molinier et Picard, 1952). La croissance verticale des rhizomes et le piégeage des sédiments contribuent à l'accrétion de la matte et donc à l'élévation des fonds marins au cours du temps (Molinier et Picard, 1952 ; Boudouresque et Jeudy de Grissac, 1983). La croissance verticale, mesurée sur plusieurs décennies, correspond à l'interaction entre les phénomènes d'accrétion, de décomposition et d'érosion (Mateo *et al*., 1997 ; Serrano *et al*., 2012). L'accrétion moyenne observée en Méditerranée est très variable, elle est estimée en moyenne entre 10 et 100 cm par siècle (Molinier et Picard, 1952 ; Picard, 1953 ; Nesteroff, 1965 ; Tchernia *et al*., 1978 ; Boudouresque *et al*., 1980 ; Boudouresque et Jeudy de Grissac, 1983 ; Romero *et al*., 1994 ; Maggi *et al*., 1997 ; Mateo *et al*., 1997, 2005 ; Lo Iacono *et al*., 2008 ; Serrano *et al*., 2012, 2014, 2016a). L'ensemble de ces processus conduit à la formation de dépôts organiques pouvant mesurer jusqu'à 14 mètres d'épaisseur et datant de plus de 6 000 ans (Molinier et

Picard, 1952 ; Miković, 1977 *in* Varda, 2015 ; Boudouresque *et al*., 1980 ; Mateo *et al*., 1997 ; Lo Iacono *et al*., 2008) considérés comme étant des puits de carbone majeurs en Méditerranée (Fourqurean *et al*., 2012). L'évaluation de l'épaisseur des mattes des herbiers à *P. oceanica* relève principalement d'observations ponctuelles depuis les escarpements de mattes (*i.e.* tombants) liés à l'érosion naturelle de la matte (Boudouresque *et al*., 2012 ; Abadie *et al*., 2015), et à de fouilles archéologiques (*e.g.* Tchernia *et al*., 1978) ou à des carottages dans les herbiers (Mateo *et al*., 1997 ; Serrano *et al*., 2012). Au cours des deux dernières décennies, la nécessité d'obtenir des enregistrements continus a été mis en évidence afin d'évaluer l'épaisseur et le volume occupé par ces puits de carbone. Dans ce contexte, plusieurs études s'appuyant sur l'utilisation de la sismique réflexion haute-résolution ont permis d'acquérir des représentations continues des couches sédimentaires superficielles et de fournir les premières estimations des épaisseurs, des volumes et de l'extension de ces réservoirs biogéochimiques (Lo Iacono *et al*., 2008 ; Tomasello *et al*., 2009).

L'accumulation et la préservation de grandes quantités de carbone sur de longues périodes de temps au sein de ces puits de carbone côtiers résultent de l'interactions de multiples facteurs biotiques et abiotiques tels que (i) la production des herbiers marins (particulièrement des organes souterrains de la plante), (ii) la composition biogéochimique de la matière organique enfouie, (iii) le taux d'accrétion du sédiment et (iv) l'apport de carbone allochtone dans le compartiment sédimentaire (Fig. 1.6. ; Serrano *et al*., 2016b ; Mazarrasa *et al*., 2018). L'accumulation de C_{org} au sein de la matte des herbiers à *P. oceanica* résulte ainsi de la forte production de biomasse de ces écosystèmes côtiers (jusqu'à 2 112 $gMS.m^{-2}$; Duarte et Chiscano, 1999) et de l'enfouissement d'environ 29 à 32 % de la production primaire nette issue de l'herbier dans les sédiments (Pergent *et al*., 1994, 1997). La proportion moyenne de C_{org} séquestré sur le long-terme dans la matte, estimée à 27 % du carbone fixé par la plante (Serrano *et al*., 2012), est cohérente avec la part de matière organique séquestrée dans les sédiments, estimée par Pergent *et al.* (1997). Bien que la séquestration en C_{org} soit très importante dans les sédiments chez *P. oceanica*, de nombreuses études ont montré qu'il existait une très grande variabilité entre les différentes espèces d'herbiers marins (Lavery *et al.*, 2013 ; Rozaimi, 2015 ; Mazarrasa *et al*., 2017). En effet, contrairement aux espèces colonisatrices (*e.g*. *Halophila* spp.) ayant une croissance rapide et un taux de renouvellement élevé, *P. oceanica* possède un taux de croissance faible, un ratio biomasse

souterraine/superficielle plus élevé et des tissus plus persistants (Duarte et Chiscano, 1999 ; Serrano *et al*., 2016b). La forte accumulation et préservation du C_{org} dans les sédiments relèvent du faible taux de dégradation des composants organiques des herbiers à *P. oceanica* (Mateo *et al*., 2006). La biomasse des herbiers marins affiche une résistance accrue à la décomposition en raison des quantités relativement élevées de composés organiques réfractaires présents dans les tissus (*e.g.* la lignine, la cellulose, les phénols ; Harrison, 1989 ; Danovaro, 1996 ; Bianchi *et al*., 1999 ; Klap *et al*., 2000, ; Torbatinejad *et al*., 2007 ; Burdige, 2007 ; Kaal *et al*., 2016 ; 2018). Comme de nombreux herbiers marins, la production de biomasse, la densité et la croissance des herbiers à *P. oceanica* sont étroitement influencée par la profondeur et la turbidité des masses d'eau contrôlant la disponibilité en lumière et l'irradiance indispensable à l'activité photosynthétique (Alcoverro *et al*., 2001 ; Collier *et al*., 2007, 2009). Bien que l'effet de la profondeur sur la production primaire et la séquestration du C_{org} dans les sédiments des herbiers marins et notamment chez *P. oceanica* ait été mis en évidence (Fig. 1.6. ; Serrano *et al.*, 2014, 2016b ; Dahl *et al*., 2016), l'influence de la turbidité est plus discutée. En effet, alors qu'une hausse de la turbidité conduit à une diminution de la production primaire chez les herbiers marins (Collier *et al*., 2009 ; Ruiz et Romero, 2001), ce phénomène peut également favoriser l'apport de particules fines et de C_{org} allochtone contribuant à une accumulation et à une préservation de C_{org} après l'enfouissement dans les sédiments (Samper-Villareal *et al*., 2016). Ainsi, une augmentation des apports en C_{org} allochtone peut potentiellement contrebalancer la réduction des apports en C_{org} autochtone et former des stocks de C_{org} identiques ou supérieures dans ces dépôts sédimentaires (Samper-Villareal *et al*., 2016 ; Serrano *et al*., 2016b).

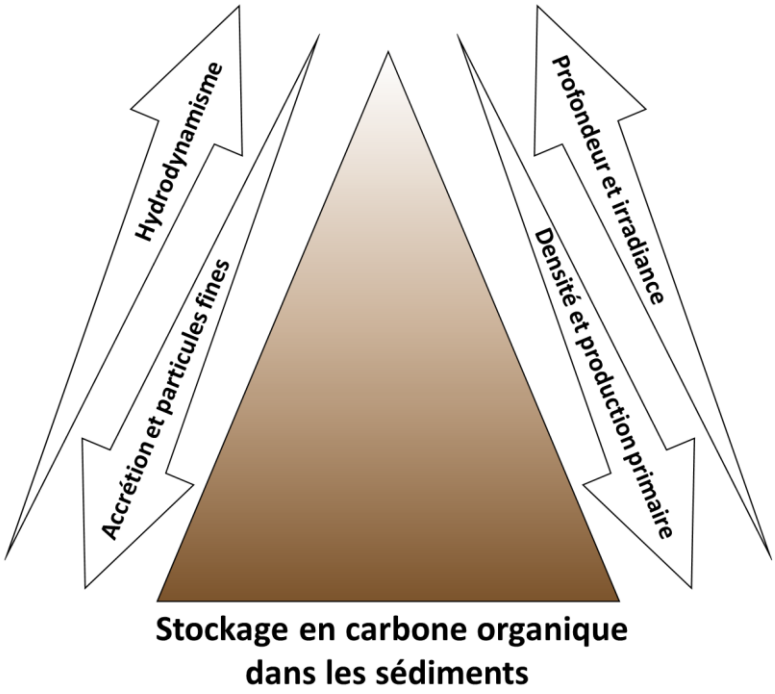

Figure 1.6. Influence des facteurs biogéochimiques sur la capacité de stockage des herbiers marins. La teneur en carbone organique dans les sédiments augmente avec le taux d'accrétion du sédiment, la teneurs en particules fines, la densité et la production primaire de l'herbier et diminue avec la profondeur, l'irradiance et l'hydrodynamisme. Adapté et traduit de Serrano *et al*., 2016b et Mazarrasa *et al*., 2018.

Bien qu'une part importante du carbone stocké dans les mattes des herbiers à *P. oceanica* soit issue majoritairement du C_{org} autochtone de la biomasse souterraine (*i.e*. rhizomes, racines et écailles), une grande partie de la séquestration résulte d'apports de C_{org} et C_{inorg} allochtone (Kennedy *et al*., 2010 ; Mazarrasa *et al*., 2015 ; Saderne *et al*., 2019). Le carbone allochtone enfoui dans ces écosystèmes côtiers réfère notamment au matériel ne provenant pas des tissus des Magnoliophytes marines et résultant essentiellement du dépôt de matières en suspension dans la colonne d'eau (*e.g.* carbone sestonique) (Kennedy *et al*., 2010) captées par la canopée de l'herbier (Gacia *et al*., 2002). Contrairement au C_{org} autochtone, issu des organes souterrains de l'herbier, le C_{org} allochtone provenant des macroalgues et du plancton est plus instable (Enriquez *et al*., 1993 ; Hendricks *et al*., 2008) et est susceptible d'être reminéralisé au début de la diagenèse (Henrichs, 1992 ; Laursen *et al*., 1996). Après son incorporation dans le compartiment sédimentaire, la reminéralisation du C_{org} allochtone est réduite contribuant ainsi à une part importante au carbone enfouie dans ces dépôts (en moyenne 50 % ; Kennedy *et al*., 2010). L'accumulation et la préservation de C_{org}

autochtone et allochtone après l'enfouissement dans les sédiments sont fortement contrôlés par l'accrétion du sédiment et la teneur en particules sédimentaires fines (*i.e.* limons et argiles ; Serrano *et al*., 2016b).

Ces paramètres sont fortement dépendants de la structure de la canopée des herbiers marins qui affecte le piégeage et la rétention des particules sédimentaires (De Falco *et al*., 2000 ; Gacia et Duarte, 2001 ; Peralta *et al*., 2008 ; Hendriks *et al*., 2010), de l'hydrodynamisme, de la disponibilité en particules fines dans la colonne d'eau, mais également la production de C_{inorg} (*i.e.* $CaCO_3$) au sein de l'herbier (De Falco *et al*., 2010 ; Mazarrasa *et al*., 2015). En effet, une densité plus importante des faisceaux, couplée à un faible hydrodynamisme et à une forte production de $CaCO_3$ contribue à une plus grande rétention des particules et à une accrétion significative des puits de carbone tel que la matte des herbiers à *P. oceanica* (Serrano *et al*., 2016b). De plus, comparé aux particules grossières (*i.e.* sables, graviers et galets), la présence de particules sédimentaires fines au sein des herbiers tend à limiter la reminéralisation de la matière organique en raison des faibles potentiels redox et de la diminution des échanges en oxygène (Hedges et Keil, 1995 ; Burdige, 2007 ; Pedersen *et al*., 2011).

La formation de puits organiques très riches en carbone résulte de l'accumulation dans les sédiments de 9 à 249 g C_{org} m^{-2} an^{-1} et de 47 à 138 g C_{inorg} m^{-2} an^{-1} (pour des hauteurs de mattes comprises entre 100 et 496 cm ; Romero *et al*., 1994 ; Mateo *et al*., 1997 ; Mateo *et al*., 2005 ; De Falco *et al*., 2008 ; Lo Iacono *et al*., 2008 ; Serrano *et al*., 2012, 2014, 2016b ; Mazarrasa *et al*., 2015). Le stock de C_{org} et C_{inorg} présent au sein de ces formations est ainsi estimé entre 30 et 176 kg C_{org} m^{-2} et 87 et 203 kg C_{inorg} m^{-2}, respectivement. L'accumulation et le stock de C_{org} et C_{inorg} présent au sein des mattes des herbiers à *P. oceanica* sont reconnus pour être parmi les plus importants des herbiers marins, mais également des écosystèmes marins et terrestres (Laffoley et Grimsditch, 2009 ; Mcleod *et al*., 2011 ; Serrano *et al*., 2012 et les références qui y sont citées). La première estimation globale des stocks de C_{org} séquestrés au sein des sédiments des herbiers marins a montré que les sédiments des herbiers à *P. oceanica* présentaient la plus grande capacité de stockage au monde (372 ± 74,5 t C_{org} ha^{-1}) (Fourqurean *et al*., 2012 ; Rozaimi, 2015).

Outre l'accumulation et la préservation du C_{org} et C_{inorg} sur de longues périodes de temps, les mattes des herbiers à *P. oceanica* constituent des réservoirs biogéochimiques (nutriments, éléments traces métalliques) et des archives biologiques uniques pour la reconstruction et l'étude des changements écologiques et climatiques passés en Méditerranée au cours de l'Holocène (Pergent et Pergent-Martini, 1999 ; Serrano *et al*., 2011 ; Mateo *et al*., 2010). L'accumulation et la conservation de matériaux hautement organiques associées au faible taux d'accrétion de ces dépôts offrent une cohérence chronostratigraphique très importante et une résolution temporelle exceptionnelle pour entreprendre des reconstructions paléoécologiques en Méditerranée (Mateo *et al*., 1997 ; Serrano *et al*., 2016a). Au cours des dernières décennies, plusieurs applications paléoécologiques ont permis de souligner l'importance des mattes comme archives pour entreprendre une reconstruction directe ou indirecte (i) de l'évolution de la végétation et des paysages littoraux, (ii) des activités anthropiques, (iii) des changements paléoclimatiques et (iv) de la productivité des herbiers au cours des derniers millénaires (López-Saéz *et al*., 2009 ; Mateo *et al*., 2010 ; Serrano *et al*., 2011, 2012, 2013 ; López-Merino *et al*., 2015, 2017 ; El Zrilli *et al*., 2017 ; Leiva-Dueñas *et al*., 2018). La préservation d'épaves ou encore de vestiges datés de l'époque romaine au sein de ces dépôts contribue aussi à souligner également leur rôle d'archive archéologique (Frost, 1969 ; Tchernia *et al*., 1978 ; Votruba *et al*., 2016). De manière similaire, les mattes participent au piégeage de restes fossiles carbonatés et siliceux provenant d'organismes marins ayant vécu au sein des herbiers à *P. oceanica* (Harmelin *et al*., 1964 ; Buia *et al*., 2000) mais aussi à la conservation de récifs biogéniques fossiles comme celui décrit par Boudouresque *et al.* (1980) en Corse.

1.4. Objectifs et structure de la thèse

Au cours de la dernière décennie, l'accent mis sur le marché du carbone[5] a intensifié l'intérêt de quantifier la capacité des écosystèmes à « Carbone Bleu » à séquestrer et stocker le carbone sur plusieurs milliers d'années (Alongi, 2018). L'estimation des stocks et des flux de carbone constitue la première approche visant à déterminer la contribution de ces écosystèmes à la réduction des émissions de GES et à l'atténuation du changement climatique. Ces inventaires des puits de carbone, encouragés par l'Accord de Paris (UNFCCC, 2016), offrent également le moyen de promouvoir leur conservation et leur restauration, mais également de les intégrer dans les processus décisionnels de création d'aires marines protégées (Adame *et al*., 2015 ; Herr *et al*., 2017).

Cependant, la capacité de séquestration et les stocks de carbone dans les sédiments de ces écosystèmes sont très variables notamment entre les différents herbiers marins, mais également au sein d'une même espèce (Lavery *et al*., 2013 ; Miyajima *et al*., 2015). Bien que des efforts conséquents aient été menés sur l'étude des facteurs favorisant ou inhibant la séquestration et la préservation du carbone au sein des sédiments des herbiers marins (*e.g.* Lavery *et al*., 2013 ; Ricart *et al*., 2015, 2017, 2020; Serrano *et al*., 2014, 2016b ; Mazarrasa *et al*., 2017, 2018), les estimations mondiales ou régionales menées au cours des dernières décennies reposent sur la prise en compte d'un nombre très limité de données (Fourqurean *et al*., 2012 ; Alongi, 2018). L'une des principales limitations rencontrées lors de la production de ces inventaires est l'estimation de la superficie couverte par les herbiers de Magnoliophytes marines (extension spatiale) mais surtout l'épaisseur et le volume occupés par les sédiments sous-jacents constituant ces puits de carbone (Pergent *et al*., 2012 ; Howard *et al*., 2014a).

[5] Système permettant l'échange de quotas d'émissions de GES visant à inciter les pays à réduire leurs émissions ou à investir dans des technologies plus propres afin de lutter contre le changement climatique.
Plus d'informations sur https://youtu.be/pH9BYRqbofk.

Dans ce contexte, les objectifs globaux de cette thèse de doctorat étaient les suivants :

- Développer une méthodologie pour l'acquisition de données terrains nécessaires à la cartographie des habitats benthiques côtiers et marins et notamment ceux impliqués dans l'atténuation du changement climatique (*e.g.* herbiers à *P. oceanica*) ➔ Optimisation des outils cartographiques pour préciser l'extension spatiale des écosystèmes à carbone bleu

- Développer une méthodologie visant à estimer la vitesse de l'onde acoustique dans la matte des herbiers à *P. oceanica* afin de calibrer les données de sismique-réflexion haute-résolution ➔ Optimisation des outils (intercalibration, validation *in situ*) permettant d'estimer l'épaisseur de la matte

- Réaliser une vaste estimation des épaisseurs et volumes occupés par les mattes sur la côte orientale de la Corse (zone Natura 2000 « FR9402014 - Grand Herbier de la Côte orientale ») ➔ Mise en application des outils précédents pour estimer le volume des mattes de *P. oceanica* sur un site atelier

- Quantifier les stocks et flux de carbone des mattes présentes au sein de ce site d'étude et caractériser la dynamique spatio-temporelle de ces puits de carbone ➔ Estimation des stocks de carbone et de leur variabilité spatio-temporelle dans ce site atelier

- Souligner le rôle des mattes comme archive pour la reconstruction et l'étude des changements écologiques et climatiques passés sur le littoral de la Corse ➔ Valider le rôle d'archive biologique de ces mattes à partir d'un exemple de paléo-construction (banc de *Cladocora caespitosa*).

Ce manuscrit est structuré en **7 chapitres** dont les objectifs sont les suivants :

Chapitre 1 : Réaliser une présentation synthétique du contexte climatique, du rôle des écosystèmes côtiers dans le cycle du carbone océanique ainsi que dans l'atténuation du changement climatique et notamment des mattes des herbiers à *P. oceanica* comme puits biogéochimiques et comme archive paléo-environnementale.

Chapitre 2 : Mettre en place une méthodologie innovante pour acquérir des données terrains en continu afin de calibrer et interpréter les données acoustiques et s'affranchir de la bande aveugle des sonogrammes en se basant sur l'utilisation simultanée d'une caméra sous-marine et d'un sonar à balayage latéral.

Chapitre 3 : Développer une méthodologie innovante basée sur l'intercalibration de données sismiques, acoustiques, optiques et de terrain pour estimer la vitesse de l'onde acoustique dans la matte (donnée nécessaire à la calibration des données de sismique réflexion). Ce chapitre a également pour objectif de s'intéresser à l'étude des relations entre la vitesse de l'onde acoustique dans la matte et les propriétés biogéophysiques.

Chapitre 4 : Utiliser la sismique réflexion haute résolution pour entreprendre une vaste estimation des épaisseurs et volumes occupés par la matte sur le site d'étude et étudier la dynamique spatio-temporelle de ces puits en fonction des conditions environnementales.

Chapitre 5 : Réaliser un inventaire des stocks et flux de carbone organique et inorganique présents au sein des matte des herbiers à *Posidonia oceanica* de notre site d'étude et étudier l'influence de plusieurs paramètres environnementaux sur ce puits de carbone.

Chapitre 6 : Utiliser la matte comme archive pour reconstruire la dynamique temporelle d'un banc de *Cladocora caespitosa* découvert au sein du site d'étude.

Chapitre 7 : Réaliser une synthèse et une discussion générale visant à souligner l'implication de ces travaux de thèse et ouvrir les perspectives de travail à l'échelon régional.

Thèse : Quantification et dynamique spatio-temporelle des puits de carbone associés aux herbiers à *Posidonia oceanica*

Chapitre 1

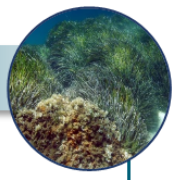

Changement climatique et les écosystèmes à carbone bleu : le rôle particulier de *Posidonia oceanica* dans la séquestration et le stockage du carbone.

Chapitre 2

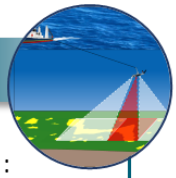

Optimisation des méthodes de cartographie des habitats marins : acquisition continue de données terrain.

Chapitre 3

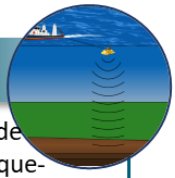

Développement d'une méthode de calibration des données de sismique-réflexion acquises au sein de la matte.

Objectifs : Optimisation des méthodes d'investigations pour estimer l'extension horizontale (spatiale) et verticale (épaisseur) des puits de carbone côtier.

Chapitre 4

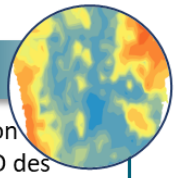

Utilisation de la sismique-réflexion pour réaliser une cartographie 3D des herbiers à *P. oceanica* du site d'étude

Chapitre 5

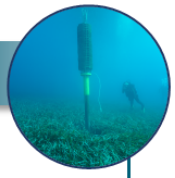

Caractérisation de la matte et analyses biogéochimiques pour déterminer les stocks et flux de carbone.

Objectifs : Estimation de l'épaisseur et du volume des mattes des herbiers à *P. oceanica,* évaluation des stocks et flux de carbone au sein de ces puits et étude de leur dynamique spatio-temporelle.

Chapitre 6

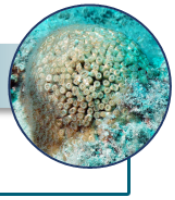

Reconstruction paléo-écologique et étude de la dynamique temporelle d'un banc de *Cladocora caespitosa* enfouie dans la matte au sein du site d'étude.

Objectifs : Valider le rôle des mattes des herbiers à *P. oceanica* comme archive biologique pour étudier les changements environnementaux et climatiques durant l'Holocène.

Liste des articles scientifiques publiés et soumis dans des revues

Chapitre 2 : Pergent, G., Monnier, B., Clabaut, C., Gascon, G., Pergent-Martini, C., Valette-Sansevin, A. (*Publié en 2017*). Innovative method for optimizing Side-Scan Sonar mapping: The blind band unveiled. Estuarine, Coastal and Shelf Science 194, 77-83. https://doi.org/10.1016/j.ecss.2017.05.016.

Chapitre 3 : Monnier, B., Pergent, G., Mateo, M.Á., Clabaut, P., Pergent-Martini, C. (*Publié en 2020*). Seismic interval velocity in the matte of *Posidonia oceanica* meadows: Towards a non-destructive approach for large-scale assessment of blue carbon stock. Marine Environmental Research 161, 105085. https://doi.org/10.1016/j.marenvres.2020.105085.

Chapitre 4 : Monnier, B., Pergent, G., Mateo, M.Á., Clabaut, P., Pergent-Martini, C. (*Soumis en 2020 dans la revue Science of the Total Environment*). Sizing the carbon sink associated with *Posidonia oceanica* seagrass meadows using very high-resolution seismic reflection.

Chapitre 5 : Monnier, B., Pergent, G., Valette-Sansevin, A., Boudouresque, C.F., Mateo, M.Á., Pergent-Martini, C. (*Soumis en 2020 dans la revue Vie & Milieu*). The *Posidonia oceanica* matte: a unique carbon sink for climate change mitigation - Preliminary results and implications for management.

Chapitre 6 : Monnier, B., Lehmann, L., Sartoretto, S., Pergent-Martini, C., Mateo, M.Á., Pergent, G. (*Soumis en 2020 dans la revue Estuarine, Coastal and Shelf Science*). Long-term dynamics of a *Cladocora caespitosa* bank as recorded by a *Posidonia oceanica* millenary archive.

Chapitre 2

© Pergent G.

Innovative method for optimizing Side-Scan Sonar mapping: The blind band unveiled

Abstract

Over the past few years, the mapping of Mediterranean marine habitats has become a priority for scientists, environment managers and stakeholders, in particular in order to comply with European directives (Water Framework Directive and Marine Strategy Framework Directive) and to implement legislation to ensure their conservation. Side-scan sonar (SSS) is recognized as one of the most effective tool for underwater mapping. However, interpretation of acoustic data (sonograms) requires extensive field calibration and the ground-truthing process remains essential. Several techniques are commonly used, with sampling methods involving grabs, scuba diving observations or Remotely Operated Vehicle (ROV) underwater video recordings. All these techniques are time consuming, expensive and only provide sporadic informations. In the present study, the possibility of coupling a camera with a SSS and acquiring underwater videos in a continuous way has been tested. During the 'PosidCorse' oceanographic survey carried out along the eastern coast of Corsica, optical and acoustic data were respectively obtained using a GoPro™ camera and a Klein 3000™ SSS. Thereby, five profiles were performed between 10 and 50 m depth, corresponding to more than 20 km of data acquisition. The vertical images recorded with the camera fixed under the SSS and positioned facing downwards provided photo mosaics of very good quality corresponding to the entire sonograms's blind band. From the photo mosaics, 94% of the different bottom types and main habitats have been identified; specific structures linked to hydrodynamics conditions, anthropic and biological activities have also been observed as well as the substrate on which the *Posidonia oceanica* meadow grows. The association between acoustic data and underwater videos has proved to be a non-destructive and cost-effective method for ground-truthing in marine habitats mapping. Nevertheless, in order to optimize the results over the next surveys, certain limitations will need to be remedied.

2.1. Introduction

Loss of marine coastal habitats (seagrass meadows, coral reefs, coralligenous assemblages) has been reported in many regions of the biosphere (Waycott *et al*., 2009; De'ath *et al*., 2012; Ponti *et al*., 2014). In the Mediterranean Sea, loss of seagrass meadows is mainly due to coastal development, trawling, eutrophication, competition with invasive species and sea level rise (Boudouresque *et al*., 2009; Pergent *et al*., 2015). The mapping of coastal benthic communities is a priority for marine environment managers, in particular for the purpose of assessing the extent of these changes and implementing management policy for the conservation of these key habitats (Gilman, 2002; Mapping European Seabed Habitats MESH, 2008; Cogan *et al*., 2009; UNEP-MAP-RAC/SPA, 2009; Lopez y Royo *et al*., 2010). It makes a fundamental contribution to environmental characterization and may therefore be considered as the key management tool (Bianchi, 2008).

Most underwater mapping methods generally use optical sensors (satellite images, aerial photographs) for shallow depths (down to 15 m) and acoustic sensors (side-scan sonar and multibeam echosounder) in deeper waters (Godet *et al*., 2009; Vela *et al*., 2008; Brown *et al*., 2011; Bonacorsi *et al*., 2013). Whatever the type of sensor used, remote-sensing systems require field data (ground truthing process; Elefteriou and McIntyre, 2005; Anderson, 2007; Coggan *et al*., 2007; Van Rein *et al*., 2009; Brown *et al*., 2011) to validate information provided by these devices (spectral response, sonograms). The acquisition of field data is often long and expensive, and the methods chosen vary according to the range and depth of the area under investigation (Kenny *et al*., 2003; UNEP-MAP-RAC/SPA, 2011; Bonacorsi *et al*., 2013). For shallow water (0 to -10 m), direct observation, on a small boat, from the surface, using a bathyscope combined with a GPS, is very rapid and accurate both in terms of identification of biocenoses and location (Vela *et al*., 2008). For intermediate depths (-10 to -40 m), scuba diving is often used, but the amount of data acquired per time unit is reduced and the acquisition cost is much greater; furthermore, the accuracy in terms of location more limited (Leriche *et al*., 2006; Holon *et al*., 2015). At depths below 50 m, two techniques are commonly used: blind samples with grabs or cores - very effective for soft bottoms - and direct observation using a wide range of tools (Remotely Operated Vehicles (ROVs), underwater video cameras, submarines, etc.), that suit all substrates and habitats without being

destructive. The images are usually produced by towed video cameras (Lefebvre *et al*., 2009; Ierodiaconou *et al*., 2011), ROVs (Micallef *et al*., 2012; Ludvigsen *et al*., 2007, 2014), Unmanned Surface Vehicles - USVs (Fumagalli *et al*., 2014) or Autonomous Underwater Vehicles - AUVs (Norgren and Skjetne, 2014, 2015).

Over the past few years, underwater video images have been more and more widely used to calibrate optical sensors, side-scan sonar and multibeam echosounder data (Smith *et al*., 2007, 2015; Lefebvre *et al*., 2009). However, ground-truthing data corresponds to sporadic information concerning only a small proportion of the seafloor (points or transects), while sensors provide broad surface area data (images, sonograms). Even if the amount of field data is considerable, it is often difficult to calibrate all the spectral responses of an image (which varies with depth for the same habitat) or the textures of a sonogram. Therefore, these methods involve a high degree of interpolation for mapping interpretation and production. The aim of this work is to test the possibility of acquiring field data in a continuous way when using a side-scan sonar in order to facilitate the mapping interpretation phase.

2.2. Material and methods

The studied site is located along the eastern coast of Corsica (Natura 2000 site “Grand Herbier de la Côte Orientale”), between 10 and 50 m depth. Acoustic data were collected during the PosidCorse survey conducted during summer 2015, aboard the Ifremer vessel, N/O L'Europe. Two complementary types of equipment were used:

- a side-scan sonar (Klein 3000™), providing acoustic data (sonograms) for the seabed (texture, grey color);

- a GoPro™ camera (HD Hero3 Black Edition) with a Subspace Picture™ underwater housing fixed under the side-scan sonar (Fig. 2.1).

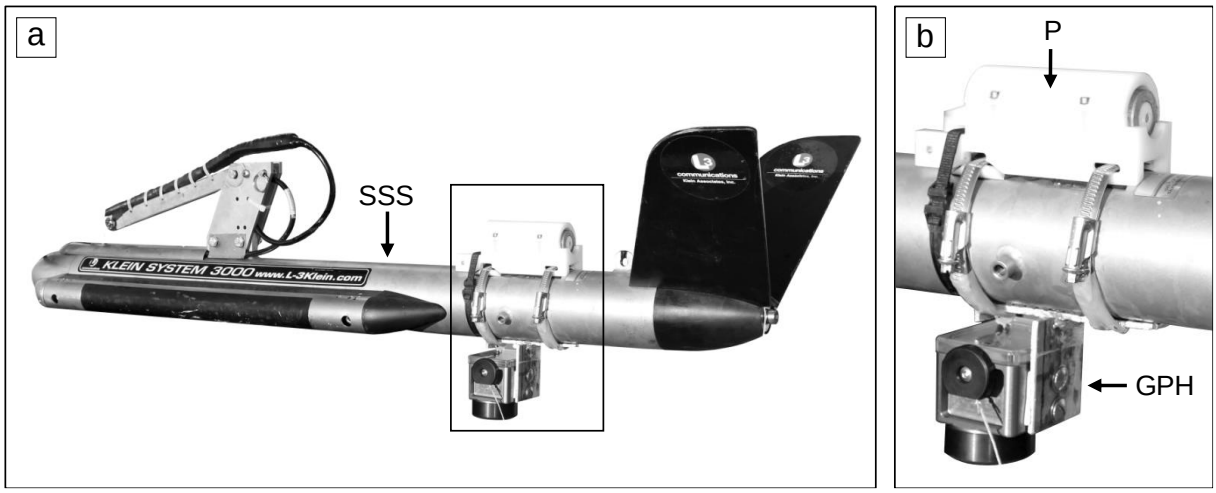

Figure 2.1. (a) Klein 3000 TM side-scan sonar (SSS) and (b) the pinger (P) with the GoPro™ camera in its housing (GPH) fixed on the towfish.

The GoPro™ camera was positioned face down to record vertical images under the side-scan sonar corresponding to the blind band (Fig. 2.2). Five profiles were performed, between 10 and 50 m depth, corresponding to more than 20 km of data acquisition with a side scan sonar range between 25 and 50 m (Table 2.1).

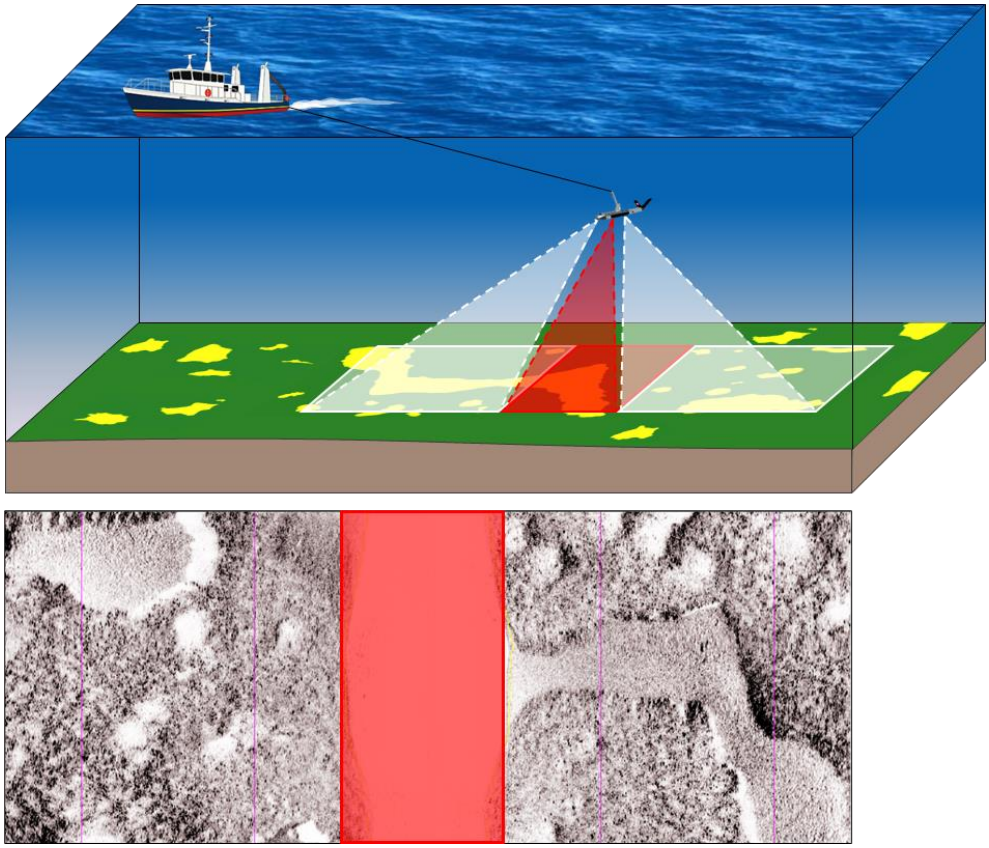

Figure 2.2. Data recorded by the two devices, GoPro™ camera in the central part (red band) and side-scan sonar on either side (white bands).

The speed of the vessel varied from 4.5 to 6.0 km h^{-1}. Different resolutions of GoPro™ camera and numbers of frame per second were tested as well as the distance between the camera and the bottom. One field of view (Medium) is used (127°). Several habitats and bottom types were investigated (*Cymodocea nodosa* beds, *Posidonia oceanica* meadows, photophilous algae, beach rocks, sandy and rocky bottom).

Table 2.1. Characteristics of transects using the GoPro™ camera and Klein 3000 side-scan sonar. fps= frame per second.

Transect	Length (m)	Time duration (min)	Bottom depth (m)	Sonar range (m)	Tow elevation (m)	GoPro resolution (pixels)	Frames (fps)
L3-102	1700	20	10 - 12	25	2.5 - 3.3	1920 × 1080	60
L3-110	1600	21	10 - 16	25	2.5 - 4.9	1920 × 1080	60
L3-128	2800	29	20 - 45	25	2.5 - 4.0	1920 × 1080	60
L4-152	8100	84	10 - 50	25	2.5 - 2.8	2048 × 1536	30
L4-166	6200	68	10 - 20	50	3.9 - 5.4	1920 × 1080	60

The videos acquired using GoPro™ camera were imported in the software Microsoft© Image Composite Editor (ICE) version 2.0.3.0, to create a high-quality panoramic image mosaic corresponding to the ground covered by the blind band. Import step options allow selection of an interval of the original video to optimize the time process and for define the photo mosaic length. ICE software autodetect mode analyzes the video, extracts images on the focal plane at a given moment, stitches the images to one another and finally composes a first photo mosaic very quickly and simply.

2.3. Results

GoPro™ camera images allow good discrimination of the different bottom types and main habitats, even if the results are less satisfactory in the deeper part (Table 2.2). It is also possible to clearly identify specific structures related to water movement (ripple marks, intermattes, accumulation of *Posidonia* dead leaves) (Fig. 2.3.a; Fig. 2.3.b) to anthropic activity (waste, boat hull, plastic bag, etc.), and also to biological activity (bioturbation of the sediment such as burrows) (Fig. 2.3.c). A large number of burrows are observed, mainly associated with

Cymodocea nodosa beds; they seem to correspond to the activity of the decapod crustaceans, such as *Pestarella tyrrhena* Petagna 1792 and *Upogebia pusilla* Petagna 1792.

Table 2.2. Percentage of bottom types and main habitats identified along GoPro transects.

Habitats and bottom types	Transect				
	L3-102	**L3-110**	**L3-128**	**L4-152**	**L4-166**
Cymodocea nodosa	38.0%			5.0%	
Posidonia oceanica		79.2%	30.7%	45.3%	96.4%
Dead matte				6.7%	1.1%
Soft bottom	62.0%	13.8%	12.5%	10.6%	2.5%
Rocky bottom		7.0%		0.3%	
Pebbles				0.5%	
Rhodolith beds			34.4%	24.8%	
Undefined habitats			22.4%	6.8%	

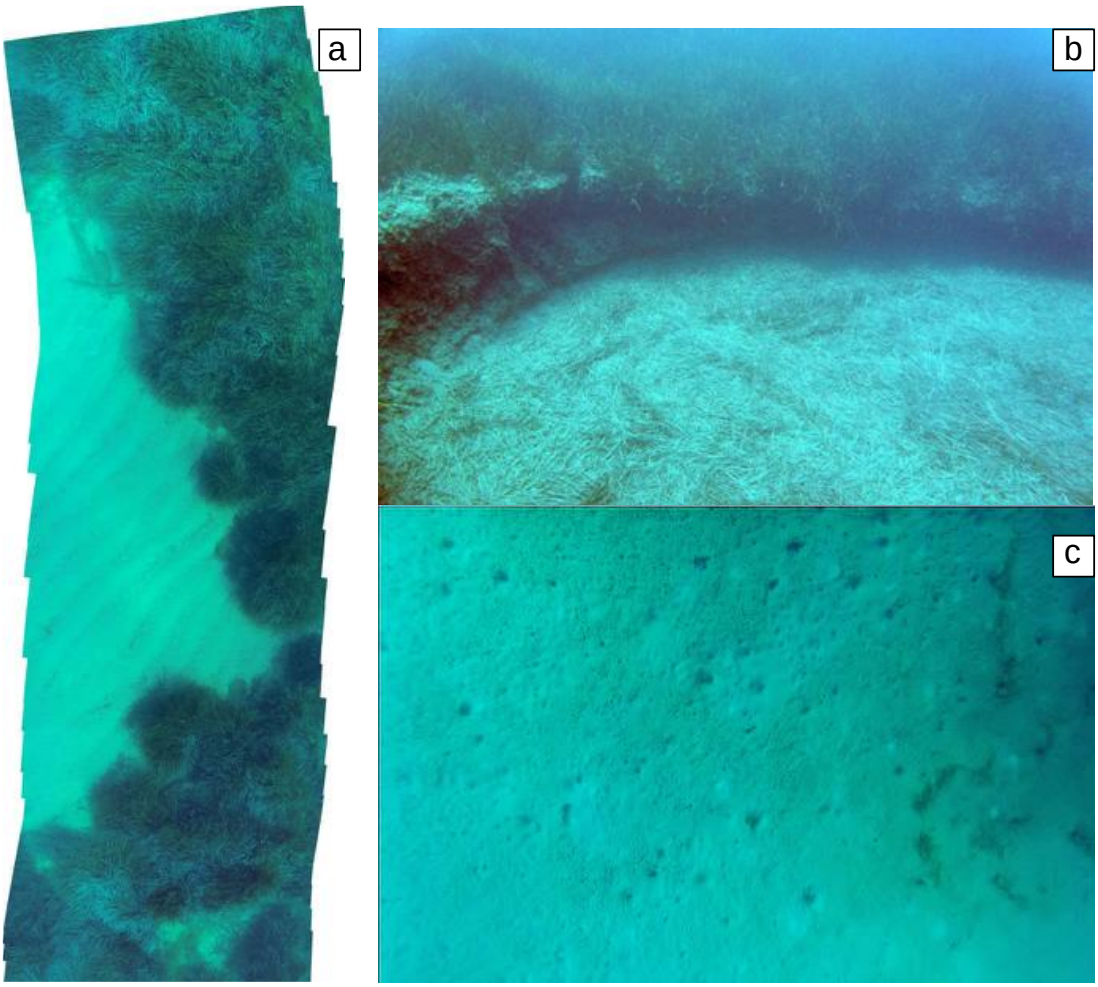

Figure 2.3. (a) Photo mosaic made by Microsoft© ICE, a part of the transect L3-1101 showing *P. oceanica* meadow and soft bottom with ripple marks, (b) accumulation of *P. oceanica* dead leaves in an intermatte and (c) and crustacean burrows in *C. nodosa* beds.

On the other hand, in some cases the substrate on which the *P. oceanica* meadow grows (soft bottom and/or matte and rocky bottom) appears clearly on the images from the GoPro™ camera; this information, not always provided by sonograms, is of great help for the interpretation of acoustic data (Fig. 2.4.a; Fig. 2.4.b). In the Natura 2000 zone, seagrass settled on rocky substrate is rarely a continuous habitat in this region and represents small areas which are confirmed by the videos.

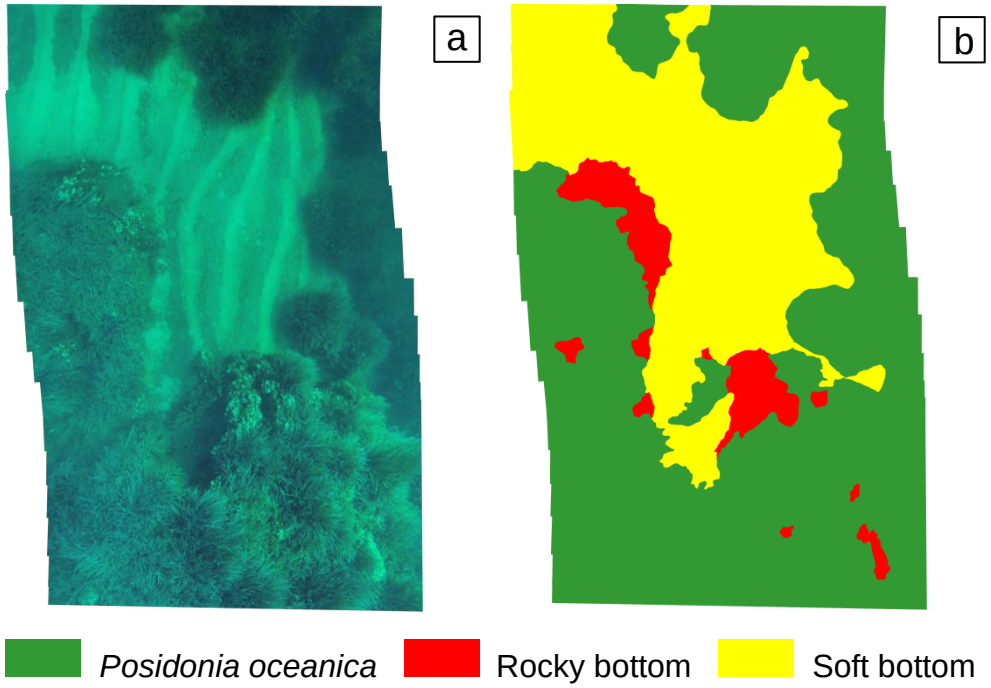

Figure 2.4. (a) Photo mosaic of *Posidonia oceanica* on rocky and soft bottom and (b) the mapping interpretation (b).

Thus, the association between acoustic data (sonograms) and images from the camera provides a wide range of information as a basis for underwater mapping, (i) It allows accurate validation (calibration) of acoustic data and precise identification of the bottom type and/or corresponding habitat (Fig. 2.3.a; Fig. 2.3.b; Fig. 2.3.c), (ii) it provides an indication concerning the nature of the substrate (Fig. 2.4.a; Fig. 2.4.b) and also (iii) provides information on the 'blind band' not sampled by the side-scan sonar. This last feature mitigates subjective interpolation. This method offers the means to map more accurately the location of the boundaries of these habitats, on each side of the blind band (Fig. 2.5.a), and also to detect small structures only present in this band (Fig. 2.5.b).

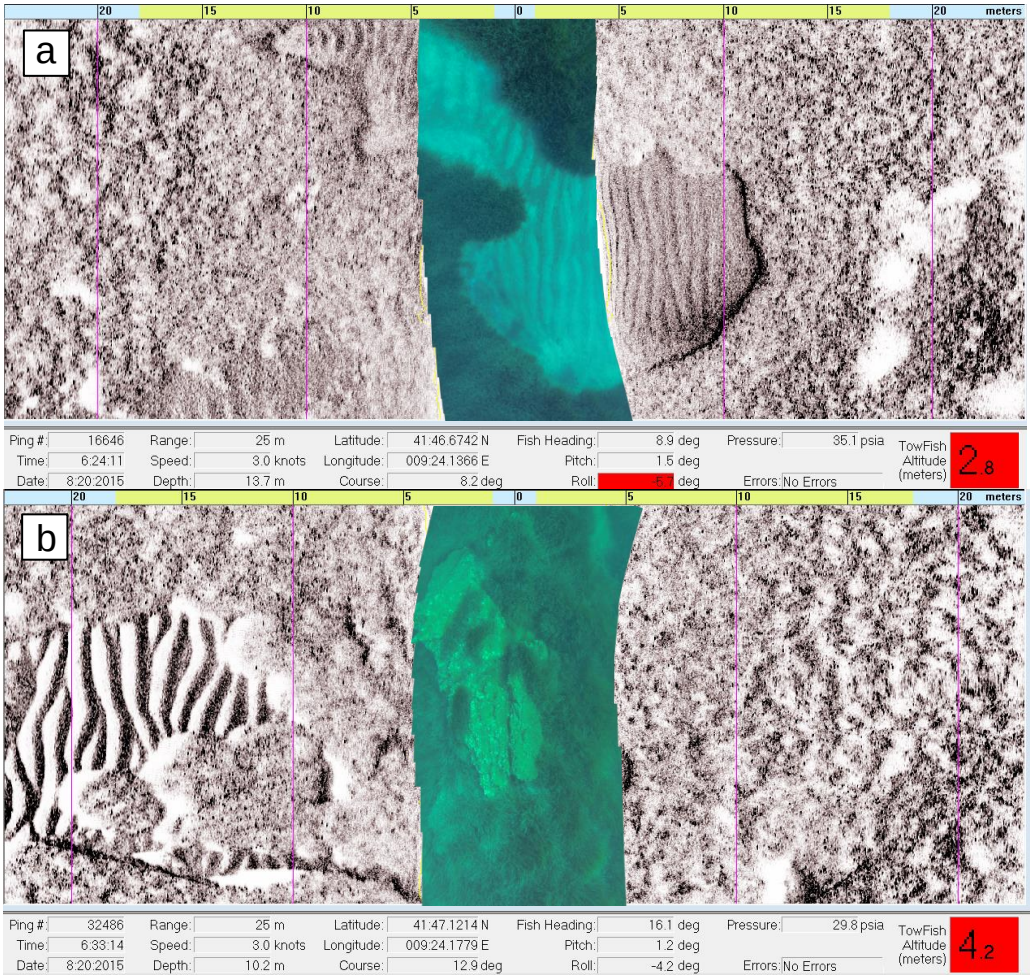

Figure 2.5. (a) Association between acoustic data (sonograms) and photo mosaic from GoPro camera: limit of sand with ripple mark and (b) rock with meadow on both sides.

2.4. Discussion

The use of acoustic sensors provides a wide range of information regarding the characterization of the seabed (bathymetry, assemblages and types of bottom). However, these data, and in particular those relative to the nature of the seabed, require validation and calibration before being used as a basis for precision mapping. For the side-scan sonar data, this validation calls for extensive experience and is based on reference sonar images for the identification of spectral signatures and characteristic textures (*e.g.* sonogram atlas; Clabaut *et al.*, 2007; Clabaut and Augris, 2014). Nevertheless, the acquisition of ground-truthing remains essential to confirm these interpretations (MESH, 2008); these data are acquired either in the course of the oceanographic survey, requiring the interruption of the data acquisition by the side-scan sonar (Bonacorsi *et al.*, 2012; 2013), or after the survey, which

means the repeated use of seagoing research facilities and a very accurate positioning system in order to be able to revisit the points to be verified (Andromède Océanologie et Stareso, 2012; Pasqualini *et al*., 2000). These operations represent a significant additional cost.

For the past few years, the use of underwater cameras has become increasingly frequent, as (i) they enable good discrimination of assemblages and species (Rooper, 2008; van Overmeeren *et al*., 2009; Hamilton *et al*., 2011; Pelletier *et al*., 2011; Bonacorsi *et al*., 2012; Chabanet *et al*., 2012; Sañé *et al*., 2016), (ii) they provide raw data banks which can be stored and reinterpreted for the purposes of monitoring over time (Barker *et al*., 1999; Lam *et al*., 2006; Lirman *et al*., 2007; Tyne *et al*., 2010; Pelletier *et al*., 2012) and (iii) they result in no degradation of the environment, in contrast to commonly used sampling methods (grab, dredge, etc.). In the present study, the coupling of a GoPro™ type camera and a side-scan sonar has therefore been tested for the purpose of validating the acoustic data for the mapping of the main habitats and bottom types occurring between 10 and 50 m depth.

This technique has made possible the continuous calibration, in real time, of sonograms with more than 94% identification of habitats and bottom types present (Table 2). It has also provided the means to determine the nature of the substrate on which the habitats have developed (*e.g*. *Posidonia oceanica* meadow) and to reveal specific structures related to water movement, anthropic and biological activities (Fig. 2.3.a; Fig. 2.3.c). In addition, for the first time, the blind band, situated beneath the sonar, has been properly surveyed (Fig. 2.5.a; Fig. 2.5.a), whereas the only techniques available hitherto consisted in using specific algorithms during the processing of the sonograms or carrying out manual interpolation.

Like the images and video footage captured by many towed systems (Rooper, 2008; Rende *et al*., 2015), the optical recordings acquired in the course of this study were very little exposed to the effects of pitching and rolling. The fins with which side-scan sonars are equipped provide effective stabilization and guarantee good image quality. The small-sized, light-weight camera housing fixed at the rear of the side-scan sonar causes no hydrodynamic turbulence or effect on the movement. The videos acquired at speeds of between 4.5 and 6 km h^{-1} provide photo mosaics of very good quality for videos of 60 fps, even if occasional distortion and blurring may be observed.

During the realization of photo mosaics with the Microsoft ICE software, the use of the time lapse mode of the GoPro™ camera with an acquisition frequency of 0.5 fps gives highly satisfactory results and avoids the problem of blurring due to the high coverage of seagrass meadow and the movement of the leaves ('canopy effect') and facilitates the stage of stitching up the different photographs (Rende *et al*., 2015).

In order to optimize the results obtained and to enable the wider application of this technique in underwater mapping, certain limitations need to be remedied. The battery life, limited to 2 h, will need to be extended to avoid having to repeatedly bring the sonar back on board. Furthermore, the sensitivity of the camera today constitutes a significant obstacle which limits the depth of acquisition to 50 m (in the Mediterranean and another areas with low turbidity) and imposes a limited height of the towfish above the bottom (2-5 m), and thus limits the range of the sonar to 50 m. Nevertheless, the high sensitivity of this type of camera is constantly being improved; today, it is 6400 ISO and should progress even further.

In addition, the use of a wider field of view (170°) is worth testing, even if greater distortion is to be expected at the edges of the image. These distortions can in fact be remedied by calibration and correction procedures (Bouguet, 2010 *in* Rende *et al*., 2015). The installation of powerful light sources to increase the depth and the height above the bottom of the photograph acquisition, by means of remotely controlled underwater systems, has also been envisaged for greater depths (Ludvigsen *et al*., 2007). However, in view of the bulkiness of this type of equipment, its use on side-scan sonar seems difficult to envisage for the moment.

Chapitre 3

Seismic interval velocity in the matte of *Posidonia oceanica* meadows: towards a non-destructive approach for large-scale assessment of blue carbon stock

Abstract

High-resolution seismic reflection data have been used over the last decades to estimate the thickness of the long-term Blue Carbon sink associated to the below-ground sediment deposit (matte) of the *Posidonia oceanica* meadows. Time-to-depth conversion of these geophysical datasets was usually performed assuming a sound velocity in this structure, but appropriate seismic interval velocity measurements is necessary to achieve accurate calibration. This study describes the first methodology to estimate the seismic interval velocity in the matte. This approach performed on the eastern continental shelf of Corsica island (France, NW Mediterranean) is based on measurements of the vertical matte profile from high-resolution seismic reflection profiles (s TWTT) and from seafloor morpho-bathymetric DTM (multibeam echosounders - MBES and Light Detection and Ranging - LiDAR surveys) calibrated with ground-truthing data. A biogeosedimentological analysis of horizontal cores sampled in vertical matte escarpments has been undertaken to identify the potential relationship of sediment and environmental parameters with sound velocity. The cross-comparison and the data intercalibration show significant correlation of MBES (R^2 = 0.872) and LiDAR datasets (R^2 = 0.883) with direct underwater measurements. Seismic interval velocities (n = 367) have been found to range between 1631.9 and 1696.8 m s^{-1} (95% confidence interval) and are estimated on average at 1664.4 m s^{-1}, which is similar to the literature for unconsolidated marine sediments. The prediction map provided by the ordinary kriging method emphasized, however, a high variability of sound velocity within the study area. The results showed that changes in sound velocity in the matte are positively and strongly correlated with sand and gravel content and environmental factors such as distance to coastal river mouths and coastline. However, it was found that a negative relationship linked sound velocity with total and coarse organic content of matte deposits.

3.1. Introduction

Coastal marine vegetation has been recently highlighted for its highly efficient carbon storage capacity (McLeod *et al*., 2011; Duarte *et al*., 2013). These habitats, in particular mangroves, salt marshes, and seagrass meadows, play a significant role in climate change mitigation due to their contribution to long-term carbon sequestration (Nelleman *et al*., 2009; Laffoley and Grimsditch, 2009). The high primary production associated with their exceptionally high burial rates provide large organic carbon (C_{org}) stocks comparable to other main terrestrial carbon sinks (McLeod *et al*., 2011). Seagrass meadows occur in a variety of marine environments (Carruthers *et al*., 2007) and cover less than 0.2% of the world's ocean surface (Short *et al*., 2016). The overall estimates of C_{org} stock in the first metre seagrass meadow soils range between 4.2 to 8.4 Pg C (Fourqurean *et al*., 2012), while their C accumulation rates range from 48 Tg C yr^{-1} to 112 Tg C yr^{-1}, representing almost 10-18% of the total carbon burial in the ocean (Kennedy *et al*., 2010; Duarte *et al*., 2013).

In the Mediterranean Sea, the endemic seagrass *Posidonia oceanica* (Linnaeus) Delile forms extensive meadows considered as a unique C_{org} sink due to the development of an outstanding terraced structure known as "matte" (Molinier and Picard, 1952). This complex belowground formation, composed of intertwined rhizomes, roots and leaf sheaths, exhibits a very low decay rate in relation with the highly refractory nature of the organic matter and the anoxic conditions (Klap *et al*., 2000; Romero *et al*., 1992; Mateo *et al*., 1997, 2006). The accretion of organic-rich material in coastal sediments beneath the *P. oceanica* meadows constitutes massive C_{org} stock ranging from 40 to 770 kg C_{org} m^{-2} and builds matte deposits up to 14-meters thick preserved over time spans from decades to millennia (Miković, 1977 *in* Varda, 2015; Boudouresque *et al*., 1980; Romero *et al*., 1994; Mateo *et al*., 1997, 2006; Lo Iacono *et al*., 2008; Serrano *et al*., 2012, 2014). However, estimates of carbon stocks beneath *P. oceanica* seagrass meadows are directly based on the analysis of a few matte cores at a very limited number of sites over the Mediterranean basin. These works have emphasized the necessity (i) increasing the number of direct measurements in seagrass sediments, and (ii) providing extensive measurements of estimated *P. oceanica* mattes thickness along the Mediterranean coast (Pergent *et al*., 2012).

Very few of the studies reported are directly focused on the assessment of the thickness, volume and spatial distribution of the matte to establish clear and robust regional estimates of carbon stocks (Lo Iacono *et al*., 2008). The assessment of matte thickness is typically approximated by core sampling or manual sounding but also by direct field observations from erosional matte escarpments referred to as "matte walls" (Mateo *et al*., 1997; Lo Iacono *et al*., 2008; Serrano *et al*., 2012; 2014; 2016a). During the last few years, other investigative methods, such as very high-resolution seismic reflection prospection, have been successfully applied at local scale (Lo Iacono *et al*., 2008; Tomasello *et al*., 2009; Blouet *et al*., 2010). The very high-resolution seismic reflection method offers the means to delineate the near-surface geological structures and to characterize the stratigraphy of soils layers (Yilmaz, 2001).

The structural seismic interpretation requires a time-to-depth strategy consisting in the conversion of data from travel time boundaries (in the time domain) to depths (in the space domain) (Assaad *et al*., 2013). While travel times are measured, the one parameter that most affects the conversion to depth is seismic velocity (Reynolds, 2011). The time-to-depth process of a specific lithological layer is performed using interval velocity (*i.e.* compressional-wave, *P*-wave or sound velocity) defined as the average velocity between two reflectors (Yilmaz, 2001). In underwater acoustical, geophysical and marine geological studies, calibration of seismic data is usually done by assuming a sound velocity in the superficial unconsolidated marine sediments, generally agreed to be near 1500 m s^{-1} (Hamilton, 1963, 1969, 1970; Hicks and Kibblewhite, 1976; Bourbié *et al*., 1986; Turgut and Yamamoto, 1990). Nevertheless, due to the complexity of the structure of seabed sediments, the sound velocity is not a constant value. The interval velocity of the seismic wave in a stratigraphic sequence is mainly influenced by several factors: lithology, porosity, density, fluid saturation, compaction, temperature, evolution and geological age (Hamilton and Bachman, 1982, Cordier, 1985; Yilmaz, 2001; Upadhyay, 2004). A calibration of data by drilling or coring has proved to be essential to ensure the quality characterization of the stratigraphic sequence (*i.e.* depth and thickness) and to improve seismic interval velocity calculation (Cordier, 1985; Bitri *et al*., 1996; Yilmaz, 2001; Onajite, 2014).

The main aims of this study are (i) to determine the seismic interval velocity in the *P. oceanica* matte based on very high-resolution seismic reflection and calibration from multibeam echosounders (MBES), Light Detection and Ranging (LiDAR) and ground-truthing data, and (ii) to evaluate the relationship between variation of seismic interval velocity and the biogeosedimentological parameters of the matte.

3.2. Material and methods

3.2.1. Study site

This study was conducted in the Natura 2000 area, FR9402014 - Grand Herbier de la Côte Orientale, on the eastern coast of Corsica Island (France, NW Mediterranean Sea). The site stretches along 106 km of sandy coast between the mouth of the Biguglia lagoon in the north and the mouth of the Solenzara river in the south (Meinesz *et al*., 1990; Fig. 3.1). This site hosts one of the largest *P. oceanica* meadows in the Mediterranean Sea, covering a surface area of 20425 ha (Valette-Sansevin *et al*., 2019). This continuous meadow is mainly settled on sandy substrate and has several landscape discontinuities naturally generated by hydrodynamics or by anthropic activities, designated by the term 'intermattes' (Blanc and Jeudy De Grissac, 1984; Abadie *et al*., 2015).

3.2.2. Data acquisition and methodology

The present study is based on the integration of different datasets, high-resolution seismic reflection, morpho-bathymetric (MBES and LiDAR) and ground-truthing data (Fig. 3.2). These datasets were mainly collected during three oceanographic cruises, Halgolo (2010), CoralCorse (2013) and PosidCorse (2015) aboard the oceanographic and research vessels 'L'Europe' and 'L'Haliotis' (Ifremer).

The high-resolution seismic reflection profiles were obtained using two sub-bottom profilers (SBP) with distinct emission frequencies : the EDO-Western ED 248 (2.5 kHz) and the Chirp 'Pesk Avel' (3.5 kHz) developed by Ifremer. Seismic data acquisition was performed using the SUBOP® software (SUb-BOttom Profiler, Ifremer) at a vessel speed of 4 knots (7.5 km h^{-1}).

Seismic data provided an average vertical record of approximately 20-40 m below the seafloor. These oceanographic surveys provided almost 3 095 km of 2D seismic profiles between 10 and 50 m depth.

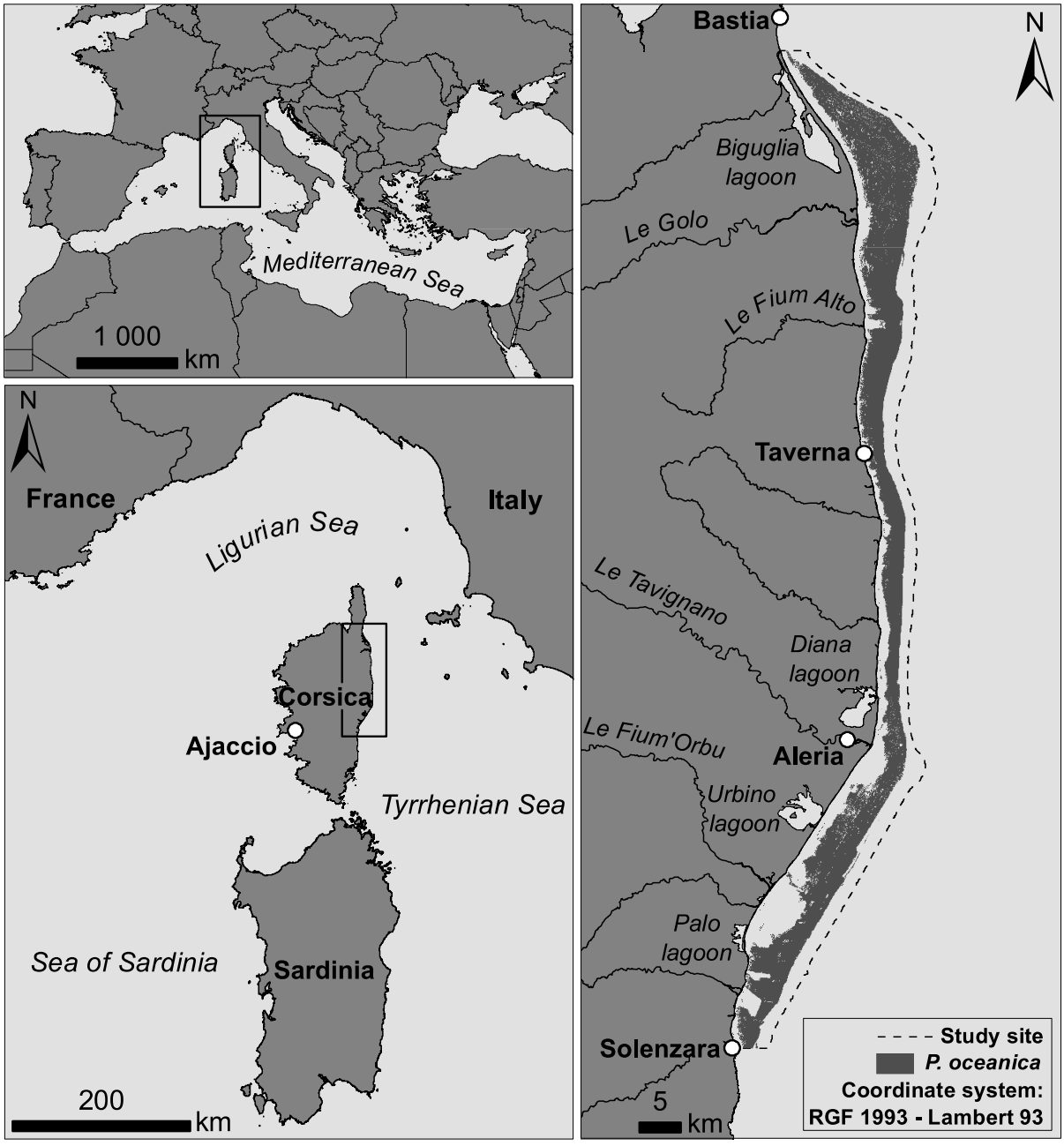

Figure 3.1. Location of the study site and the distribution of the *P. oceanica* meadow surveyed along the eastern continental shelf of Corsica Island.

The pre- processing step for the raw files (SEG-Y format) was initiated using the MATLAB® software. The signal to noise ratio was improved by using bandpass filter adapted to the emission frequency of each device. The post-processing and 2D seismic data analysis were undertaken with the seismic and geological interpretation software Kingdom® 8.7.1. The interpretation of seismic profiles was performed by manually picking lines corresponding to the top (upper horizon) and the base of the matte walls (lower horizon). This interpretation of seismic profiles is mostly based in accordance with the features of the eastern continental shelf of Corsica reported in the literature (Pluquet, 2006; Dupouy, 2011). After this step, the reference (seismic shotpoint) and the geographical position of each matte wall were exported.

Bathymetric data collection was performed using several MBES (Kongsberg-Simrad EM1000®, EM2040®, ME70®) with a frequency range of 250-400 kHz. The vessel absolute decimetric position was determined using a differential GPS (Global Positioning System). The data surveyed were processed with the Caraibes 4.4® system (Alami *et al.*, 2014). Daily sound velocity profiles were collected before operations to correct for local variations in sound velocity through the water column during processing. The morpho-bathymetric data were compiled in a Digital Terrain Model (DTM) raster mosaic with a spatial resolution of 5 x 5 m and a vertical accuracy of 0.2 m. LiDAR data were collected in October 2017 by the airborne Leica HawkEye™ III topographic and deep water bathymetric multi-sensor in double-hatch configuration (Chiroptera and Deep Channel). Data processing was undertaken with the Fledermaus 7.0 software and structured in a DTM raster mosaic (1 km^2-slabs) with a spatial resolution of 1 x 1 m and a vertical accuracy of 0.2 m (SHOM-CDC-DREAL Corse, 2019).

The MBES and LiDAR DTM were integrated (Mercator projection - WGS 1984) in a Geographic Information System (GIS) software (ArcGIS® 10.0; ESRI, 2011). Shading was applied on the raster data to highlight the morphology and topology of the sea bottom and especially the matte walls and intermattes. After importing geographical positions of previously calculated measurements from seismic profiles, bathymetric and LiDAR data were used to directly perform 3 matte walls measurements on each raster mosaics. By means of underwater surveys performed by scuba diving, it was possible to directly calculate the average matte wall heights from 5 measures collected at the same location from the seismic profiles. The measurements are taken at the base and at the top of the matte walls using dive

computer (vertical resolution: 10 cm). During ground-truthing, substrate and matte walls images were collected together with *in situ* information concerning morphology and seabed features.

Time-to-depth conversion of matte thickness was undertaken by using heights of vertical matte escarpments from the seismic profiles (ms TWTT) and metric data from morpho-bathymetric DTM. Intercalibration of morpho-bathymetric data was performed using scuba diving and LiDAR measurements to ensure consistent data quality. Seismic interval velocity is defined as the thickness of a stratigraphic layer divided by the time it takes to travel from the top of the layer to its base. This velocity is also equal to twice the interval thickness (meters) divided by the two-way travel time (seconds) following this formula:

$$v_{int} = \frac{2\Delta z}{\Delta T} = \frac{2\,(z_n - z_{n-1})}{T_n - T_{n-1}}$$

where v_{int} is the seismic interval velocity within the layer bounded by the $n-1$ layer boundary above and the n layer boundary below, z_n and z_{n-1}, T_n and T_{n-1} are the corresponding depths and two-way travel times at the respective previous reflector of the lithological or sediment layer (Sengbush, 1983; Kearey *et al*., 2002; Onajite, 2014).

3.**2.3. Sampling and laboratory analysis**

Samples were collected along 9 matte walls (80 to 280 cm high; Fig. 3.3.a), distributed between 13 and 21 m depth (mean depth ± S.D.: 15.1 ± 2.4 m) and equidistantly at the study site between 5-10 km (mean distance ± S.D.: 6.0 ± 2.7 km). The distances of the different stations from the coast and to the mouth of the nearest coastal river mouth (Class 1 to 3) were also calculated on the GIS software from the datasets of the national geographic reference for the coastline (HISTOLITT®) and the French hydrographic network (BD CARTHAGE®).

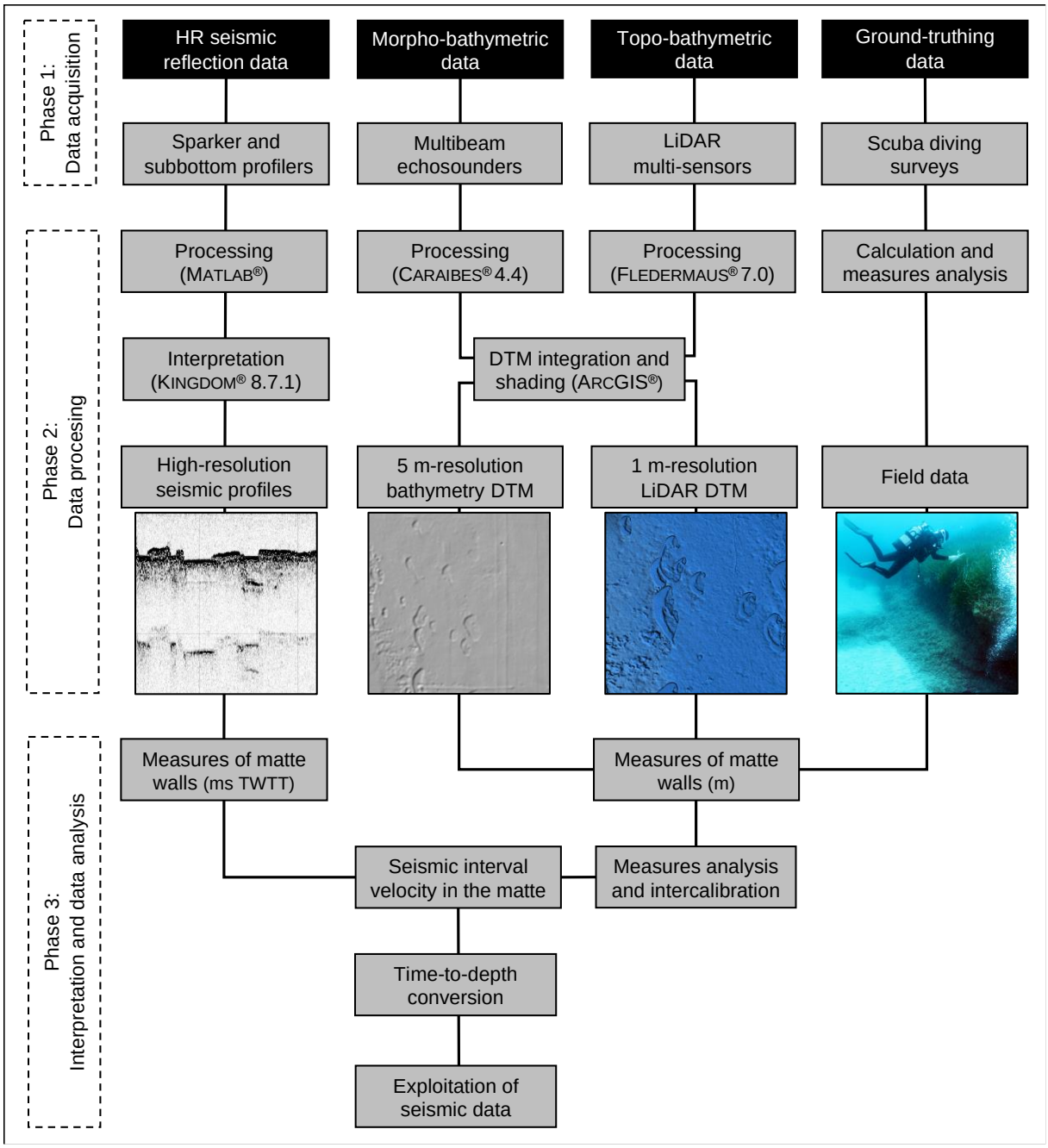

Figure 3.2. Different steps followed for the calculation of the seismic interval velocity in the *P. oceanica* matte and the calibration of the high-resolution seismic reflection data. DTM: Digital Terrain Model; LiDAR: Light Detection and Ranging; TWTT: Two-way travel time.

For each *P. oceanica* matte wall, horizontal cores were directly sampled by scuba diving (Pedersen *et al.*, 2011; Serrano *et al.*, 2016a). Three replicates spaced approximately 50 cm apart were collected at 3 different levels (Fig. 3.3.b). The coring was carried out using 100 cm-long PVC tubes (internal diameter 50 mm). The external 10 cm of the horizontal cores was removed to eliminate any contamination. The remaining material was homogenized and

subsampled (triplicates per level) in polypropylene vials. The samples were stored at 5°C before processing and analyses.

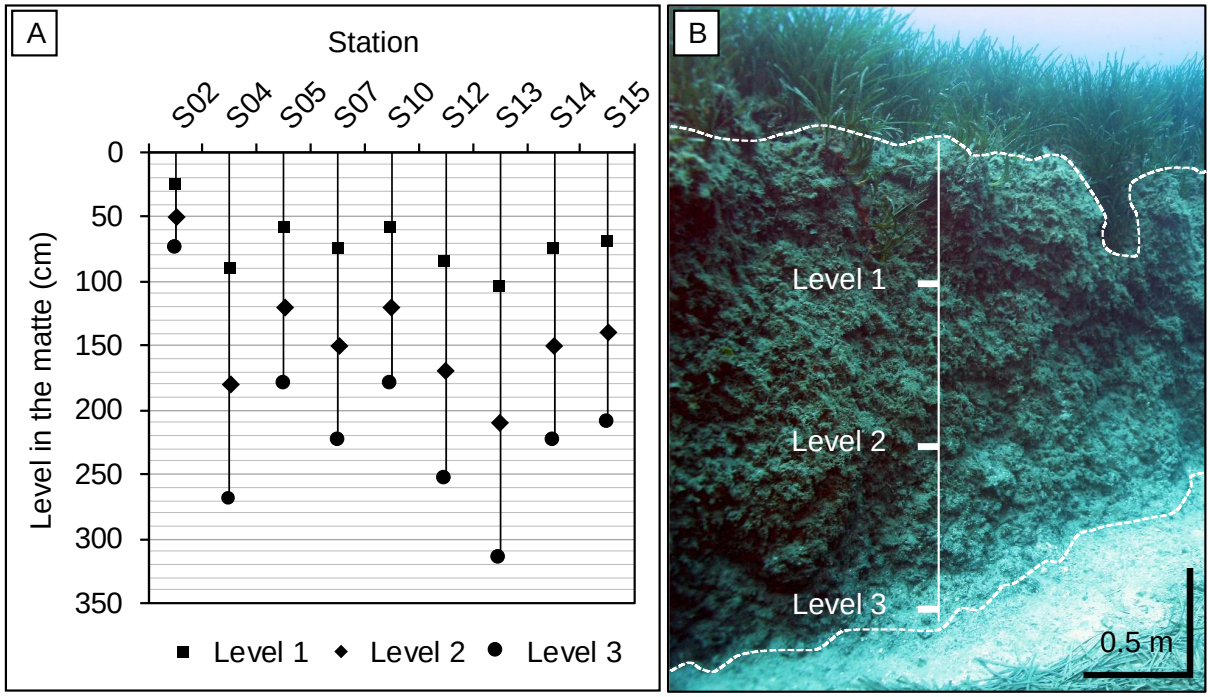

Figure 3.3. (a) Distribution of the horizontal cores collected along the *P. oceanica* matte walls surveyed in this study. Level 3 coincides with the bottom-most level of the matte wall sampled. (b) Example of one of the matte wall sampled in this study showing the levels where the horizontal cores were taken. The geographic location of the different sampling stations is shown in Figure 3.4.c.

Bulk density (ρ_d) and porosity of sediment (ϕ) were measured after drying samples at 70°C until constant weight (Howard *et al*., 2014a). The samples are sieved and weighed after drying and then separated into two fractions: the fine (<2 mm) and coarse fraction (>2 mm). The fine fraction is composed of the inorganic and organic matter of the sediment (SOM). The coarse fraction was sorted into 3 different categories, (i) the coarse organic fraction (COM, fragments of *P. oceanica*), (ii) the coarse mineral fraction (gravel), and (iii) the coarse carbonate fraction (shells and biogenic debris). After the sorting step, the COM was ground, homogenized and integrated into the fine fraction. The total organic matter (TOM) and calcium carbonate contents ($CaCO_3$) were determined by the method of loss on ignition at 500°C for 5 h and 950°C for 2 h in a muffle furnace (Heiri *et al*., 2001). The TOM content represents the total amount of SOM (<2 mm) and COM (>2 mm). Reference samples of pure calcium carbonate ($CaCO_3$, Merck EMSURE®, Darmstadt, Germany) were used for the 950°C combustions in order to correct any incomplete combustions. The particle size distribution for

the fine fraction was performed by wet sieving a 25 g subsample of dry sediment through a 0.063 mm stainless steel sieve. The very fine organic fibrous debris were previously extracted manually. The organic matter in the sandy-silt sediment was removed after treatment with 30% hydrogen peroxide (H_2O_2) for 24 h (Carver, 1971). Vigorous cleaning and rinsing of remaining material were achieved with MilliQ ultrapure water to remove soluble salts before wet sieving (Erftemeijer and Koch, 2001). The sediment was divided into 3 size classes: gravel (>2 mm), sand (<2 mm and >0.063 mm) and clay and silt (<0.063 mm, mud) according to the Wentworth classification scale (Wentworth, 1922).

3.2.4. Numerical analysis

Statistical analyses were performed using the statistics software package XLSTAT (Addinsoft, 2019) for Microsoft Office Excel® 2016. Normality of structural parameters values was checked using a Shapiro-Wilk test. A multiple linear regression model was computed between the three datasets (*i.e.* MBES, LiDAR and ground-truthing data) to identify the most appropriate tools to perform matte wall measurements. Inter-relationships between the seismic interval velocity in the matte, the biogeophysical parameters (*i.e*., dry-bulk density, porosity, organic and inorganic content) and the environmental parameters (*i.e*., bathymetry, depth in the soil, distance from the coast, distance from the nearest coastal river mouth) were investigated by performing Pearson correlation test. The correlation coefficient was calculated together with p-values to determine the significance and strength of each relationship. A significant difference is considered as a p-value <0.05. A hierarchical cluster analysis was performed using the Ward method and Euclidean distances between individuals (stations) for testing dissimilarity. Data were standardized (centered and reduced) before analysis to take into account the difference of units. In a first approach, separate analyses were performed for environmental parameters and biogeosedimentological parameters and finally computed together in order to study the combined influence of these parameters on the study site.

3.3. Results

3.3.1 Matte escarpment measurements

The high-resolution seismic reflection datasets were characterized by multiple horizontal reflectors from the layer boundaries highlighting a strong continuity in the stratigraphy of the eastern continental shelf of Corsica. The morphology and topography of the upper sedimentary sequences have contributed to identification of continuous *P. oceanica* meadow and the base of the matte, as well as areas with fragmentation of the meadow (*i.e.* intermattes). These numerous landscape fragmentations enclose sand patches and are bordered by matte walls (Fig. 3.4).

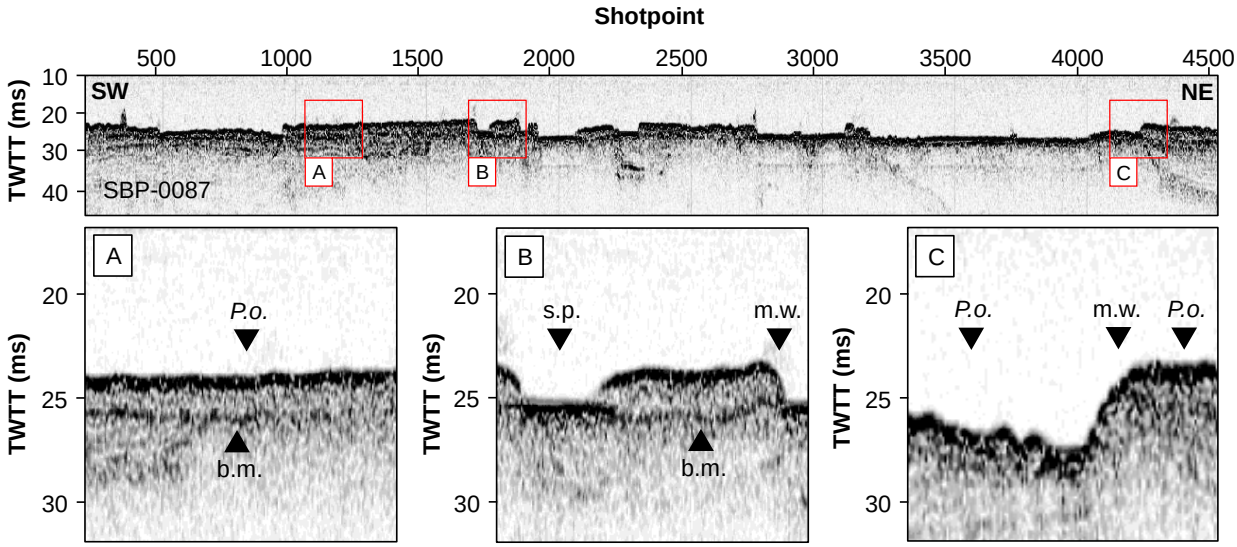

Figure 3.4. Example of high-resolution seismic reflection profile (#SBP-0087) characterized by area with (a) continuous *P. oceanica* meadow (*P.o.*) where we can observe the base of the matte (b.m.), (b) matte walls (m.w.) and intermattes with sand patches (s.p.) and (c) high matte walls in *P. oceanica* meadow.

These erosion escarpments mainly appear within the shallow bathymetric depth range near the upper limit of the *P. oceanica* meadow (*i.e.* ~10-20 m depth) and in very specific coastal areas (*i.e.* mouth of coastal rivers and coastal lagoons). Analysis of the seismic profiles made it possible to collect 367 measurements of matte walls. The analysis of MBES data has contributed to providing a near continuous morpho-bathymetric DTM within the study area (approximately 30 000 ha covered). The bathymetric mapping offers an accurate

geomorphological representation of seabed and habitat composition on the shallow eastern continental shelf of Corsica. The textural and topographical analyses contribute to identifying *P. oceanica* matte walls and also to acquiring 367 measurements of matte thickness (Fig. 3.5a).

These matte walls mainly occur in the bathymetric range between -10 and -20 m. In parallel, exploitation of data enabled collection of 133 LiDAR DTM (Fig. 3.5b) and 34 scuba diving measurements within the study site (Fig. 3.5.c.). The mean matte wall height was of 215 ± 59 cm for the raster mosaics (mean ± S.D.; Fig. 3.5a., Fig. 3.5b; Fig. 3.5) and 186 ± 50 cm for the field data (Fig. 3.5c; Fig. 3.6.).The thickness of matte walls extracted from morpho-bathymetric DTM showed a significant correlation with scuba diving surveys (R^2 = 0.872) and with LiDAR data (R^2 = 0.765; Fig. 3.6). Among the digital data, LiDAR measurements were the most similar to the data extracted from the field measurements (R^2 = 0.883; Fig. 3.6). The measurements collected on the LiDAR DTM coupled with the data collected during the scuba diving surveys allowed the intercalibration of the DTM morpho-bathymetric data. Thus, the intercalibration process was undertaken with 150 measurements, including 34 from underwater direct records and 116 from the LiDAR raster mosaic prior to performing the calculation of the seismic interval velocity.

3.3.2 Seismic interval velocity in the matte

Calculation of the seismic interval velocity in the matte performed on the study site (n = 367) showed very heterogeneous values ([CV%] = 19.0%) ranging between 757.9 and 2 791.1 m s^{-1}. The mean seismic interval velocity in the matte was established at 1 664.4 ± 316.9 m s^{-1}. The 95% confidence interval showed a seismic interval velocity variation between 1 631.9 and 1 696.8 m s^{-1}.

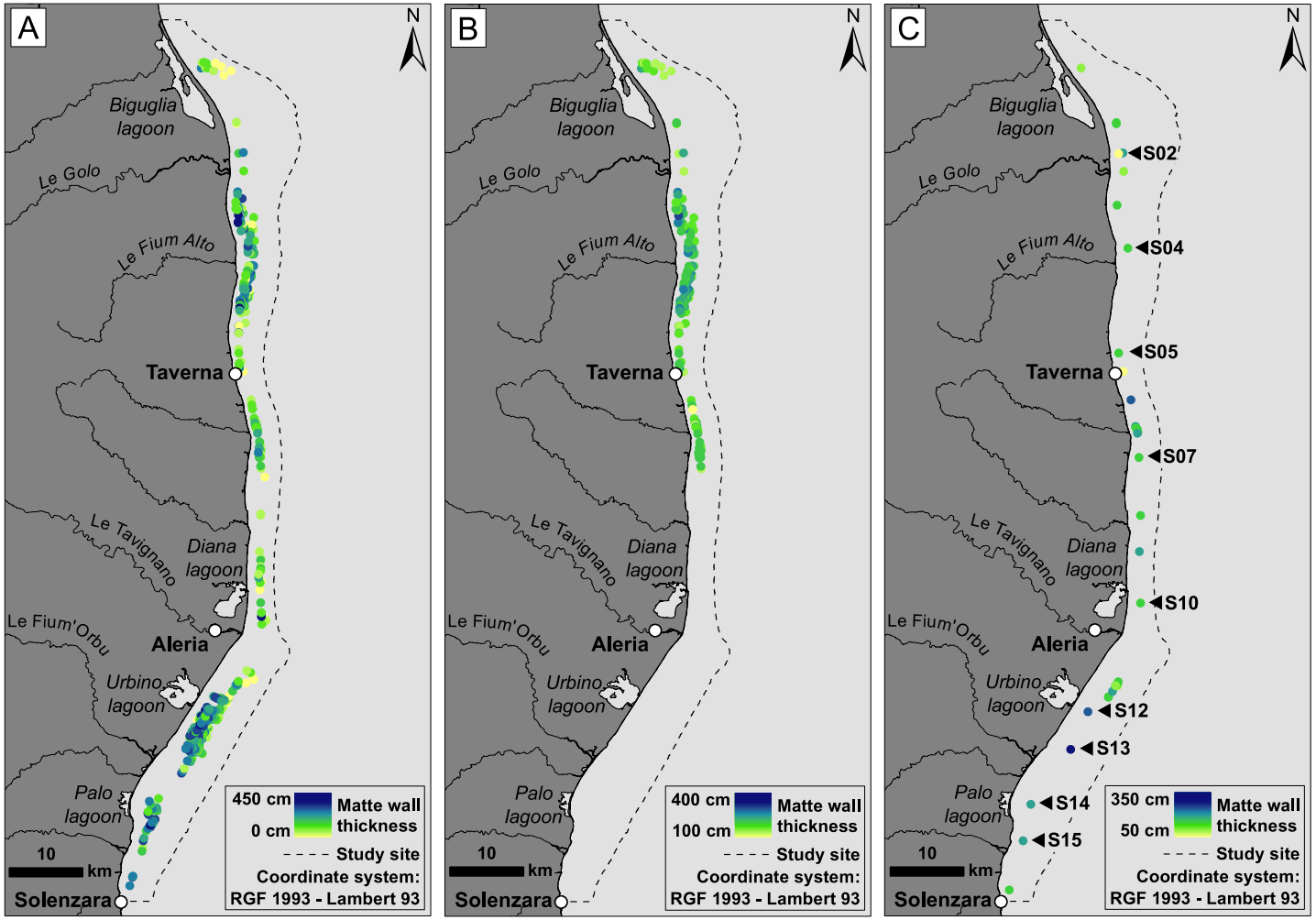

Figure 3.5. Distribution of matte walls measurements with the (a) morpho-bathymetric DTM (MBES data), (b) topo-bathymetric DTM (LiDAR data) and from (c) ground-truthing (scuba diving data). The geographical extension of matte wall measures on Figure II.4b correspond of the LiDAR data available. DTM: Digital Terrain Model; MBES: Multibeam Echosounders; LiDAR: Light Detection and Ranging.

Data interpolation achieved by ordinary kriging method highlighted a spatial heterogeneity of the seismic interval velocity values on the eastern coast of Corsica (Fig. 3.7). In GIS software, values were divided into 10 classes using Jenk's natural breaks (Jenks, 1967). Among the miscellaneous values, sound velocities under 1100 m s^{-1} (n = 9) and above 2100 m s^{-1} (n = 15) were very widely under-represented and patchy throughout the study site. Consequently, these values were not taken into account during the interpolation process by ordinary kriging (Fig. 3.7).

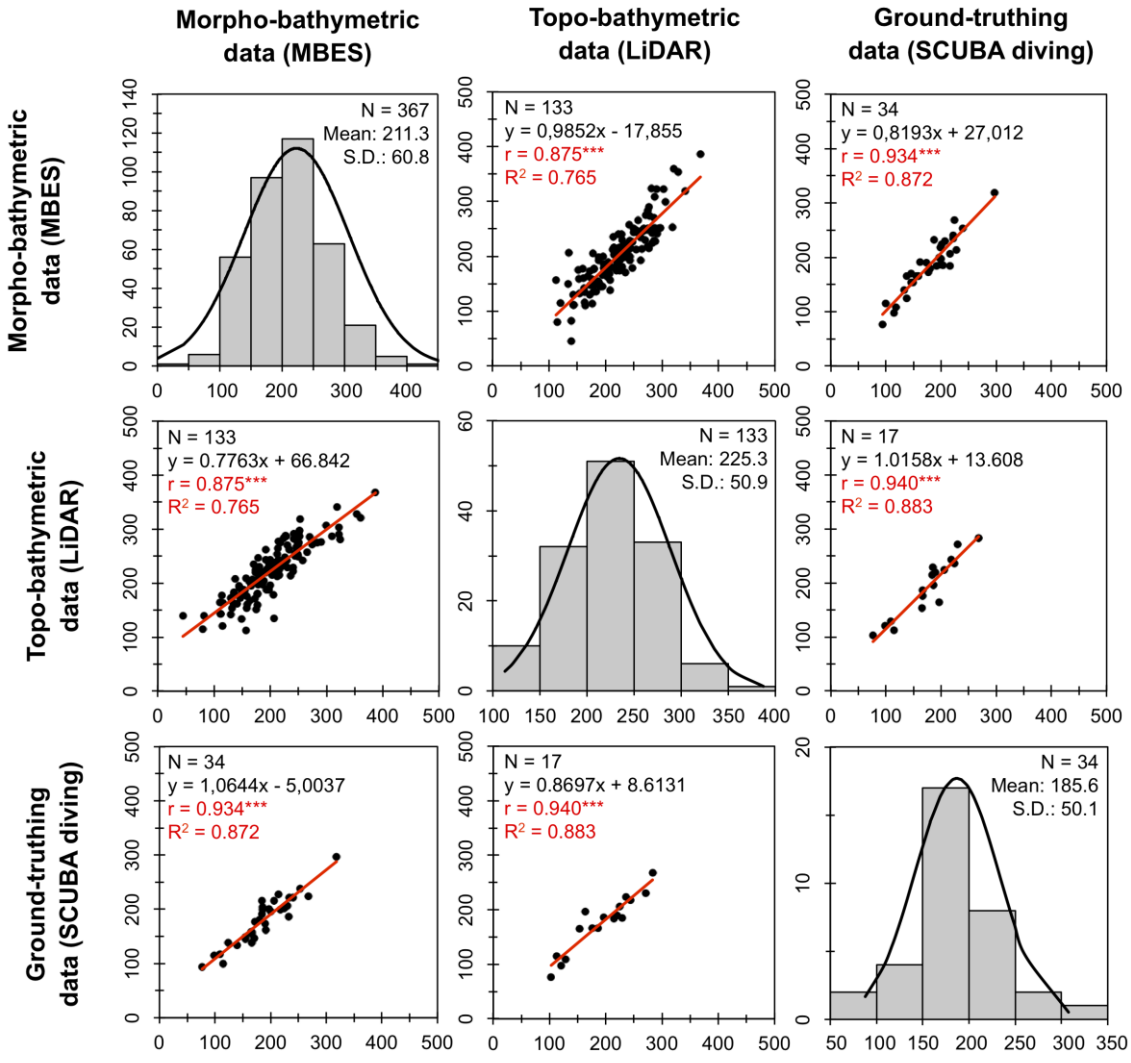

Figure 3.6. Multiple linear regression model computed between the matte wall measures collected with the three methods (morpho-bathymetric, topo-bathymetric and ground-truthing data). Levels of significance: *P≤0.05, **P≤0.01, ***P≤0.001. Significant correlations in red (r value). Matte wall measures are expressed in centimeters. Frequency histograms x-axis and y-axis correspond respectively to the measures (centimeters) and the observations number for each measurement intervals.

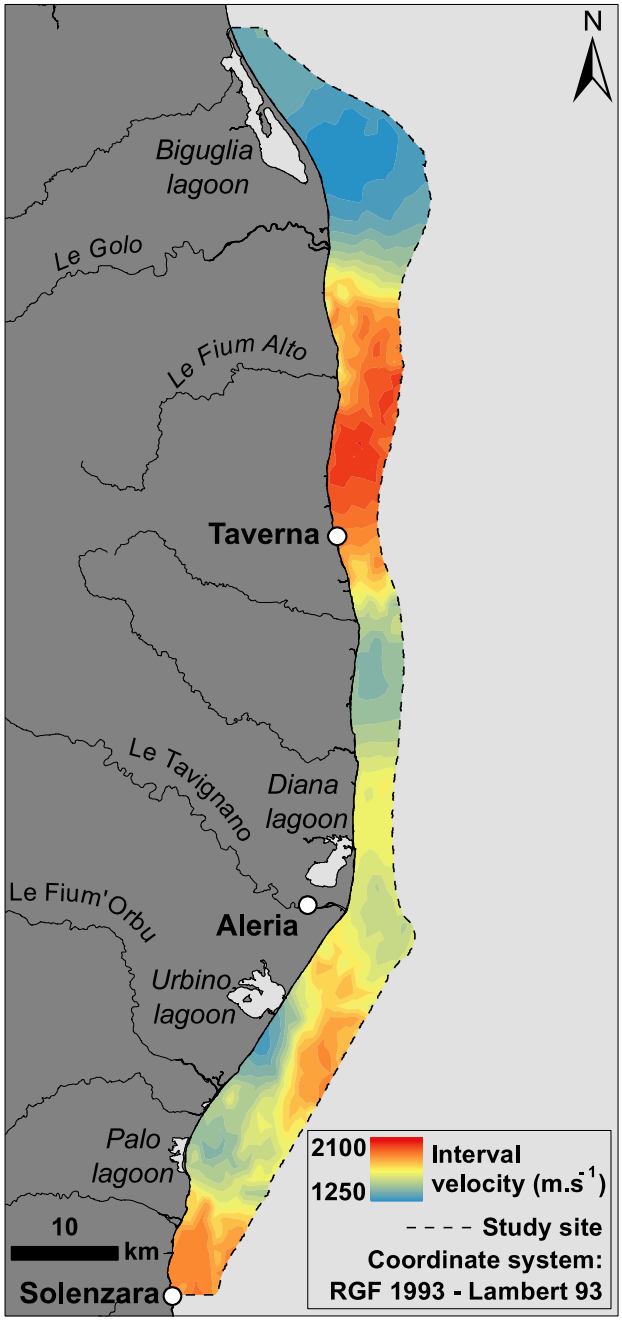

Figure 2.7. Seismic interval velocity prediction map in the *P. oceanica* matte over the Natura 2000 site. Prediction results are calculated using the velocity values from this study (n = 343).

The geographical area located between the mouth of the Golo river and the port of Taverna was characterized by the highest values ranging between 1650 and 2100 m s^{-1}. The interpolation map also highlighted other sectors with high sound velocity, such as off Urbino lagoon (1600-1800 m s^{-1}) and at the southern part of the area between the coastal lagoon of

Palo and Solenzara harbor (1600-1850 m s^{-1}; Fig. 3.7). In contrast, the lowest seismic interval velocity values were observed at the northern end of the site between Biguglia lagoon and the mouth of the Golo river (1250-1400 m s^{-1}), and locally in the shallow part near Urbino lagoon and between Taverna and Diana lagoon (1350-1450 m s^{-1}; Fig. 3.7). Thus, the central part of the alluvial delta of the Golo river was defined by an area with the lowest sound velocity over the whole study site (1250 m s^{-1}; Fig. 3.7).

3.3.3. Biogeosedimentological characterization of the matte

The eighty-one matte samples collected on the eastern continental shelf of Corsica are mainly constituted of seagrass meadows remains (sheaths, rhizomes and roots) incorporated into a dark brown sandy-muddy sedimentary matrix. The material analysis has enabled identification of extensive well-preserved seagrass organic debris buried both in the superficial parts of the matte and in the deepest parts (300-350 cm).

Dry-bulk density and soil porosity ranged from 0.52 to 1.35 g DW cm^{-3} and from 15.69 to 73.20% respectively, with an average value of 0.77 ± 0.11 g DW cm^{-3} (mean ± S.D.) and 53.38 ± 7.45% (Fig. 3.8; Table 3.1). The average composition of matte cores was mainly characterized by the inorganic content (mineral and carbonate; 77.02 ± 7.43%; Fig. 3.9.a; Fig. 3.9.b) and by the organic content (TOM; 22.98 ± 7.43%; Fig. 3.9.a; Fig 3.9.c; Table 3.1). The sandy and muddy grain-size fractions were the most dominant in the inorganic component in the matte, with an average content of 46.05 ± 9.33% and 29.26 ± 10.69%, respectively while gravel fraction was very poorly represented (0.16 ± 0.41%; Fig. 3.9.a). Similarly, the average total carbonates content accounted for an important part of the seagrass soil (13.42 ± 6.26%) and ranged from 6.09% to 39.24% (Table 3.1; Fig. 3.9.b). The high carbonate content found in seagrass soil was mostly composed by the fine carbonate fraction of the sediment, which ranged in average from 5.99 to 36.35% (Table 3.1). Inversely, organic matter content was mainly represented by coarse material (COM; 18.48 ± 10.53 %) and to a lesser degree by finer organic fractions of the soil (SOM; 4.49 ± 4.24%; Table 3.1; Fig. 3.8.a).

Although different sediment depths and locations are compared, parameters and soil properties of the cores changed with depth in seagrass meadows. The vertical trends with depth highlight a slow decrease in organic fractions while mineral and carbonate fractions increase (Fig. 3.9.a; Fig. 3.9.b; Table 3.2). Despite the occurrence of well-preserved *P. oceanica* fragments in the deeper matte sections, average organic matter patterns showed an approximately two-fold decrease of COM below the top 200 cm of the matte (Fig. 3.9.a; Fig. 3.9.c) and was negatively correlated with depth, density and mud content (Table 3.2). Conversely, a positive correlation was observed between SOM proportion and matte level (Table 3.2). Thus, SOM content increased slightly from 3.45% at the 0-200 cm matte layers to 7.63% down to the bottom end of the core (200-350 cm; Fig. 3.9.a).

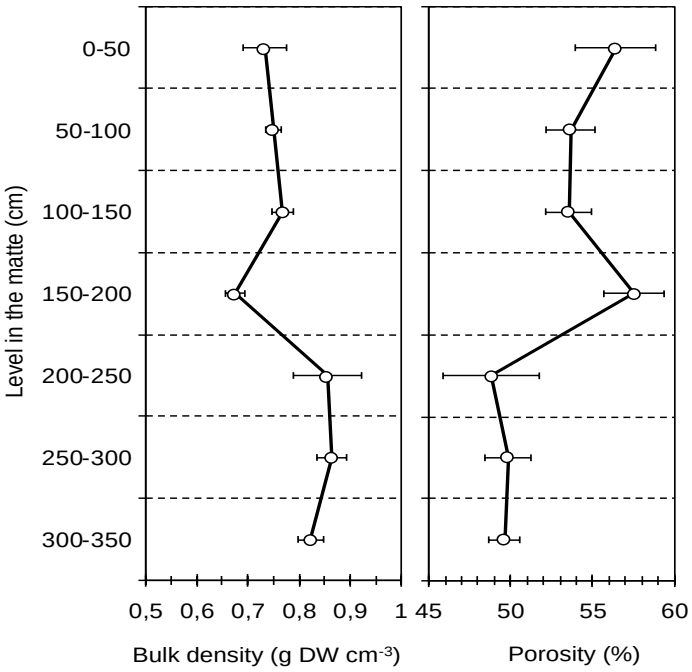

Figure 3.8. Mean bulk density and soil porosity changes along matte samples (n = 81) from the study site. Error bars represent the standard deviation (S.D.).

Similarly, the average sand and mud content followed a comparable trend, but no clear tendency emerges from gravel proportion with soil depth (Fig. 3.9.a; Fig. 3.9.c). However, the coarse mineral fractions (gravel and sand) showed negative correlations respectively with distance to the coast and with bathymetry, respectively (Table 3.2). In contrast to sand, mud and carbonate content appeared to be also positively connected with bathymetry. Analysis of

sedimentary sequences also highlighted an increase in the average total carbonate content with soil depth, in particular for the coarse fraction in the bottom-most sediment interval (300-350 cm; Fig. 3.9.b). In addition, changes of mean bulk density and porosity of the matte were observed with depth (Table 3.1; [CV%] = 14.7% and 13.95%, respectively). With regard to both the environmental and biogeosedimentological parameters of the matte, the majority were positively or negatively correlated to bulk density of sediment.

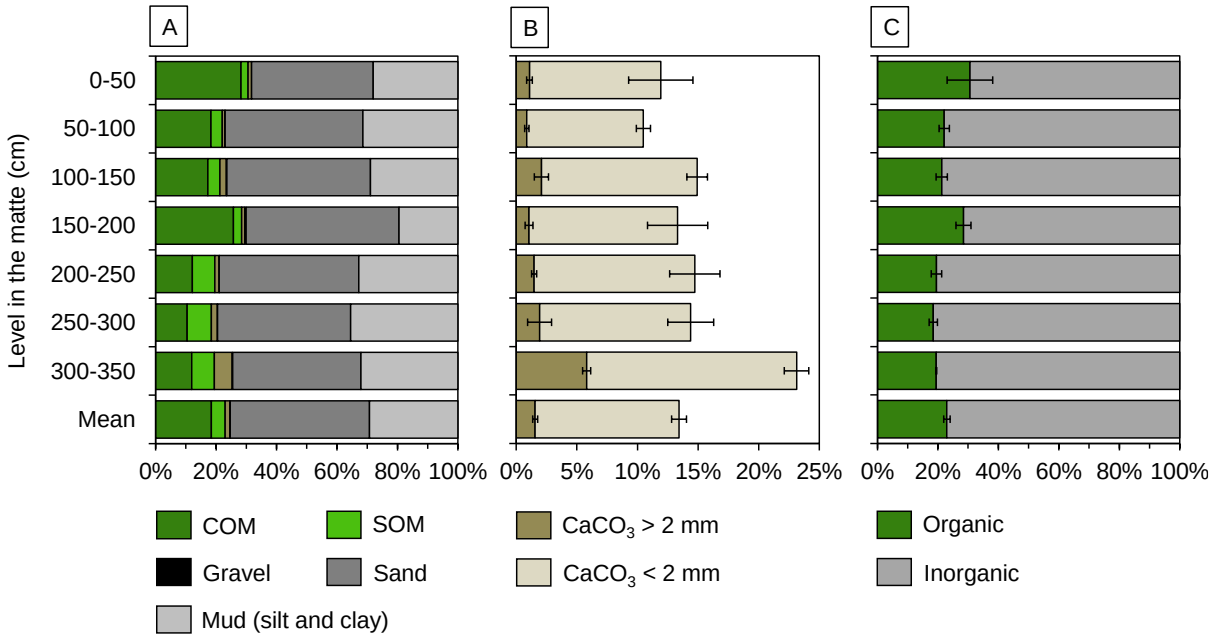

Figure 3.9. Mean values for the main variables studied along the matte cores collected over the studied area. Inorganic content, organic content, total carbonate content, TOM, COM and SOM contents are expressed as percentage of the total sample dry weight. Inorganic content encompasses inorganic and organogenic carbonates, and the rest of mineral fractions.

Higher sediment density values were positively associated with an increase in mud and SOM content, but also soil depth and distance from the coast. However, density was negatively correlated with porosity, COM and gravel content (Fig. 3.8; Table 3.2). One of the main results observed after the biogeosedimentological analysis of *P. oceanica* matte cores was the positive correlation of the seismic interval velocity with the gravel ($r = 0.316$; $p<0.01$) and sand content ($r = 0.290$; $p<0.05$) in the matte of *P. oceanica* (Table 3.2). However, the seismic interval velocity was negatively correlated with the total organic content (TOM; $r = -0.341$; $p<0.01$) and the coarse organic fraction (COM; $r = 0.314$; $p<0.01$) (Table 3.2). Furthermore, the analysis of environmental parameters showed that the seismic interval

velocity in the matte was strongly correlated with the distance from the coast and from an estuary outfall (Table 3.2).

Table 3.1. Descriptive statistics of the variables studied along the mat core. N (number of analyses); Mean ± Standard Deviation (S.D.); minimum and maximum values measured among the variables studied and matte depth. Bulk density, inorganic content, total carbonate content, total organic matter (TOM), coarse organic matter (COM) and sediment organic matter (SOM) are expressed in dry weight percentage referred to the total sample dry weight (%).

	N	Mean	S.D.	Minium	Maximum	Coefficient of variation [C.V.]
Bulk density (g DW cm^{-3})	81	0.767	0.113	0.524	1.348	14.697
Porosity (%)	81	53.384	7.446	15.688	73.197	13.948
Inorganic content (%)	81	77.022	9.441	31.149	93.462	12.257
Mineral content (%)	81	75.466	9.277	30.077	88.279	0.123
Gravel content (%)	81	0.156	0.408	0.000	3.020	220.399
Sand content (%)	81	46.045	9.336	24.496	70.738	31.007
Mud content (%)	81	29.265	10.689	5.481	48.902	45.145
Total carbonate content (%)	81	13.423	6.256	6.092	39.239	46.610
$CaCO_3$ >2 mm (%)	81	1.556	1.734	0	9.247	1.114
$CaCO_3$ <2 mm (%)	81	11.867	5.222	5.996	36.346	0.440
TOM (%)	81	22.978	9.441	6.537	68.851	36.983
COM (%)	81	18.485	10.534	4.163	68.303	50.303
SOM (%)	81	4.493	4.243	0.005	20.398	101.933

The cluster analysis performed on environmental parameters identified four classes connecting the most distant stations from the coast and the mouth of a coastal river (S13 and S14) while the shallowest and nearest stations to the coast were grouped (S02, S05, S07 and S15), thus isolating the deepest station (S10) and the stations with the high thicknesses of matte (S04 and S12; Fig. 3.10.a). The dendrogram of the cluster analysis using biogeosedimentological parameters underlines changes between the four classes linking stations S05 and S07 together, aggregating S10 with S12, the stations at the southern end (S13, S14 and S15) with S04, leaving the northern S02 alone (Fig. 3.10.b). By combining the biogeosedimentological parameters with the environmental ones, no significant variations are observed between the four clusters previously described (Fig. 3.10.c).

Table 3.2. Pearson's correlation matrix between the seismic interval velocity, environmental and biogeosedimentological parameters analyzed in the *P. oceanica* matte cores. 'Velocity' stands the seismic interval velocity. Level of significance: *P≤0.05, **P≤0.01, ***P≤0.001; NS, P≥0.05; Significant correlations in bold (r value).

	Density	**Porosity**	**Gravel**	**Sand**	**Mud**	**$CaCO_3$**	**TOM**	**COM**	**SOM**	**Velocity**	**Level**	**Depth**	**Coastline**	**Estuary**
Density		**-0.833**	**-0.265**	0.031	**0.266**	-0.028	**-0.335**	**-0.414**	**0.283**	0.042	**0.286**	0.062	**0.337**	0.182
Porosity	***		0.184	0.036	-0.161	0.052	0.135	0.215	**-0.235**	-0.049	-0.230	0.134	-0.193	-0.088
Gravel	*	NS		0.101	-0.116	-0.054	-0.037	0.017	-0.126	**0.316**	0.078	-0.203	**-0.286**	-0.012
Sand	NS	NS	NS		**-0.578**	**-0.350**	**-0.287**	-0.190	-0.166	**0.290**	0.044	**-0.358**	-0.058	0.064
Mud	*	NS	NS	***		**0.252**	**-0.601**	**-0.610**	0.175	0.009	0.062	**0.371**	0.165	-0.015
$CaCO_3$	NS	NS	NS	**	*		-0.063	-0.102	0.113	0.075	**0.279**	**0.425**	-0.045	**-0.342**
TOM	**	NS	NS	*	***	NS		**0.915**	-0.048	**-0.341**	-0.174	-0.108	-0.120	-0.007
COM	***	NS	NS	NS	***	NS	***		**-0.446**	**-0.314**	**-0.310**	-0.170	**-0.265**	-0.094
SOM	*	*	NS	NS	NS	NS	NS	***		0.020	**0.383**	0.182	**0.389**	0.218
Velocity	NS	NS	**	*	NS	NS	**	**	NS		0.220	0.130	**0.256**	**0.399**
Level	*	NS	NS	NS	NS	*	NS	**	***	NS		0.169	0.219	-0.023
Depth	NS	NS	NS	**	**	***	NS	NS	NS	NS	NS		0.179	-0.042
Coastline	**	NS	*	NS	NS	NS	NS	*	***	*	NS	NS		**0.790**
Estuary	NS	NS	NS	NS	NS	**	NS	NS	NS	***	NS	NS	***	

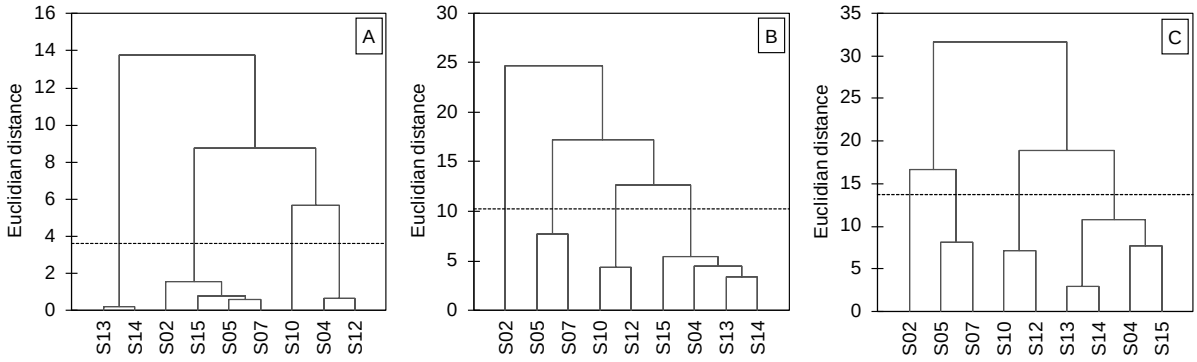

Figure 3.10. Cluster analysis dendrograms described by (a) environmental parameters, (b) biogeophysical parameters and (c) environmental and biogeophysical parameters of the sampling station. The dotted line materializes classes separation according to their dissimilarity. Stations location is depicted in Figure 3.4.c.

3.4. Discussion

This study has outlined a first methodological approach aiming to estimate the seismic interval velocity in the *P. oceanica* matte for the calibration of high-resolution seismic reflection data. The process described in this work was based on the combined use of matte wall measurements from high-resolution seismic reflection data and surveys collected both from scuba diving surveys and from seafloor morpho-bathymetric models of the study area.

3.4.1. High-resolution seismic reflection data: strengths and weaknesses

The integration of data from seismic profiles combined with the continuous mapping of the marine and coastal habitats of Corsica (Valette-Sansevin *et al.*, 2019) has made it possible to attest the presence of numerous discontinuities within the *P. oceanica* meadow identified as intermattes bordered by erosive matte walls. Although identification of these escarpments formations within marine vegetation is easily obtainable, the main limitation is linked to the vertical resolution of seismic records affecting the measurement of matte wall heights. This is the case for sparker seismic sources frequently used for a wide range of applications from coastal surface sediments (100 m) with moderate resolution (2 m) to deep stratigraphic layers (>1 km) where the resolution is low (Mosher and Simpkin, 1999; Kearey *et al.*, 2002; Duschesne and Bellefleur, 2007). The vertical resolution of a stratigraphic sequence, defined as the measure of the ability to recognize individual, closely spaced reflectors, is

closely linked to the emission frequency of the source (Sheriff and Geldart, 1995; Bitri *et al*., 1996; Yilmaz, 2001). Thus, a higher frequency (f) results in a shorter wavelength (*i.e.* $\lambda = v/4f$) and a higher vertical seismic resolution (Crutchley and Kopp, 2007). Therefore, considering a mean seismic interval velocity in the matte of 1 664.4 m s^{-1} and an emission frequency of 2.5 to 3.5 kHz for the two sub-bottom profilers, the vertical resolution ranges between ~0.1 and 0.2 m. Therefore, in view of the information provided and the precision required for the calculation of the seismic interval velocity in the matte, these devices have been selected for the measurements of matte walls. Here, the use of seismic records with sparker source (1.0 kHz) would be inadequate for an accurate interpretation due to the lower vertical resolution (~0.5 m). Nevertheless, the acquisition of seismo-acoustic records with high-resolution non-linear parametric echosounders seems to produce better results in matte and should be explored for this application (Lo Iacono *et al*., 2008; Tomasello *et al*., 2009). The use of the Innomar SES-2000 compact system generates seismic records imaging with high horizontal and vertical resolutions (a few centimeters). The advantage of the parametric effect lies notably in their ability to produce two high frequencies, which contributes to the detection of small impedance variations in the sub-bottom stratigraphy (Grant and Schreiber, 1990; Spieß, 1993; Hamilton and Blackstock, 1998).

3.4.2. Morpho-bathymetric and ground-truthing data: strengths and weaknesses

Whatever the type of seismic sources used (*i.e.* boomers, sparker, chirp), data require a calibration process to validate the information provided by these devices (Cordier, 1985; Lo Iacono *et al*., 2008; Brambilla *et al*., 2019). Ground-truthing data was conducted in the first instance by scuba diving (i) to attribute the signal response detected on high-resolution seismic imaging to morphological and substrate features observed *in situ*, and (ii) to gather direct measurements of matte walls necessary to undertake the seismic interval velocity calculation. However, even though underwater inspections by scuba diving remains one of the most accurate techniques to obtain seafloor data (Bonacorsi *et al*., 2013; Holon *et al*., 2015), there can be limitations. Direct underwater measures of matte walls during ground-truthing is a time-consuming and expensive process which only provides sporadic information (Komatsu *et al*., 2003).

In this study, the acquisition of matte wall measurements was mainly achieved using continuous elevation models of the seafloor from hull-mounted hydroacoustic (MBES) or airborne optic sensors (LiDAR), and these approaches offer many advantages for data acquisition (*e.g.* speed, positioning, accuracy, safety; Di Maida *et al*., 2011). Moreover, contrary to others acoustic sensors such as side-scan sonar (SSS) or single beam echo sounder, the high-resolution MBES datasets offer the advantage both of (i) providing boundary location information for marine benthic habitats such as *P. oceanica* meadows, and of (ii) establishing continuous shaded-relief topographic maps representing seafloor morphology (Kenny *et al*., 2003; Brown *et al*., 2011; Micallef *et al*., 2012). Even if acoustic methods are mainly used to identify geological formations and seabed elevations, biological formations have also been identified in this way (*e.g.* coral reefs, mussel and oyster beds; Shumchenia and King, 2010 and references therein), and more specifically submerged marine vegetation, by generating 3D information and allowing visualization of community distribution and vertical structure (Komatsu *et al*., 2003). Recently, MBES have been also efficiently applied on the Mediterranean coast to develop mapping of *P. oceanica* meadows by identifying bathymetric elevation boundaries formed between matte walls and sand patches (Di Maida *et al*., 2011).

LiDAR data have been also applied with success in this study to measure matte wall heights. In comparison with many recent studies, this bathymetric tool has been efficiently used to produce extensive DTMs of the seafloor and to map aquatic vegetation (Wang and Philpot, 2007; Silva *et al*., 2008 and references therein). Like many other remote sensing sensors, LiDAR systems generate 3D datasets from travel time differences of high-frequency laser pulse from the source to the receiver (Silva *et al*., 2008). Although the major factor interfering the LiDAR response is water absorption and scattering of laser signal by suspended material in the water column (Hopkinson *et al*., 2005; Wang and Philpot, 2007), it is particularly worth emphasizing the wide bathymetric range covered by LiDAR data within this area. The exceptional quality of the coastal and marine waters of the Corsica island in particular in this sector, has made it possible to extract measurements up to a depth of approximately 25-30 m. In total, the combination of MBES and LiDAR data has enabled the collection of approximately 500 accurate measurements of matte walls. The results showed that these two complementary methods represent a powerful and innovative methodology for a fast and accurate technique to gather *P. oceanica* matte wall measurements.

3.4.3. Intercalibration of matte wall measures

Calculation of the seismic interval velocity in the matte requires a high precision data. Considering the main aim of this study, the proper calibration and validation of numerical data with ground-truth data remains paramount (Hopkinson *et al*., 2006). Thus, to assess the error of matte wall height measurements, a multiple comparison has been undertaken between the numerical data (MBES and LiDAR) and ground-truthing surveys. The results have showed a significant correlation (R^2 >0.87; Fig. 3.6) of numerical data with field records proving the efficiency of the methodology. The mean difference of measurements estimated by digital and field data was 16.4 cm and is similar to error detection observed by Komatusu *et al.* (2003). These measurement errors could be attributed to the detection of *P. oceanica* canopy, unlike field data where matte heights take into account only the belowground parts of the structure.

Furthermore, the overall comparison has highlighted that LiDAR data provides a better prediction of matte heights in comparison with ground-truthing measurements (R^2 = 0.883; Fig. 3.6). Despite the similar vertical accuracy range (~0.2 m) of numerical datasets, the slight dissimilarity of ~1.1% between seafloor models (R^2 = 0.011) could result from the spatial resolution difference of LiDAR (1 m) and MBES data (5 m). The spatial resolution of the DTM is a key factor which can create uncertainty in the 3D bathymetric model of the seafloor and consequently can modify the interpretation of data. Malik (2019) has clearly demonstrated the limitation linked to this parameter by using the Horn method for various grid cell size resolutions to compute the seafloor slope (Horn, 1981). Thus, an increase in the grid cell size reduces the information content of the slope estimates and contributes to affecting the accuracy of bathymetric models. Although LiDAR data provide better results for matte wall measurements, a significant correlation has been also observed between the two numerical datasets (R^2 = 0.765). Taking into account these last outcomes and many other factors (*e.g.* high data density, high spatial extent of data), MBES height measurements have been selected to assess the seismic interval velocity in the matte. The intercalibration of these measurements has been successfully achieved by using the ground-truthing measurements in a first approach, and then, LiDAR measurements calibrated with the ground-truthing records.

This procedure is one of the most important steps to generate the accurate measurements needed for the next steps of the methodology.

3.4.4. Seismic interval velocity in the matte and relationship with sediment properties

This study presents the first estimates of seismic interval velocity in the matte of *P. oceanica* which have been calculated from time measures and calibrated metric measures of matte thickness distributed within the study site. Calculation and spatial prediction of sound velocity showed a high variability of values, but similar ones are recorded for unconsolidated marine sediments. Typical sound velocity of water-saturated sand and silt-clay sediments are within the 1 400-2 000 m s^{-1} range (Hamilton, 1956, 1971; Nafe and Drake, 1957, 1961; Schreiber, 1968; Kermabon *et al*., 1969; Turgut and Yamamoto, 1990; Kearey *et al*., 2002). The acoustic nature of unconsolidated marine sediments is closely related to the composition and physical properties such as bulk density, porosity, water content and mean grain size. Many works have already studied the density-velocity, porosity-velocity and grain size-velocity relationships in the marine sediments (Hamilton *et al*., 1956; Nafe and Drake, 1957; Sutton *et al*., 1957; Shumway, 1960a, 1960b; Hamilton, 1963; Breslau, 1967; Horn *et al*., 1968; Morgan, 1969; Orsi and Dunn, 1991), showing that an increase in the mean grain size of the sediment, associated with higher porosity and lower density, results in a greater sound velocity in the sediment.

Unlike marine sediments, *P. oceanica* matte is not constituted of a homogeneous accumulation of sediments characterized by solid particles and interstitial salted water filling the porous spaces (Akal, 1972). There has been recent interest in exploring the whether or not seagrass substrates can meet the requirements to qualify as soils (Serrano *et al*., 2012; Piñeiro-Juncal *et al*., 2020). Although the matte appears to be mainly constituted of the inorganic elements including lithoclastic (mineral particles) and bioclastic fractions (calcareous debris) (Boudouresque and Jeudy de Grissac, 1983; Jeudy de Grissac and Boudouresque, 1985; De Falco *et al*., 2000; 2003), this structure is also characterized by a dense belowground rhizosphere and an abundance of autochthonous - allochthonous organic matter (Mateo *et al*., 1997; 2006; Kennedy *et al*., 2010; Serrano *et al*., 2012). The physical and chemical characteristics of the matte have been found to be very heterogeneous owing to the

interplay of a number of factors (*e.g.* depth, depositional environment, currents, marine and terrestrial landscape configuration; Serrano *et al*., 2012, 2014, Ricart *et al*., 2015).

Here, the biogeosedimentological analysis of matte samples has contributed to the identification of differences of the parameters studied at different levels of the matte and environmental conditions. No significant correlation was obtained between density and porosity of the matte. Even though cores were collected, transported and analyzed with extreme care, the subsampling strategy implemented in this study could lead to sediment disturbance. In spite of this, a significant relationship of the mineral content (sand and gravel) with the seismic interval velocity in the matte was found, but not with the mud (silt-clay) fraction (Table 3.2). Also, results highlighted a positive relationships of seismic interval velocity in the matte with the distance from the coastline and from the nearest river mouth. These significant correlations were supported by coupling the prediction map of seismic interval velocity in the matte from this study with the sedimentological mapping of eastern continental shelf of Corsica established by recent studies over the last decades (Bouysse *et al*., 1981, Guennoc *et al*., 2001; Pluquet, 2006). Terrestrial sedimentary inputs in the area experience high seasonal and inter-annual variability (Mulder and Maneux, 1999; Gervais, 2002), leading to an also highly variable particle size composition, (encompassing fractions from gravel and coarse sand, to fine silt and clay; Gervais *et al*., 2006; Deptuck, 2008). In the north-south axes (parallel to the isobaths), fine sands were dominant in areas closest to the shore (Biocenosis of well sorted fine sand – WSFS; Pérès and Picard, 1964), giving place to a discontinuous band of coarse sand and gravel down to the lower limit of the *P. oceanica* meadow. These observations were also captured by (i) the lowest predicted velocity values observed in the shallow areas near the mouths of the Urbino and Tavignano rivers, and (ii) the cluster analysis which grouped the stations S10-S12 in this sector (mainly constituted by the highest mud content, 33.3-42.6%; Fig. 3.10.c). Similar results were highlighted by the cluster analysis for stations S13-S14, both characterized by the same environmental and biogeosedimentological parameters and found in a predicted area with low sound velocities. However, although the lowest seismic interval velocities were also observed at the northern end of the site (Fig. 3.7), mud content was not the most represented fraction in the S02 sediment samples. This station is characterized by its proximity with the mouth of the Golo river and located in the most extensive area of the eastern margin (Golo river fan; Pluquet, 2006). Nonetheless, the

particularity of this station was not highlighted by the cluster analysis with the environmental parameters, but with the biogeosedimentological ones (Fig. 3.10.b; Fig. 3.10.c). Station S02 station shows the highest mean TOM (37.4%) and COM content (35.8%). These features presented a strong negative correlation with the sound velocity (Table 3.2), possibly explaining the lowest sound velocities observed between the Biguglia lagoon and the mouth of the Golo river. Garlan (2004) showed how carbon organic content can influence sound velocity in marine sediment but many other factors can also lead to a low seismic interval velocity in the matte (<1 400 m s^{-1}). Among them, gas bubbles (usually methane) that occur in void space in marine sediments can impact the propagation of sound velocity. Thus, *in situ* or laboratory measurements of sound velocities in gassy sediments can commonly reach values below 1 000 m s^{-1} (Leighton and Robb, 2008 and references therein).

In contrast, high sound velocities are observed coincidentally with coarse sand and gravel fractions as depicted on the sedimentological map of Guennoc *et al.* (2001). This is notably the case between the mouth of the Golo river and the Taverna harbor where the highest seismic interval velocities were recorded. These results were supported by the biogeosedimentological analysis performed on stations S05 and S07, recognized as a cluster and defined by the highest gravel (S05: 0.86%) and sand content (S07: 60.1%). Moreover, seafloor pictures taken at the base of matte walls during underwater surveys between the south of the Golo river and Taverna harbor underlined the existence of rocky substrate layers. According to the Wentworth classification (Wentworth, 1922), coarse grain sizes ranging from pebbles (>4 mm and <64 mm) to cobbles (>64 mm to <256 mm) were identified at the base of the *P. oceanica* meadows, which could correspond to the original substrate and could be associated with the higher sound velocity. Similar high velocities occurred in the offshore part of the site between the mouths of the Urbino lagoon and the Fium'Orbu river (Fig. 3.7). Coarse sediment facies (Biocenosis of coarse sands and fine gravels under the influence of bottom currents – CSFG; Pérès and Picard, 1964) indicated by Pluquet (2006) in the same area could be related to these results.

One of the main aims of this work was to identify the major relationship between the seismic interval velocity and the biogeosedimentological features of the *P. oceanica* matte. According to the literature, many other parameters can influence the acoustic signals such as

grain wear, cohesion, bioturbation or the presence of calcium carbonate (Schreiber, 1967; Sutton 1975). Therefore, the study of the relationships established between the parameters of the sediment and the sound velocity requires consideration of not only the central parameters (porosity, density, grain size) but also the mode of deposition, the particle shape or even the nature of the interstitial fluid. Moreover, the comparison of different empirical models from the literature illustrating the porosity-velocity relationship shows that the quality and the measurement protocols can cause deviations of up to 150 m s^{-1} (Garlan, 2004). Many empirical models and statistical equations have been developed in the literature based on a major core or sediment sampling effort. In this study, only few matte samples were collected and analyzed to ensure clear, robust and accurate relationships of physical and textural parameters with sound velocity. Consequently, further research would be required (i) to compare seismic interval velocity estimates from this study with sound velocity measurements by using laboratory (*e.g.* Hamilton, 1971; Kim *et al*., 2001, 2008) or *in situ* acoustic analysis (*e.g.* Hamilton *et al*., 1956; Gorgas *et al*., 2002; Kim *et al*., 2008) and (ii) to explore in more depth the relationship between sound velocity and the properties of the deposits beneath the *P. oceanica* seagrass meadows.

3.5. Conclusion

This study provides the first detailed methodology to estimate the seismic interval velocity in the soil of a seagrass meadow for the accurate time-to-depth conversion and calibration of high-resolution seismic reflection data. The strategy developed in this work was based on the combined use of (i) high-resolution seismic reflection data, (ii) direct measurements using scuba diving, and (iii) seafloor morpho-bathymetric models, to measure the height of *P. oceanica* matte walls. The cross-comparison and the data intercalibration proved that the non-destructive methods constitute an accurate, time-saving, and cost-effective alternative to measure the matte wall thickness. The biogeosedimentological analysis performed on matte samples contributed to providing a first description of the parameters interfering with sound velocity in these exceptional marine sediments. The development of empirical models coupling the physical and textural parameters and the seismic interval velocity in further studies will provide precious structural information

contributing to size estimation and characterization of the long-term Blue Carbon sink associated with *P. oceanica* and eventually with other seagrass species.

Chapitre 4

Sizing the carbon sink associated with *Posidonia oceanica* seagrass meadows using very high-resolution seismic reflection

Abstract

Among coastal blue carbon ecosystems, seagrass meadows have been highlighted for their contribution to the global ocean carbon cycle and the climate change mitigation because of their capacity in the storage of large amount of carbon over long period of time in their sediments. Most of actual carbon stocks estimates beneath seagrass meadows are based on the analysis of a very limited number of sediment cores. High-resolution seismic reflection method has been applied at local scale to provide accurate estimates of the potential size occupied by the several meters thick organic deposit (matte) found beneath the Mediterranean seagrass meadows *Posidonia oceanica*. In this study, high-resolution seismic profiles (~1400 km) were collected along the eastern continental shelf of Corsica Island (France, NW Mediterranean) to perform the largest estimates of carbon stock in seagrass sediments. The seismic data were ground-truthed by sampling sediment cores and using calibrated seismo-acoustic surveys. The prediction map calculated by data interpolation (ordinary kriging method) highlighted a strong spatial heterogeneity of the matte thickness in the investigated site. The height of matte deposits, estimated in average at 251.9 ± 0.2 cm, increase in shallow waters (-10 m to -20 m), near river mouths (Golo, Tavignano and Travo) and lagoon inlets (Diana and Urbino) where matte thickness reaching 867 cm have been recorded, and locally in deepest areas (-30 m to -40 m). Radiocarbon datings performed at the base of matte deposits reveal the presence of the seagrass meadows since the mid-Holocene period (7000-9000 cal. yr BP). For the top 100 cm of soil, the age of the matte was ranged between 440 and 5331 cal. yr BP and the mean age was calculated at 1656 ± 528 cal. yr BP. The accretion rate of the matte, estimated in average at 1.02 ± 0.21 mm yr^{-1}, show a high variability resulting in a complex interplay of multiple biotic and abiotic factors (*e.g.* meadow features, water depth, exposure to hydrodynamic energy, geomorphology). Based on the surface occupied by these seagrass meadows, the average thickness of matte and data from literature, the volume of matte and total C_{org} stock were estimated at 403.5 ± 49.4 million m^3 (ratio: 2.2 m^3 m^{-2}) and 15.6 ± 2.2 million t C_{org}, respectively. The application of the high-resolution seismic reflection method to size the potential thickness and volume of matte has emphasized the necessity to perform large-scale assessment of spatial extent of blue in order to precise carbon stock estimates beneath seagrass meadows in Mediterranean and worldwide.

4.1. Introduction

Seagrass meadows, mangroves and tidal salt marshes have been highlighted for their highly efficient carbon storage capacity (Mcleod *et al*., 2011; Duarte *et al*., 2013). This coastal marine vegetation plays a significant role in climate change mitigation due to their contribution to long-term carbon sequestration (Nelleman *et al*., 2009; Laffoley and Grimsditch, 2009). The high primary production of these ecosystems associated with their exceptionally high burial rates provide large organic carbon (C_{org}) stocks comparable to other main terrestrial carbon sinks (Mcleod *et al*., 2011). Unlike most terrestrial ecosystems and similarly than peatlands, the carbon sequestered in coastal soils can be massive and remain trapped for very long periods of time resulting in very large carbon stocks (Duarte *et al*., 2005; Lo Iacono *et al*., 2008). The water-saturated and highly anoxic soil of blue carbon ecosystems limiting the aerobic microbial carbon oxidation and their continually vertical accretion at high rates result in a continuous build-up of a carbon-rich organic matter deposit over time (Schlesinger and Lichter, 2001; Chmura *et al*., 2003). Among these coastal ecosystems, seagrass meadows occur in a variety of marine environments (Carruthers *et al*., 2007) and cover nearly 0.2% of the world's ocean surface (Short *et al*., 2016). The overall estimates of C_{org} stock in the first meter seagrass meadow soils range from 4.2 to 8.4 Pg C (Fourqurean *et al*., 2012), while their carbon accumulation rates range from 48 to 112 Tg C_{org} yr^{-1}, representing almost 10-18% of the total carbon burial in the ocean (Kennedy *et al.* 2010; Duarte *et al*., 2013).

In the Mediterranean Sea, the endemic seagrass *Posidonia oceanica* (Linnaeus) Delile constitutes extensive meadows considered as a unique Corg sink due to the development of an outstanding structure known as "matte" (Molinier and Picard, 1952). This complex belowground formation, composed of intertwined rhizomes, roots and leaf sheaths, exhibits a very low decay rate in relation with the highly refractory nature of the organic matter and the anoxic conditions (Klap *et al*., 2000; Romero *et al*., 1992; Mateo *et al*., 1997, 2006). The accretion of organic-rich material in coastal sediments beneath the *P. oceanica* meadows constitutes massive C_{org} stock ranging from 40 to 770 kg C_{org} m^{-2} preserved over time spans from decades to millennia (Romero *et al*., 1994; Mateo *et al*., 1997, 2006; Serrano *et al*., 2012, 2014, 2016a). Matte deposits constitute one of the largest carbon stocks in coastal sediments

(Howard *et al*., 2014a). The matte thickness recorded in the literature typically ranges between 2 and 6-meters high (Molinier and Picard, 1952; Lo Iacono *et al*., 2008; Serrano *et al*., 2012, 2016a; Monnier *et al*., 2020) but reaches up to 14-meters in Montenegro (Miković, 1977 *in* Varda, 2015).

Since the last decades, the global importance of *P. oceanica* meadows as a long-term carbon sink have been widely recognized due to the large amount of carbon stored and their high distribution in the Mediterranean Sea (Pergent *et al*., 2012, 2014). However, estimates of carbon stocks beneath *P. oceanica* seagrass meadows are directly based on the analysis of a few matte cores at a very limited number of sites over the Mediterranean basin (Mateo *et al*., 1997; Lo Iacono *et al*., 2008; Serrano *et al*., 2012, 2014; Fourqurean *et al*., 2012). These limited estimates have emphasized the necessity to include a better estimate of the variability among seagrass habitats by (i) increasing the number of direct measurements in seagrass sediments, and (ii) providing extensive measurements of estimated *P. oceanica* mattes thickness along the Mediterranean coast (Pergent *et al*., 2012). Historically, the first assessment of *P. oceanica* matte thickness has been approximated by direct ground-truth observations from erosional matte escarpments referred as “matte walls” during mapping of benthic habitats (Molinier and Picard, 1952; Ribera *et al*., 1997; Abadie *et al*., 2015) and research in sediment dynamics of seagrass beds (Jeudy de Grissac, 1975; Blanc and Jeudy de Grissac, 1978, 1984). Large matte deposits were also recorded after the destruction of the *P. oceanica* meadows during coastal constructions (*i.e.* harbor, sea outfall) (Molinier and Picard, 1952; Miković, 1977 *in* Varda, 2015), underwater archeological excavation (Roman wrecks; Frost, 1969 ; Tchernia *et al*., 1978) and paleo-landscape studies (Votruba *et al*., 2016). Manual sounding during environmental impact studies (*e.g.* STARESO, 1991; Vela and Garrido-Maestracci, 2008; Vela *et al*., 2010) or core sampling during carbon stock inventories (Mateo *et al*., 1997, 2018; Lo Iacono *et al*., 2008; Pedersen *et al*., 2011; Serrano *et al*., 2011, 2012, 2014) was equally carried out to achieve accurate but sporadic assessment of matte thickness.

There are, to date, very few of the studies reported are directly focused on the assessment of the thickness, volume and spatial distribution of the matte to establish clear and robust regional estimates of carbon stocks (Lo Iacono *et al*., 2008). During the last decades, other methods, such as very high-resolution seismic reflection prospection, have

been successfully applied at local scale (Lo Iacono *et al*., 2008; Tomasello *et al*., 2009; Blouet *et al*., 2014). Since the 1970s, this geophysical method has been used to approximate the thickness of *P. oceanica* in coastal areas. To our knowledge, the first use of seismo-acoustic devices was undertaken in France where matte deposits up to 6-meters thick was found (Chassefière *et al*., 1974 *in* Blanc and Jeudy de Grissac, 1978). Similar studies involving mapping of benthic habitats in Italy (Colantoni *et al*., 1982) and Spain (Rey and Diaz del Rio, 1989) based on seismic technologies did not obtain conclusive results and only the superficial layers of *P. oceanica* could be identified. However, although the very high-resolution seismic reflection method proved to be cost-effective tool to estimate the potential size of carbon stocks associated to the *P. oceanica* matte, calibration of data by coring remains essential to ensure a good interpretation of the stratigraphic sequence (*i.e.* depth and thickness ; Onajite, 2014) but also to precise the C_{org} content and the spatio-temporal dynamic of these belowground formations (Lo Iacono *et al*., 2008). Indeed, several studies have underlined that matte accretion and carbon accumulation over long periods of time are influenced by the complex interactions of multiple biotic or abiotic factors (Mateo *et al*., 1997, 2002; Serrano *et al*., 2016b; Mazarrasa *et al*., 2018).

The main aims of this study are (i) to perform a large scale estimate of the thickness of *P. oceanica* matte based on a high-resolution seismic reflection dataset, (ii) to use the prediction model of matte and the surface covered by the meadows to calculate the total volume occupied by these organic deposits in the area surveyed, (iii) to provide a preliminary estimate of the total amount of C_{org} stocks buried beneath *P. oceanica* meadows in the study area and (iv) to investigate which parameters could be involved in the spatio-temporal dynamic of matte accretion throughout the study area.

4.2. Material and methods

4.2.1. Study site

This study was conducted in the Natura 2000 area, “FR9402014 - Grand Herbier de la Côte Orientale”, on the eastern continental shelf of Corsica Island (France, NW Mediterranean Sea; Fig. 1a; Fig. 1b). The site stretches along 106 km of sandy coast between the mouth of

the Biguglia lagoon in the north and the mouth of the Solenzara river in the south (Meinesz *et al*., 1990; Fig. 1c). This site is bordered by numerous in-land protected areas characterized by the presence of wetlands and coastal lagoons (Biguglia, Diana, Urbino, Palo) (Cannac-Padovani *et al*., 2014). The shelf is characterized by a 5-12 km-width range with a low gradient slope (~1-2°) (Gervais *et al*., 2006; Pluquet, 2006). This site hosts one of the largest *P. oceanica* meadows in the Mediterranean Sea, covering a surface area of 20425 ha (Fig. 1c) corresponding to 52% of sea bottom between 0 and 50 depth (Valette-Sansevin *et al*., 2019). This continuous meadow is mainly growing on a sandy substrate and interspersed by several landscape discontinuities (intermattes') naturally generated by hydrodynamics or by anthropic activities (Blanc and Jeudy de Grissac, 1984; Abadie *et al*., 2015).

4.2.2. Seismic data and methodology

The present study is based on the integration of different datasets, high-resolution seismic reflection and ground-truthing data (Fig. 4.1.d; Fig. 4.1.e). These datasets were mainly collected during three oceanographic surveys: CoralCorse (2013), PosidCorse (2015) and Carbonsink (2018). The high-resolution seismic reflection profiles were obtained using a Western ED 248 sub-bottom profiler called Manta EDO (Ifremer) operating at 2.5 kHz. Seismic data acquisition was performed with the oceanographic vessel 'L'Europe' (Ifremer) using the SUBOP® software (SUb-BOttom Profiler, Ifremer). The acquisition was performed at a vessel speed of 4 knots (7.5 km h^{-1}) and the absolute decimetric position of the vessel was determined using a differential GPS (Global Positioning System). Seismic data provided an average vertical record of approximately 20-40 m below the seafloor. These oceanographic surveys provided almost 1380 km of high-resolution, single-channel, seismic profiles between 10 and 50 m depth in the investigated sector (Fig. 4.1.d).

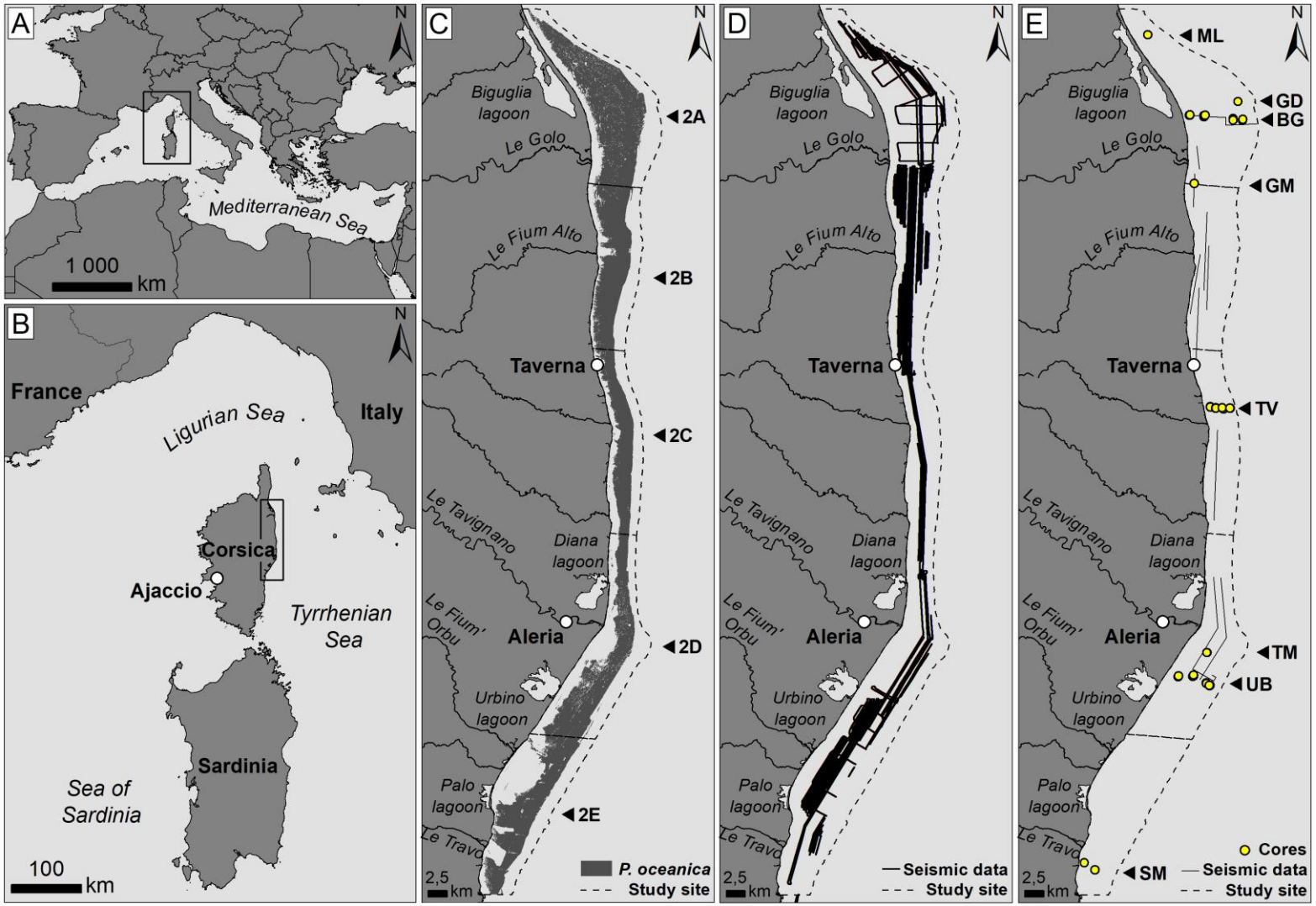

Figure 4.1. (a, b) Location of the study site on the eastern continental shelf of Corsica island, (c) distribution of the biocenosis of the *Posidonia oceanica* meadow and location of the sectors (2A, 2B, 2C, 2D and 2E), (d) seismic data profiles and (e) ground-truthing data. ML: Marana lido; GM: Golo river mouth; GD: Golo river delta; BG: Biguglia; TV: Taverna; TM: Tavignano river mouth; UB: Urbino; SM: Solenzara.

The pre-processing step for the raw files (SEG-Y format) was initiated using the MATLAB® software by applying a first set of corrections and options. The signal to noise ratio was improved by using bandpass filter adapted to the emission frequency. The post-processing and 2D seismic data analysis were undertaken with the seismic and geological interpretation software Kingdom® 8.7.1 on seismic profiles with better resolution for matte thickness discrimination. The interpretation of each seismic profiles was performed by manually picking lines corresponding to the top (upper horizon) and the base of the matte (lower horizon). This interpretation of seismic profiles is mostly based in accordance with the features of the eastern continental shelf of Corsica from former interpretations reported in the literature on the regional geology (Pluquet, 2006; Dupouy, 2011) and the benthic habitat distribution of the area (Valette-Sansevin *et al*., 2019). Interpretation of this seismic dataset was also referred to almost 55 km of very high-resolution seismic reflection dataset collected during the Sismat survey (2018) with the Innomar SES-2000 sub-bottom profiler (8 kHz; Fig. 4.1.e). These relevant seismo-acoustic profiles were processed using the software Innomar-ISE 2.9 (Interactive Sediment layer Editor) and interpreted following the previous methodology (unpublished data). The high-resolution seismic reflection profiles were mainly ground-truthed by several *P. oceanica* matte cores (Fig. 4.1.e) sampled using a gravity corer (see section below) but also by visual observations and matte walls measurements achieved during scuba diving operations (Monnier *et al*., 2020).

Height measurements, the reference (seismic shotpoint), and the geographical position of each matte thickness were exported and integrated (Mercator projection - WGS 1984) in a Geographic Information System (GIS) software (ArcGIS® 10.0; ESRI, 2011). Time-to-depth conversion of matte thickness, consisting in the conversion of data from travel time boundaries (in the time domain) to depths (in the space domain), was undertaken by using the average seismic interval velocity of 1664.4 m s^{-1} calculated in the matte of the *P. oceanica* by Monnier *et al.* (2020). The thickness was estimated by subtracting the elevation value of the matte base and the top of the matte for each shotpoint. The model of the matte thickness was created with the GIS geostatistical analysis tools by using the ordinary kriging method. The interpolation of the data was performed between the upper and lower limits of the *P. oceanica* meadows for the whole investigated site. The prediction model of matte thickness was splitted in five sectors (2A, 2B, 2C, 2D and 2E; Fig. 4.1.c) according to the segmentation

established in the framework of the benthic habitat mapping in Corsica (Meinesz *et al*., 1990; Pergent-Martini *et al*., 2015) to improve data analysis. Cross validation of prediction model was achieved in a first approach by comparing the predicted values with measured values from seismic data. A standard error map showing the uncertainty related to the predicted matte thickness values was computed throughout the study site. A second cross validation was performed to compare the prediction model with the ground-truthing dataset (*i.e.* seismo-acoustic data and sediment cores). The recognized submerged matte thicknesses were classified into categories at 0.5 m intervals. The matte volumes were estimated from the digital model of the thickness coupled to the surface area occupied by seagrass meadows. The error range in the volume estimation of the matte was calculated considering the difference between the minimum and maximum of the different classes.

4.2.3. Sediment sampling and laboratory analysis

The matte was sampled using a Kullenber gravity corer in 2018 during the oceanographic research survey Carbonsink aboard the R/V 'L'Europe' (Ifremer; Appendix A2). The sediment cores were collected in the *P. oceanica* seagrass meadow (water depth of 10–40 m) mainly along three transects (Biguglia (BG), Taverna (TV) and Urbino (UB) (Fig. 4.1.e; Table 4.1). Additional cores were also sampled in specific stations over the study site; Marana lido (ML), Golo river mouth (GM), Golo river delta (GD), Tavignano river mouth (TM) and Solenzara river mouth (SM) (Fig. 4.1.e; Table 4.1). The replicates cores sampled in each station (n = 2 to 3; α, β and γ) were spaced by ~50 m. The core barrel consists of a stainless-steel tube of 5 meters-long with a PVC tube (internal diameter 90 mm) inside it and surmounted by a lead weight of approximately 1 ton. The coring head is constituted by a sharp edge to cut the fibrous matte material and minimize the effects of compression during sediment sampling. Compression of unconsolidated sediment during coring was inevitable and corrections were applied (*i.e.* linear regression; Serrano *et al*., 2012) to decompress the sediment sequence and obtain the corrected core lengths.

In the laboratory, the core barrels were cut lengthwise and a biogeosedimentological description of the log stratigraphic sequences were performed. The cores were sub-sampled into 1 cm-wide slices (every 5 cm) and stored in polypropylene vials at 5°C before further

processing. The dating and the chronostratigraphic reconstruction of matte cores were achieved from radiocarbon (^{14}C) measurements by Accelerator Mass Spectrometry at the DirectAMS laboratory (Accium BioSciences, Seattle, WA). Samples of *P. oceanica* remains (n = 2) were only taken in cores collected at 10- and 20-meters depth spaced along the core. Before ^{14}C measurements, seagrass debris were first rinsed with ultrapure MilliQ™ water to remove fine sediment particles, placed in an ultrasonic bath of ultrapure MilliQ™ water for 5 minutes and finally inspected under a stereomicroscope for any attached materials. Then, samples were placed in baths of hydrochloric acid (HCl 1M, 80°C for 30 min) and sodium hydroxyde (NaOH 0.2M, 80°C for 30 min) in order to eliminate the carbonates, the fulvic and humic acids and the atmospheric carbon dioxide respectively (acid-base-acid treatment – ABA; Brock *et al*., 2010).

Radiocarbon data, expressed as years before present (yr BP), were subsequently calibrated for the local marine reservoir effect (ΔR = 46 years, error ΔR = 40 years; Siani *et al*., 2000) using the CALIB 7.1.0 software (Stuiver and Reimer, 1993) in conjunction with the Marine 13.14C calibration curve (Reimer *et al*., 2013). After corrections, the calibrated ages before present (cal. yr BP) were used to produce age-depth models using the clam package in R software (Blaauw, 2010). The best-fitted chronostratigraphic models were obtained with the linear model (Appendix A3) for approximate the respective mean sediment accumulation rate (SAR; mm yr^{-1}) and the resolution (yr cm^{-1}). Due to variability in core lengths sampled, the calibrated age, SAR and resolution of matte were standardized to stratigraphic depths of 30 cm and 100 cm to allow comparisons as performed by Rozaimi (2015). The limit of 30 cm was selected to obtain values in shallow sediments and 100 cm to performed comparison between stations. For temporal-based accumulations of the matte, the mean ages were determined as in the stratigraphic-based method within the thickness corresponding to the calibrated age of 100 and 1000 cal. yr BP.

4.3. Results

4.3.1. Application of the high-resolution seismic data on *Posidonia oceanica* matte

The high-resolution seismic reflection datasets contributed to provide a morphological and topographical representation of seabed features and superficial layers of sediment in the shallower part of the eastern continental shelf of Corsica. The infralittoral area was mainly constituted by a *P. oceanica* meadow alternated with sandy bioclastic patches ('intermattes'; Fig. 4.2.a; Fig. 4.2.b). The interpretation of seismic profiles contributed to highlight discontinuities and irregularities in the seafloor topography due to the presence of elevated erosive structures called 'matte walls' (Fig. 4.2.b). The seagrass meadow was delimited by these vertical escarpments reaching up to 3 m mainly located near the upper limit of the *P. oceanica* meadow (*i.e.* ~10-20 m depth).

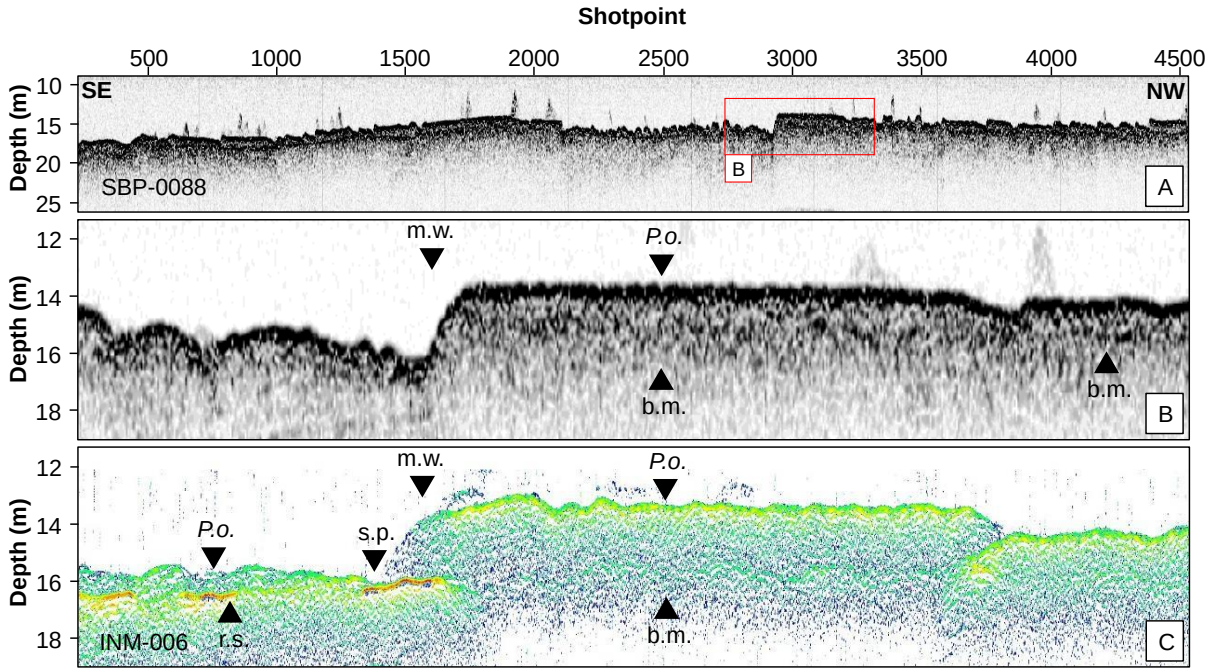

Figure 4.2. (a) Example of high-resolution seismic reflection profile (SBP-0087) recorded on the eastern coast of Corsica. (b) Section of the seismic profile displaying a continuous *P. oceanica* meadow (*P.o.*), the base of the matte (b.m.), a matte wall (m.w.) and a sand patch (s.p.). (c) Comparison with a seismo-acoustic profile (INM-006) where we can observe the rocky substrate (r.s.).

The analysis of stratigraphic structures and seismic profiles has also highlighted the presence of multiple horizontal reflectors with various contrasts of impedance. The heterogeneous composition of the substratum which occurred at the base of the matte provided different contrasts generating distinct seismic reflectors interpreted as rocky substrate and diffuse reflectors suggesting a sandy-muddy sediment basement associated to a progressive degradation of the matte. The identification of the native *P. oceanica* meadow substratum where the seagrass settled for the first time was completed by ground-truthing: sediment cores (see section below) and very high-resolution seismo-acoustic data. The use of data acquired with the seismo-acoustic sub-bottom profiler Innomar SES-2000 has offered the opportunity to improve both the detection of thin layers of matte (<0.5 m thick) and also the delineation and characterization of the sediment layer which constitute the base of the matte in comparison with seismic data acquired with the sub-bottom profiler Manta EDO (Fig. 4.2.b; Fig. 4.2.c).

4.3.2. Settlement and dynamic of *Posidonia oceanica* meadow

The sediment cores (n = 44), used to characterize the sediment layers and also to calibrate the base of the matte, were ranged from 57 cm to 380 cm (mean ± S.E.: 212 ± 13 cm; Table 4.1). The base of the matte was reached by 31 of the cores and the mean thickness recorded was estimated at 143 ± 14 cm (Table 4.1). The minimum and maximum matte thickness collected in the cores were 25 cm (TM-20-γ) and 340 cm (BG-10-γ), respectively. Matte deposits were also found at 40 meters depth but only for stations GD-40-α (100 cm) and UB-40-β (100 cm). The substrate at the base of the matte was mainly constituted by coarse sandy bioclastic sediment layers. Equally, *P. oceanica* matte has been observed on muddy substrate in deeper and locally near river mouths defined by terrestrial inputs (*e.g.* Golo and Tavignano rivers), but also on rocky substrates (pebbles and cobbles according to Wentworth, 1922) in shallower areas characterized by high-energy hydrodynamics. This is corroborated by the higher fragmentation of *P. oceanica* meadows in shallower areas and the presence of coarse-grained sediments in the intermattes (*i.e.* pebbles, cobbles, rhodoliths debris).

Table 4.1. Minimum, maximum and mean cores length and matte thickness sampled in the investigated site at different depth.

	Core length (cm)			Matte thickness (cm)		
Depth	**Minimum**	**Maximum**	**Mean ± S.D.**	**Minimum**	**Maximum**	**Mean ± S.D.**
10	57	380	259 ± 113	55	340	203 ± 93
20	85	356	211 ± 73	25	275	138 ± 79
30	60	247	145 ± 62	0	80	54 ± 24
40	120	310	228 ± 71	0	105	26 ± 48

Matte ages (n = 20) were ranged between 389 ± 94 and 9073 ± 181 cal. yr BP (Table 4.2). The earlier radiocarbon ages were recorded for the stations TM-20-β (264 cm) and GM-10-α (305 cm) attesting the seagrass meadow presence in the eastern coast of Corsica between 7000 and 9000 cal. yr BP (Northgrippian age, mid-Holocene). Age increased regularly with the depth of sediment (Table 4.2), but showed a strong variability between cores, even among cores taken at the same station (*e.g.* TM-20-α and TM-20-β; Table 4.2). Considering all the radiocarbon dates throughout the site, the ages were positively and significantly correlated with depth in the soil ($r = 0.578$; $R^2 = 0.334$; p-value<0.01; Pearson correlation test).

Considering each respective cores, the age of the matte ranged between 90 and 1552 cal. yr BP and 440 and 5331 cal. yr BP at 30 cm and 100 cm from the top of the matte, respectively (Fig. 4.3). The minimum age was calculated for the stations located in the transect UB at 30 cm and 100 cm (164 ± 36 and 644 ± 167 cal. yr BP, respectively). Conversely, for the same depth of sediment, the stations of the TM transect exhibited five-fold older age estimated at 896 ± 656 and 3146 ± 2185 cal. yr BP, respectively. Whatever the soil depth considered, the age of matte increase with the bathymetry (Fig. 4.3). Thus, the respective age at 30 cm and 100 cm depth were estimated at 180 ± 61 and 729 ± 215 cal. yr BP at 10 m depth whereas values were ranged between 729 ± 215 and 2514 ± 821 cal. yr BP at 20 m depth. Similarly, whatever the soil depth considered, seagrass meadows dominated by higher influence of alluvial inputs and located near river estuaries (GM, TM, SM; <3.5 km) were older than open sea meadows distant from river mouths (BG, TV, UB; >6 km) (Fig. 4.3).

The mean sediment accretion rate (SAR) was ranged between 0.19 and 2.64 mm yr^{-1} with an average value of 1.05 ± 0.26 mm yr^{-1}. For the top 30 cm and 100 cm of matte, the

mean SAR of open sea meadows (1.17 ± 0.23 and 1.26 ± 0.30 mm yr^{-1}, respectively) was two-fold higher than estuary meadows (0.64 ± 0.16 and 0.65 ± 0.17 mm yr^{-1}, respectively) (Fig. 4.3). Similar trend was observed with depth gradient where shallow meadows (-10 m) exhibited two-fold higher values (1.39 ± 0.25 and 1.57 ± 0.33 mm yr^{-1}) than deep meadows (-20 m; 0.67 ± 0.14 and 0.64 ± 0.16 mm yr^{-1}) (Fig. 4.3). For the top 100 cm of matte, the respective lowest and highest mean SAR were recorded for the TM stations (0.58 ± 0.39 mm yr^{-1}) and for the UB stations (1.65 ± 0.21 mm yr^{-1}) with in average 1.02 ± 0.21 mm yr^{-1} (Fig. 4.3). Through the investigated site, the mean calibrated age of matte at 30 cm and 100 cm depth is estimated at 370 ± 128 and 1656 ± 528 cal. yr BP, respectively (Fig. 4.3).

The mean resolution ranged between 4.56 and 54.03 yr cm^{-1} with better resolution for the top 30 cm and 100 cm of matte in open sea stations (10.94 ± 2.57 and 15.85 ± 6.96 yr cm^{-1}, respectively) and in shallow stations (-10 m) with 8.32 ± 2.04 and 7.98 ± 2.15 yr cm^{-1}, respectively (Fig. 4.3). Considering the top 100 cm of soil, the lowest and highest mean resolution were calculated for the TM stations (32.19 ± 21.85 yr cm^{-1}) and for the UB stations (7.06 ± 1.59 yr cm^{-1}), respectively (Fig. 4.3). For the whole site, the temporal accumulations of matte were estimated at 16.30 ± 2.79 cm (100 cal. yr BP/century) and 128.00 ± 27.94 cm (1000 cal. yr BP/millennia). Since the sampling year of matte cores, the accumulation of matte was assessed at 12.60 ± 3.32 cm for the last century and at 119.45 ± 25.62 cm since the last millennia.

Table 4.2. Radiocarbon ages, mean sediment accretion and resolution for *Posidonia oceanica* matte samples. Sample depth was corrected for core compression. Sediment accretion and resolution were calculated using clam R package. *na: possible sediment mixing

Sector	Replicate core ID	Core lenght (cm)	Matte thickness (cm)	Sample depth (cm)	Radiocarbon (^{14}C) age (yr BP)	Calibrated ^{14}C age (cal. yr BP - 2σ)	Mean accretion (mm yr^{-1})	Mean resolution (yr cm^{-1})
2A	BG-10-α	365	270	151	1476 ± 33	1001 ± 125		
				263	3917 ± 35	3860 ± 157	0.98	15.00
	BG-20-γ	188	182	92	2090 ± 31	1629 ± 134		
				142	3584 ± 33	3438 ± 128		
				182	4259 ± 45	4307 ± 175	0.45	24.02
	GM-10-α	364	305	159	2531 ± 29	2207 ± 91		
				305	7275 ± 40	7697 ± 119	0.49	25.49
2C	TV-10-γ	206	185	87	802 ± 26	389 ± 94		
				177	1224 ± 27	741 ± 101	2.24	4.56
	TV-20-γ	138	110	42	1299 ± 27	747 ± 102		
				102	4722 ± 36	4926 ± 135	0.30	49.16
2D	TM-20-α	356	193	93	1399 ± 23	890 ± 114	0.97	10.34
	TM-20-β	275	110	92	4688 ± 39	4898 ± 133	0.19	54.03
				264	8488 ± 46	9073 ± 181	*na	*na
	UB-10-γ	300	154	72	852 ± 27	416 ± 96		
				145	1065 ± 27	592 ± 74	2.64	4.59
	UB-20-α	215	185	82	1257 ± 32	771 ± 108		
				157	1642 ± 31	1154 ± 115	1.33	7.79
2E	SL-20-α	220	220	87	1660 ± 26	1165 ± 106		
				183	2464 ± 34	2059 ± 157	0.90	11.60

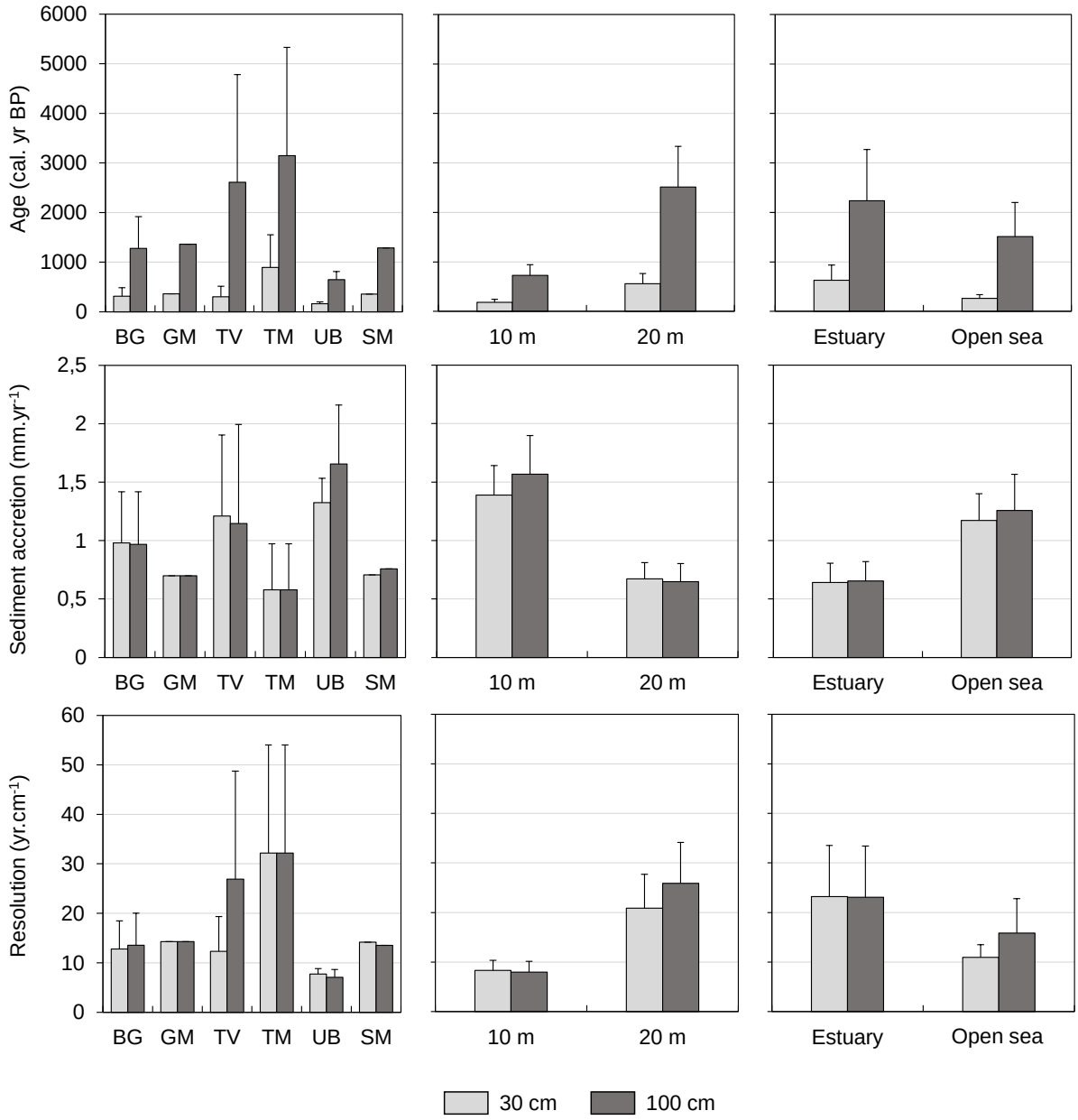

Figure 4.3. Mean value (± S.E.) of calibrated ^{14}C age, sediment accretion and resolution for the top 30 cm and 100 cm of matte at the different stations, bathymetric depth (-10 m and -20 m) and depositional environment (estuary or open sea).

4.3.3. Estimates of the *Posidonia oceanica* matte thickness and volume

The spatial prediction of the thickness of the *P. oceanica* matte on the study site was performed from a high number of measures (n = 861544) ranging between 0 and 867 cm (Fig. 4.4). The mean thickness in the matte was established at 251.9 ± 0.2 cm for the Natura 2000 area (Fig. 4.4). The 95% confidence interval showed a matte variation between 251.5 and 252.3 cm. The highest mean matte thickness was observed in the southern sector of study site

(sector 2E; 297.4 cm). In GIS software, data interpolation was achieved by using ordinary kriging method. Calculation of matte thickness was performed by separating values into classes at 0.5 m intervals for the study area and for each sector (2A to 2E). The values widely under-represented and patchy found throughout the study site (*e.g.* matte thicknesses up to 700 cm for the sector 2A; <1% of data for this sector) were not considered for the interpolation of data.

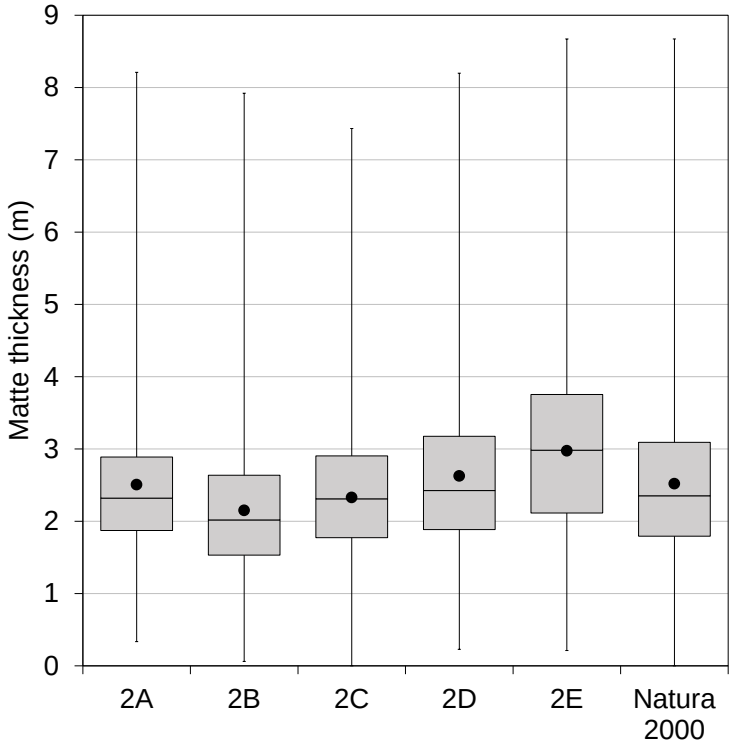

Figure 4.4. Box plot representation of the matte thickness observed within the different sectors and in the Natura 2000 area. The mean and median values are represented by the black dots and by the crossbar lines in the boxes, respectively. The minimum and maximum values are indicated by the external bars outside the boxes.

The prediction map calculated for the whole site highlighted a spatial heterogeneity of the matte thickness (Fig. 4.5.a). The standard error map evidenced that about 80% of the map surface was concerned by a standard error less than 48.6 cm (Fig. 4.5.b). Cross validation displayed a significant and positive correlation ($r = 0.913$; p-value<0.001; Fig. 4.6.a) between predicted values from kriging method and the measured values collected on high-resolution seismic reflection data. The mean error obtained between these two values highlighted a slight underestimation of the predicted compared to the measured values from the seismic profiles (-1.26 ± 0.07 cm; Fig. 4.6.a). Similarly, the cross validation performed between ground-

truthing data and predicted matte thicknesses showed that these values were underestimated (-6.62 ± 2.29 cm in average; Fig. 4.6.b). In spite of this, the linear relationship exhibited a significant and positive correlation between the predicted values and the ground-truthed data (r = 0.817; p-value<0.001; Fig. 4.6.b).

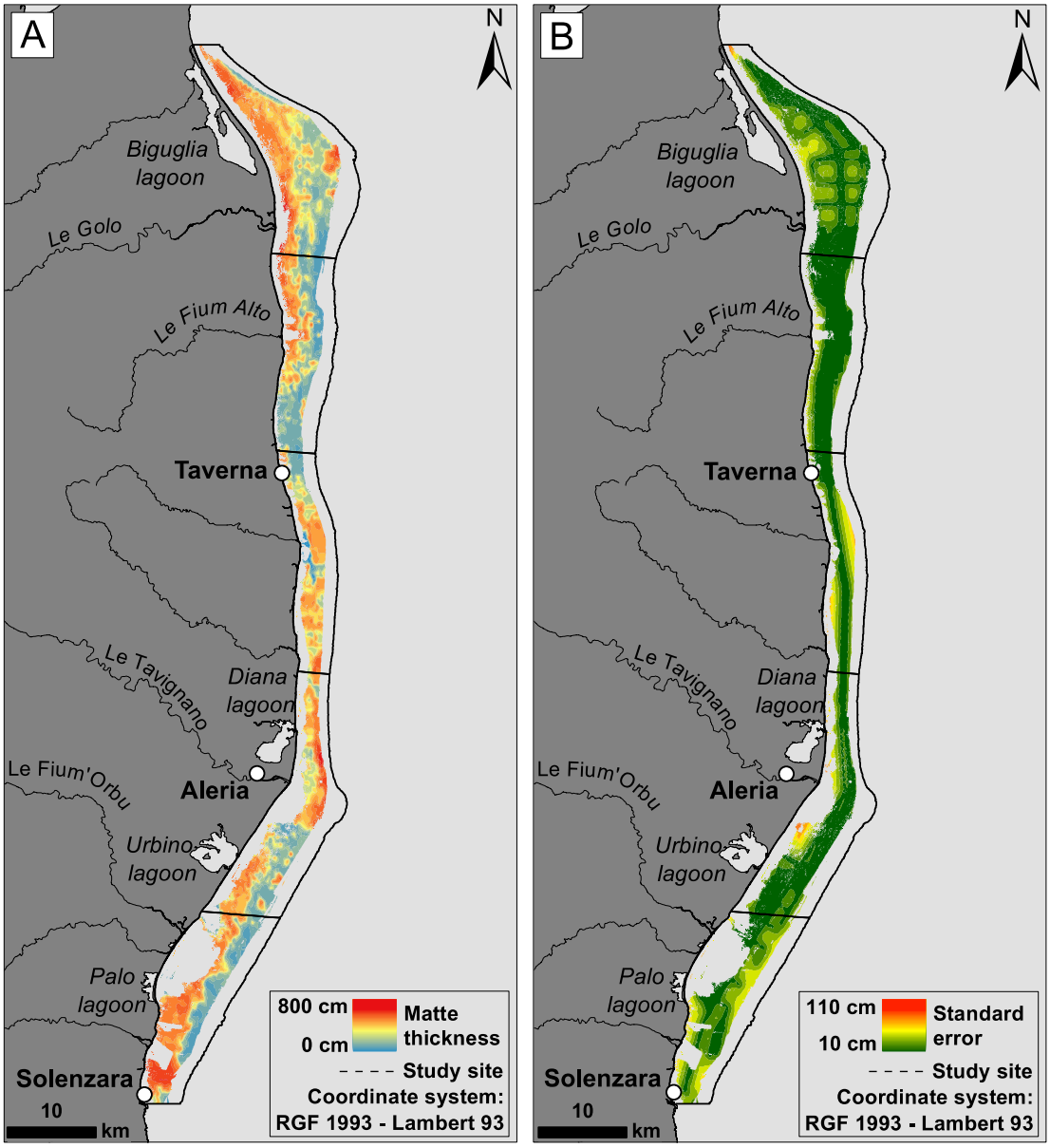

Figure 4.5. (a) Prediction map of the *Posidonia oceanica* matte thicknesses in the study site and (b) standard error of the kriging.

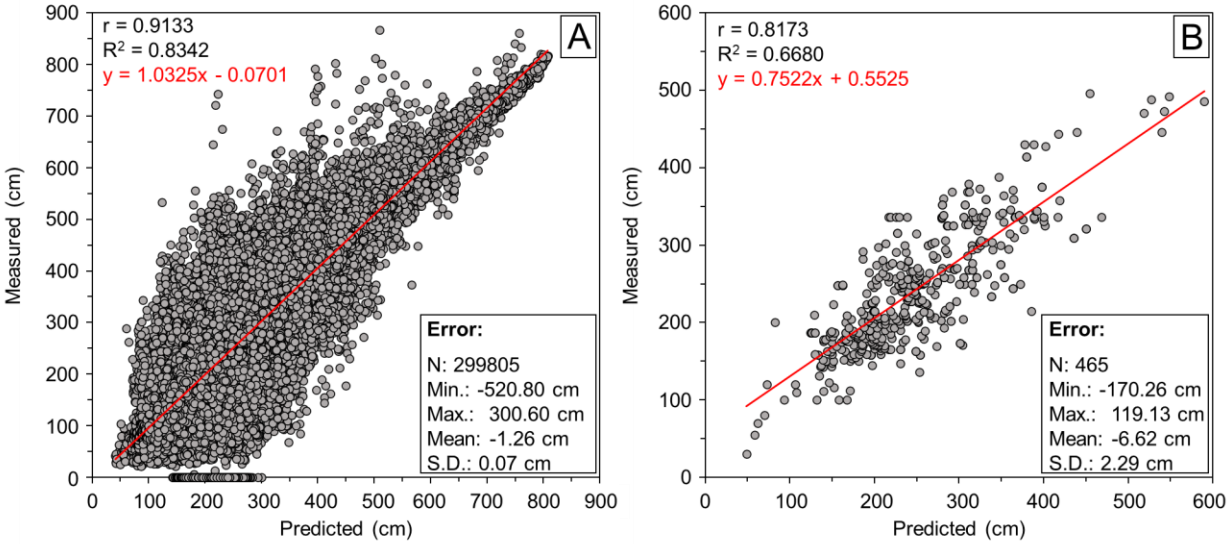

Figure 4.6. (a) Relationships between matte thicknesses measured with seismic data and predicted by kriging method and (b) relationship between matte thicknesses measured with ground-truthing data and predicted by kriging method.

The sector 2A is characterized by a very important extension of the meadow towards the open sea due to a very gentle slope (the -40 m isobath is generally more than 5 km away from the coast). In this area, the matte thickness ranged between 100 and 700 cm (Fig. 4.7.a). The thickest matte deposits were observed from the upper limit of the seagrass meadow to the 20-25 m bathymetric range (200-700 cm), notably near the mouth of the Golo river (up to 300 cm of matte). Occasionally, higher matte thicknesses were recorded in the easternmost deep part of the Golo submarine delta (-30 m to the lower limit of the *P. oceanica* meadow) (Fig. 4.7.a). In sectors 2B and 2C, characterized by a narrower eastern continental shelf, significant matte deposits up to 500 cm-thick were also observed (Fig. 4.7.b; Fig. 4.7.c). The highest matte thicknesses (>250 cm) recorded in sector 2B were observed in the shallower part (5 to 20 m depth) near the mouth of the Fium'Alto river (Fig. 4.7.b). In sector 2C, the thickness of *P. oceanica* deposits showed a highly heterogeneous distribution of values but the presence of high matte thicknesses (250-500 cm) was revealed in deeper areas (>20 m depth) off river mouths (*e.g.* Alesani and Bravona rivers; Fig. 4.7.c). The extension of the meadow up to 5 km from the coast corresponds to a widening of the eastern platform in sectors 2D (Fig. 4.7.d). This sector is notably characterized by the higher matte thickness observed on the prediction map (800 cm; Fig. 4.7.d). Likewise, highest matte thicknesses were located at the shallower depth range (10 to 20 m depth) near the Urbino lagoon outlet. However, significant matte thicknesses were not only limited to shallow waters on this sector.

The prediction map contributed to identify major matte heights in deeper areas (>25 m depth) between the Diana lagoon and the Tavignano estuary (Fig. 4.7.d).

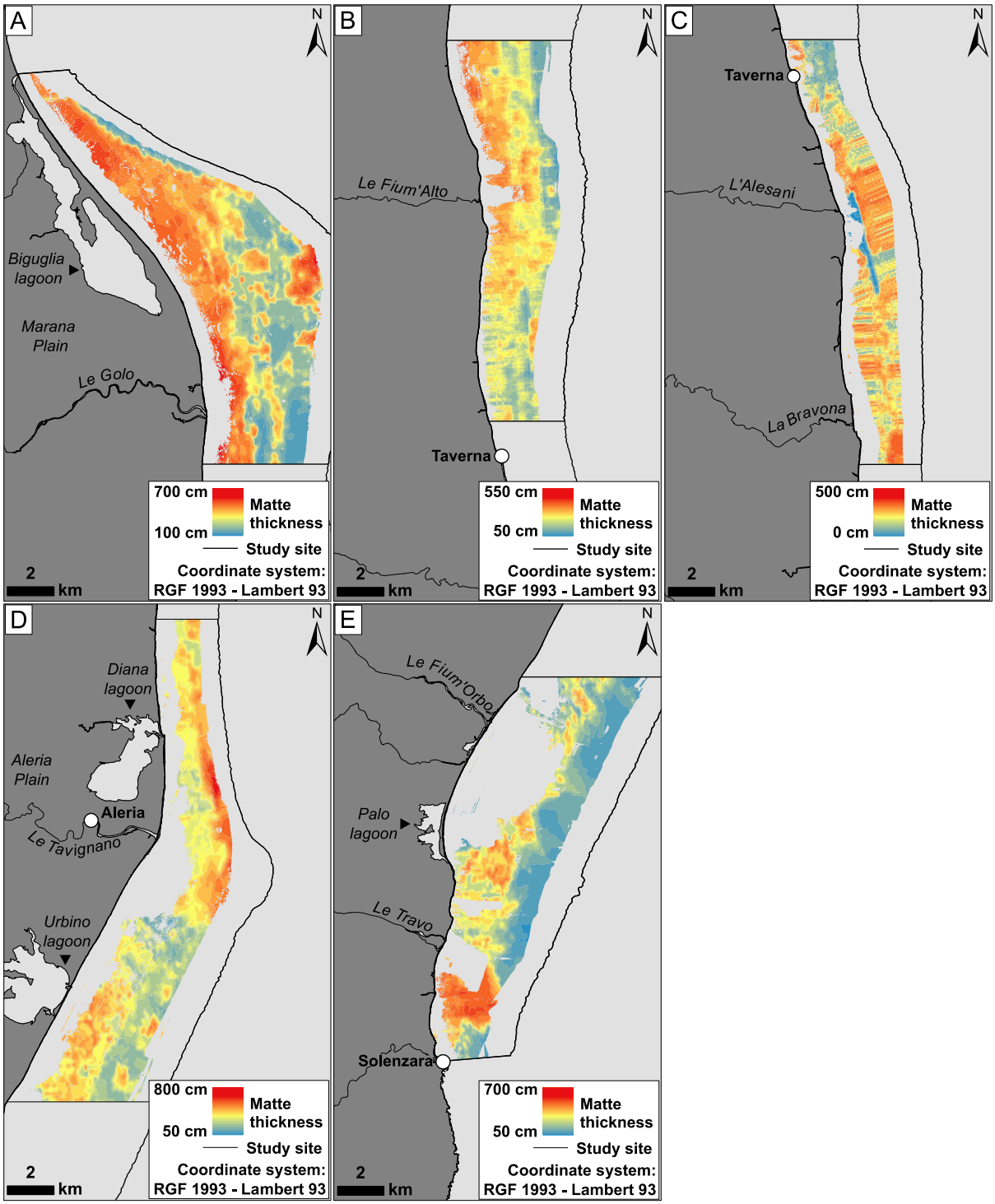

Figure 4.7. (a) Prediction map of the *Posidonia oceanica* matte thickness in sector 2A, (b) sector 2B, (c) sector 2C, (d) sector 2D and (e), sector 2E.

Finally, the *P. oceanica* meadow of the sector 2E, characterized by a decrease in its extension off the Fium'Orbo river estuary, exhibited matte thicknesses between 50 and 700 cm (Fig. 4.7.e). The highest matte deposits occurred near the coast notably between the Travo river and Solenzara river estuaries. Prediction map has also highlighted a continuous and linear section parallel to the bathymetric isobaths (25-40 m depth range) defined by thinner mattes (<200 cm).

When considering the thickness of the *P. oceanica* matte and the surface occupied by each category, the minimum, maximum and mean volumes of matte were calculated for each sector (Appendix A4) and for the entire site (Table 4.3). In total, the matte volume was estimated between 354.1 and 453.0 million m^3 with in average of 403.5 ± 49.4 million m^3 (Table 4.3). In the investigated site, approximately 53.2% of the total volume of matte (214.5 ± 40.7 million m^3) was represented by the 2.0-3.0 m matte thickness (Table 4.3). Among the different sector, sectors 2D and 2E showed the highest matte volumes (104.9 ± 10.1 million m^3 and 103.8 ± 9.6 million m^3, respectively), the lowest volumes being recorded for the sector 2C (66.2 ± 6.6 million m^3) (Appendix A4).

Table 4.3. Surface and volumes occupied by each categories of matte thickness in the study site.

Matte thickness (m)	Surface (km^2)	Minimum Volume ($\times 10^6$ m^3)	Maximum Volume ($\times 10^6$ m^3)	Mean Volume ($\times 10^6$ m^3)	± S.E. ($\times 10^6$ m^3)
0 - 0.5	0.3	0.0	0.2	0.1	0.1
0.5 - 1.0	0.6	0.3	0.5	0.4	0.1
1.0 - 1.5	10.9	10.9	10.4	10.7	0.2
1.5 - 2.0	40.4	52.3	64.3	58.3	6.0
2.0 - 2.5	61.7	88.9	139.6	114.2	25.4
2.5 - 3.0	45.0	84.9	115.6	100.3	15.3
3.0 - 3.5	25.8	58.6	66.7	62.6	4.0
3.5 - 4.0	9.5	24.4	26.6	25.5	1.1
4.0 - 4.5	4.5	12.2	14.3	13.3	1.1
4.5 - 5.0	2.4	7.8	6.7	7.2	0.6
5.0 - 5.5	1.7	6.8	3.4	5.1	1.7
5.5 - 6.0	0.9	4.4	1.7	3.0	1.3
6.0 - 6.5	0.3	1.4	1.4	1.4	0.0
6.5 - 7.0	0.1	0.6	0.9	0.7	0.2
7.0 - 7.5	0.1	0.4	0.4	0.4	0.0
7.5 - 8.0	0.0	0.3	0.3	0.3	0.0
Total	204.2	354.1	489.1	403.5	49.4

4.4. Discussion

The high-resolution seismic reflection method has confirmed to be a reliable and powerful tool to size the potential thickness and volume of the matte underneath *P. oceanica*. The use of this non-destructive geophysical method has contributed in imaging the sedimentary structure of the matte of *P. oceanica* meadows over than 1300 km of profiles along the eastern coast of Corsica. Although the vertical resolution of the EDO-Western ED 248 sub-bottom profiler has allowed to detect thin matte deposits (Monnier *et al*., 2020), the main limitation is related to the detection of very low matte thicknesses. Thus, the delimitation of thin matte deposits located in the upper and lower limits of the *P. oceanica* meadow and below sand patches (*i.e.* intermattes) remains very difficult during interpretation on seismic data. Inversely, the use of the high-resolution non-linear parametric echosounder Innomar SES-2000 compact system has provided seismic records imaging with high vertical resolution (<10 cm). The detection of small impedance variations in the seagrass sediment by the Innomar SES-2000 lies notably in the parametric effect and its ability to produce two high frequencies (8 kHz) (Grant and Schreiber, 1990; Spieß, 1993; Hamilton and Blackstock, 1998). Such seismo-acoustic prospection has been already applied with success to size *P. oceanica* matte deposit (Lo Iacono *et al*., 2008; Tomasello *et al*., 2009; Blouet *et al*., 2014). In this study, seismo-acoustic dataset has contributed to validate the presence of small matte heights in the upper limit of the *P. oceanica* meadow but also settled on rocky substrate characterized by strong reflection (Fig. 4.2.c). In some case, the reflectivity between two sediment layers provided not enough acoustic impedance contrast to generate strong seismic reflectors due to velocity and density contrasts inherent in seafloor sediments (Crutchley and Kopp, 2018). Thus, the heterogeneous composition coupled to the vertical degradation of the matte over millennia result in difficulties in associating the structure of the matte with specific seismic facies (Lo Iacono *et al*., 2008).

Despite these limitations, matte thickness predicted throughout the investigated site showed to be significantly related to the original seismic dataset and ground-truthing measures (Fig. 4.5.a, Fig. 4.6.a; Fig. 4.6.b). The vertical thickness of these deposits appeared to be highly consistent with values recorded throughout the Mediterranean (Molinier and Picard, 1952; Mateo *et al*., 1997; Lo Iacono *et al*., 2008; Serrano *et al*., 2012, 2014, 2016a).

Although this deposit is one of the largest examples of carbon stocks in seagrass ecosystems (Fourqurean *et al*., 2012), organic accumulations were also recorded for other seagrass species (*e.g. Posidonia australis*: Shepherd and Sprigg, 1976; Rozaimi *et al*., 2016; Serrano *et al*., 2016a; *Thalassodendron ciliatum*: Lipkin, 1979; Colin, 2018). Similarly, accreted carbon-rich deposits reaching 1 m to over 10 m thick were also observed for other blue carbon ecosystems like mangroves (Woodroffe *et al*., 1993; McKee *et al*., 2007; McKee, 2010; Kauffmann *et al*., 2014, 2016; Sanders *et al*., 2016) and tidal salt marshes (Scott and Greenberg, 1983; Wood, 1991; Chmura *et al*., 2003; Johnson *et al*., 2007; Drexler *et al*., 2011). In terrestrial ecosystems, organic carbon deposits reaching several meters in thickness were recorded for peatlands (Clymo, 1992; Agus *et al*., 2011; Hribljan *et al*., 2016; Silvestri *et al*., 2019) and permafrost (deposits of organic-rich frozen loess) where 90 m thick accumulation have been observed in Siberia (Botch *et al*., 1995; Smith *et al*., 2004; Zimov *et al*., 2006).

According to the curve of the Holocene sea level change predicted along the Corsican (Vacchi *et al*., 2017b) and western Mediterranean coasts (Vacchi *et al*., 2016), the relative sea level was placed ~10.0 m (8000 cal. yr BP) and ~4.0 below the present mean sea level in the late Neolithic period (~6000-5000 cal. yr BP). During the Holocene, no major isostatic highstand was reported in this sector of the Mediterranean and since the last interglacial, the Sardinia-Corsica block remained tectonically stable (Lambeck and Purcell, 2005; Ferranti *et al*., 2006; Antonioli *et al*., 2009; Vacchi *et al*., 2016). Thus, assuming that seagrass meadows were located at the same position since the mid-Holocene, the radiocarbon dating of the basal part of matte deposits were coherent with the evolution of the relative sea level. This is confirmed by the higher age of the matte at 20 m than at 10 m depth for the top 30 cm and 100 cm of sediment (Fig. 4.3). The maximum thicknesses of matte found in the investigated site were also in accordance with the maximum potential thickness of *P. oceanica* seagrass mattes estimated between 8 and 13 m by Serrano *et al*. (2016a). The spatial prediction map has underlined also a high variability in the thickness of the matte throughout the site. This vertical accumulation of organic rich material in the *P. oceanica* matte results of the balance between the seagrass production and seagrass decomposition, sedimentation and erosion (Mateo *et al*., 1997, 2006; Pergent *et al*., 1997; Gacia *et al*., 2002). Here, the SAR based on the chronostratigraphic age-depth models show a strong variability even in nearby stations (*e.g.* TM-20-α was five-fold higher than TM-20-β, only 25 m away). Analogous spatial and temporal

differences in SAR of matte were also recorded by Mateo *et al*. (1997) and Serrano *et al*. (2012) in nearby station. This irregularity in SAR of seagrass meadows from one station to another have proven to be influenced by the complex interactions of multiple factors from regional to local scales (*e.g.* productivity, density and meadow cover, exposure to hydrodynamic energy, sedimentation; Mateo *et al*., 1997; Serrano *et al*., 2016b; Belshe *et al*., 2018). The SAR and the accumulation of C_{org} in the belowground part of seagrass meadows are mainly affected by light attenuation (*i.e.* irradiance) closely related to water depth influencing the photosynthetic activity (net primary production), morphology, shoot density and growth of seagrass meadows (Pergent *et al*., 1994; Alcoverro *et al*., 2001; Collier *et al*., 2007; Serrano *et al*., 2014). Indeed, greater trapping and retention of fine sediment particles enhancing soil accumulation (Serrano *et al*., 2016b) are highly related to the structure of the canopy and, specially, to shoot density and meadow cover (Jeudy de Grissac and Boudouresque, 1985; Boudouresque and Jeudy de Grissac, 1983; De Falco *et al*., 2000; Gacia and Duarte, 2001). The effects of water turbidity in coastal and estuarine areas evidenced by several shading experiments have proven to cause comparable effects as to those of a water depth gradient (Duarte *et al*., 1991; Ruiz and Romero, 2001; Samper-Villarreal *et al*., 2016). However, high availability of fine-grained suspended particles from the water column can potentially lead to a greater accumulation of allochthonous material of seagrass soils and offset the reduction in autochthonous inputs from the seagrass meadows (Samper-Villarreal *et al*., 2016). Hydrodynamic energy and marine currents play also a role in the SAR of seagrass meadows by determining the patterns of sedimentation and erosion (Mazarrasa *et al*., 2017, 2018; Serrano *et al*., 2016b). Thus, lower exposure to waves and marine currents results in a higher accumulation of allochthonous fine sediment particles in seagrass meadow. This higher deposition of fine sediments compared to medium and coarse sands in sheltered meadows contribute to a greater preservation of belowground biomass after burial (Keil and Hedges, 1993; Burdige, 2007) and reducing the remineralization of organic material stored due to lower oxygen exchange and redox potentials (Mateo *et al*., 2006; Pedersen *et al*., 2011).

In this study, the higher matte thickness observed in shallow waters (Fig. 4.5.a; Figs. 4.7) could be attributed to the higher SAR recorded near the coast (10 m depth; Fig. 4.3). Analogously, these conditions may also contribute to higher burial and lower decay rates of the belowground biomass in shallow depths (Serrano *et al*., 2014; 2016a; 2016b). Higher

matte accumulation rates were also evidenced in shallow waters throughout the Mediterranean Sea by compiling the available data (Fig. 4.8). The occurrence of patterns in SAR with water depth were also observed in *Posidonia sinuosa* (Serrano *et al*., 2014) and *Posidonia australis* meadows (Serrano *et al*., 2016a). However, though the SAR of matte appears to be highly related to water depth, more contrasting results are observed as influenced by the depositional environment. While massive matte deposits (>3 m) are found near the river estuaries (Golo, Tavignano and Travo) and locally next to lagoon outlets (Diana, Urbino and Palo), estuarine stations exhibited in average a two-fold lower SAR than open sea stations (Fig. 4.3).

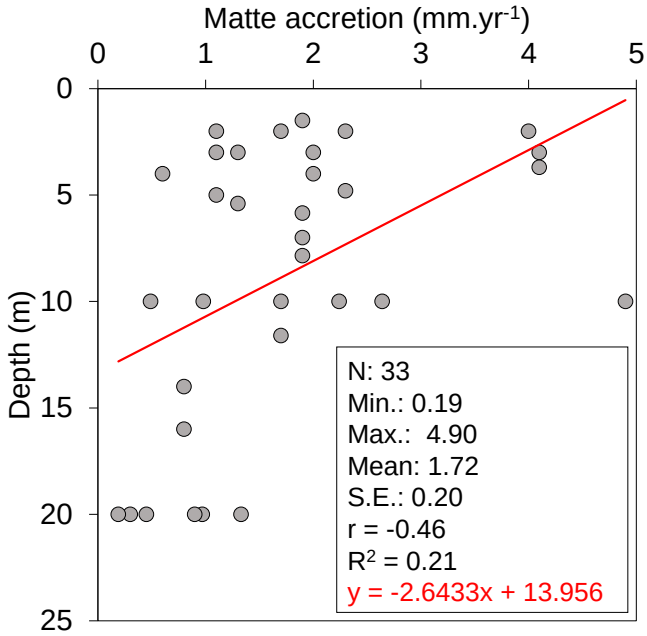

Figure 4.8. Compilation of available data on matte accretion rates of *Posidonia oceanica* meadow according to depth recorded in the Mediterranean basin. Data from Romero *et al*., 1994; Mateo *et al*., 1997, 2005; Lo Iacono *et al*., 2008; Serrano *et al*., 2012, 2014, 2016a; this study).

The distribution of *P. oceanica* seagrass meadows on the eastern coast of Corsica are mainly influenced by the water depth in the lower limit and, by exposure to physical disturbance (*i.e*. waves and marine currents) and by lower salinity of coastal waters resulting from land-based freshwater inputs (*i.e.* rainfall and river flow) in its upper limit. Thus, the significant thickness of matte observed near estuaries was found generally at a greater distance from the coast (and consequently water depth) than open sea meadows. These estuary meadows are influenced by a higher water turbidity has been evidenced by the

greater content in mud fraction found in cores collected near river estuaries. This higher deposition of fine sediment particles typically contributes to a better preservation of the organic deposits after burial and, concomitantly to the formation of larger C_{org} sedimentary deposits as observed in these sectors compared to those in more exposed stations such as open sea meadows (Serrano *et al*., 2016b; Mazarrasa *et al*., 2018). Indeed, the very disturbed geomorphology and sea bottom topography (*i.e.* submarine sand barriers; Guennoc *et al*., 2001; Pluquet, 2006) coupled to the high density naturally-induced matte escarpments and sand patches observed in open sea meadow (Abadie *et al*., 2015; Monnier *et al*., 2020) suggest a greater influence of wave energy and marine currents in these stations. Exposed meadows are more susceptible to hydrodynamic action and erosion, resulting in higher export rates, higher aeration of the soil (Burdige, 2007; Serrano *et al*., 2016b), and in lower sedimentation of fine allochthonous particles (Mateo and Romero, 1997) all together factors leading to a lower sedimentary C_{org} accumulation. This hypothesis seems to be confirmed by the lower age observed for the first meter of matte in open sea meadows (1510 ± 691 cal. yr BP) respect to those near estuaries (2234 ± 1035 cal. yr BP; Fig. 4.3).

Global estimates of the contribution of vegetated coastal ecosystems to mitigate climate change necessitate knowledge about the spatial extent and distribution of ecosystems involved in the sequestration and storage of blue carbon in their sediments (Pergent *et al*., 2012; Howard *et al*., 2014a; Lovelock and Reef, 2020). The mapping of seagrass meadows achieved in the last decades along the eastern coast of Corsica (Pergent-Martini *et al*., 2015; Valette-Sansevin *et al*., 2019) coupled to the large-scale prediction of matte thickness performed in this study has allowed to perform the widest estimation of the potential size occupied by the blue carbon stocks associated to *P. oceanica*. The matte edification index (MEIx; Tomasello *et al*., 2009), obtained by the ratio between the amount of matte (403.5 million m^3; Table 4.3) and the surface occupied by these structure within the investigated site (204.2 million m^2; Table 4.3), correspond to a mean value estimated at ~2.2 m^3 m^{-2} which appears to be closely similar to the mean matte thickness recorded in this study (Fig. 4.4). This ratio is also comparable to the results obtained in the Gulf of Palermo (~1.6 m^3 m^{-2}) by Tomasello *et al*. (2009) but still well below the value recorded in Portlligat (5.0 m^3 m^{-2}) by Lo Iacono *et al*. (2008). Based on the average thickness of matte (251.9 cm; Fig. 4.4) and the average C_{org} content in the matte of *P. oceanica* meadows (75 ± 13 kg C_{org} m^{-2} for the top 247

± 36 cm of matte; Serrano *et al*., 2016a), the total C_{org} stock in the study area could be estimated at 15.6 ± 2.2 million t C_{org}. This estimation of the total C_{org} accumulation confirms the significant role played by *P. oceanica* seagrass meadows in the storage of blue carbon in Mediterranean coastal sediments. In future studies, a complete analysis of the sediment cores collected in the matte during the Carbonsink oceanographic surveys should provide a more accurate spatio-temporal characterization of carbon stocks and fluxes associated with the *P. oceanica* meadows. The results obtained in this study using high-resolution seismic reflection method has proven to be a powerful, non-destructive technology to size the potential thickness and volume of the matte accumulated by *P. oceanica* since the mid-Holocene. The application of this marine geophysical method has also put in evidence the necessity to perform large-scale survey to properly assess the extent of the highly variable carbon stocks beneath seagrass meadows worldwide and their contribution in the mitigation of climate change.

Chapitre 5

Large-scale estimate of carbon stocks and fluxes associated with a *Posidonia oceanica* meadow (Corsica, NW Mediterranean)

Abstract

In the last decades, the increasing necessity to reduce atmospheric carbon dioxide (CO_2) concentrations has recently intensified interest in quantifying the capacity of coastal ecosystems to sequestered carbon referred commonly as 'Blue Carbon' (BC). Among coastal habitats, seagrass meadows are considered as important natural carbon sinks due to their capacity to store large amount of carbon over long period of time in their sediments. However, the spatial heterogeneity of carbon burial and storage in seagrass sediments needs to be better understood to improve accuracy of BC assessments, particularly when high a high environmental variability is present. In the Mediterranean Sea, *Posidonia oceanica* (L.) Delile constitutes extensive meadows considered as long-term carbon sinks due to the development of an outstanding structure known as 'matte', reaching several meters thick in height and which can be preserved over millennia. In order to estimate the contribution of *P. oceanica* meadows to the climate change mitigation, an estimate of carbon stocks has been conducted in the Natura 2000 area 'Grand Herbier de la Côte Orientale' in Corsica (France, NW Mediterranean). This experimental approach is mainly based on the collection and the biogeochemical analysis of 39 sediment cores. The results showed a high variability in the organic and inorganic carbon (C_{org} and C_{inorg}, respectively) stocks and fluxes within study site. Estimates of C_{org} and C_{inorg} stocks (mean: 327 ± 150 t ha^{-1} and 245 ± 45 t ha^{-1}, respectively), show high variability related to water depth, sedimentary matrix (sandy *vs* rocky substrate) or the depositional environment (open sea *vs* estuary). Isotopic signature ($\delta^{13}C$) allowed to reveal a substantial contribution of allochthonous inputs of organic matter (macroalgae and sestonic sources) mainly in estuarine environment and shallow areas. Overall estimates of the amount of carbon stored over the first 250 cm of matte (average thickness at site level) were estimated between 4.5 and 13.2 million t C_{org}. By converting these results into CO_2 equivalent (CO_{2e}), the quantities thus trapped would correspond to 16.5 and 48.3 million t CO_{2e}, the equivalent of 9.4 to 27.4 years of CO_2 release from the entire population of Corsica. Extrapolation of data to the regional scale shows that seagrass meadows would have stored the equivalent of 26.6 to 72.0 years of CO_2 release.

5.1. Introduction

The implementation of reduction strategies of atmospheric greenhouse gas (GHG) and notably carbon dioxide (CO_2) is a crucial step for meeting the objectives of the Paris Agreement (UNFCCC, 2016) and for climate change mitigation. In the last decades, the emission reduction strategy instigated to reduce CO_2 concentrations and mitigate climate change combine the reduction of anthropogenic emissions sources with natural-based approaches promoting conservation and restoration of world's ecosystems recognized as major natural CO_2 sinks (Herr *et al*., 2017). Among them, 'Blue Carbon' initiatives have been dedicated to the protection and the restoration of coastal and marine vegetated ecosystems contributing to the sequestration and the storage of organic carbon referred commonly as 'Blue Carbon' (BC) (Laffoley and Grimsditch, 2009; Nellemann *et al*., 2009). Coastal vegetated ecosystems, mainly tidal marshes, mangroves forests and seagrass meadows, are among the most productive habitats on Earth (Duarte *et al*., 2005). Although these ecosystems represent less than 1% of the world's ocean surface, they are particularly effective in the capture of CO_2 from atmosphere and its sequestration as organic carbon in their sediments for long-term period. The organic carbon sequestration rates in BC ecosystems soils are 30- to 50-fold greater than those of many terrestrial ecosystems (Mcleod *et al*., 2011; Duarte *et al*., 2013) contributing to the storage of large amount of carbon in coastal areas and the formation of significant natural carbon sinks (Chmura *et al*., 2003; Fourqurean *et al*., 2012; Atwood *et al*., 2017).

Seagrass meadows occur in a wide range of habitat types (from marine to estuarine environments) along the shores of all continents except in Antarctica, from intertidal and shallow waters to maximum depths of up to 50 m (Hemminga and Duarte, 2000; Carruthers *et al*., 2007). Seagrass meadows are highly productive ecosystems (Duarte and Chiscano, 1999) and provide key ecological functions and services of high value in comparison with other marine and terrestrial habitats (Costanza *et al*., 1997). Since the early 1980s, these ecosystems have been recognized for accumulating amounts of organic carbon (C_{org}) of potential global significance (Smith, 1981). In the context of climate change mitigation, the necessity to reduce CO_2 concentrations has intensified the interest in quantifying the capacity of seagrass meadows to store C_{org} (Duarte *et al*., 2005, 2010, 2013; Mcleod *et al*., 2011; Fourqurean *et al*., 2012; Serrano *et al*., 2012, 2016, 2016a, 2016b; Lavery *et al*., 2013; Miyajima *et al*., 2015;

Gullström *et al*., 2018). Although seagrass meadows occupy a relatively small area of the ocean surface (~0.2%; 160 000-600 000 km^2), their C_{org} accumulation rates range from 48 to 112 Tg C_{org} yr^{-1} representing almost 10-18% of the total carbon burial in the ocean sediment (Duarte *et al*., 2005, 2013; Kennedy *et al*., 2010; Mcleod *et al*., 2011; McKenzie *et al*., 2020). Through their high C_{org} burial rates, seagrass ecosystems worldwide constitute large organic carbon stocks estimated in the top meter of sediment from 4.2 to 8.4 Pg C_{org} (Fourqurean *et al*., 2012). Unlike terrestrial ecosystems where C_{org} stocks are mainly found in living biomass and preserved for decades or centuries, the C_{org} stored by seagrass meadows in their sediments could be preserved over millennia (Mateo *et al*., 1997; Nellemann *et al*., 2009; Serrano *et al*., 2012; Howard *et al*., 2014a). The long-term carbon sinks constituted by seagrass meadows result from both the direct accumulation in the sediment matrix of C_{org} from autochthonous sources (*i.e.* seagrass belowground tissues and detritus) and allochthonous sources (*i.e.* macroalgae, epiphytes and suspended particulate organic matter – SPOM, terrestrial inputs) (Gacia and Duarte, 2001; Kennedy *et al*., 2010).

The sequestration and the preservation of C_{org} over long time period in seagrass soils is mainly related to (i) the seagrass meadow productivity and biomass accumulation, (ii) the sediment accretion rates resulting from the trapping of fine allochthonous particles by seagrass canopies, (iii) the biogeochemical composition and the proportion of degradation-resistant organic compounds stored (*e.g.* lignin and cellulose) and, (iv) the anoxic conditions promoting a slow microbial decomposition in the sediments (Klap *et al*., 2000; Mateo *et al*., 2006; Hendriks *et al*., 2008; Serrano *et al*., 2016b; Mazarrasa *et al*., 2018). The research efforts undertaken in the last decades have demonstrated a high variability in the sedimentary C_{org} stocks of seagrass ecosystems worldwide (Lavery *et al*., 2013; Miyajima *et al*., 2015; Mazarrasa *et al*., 2017). This variability in the accumulation and storage of C_{org} has been associated to the interactions of multiple biotic and abiotic factors as seagrass species characteristics (*e.g.* density, cover and biomass productivity; Lavery *et al*., 2013; Miyajima *et al*., 2015; Serrano *et al*., 2016b), water depth and light availability (*e.g.* Mateo *et al*., 1997; Serrano *et al*., 2014, 2016b), hydrodynamic exposure and turbidity (*e.g.* Samper-Villareal *et al*., 2016; Mazarrasa *et al*., 2017), geomorphological settings (*i.e.* landscape configurations; Ricart *et al*., 2015, 2017; Gullström *et al*., 2018) and depositional environments (*i.e.* fluvial inputs; Kennedy *et al*., 2010; Ricart *et al*., 2020).

The recognition of seagrass meadows as carbon sinks in coastal areas has focused the effort in quantifying their capacity to sequester and store C_{org}. However, inorganic carbon (C_{inorg}) provided by calcifying organism associated with seagrass habitats and buried in their sediments represent a substantial carbon stock which may exceed C_{org} (Mazarrasa *et al*., 2015). The production of C_{inorg} through calcification process may represent a source of CO_2 to the atmosphere, with a ratio of ~0.6 mol of CO_2 emitted per mol of $CaCO_3$ precipitated (Ware *et al*., 1992; Frankignoulle *et al*., 1994; Gattuso *et al*., 1998; Smith, 2013). Recently, these ecosystems have been also highlighted for the significant sequestration of C_{inorg} imported from adjacent ecosystems like coral reefs or terrestrial lithogenic sources (Saderne *et al*., 2019). The global annual burial of $CaCO_3$ in seagrass sediments ranged between 12 and 62 Tg C_{inorg} yr^{-1} is mainly supported by tropical meadows (~90%; Saderne *et al*., 2019) and constituted substantial C_{inorg} carbon stocks estimated between 11 and 39 Pg C_{inorg} (Mazarrasa *et al*., 2015). Thus, understanding the amount and the source of carbonate in seagrass ecosystems is crucial to determine the role as carbon sink or carbon source (Mazarrasa *et al*., 2015; Macreadie *et al*., 2017; Gullström *et al*., 2018; Saderne *et al*., 2019).

In the Mediterranean Sea, the endemic seagrass species *Posidonia oceanica* (Linnaeus) Delile constitutes extensive meadows considered as a unique carbon sink due to the development of an outstanding structure known as “matte” (Molinier and Picard, 1952). This complex belowground formation, composed of intertwined rhizomes, roots and leaf sheaths embedded in the sediment, exhibits a very low decay rate in relation with the highly refractory nature of the organic matter and the anoxic conditions (Romero *et al*., 1992; Mateo *et al*., 1997, 2006; Kaal *et al*., 2018). The accretion of organic material in coastal sediments beneath the *P. oceanica* meadows constitutes one of the largest carbon sinks in coastal areas worldwide which can reach several meters in height and remain over millennia (Lo Iacono *et al*., 2008; Serrano *et al*., 2012). The global importance of *P. oceanica* meadows as a long-term carbon sink have been widely recognized due to the formation of large carbon stocks and their high distribution in the Mediterranean Sea (Romero *et al*., 1994; Mateo *et al*., 1997, 2006; Serrano *et al*., 2012, 2014, 2016a).

However, estimates of carbon stocks beneath *P. oceanica* seagrass meadows are directly based on the analysis of a relatively low number of sediment cores at a very limited number of sites therefore, not accounting for the potential spatial variability in seagrass sedimentary carbon stocks (Mateo *et al*., 1997; Lo Iacono *et al*., 2008; Serrano *et al*., 2012, 2014, 2016a; Fourqurean *et al*., 2012). The works performed in the last decade have emphasized the necessity to improve the global estimates of carbon stocks and fluxes (i) by increasing the number of direct measurements in seagrass sediments and (ii) by accounting for biogeochemical factors driving variability within habitats (Pergent *et al*., 2012, 2014; Mazarrasa *et al*., 2018). For this purpose, the current study aimed (i) to understand the spatial variability in the sequestration and the storage of C_{org} and C_{inorg} in the matte of a *P. oceanica* meadow located in the eastern coast of Corsica, (ii) to identify the factors which enhance or diminish the burial and storage of carbon in the sediments at the site-level and (iii) to provide a global estimate of the C_{org} and C_{inorg} stored.

5.2. Material and methods

5.2.1. Study site

This study was conducted in the eastern continental shelf of Corsica Island (France, NW Mediterranean Sea; Fig. 5.1.a; Fig. 5.1.b). This large geographical area was selected because it presents a wide range of environmental conditions (Table 5.1).

The study was mainly conducted in the Natura 2000 area, "FR9402014 - Grand Herbier de la Côte Orientale", located between the mouth of the Biguglia lagoon in the north and the mouth of the Solenzara river in the south (Meinesz *et al*., 1990). The site stretches along 106 km sandy coast and is characterized by the presence of multiple lagoons (*e.g.* Biguglia, Diana, Urbino, Palo) and by freshwater inputs from the main coastal rivers of Corsica (*e.g.* Golo, Tavignano, Travo; Cannac-Padovani *et al*., 2014). This site hosts one of the largest *P. oceanica* meadows in the Mediterranean Sea, covering a surface area of 20 425 ha (Fig. 5.1.c), what represents 52% of the sea bottom between 0 and 50 depth (Valette-Sansevin *et al*., 2019). This continuous meadow grows on a sandy substrate and is influenced by local high-energy hydrodynamic currents as suggested by the presence of frequent intermattes (Abadie *et al*., 2015).

Others investigations were performed between the Solenzara mouth in the north and the gulf of Porto-Vecchio in the south (Fig. 5.1.c). This area occurred along a 25 km rocky coast and is constituted by a succession of small pocket beach and bays. The irregular topography of the sea bottom is mainly dominated by hard substrate with infralittoral photophilous algae and *P. oceanica* seagrass meadows. Influence of nearshore high exposure to hydrodynamic energy and wave action in the *P. oceanica* meadow was evidenced by the presence of erosive structure as 'return rivers' (*i.e.* sand channel parallel to the coast; Boudouresque and Meinesz, 1982) and the presence of meadows from ca. 10 meters below the sea level (Vacchi *et al*., 2016). Geomorphology and the slope of the continental shelf along this sector limited the meadow extension toward the open sea (20-25 meters depth; Pluquet, 2006).

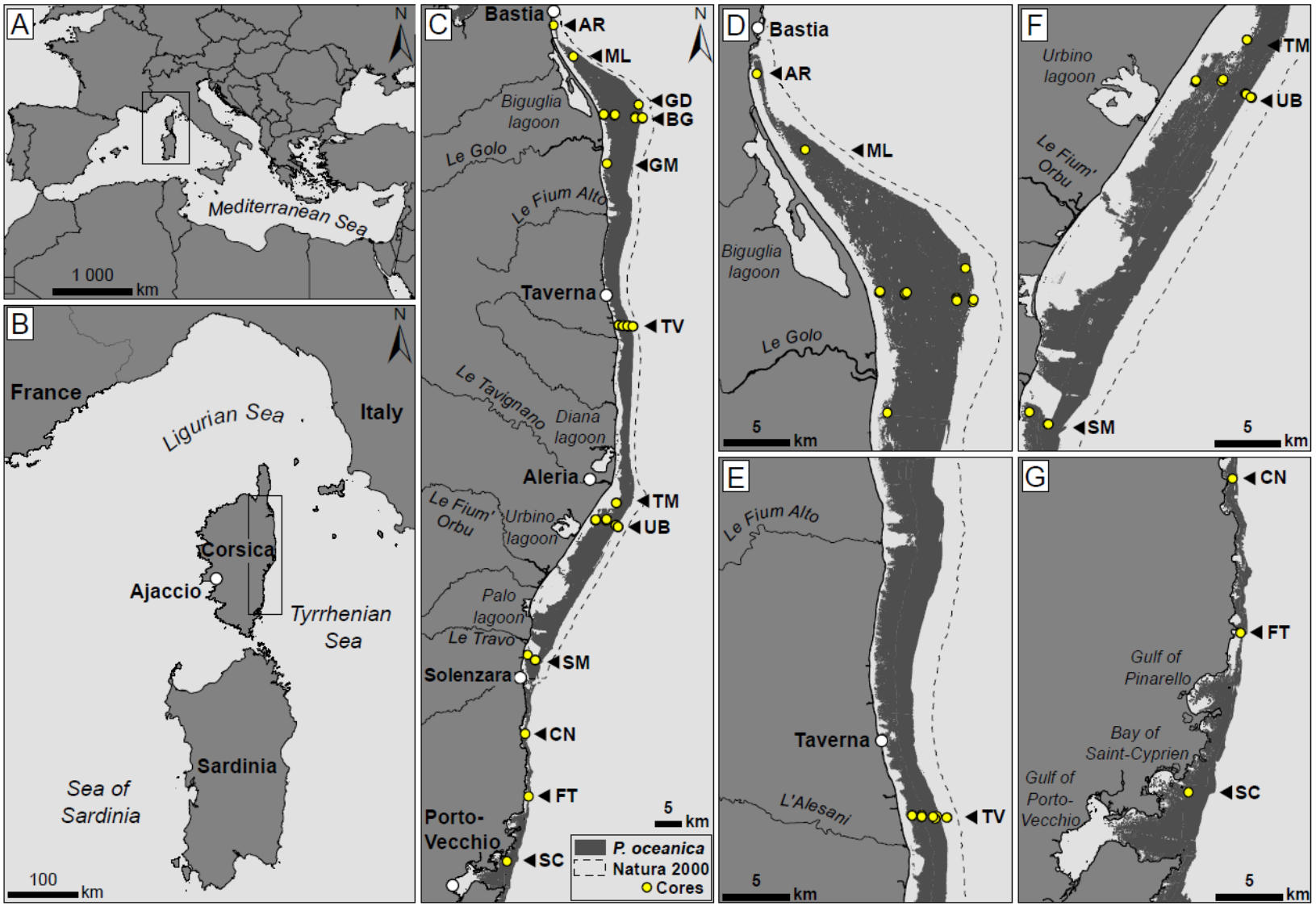

Figure 5.1. Location of the area of study on the eastern continental shelf of Corsica island (a, b), distribution of the biocenosis of the *Posidonia oceanica* meadow and location of the sampling stations (c, d, e, f, g).

Table 5.1. Geographical location and environmental features of the studied *P. oceanica* meadows. Substrate type was determined from the analyses performed on the sediment cores. The depositional influence of each investigated meadows was determined by calculating the distance to the nearest major river mouth (Class 1 to 3) defined by the French hydrographic network (BD CARTHAGE®). Estuary: <3.5 km; Open sea: >3.5 km.

Location	Lab code	Coordinates		Replicates	Depth (m)	Substrate	Depositional influence
Arinella	AR-15	42°40'32"N	9°27'80"E	1	15.0	Medium sand	Open sea
Marana lido	ML-20	42°38'13"N	9°29'70"E	1	10.0	Fine to coarse sand	Open sea
Biguglia	BG-10	42°33'53"N	9°32'12"E	3	10.0	Medium sand to gravel / pebbles	Open sea
	BG-20	42°33'52"N	9°33'14"E	3	20.0	Coarse sand to gravel / pebbles	Open sea
	BG-30	42°33'41"N	9°35'22"E	3	30.0	Fine to medium sand / rhodoliths	Open sea
	BG-40	42°33'36"N	9°36'20"E	2	40.0	Medium to coarse sand / rhodoliths	Open sea
Golo mouth	GM-10	42°30'13"N	9°32'30"E	1	10.0	Fine to medium sand / pebbles	Estuary
Golo delta	GD-40	42°34'37"N	9°35'43"E	1	40.0	Fine to coarse sand	Open sea
Taverna	TV-10	42°18'70"N	9°33'42"E	3	10.0	Coarse sand / pebbles	Open sea
	TV-20	42°18'50"N	9°34'60"E	3	20.0	Coarse sand to gravel / pebbles	Open sea
	TV-30	42°18'40"N	9°34'36"E	3	30.0	Medium sand	Open sea
	TV-40	42°18'30"N	9°35'70"E	2	40.0	Fine to medium sand	Open sea
Tavignano mouth	TM-20	42°04'47"N	9°33'27"E	3	20.0	Sandy mud to fine sand	Estuary
Urbino	UB-10	42°03'31"N	9°31'21"E	3	10.0	Medium to coarse sand / pebbles	Open sea
	UB-20	42°03'31"N	9°32'27"E	3	20.0	Medium to coarse sand / pebbles	Open sea
	UB-30	42°03'80"N	9°33'24"E	3	30.0	Fine to medium sand	Open sea
	UB-40	42°03'10"N	9°33'39"E	3	40.0	Fine to medium sand	Open sea
Solenzara mouth	SM-10	41°53'21"N	9°24'30"E	1	10.0	Fine to medium sand	Estuary
	SM-20	41°52'58"N	9°25'15"E	3	20.0	Mud to fine sand	Estuary
Canella	CN-10	41°47'24"N	9°24'14"E	1	10.0	Gravel to rock	Open sea
Fautea	FT-10	41°42'40"N	9°24'34"E	1	10.0	Rock	Open sea
Saint Cyprien	SC-10	41°37'47"N	9°22'26"E	1	10.0	Gravel to rock	Open sea

5.2.2. Matte sampling in *Posidonia oceanica* meadows

The sediment sampling was performed in 2018 during the oceanographic research survey Carbonsink aboard the R/V 'L'Europe' (Ifremer) to characterize the matte deposits. In total, 48 cores were sampled at 12 locations and 22 stations (Fig. 5.1.c; Table 5.1; Table 5.2). On each station, one to three replicates were sampled (α, β and γ) ca. 50 m from each other. On the sandy coastline, the cores were mainly collected between 10- and 40-meters depth along three transects; Biguglia (BG), Taverna (TV) and Urbino (UB) (Fig. 5.1.d; Fig. 5.1.e; Fig. 5.1.f; Table 5.1). Through the study area, additional cores were also sampled in specific stations; Arinella (AR), Marana lido (ML), Golo river mouth (GM), Golo river delta (GD), Tavignano river mouth (TM) and Solenzara river mouth (SM). Additionally, three cores, equidistantly distributed along the rocky coastline, were sampled; Canella (CN), Fautea (FT) and Saint-Cyprien (SC) (Fig. 5.1.c; Fig. 5.1.g). The sediment sampling was achieved by using a Kullenberg gravity corer. The corer barrel consisted of a stainless-steel tube of 3 to 5 meter-long with a PVC tube (internal diameter 90 mm) inside it and surmounted by a lead weight of approximately 1 ton (Appendix A2). Compression of unconsolidated sediment during coring is an inevitable phenomenon. In order to minimize this effect, the core head was constituted by a sharp edge to cut the fibrous material of the matte. Corrections were applied to decompress the sediment sequence by distributing the spatial discordances proportionally to the expected and the observed soil column layers (Glew *et al*., 2001; Howard *et al*., 2014a). For the different cores, the average compression was estimated between 10% and 20% and the corrected core lengths ranged from 40 to 380 cm (Table 5.2).

For the elemental and isotopic composition analysis of the main allochthonous or autochthonous potential carbon sources contributing to the carbon sink, *P. oceanica* shoots, macroalgae and epiphytes were manually collected for each station of the Taverna (TV) transect (10 m radius). In addition, 10 liters of seawater were collected from 2 m above the sea bottom (GM, BG, TV, TM, and UB stations) with Niskin bottle (General Oceanics, Miami, USA) and filtered into prewashed and precombusted (450°C, 3 h) Whatman GF/F 47 mm filters directly after collection for SPOM elemental and isotopic analysis. All the samples were kept frozen at 5°C until analysis in the laboratory.

Table 5.2. Features of core sediments. Regular subsampling: 1 cm-thick slices every 5 cm; Irregular subsampling: 1 cm-thick slices every 5-10 cm in the top 50 cm of cores and every 20-25 cm over the rest of the core. *Cores not taken into account in this study.

Location	Depth (m)	Lab code	Subsampling strategy	Corrected core lenght (cm)	Matte thickness (cm)
Arinella	10.0	AR-15-α	Irregular	185	185
Marana lido	20.0	ML-20-α	Irregular	312	275
Biguglia	10.0	BG-10-α	Regular	365	270
		BG-10-β	Irregular	343	300
		BG-10-γ	Irregular	380	340
	20.0	BG-20-α	Irregular	294	70
		BG-20-β	Irregular	256	0*
		BG-20-γ	Regular	188	145
	30.0	BG-30-α	Irregular	60	60
		BG-30-β	Irregular	70	65
		BG-30-γ	Regular	105	75
	40.0	BG-40-α	Irregular	237	0*
		BG-40-β	Irregular	166	0*
Golo mouth	10.0	GM-10-α	Irregular	364	305
Golo delta	40.0	GD-40-α	Irregular	260	100
Taverna	10.0	TV-10-α	Irregular	170	105
		TV-10-β	Irregular	57	55
		TV-10-γ	Regular	206	185
	20.0	TV-20-α	Irregular	170	167
		TV-20-β	Irregular	85	45
		TV-20-γ	Regular	138	110
	30.0	TV-30-α	Irregular	247	70
		TV-30-β	Regular	117	80
		TV-30-γ	Irregular	165	50
	40.0	TV-40-α	Irregular	160	0*
		TV-40-β	Regular	120	0*
Tavignano mouth	20.0	TM-20-α	Regular	356	193
		TM-20-β	Regular	275	110
		TM-20-γ	Irregular	158	25
Urbino	10.0	UB-10-α	Irregular	215	215
		UB-10-β	Irregular	338	200
		UB-10-γ	Regular	300	154
	20.0	UB-20-α	Regular	215	185
		UB-20-β	Irregular	122	75
		UB-20-γ	Regular	205	205
	30.0	UB-30-α	Irregular	183	0*
		UB-30-β	Irregular	157	50
		UB-30-γ	Irregular	200	40
	40.0	UB-40-α	Irregular	265	0*
		UB-40-β	Regular	310	105
		UB-40-γ	Irregular	307	0*
Solenzara mouth	10.0	SL-10-α	Regular	107	105
	20.0	SL-20-α	Regular	220	220
		SL-20-β	Irregular	190	190
		SL-20-γ	Irregular	172	172
Canella	10.0	CN-10-α	Regular	40	28
Fautea	10.0	FT-10-α	Regular	80	25
Saint-Cyprien	10.0	SC-10-α	Regular	40	7*

5.2.3. Laboratory analyses

All cores collected were subsampled on the research vessel according two strategies. The first strategy consisted in subsampling sediment cores (1 cm-thick slices every 5 cm) in order to have a detailed and regular pattern of biogeochemical parameters in the matte. The second strategy corresponds to the subsampling of sediment cores at irregular intervals (1 cm-thick slices every 5-10 cm in the top 50 cm of cores and every 20-25 cm over the rest of the core, in order to have punctual replicates at the same soil depth with the regularly subsampled core (Mateo *et al*., 2018). Bulk density (g DW cm^{-3}) was measured after drying samples at 70°C until constant weight (Howard *et al*., 2014a). Each sample was disaggregated manually with spatula, sieved through a 2 mm-mesh sieve and then separated into two fractions: fine (<2 mm) and coarse (>2 mm). The fine fraction was composed of the inorganic and organic matter of the sediment (SOM). The coarse fraction was sorted into 3 different categories, (i) the coarse organic fraction (COM, fragments of *P. oceanica*), (ii) the coarse mineral fraction (gravel), and (iii) the coarse calcium carbonate fraction (shells and biogenic debris; $CaCO_3$ >2 mm). After the sorting step, the COM was integrated with the fine fraction, ground, and homogenized for further analysis (Monnier *et al*., 2020).

The total organic matter (TOM) and calcium carbonate contents ($CaCO_3$ <2 mm) sediment samples (ca. 3 g aliquots) were determined by the method of loss on ignition at 500°C for 5 h and 950°C for 2 h in a muffle furnace (Heiri *et al*., 2001). Reference samples of sediment (SETOC 776, WEPAL) and pure $CaCO_3$ (Merck EMSURE®, Darmstadt, Germany) were used to correct for any incomplete combustions. The TOM content represents the total amount of SOM (<2 mm) and COM (>2 mm) and the total $CaCO_3$ content correspond the total amount of CaCO3 <2 mm and >2 mm. The total content in inorganic carbon ($\%C_{inorg}$) was calculated through stoichiometry using the mass of carbon (A_r= 12) and the molecular weight of $CaCO_3$ (M_r = 100) according to Rozaimi *et al*. (2016). Another aliquot of ground sub-samples (ca. 1 g) was used for elemental composition ($\%C_{org}$) and isotopic analyses ($\delta^{13}C$) by firstly acidifying them with hydrochloric acid (HCl 1M) to remove all C_{inorg} (*i.e.* $CaCO_3$). After cessation of effervescence, the sediment was centrifuged (3500 RPM, 2-3 min), rinsed with deionized (MilliQ™) and the supernatant with acid residues removed using a pipette. Deionized water was added to wash off the residual acid, centrifuged again and the supernatant removed until

pH = 7. The residual samples were re-dried (70°C), weighted and placed in tin capsules (10-20 mg). The elemental and isotopic composition was also analyzed in seagrass, epiphytes, macroalgae and SPOM samples. The macrophytes, mainly *Cladophora prolifera*, *Codium bursa*, *Dictyota implexa*, *Flabellia petiolata*, *Osmundaria volubilis*, *Padina pavonica*, *Peysonnelia squamaria* and *Rytiphlaea tinctoria*, were successively cleaned in deionized water, decarbonated following acidification with HCl 0.1N, re-rinsed with deionized water and finally dried at 70°C. The filters in which SPOM was collected were dried to constant weight and fumed under concentrated HCl fumes (2M) overnight at room temperature in glass desiccator and under vacuum. After decarbonation, plant samples and filters were also placed in tin capsules.

Measurements of C_{org} elemental composition and stable isotope ratios were performed using an elemental analyzer EA2000 (Thermo Scientific, Milan, Italy) coupled to a continuous-flow isotope-ratio mass spectrometer (IRMS) analyzer Delta V Advantage (Thermo Scientific, Bremen, Germany) through a Conflo IV interface (Thermo Scientific, Milan, Italy) at the LIENSs Stable Isotope Facility (UMR CNRS 7266, University of La Rochelle, France). The certified standard samples used during analyses were USGS-61 (Caffeine; $\delta^{13}C$: -35.05 ± 0.04‰) and USGS-62 (Caffeine; $\delta^{13}C$: -14.79 ± 0.04‰) (USGS, Reston Stable Isotope Laboratory; Schimmelmann *et al*., 2016). Carbon isotope ratios are expressed as δ values in parts per thousand (‰) relative to VPDV (Vienna Pee Dee Belemnite) according to standard notation ($\delta^{13}C = [(R_{sample} / R_{standard}) - 1] \times 10^3$, where R is the ratio $^{13}C/^{12}C$).

5.2.4. Radiocarbon dating and age-depth models

The dating and the chronostratigraphic reconstruction of matte cores were achieved from radiocarbon (^{14}C) measurements by Accelerator Mass Spectrometry at the DirectAMS laboratory (Accium BioSciences, Seattle, USA). Samples of *P. oceanica* remains (n = 2 to 3) were taken in cores collected at 10- and 20-meters depth . A first sample was sampled at the bottom end of the matte sequence and the other ones were equally collected in the middle part (n = 1) or at one-third and two-third of the core section corresponding to the matte (n = 2). Before ^{14}C measurements, seagrass debris were first rinsed with deionized water to remove fine sediment particles, placed in an ultrasonic bath of ultrapure deionized water (5

min) and finally inspected under a stereomicroscope for any attached materials. Samples were successively acid-base-base treated following standard protocol (Brock *et al*., 2010). Radiocarbon data, expressed as years before present (yr BP), were subsequently calibrated for the local marine reservoir effect (ΔR = 46 years, error ΔR = 40 years; Siani *et al*., 2000) using the CALIB 7.1.0 software (Stuiver and Reimer, 1993) in conjunction with the Marine 13.14C calibration curve (Reimer *et al*., 2013). After corrections, the calibrated ages before present (cal. yr BP) were used to produce age-depth models using the clam package in R software (Blaauw, 2010). The chronostratigraphic age-depth model was obtained with the linear regression to approximate the respective sediment accumulation rate (SAR; mm yr^{-1}).

5.2.5. Numerical procedures

The analysis of elemental composition in C_{org} was performed in a limited number of samples (7 to 25) for regularly subsampled cores. The C_{org} content in the remaining samples was inferred using the equation obtained from the linear regression existing between TOM (%DW) and C_{org} (%DW) contents measured in the same sample for each core. Similarly, the C_{org} content of cores subsampled at irregular intervals (see above) was determined using the equation obtained in adjacent cores (*i.e.* cores with same depth and located at relative proximity). The C_{org} content was referred to the initial bulk sediment weight (*i.e.* pre-sieved and pre-acidified) and expressed as a percentage (%).

The organic and inorganic carbon density in each sample was calculated by multiplying the sediment dry bulk density (g cm^{-3}) by the organic or inorganic carbon content (%C_{org} or %C_{inorg}) to obtain the carbon density (g C_{org} cm^{-3} or g C_{inorg} cm^{-3}). The carbon density was multiplied by the sediment thickness considered to obtain the stock in the sample per unit area (g C_{org} cm^{-2} or g C_{inorg} cm^{-2}). The cumulative C_{org} and C_{inorg} stock per core was computed by adding the value of all samples and normalized to stratigraphic depths of 30 cm and 100 cm thick deposits to allow comparisons. The limit of 100 cm was based to compare values with other studies and 30 cm to obtain values in shallow sediments as performed by Rozaimi (2015). The C_{org} and C_{inorg} fluxes into the sink were performed in a limited number of cores (n = 11; see below) with ^{14}C dating. This accumulation rates of C_{org} (g C_{org} m^{-2} yr^{-1}) and C_{inorg} (g

C_{inorg} m^{-2} yr^{-1}) were estimated for 30 cm and 100 cm thick deposits by dividing the C_{org} and C_{inorg} inventories in the soil by the age at 30 cm and 100 cm, respectively.

Statistical analyses were performed using the statistics software package XLSTAT (Addinsoft, 2019) for Microsoft Office Excel® 2016. Normality of parameter values was checked using a Shapiro-Wilk test. Any differences among sites, depth, matrix (*i.e.* sand matrix/rock matrix) and depositional environment in bulk density, TOM and $CaCO_3$ content, C_{org} and C_{inorg} content (%), $\delta^{13}C$ (‰), and carbon stocks (kg C_{org} m^{-2} and kg C_{inorg} m^{-2}) were analyzed using one-way Analysis of Variance (ANOVA). When significant effects were detected by ANOVA, pairwise *a posteriori* comparisons were performed using Tukey's honest significant difference (HSD) tests. When necessary, data were log transformed to meet ANOVA assumptions. The relationships between the variables and the environmental parameters were analyzed using the Pearson correlation coefficient. The correlation coefficient was calculated together with p-values to determine the significance and strength of each relationship. When necessary, the data were log transformed to improve linearity.

The global estimates of C_{org} and C_{inorg} stored in the matte of *P. oceanica* meadows were performed using multibeam echosounder (MBES) data compiled in a morpho-bathymetric Digital Terrain Model (DTM) raster mosaic with a spatial resolution of 10 x 10 m and a vertical accuracy of 0.2 m (Monnier *et al*., 2020). The DTM was integrated (Mercator projection - WGS 1984) in a Geographic Information System (GIS) software (ArcGIS® 10.0; ESRI, 2011). Benthic habitat mapping of sea bottom was used to select the surface occupied by the *P. oceanica* meadows on the study site (Valette-Sansevin *et al*., 2019). The global C_{org} and C_{inorg} stock was estimated to the normalized depth of 100 cm (*i.e.* standard depth) and 250 cm (*i.e.* mean thickness of matte found in the study site). The C_{org} and C_{inorg} stocks for 250 cm matte thickness were inferred for the remaining cores by using logarithmic regression. The values collected for 100 cm and 250 cm in the different depths throughout the study site were used to fit logarithmic regression functions integrated to the DTM of sea bottom.

5.3. Results

5.3.1. Biogeosedimentological characterization of the matte

Among the 48 cores collected on the eastern continental shelf of Corsica, 39 were mainly constituted by seagrass meadows remains (sheaths, rhizomes, and roots) incorporated into a dark brown sandy-muddy sedimentary matrix (Table 5.2). The material analysis has enabled identification of extensive well-preserved seagrass organic debris buried until the deepest parts of sediment (>350 cm). The biogeosedimentological features of the *P. oceanica* matte changed substantially across stations (Figs. 5.2), environmental parameters (*i.e.* water depth, sediment matrix, and depositional environment; Figs. 5.3) and stratigraphy (*i.e.* level in the soil) through the site (Table 5.3; Appendix A5).

Considering the first meter of cores, the bulk density ranged from 0.15 to 1.91 g DW cm^{-3} with an average value of 1.07 ± 0.02 g DW cm^{-3} (mean ± S.E.; Fig. 5.2.a). Bulk density showed significant differences between stations (Fig. 5.2.a; ANOVA, $p<0.0001$) but not with depth, matrix, and depositional environment (Fig. 5.3.a). However, bulk density decreased significantly with level in the sediment ($r = 0.575$; $p<0.001$; Table 5.3), from 0.67 ± 0.07 to 1.23 ± 0.08 g DW cm^{-3}.

The average composition of matte cores was characterized by a high content in organic compounds. The TOM content (%TOM), estimated in average at 7.62 ± 0.25% in the top 100 cm of matte (Fig. 5.2.b), declined with level in the soil ($r = -0.418$; $p<0.001$; Table 5.3) and depth (Fig. 5.3.b; $p<0.0001$). Indeed, the %TOM was two-fold higher in 10-20 m stations than in 30-40 m stations, with 8.22 ± 0.54 and 4.19 ± 0.54% respectively (Fig. 5.3.b). The mean higher and lower %TOM in the matte were observed at the Golo mouth (GM-10; 11.13 ± 0.75%) and the deepest stations in Taverna transect (TV-30; 2.50 ± 0.38%). Though there was a weak difference in %TOM between open sea and estuary stations (7.38 ± 0.29% and 8.41 ± 0.49%, respectively), meadows located near estuary areas had significantly higher %TOM ($p<0.01$; Fig. 5.3.b).

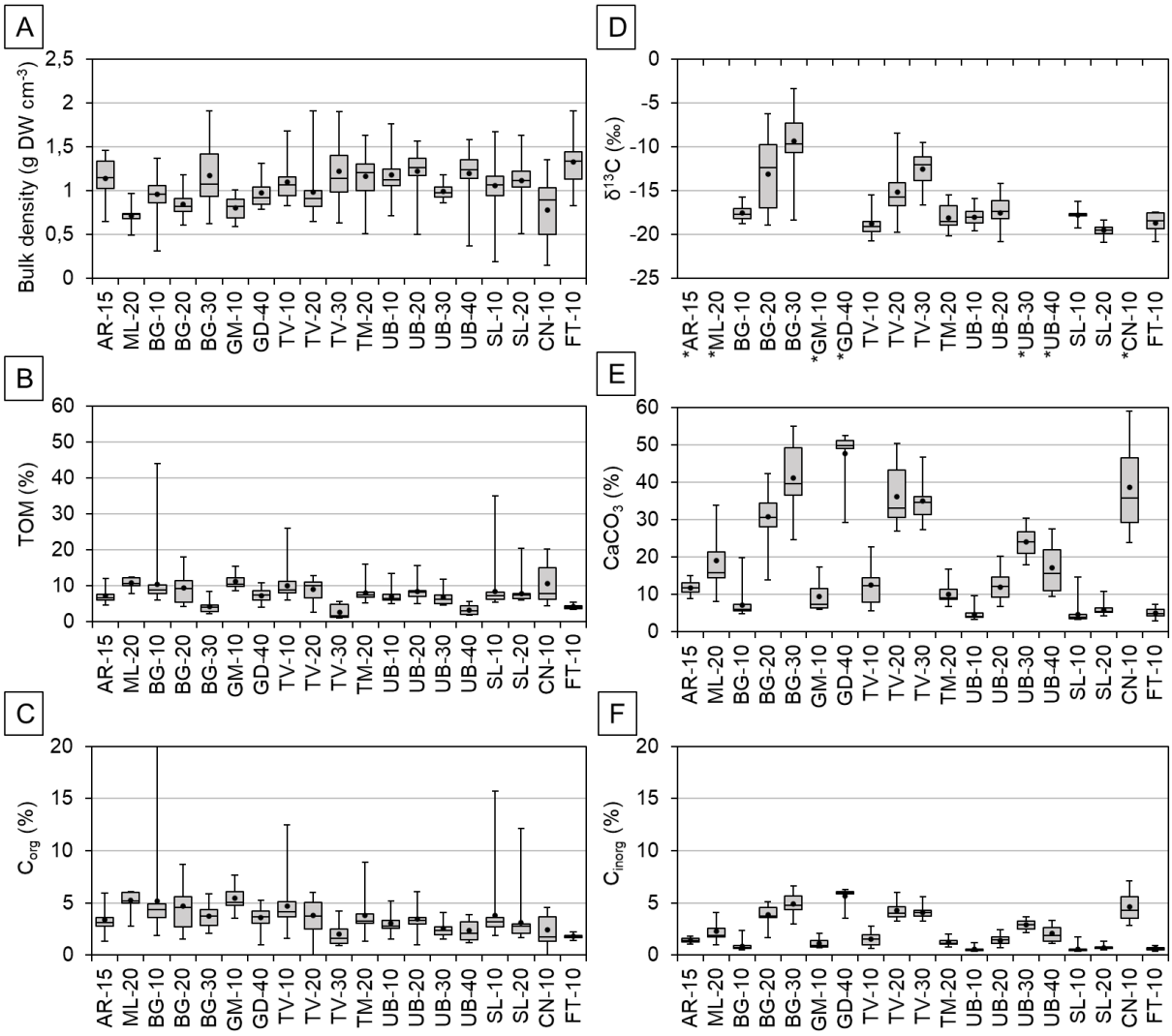

Figure 5.2. Box plots of (a) bulk density, (b) %TOM, (c) $\%C_{org}$, (d) $\delta^{13}C$ isotopic signatures of the sedimentary C_{org} (e) $\%CaCO_3$, and (f) $\%C_{inorg}$ through the investigated stations from north to south (normalized for a top 100 cm thickness of matte). Black circles represent the mean value. The maximum $\%C_{org}$ content observed at BG-10 was estimated at 23.37%. *No isotopic signature was obtained.

Organic carbon content ($\%C_{org}$), ranged between 0.88 and 23.27% (average: 3.67 ± 0.12%; Fig. 5.2.c) showed similar two-fold vertical variation as %TOM, with high values in the surface layers (7.25 ± 1.23%) declining within the matte (3.05 ± 0.31%; r = -0.364; p<0.001; Table 5.3). The top meter of the mattes near the upper limit of the *P. oceanica* meadows (10-20 m) were significantly richer in C_{org} than deeper ones (30-40 m) (p<0.0001; Fig. 5.3.c) with 3.76 ± 0.28% and 2.81 ± 0.22%, respectively. The higher and lower $\%C_{org}$ in the matte were observed at the Golo mouth (GM-10; 5.27 ± 0.26%) and the rocky stations of Fautea (FT-10; 1.82 ± 0.10%). In contrast to TOM, $\%C_{org}$ showed no significant difference between the two

depositional environment. However, matte surrounded rocky substrate showed significantly lower $\%C_{org}$ compared to *P. oceanica* meadows growing on sandy substrate ($p<0.0001$), with 3.74 ± 0.12% and 2.16 ± 0.32%, respectively (Fig. 5.3.c).

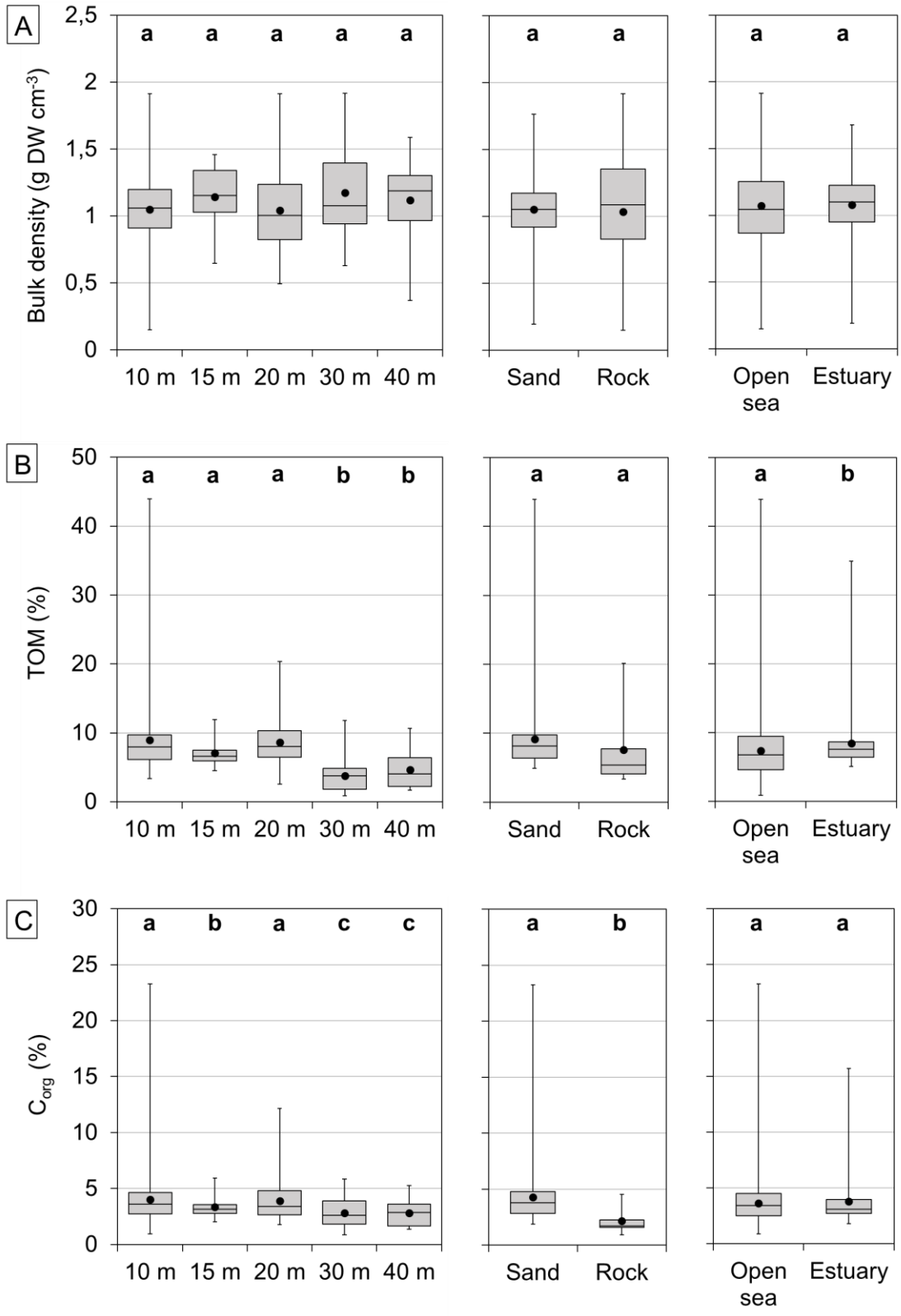

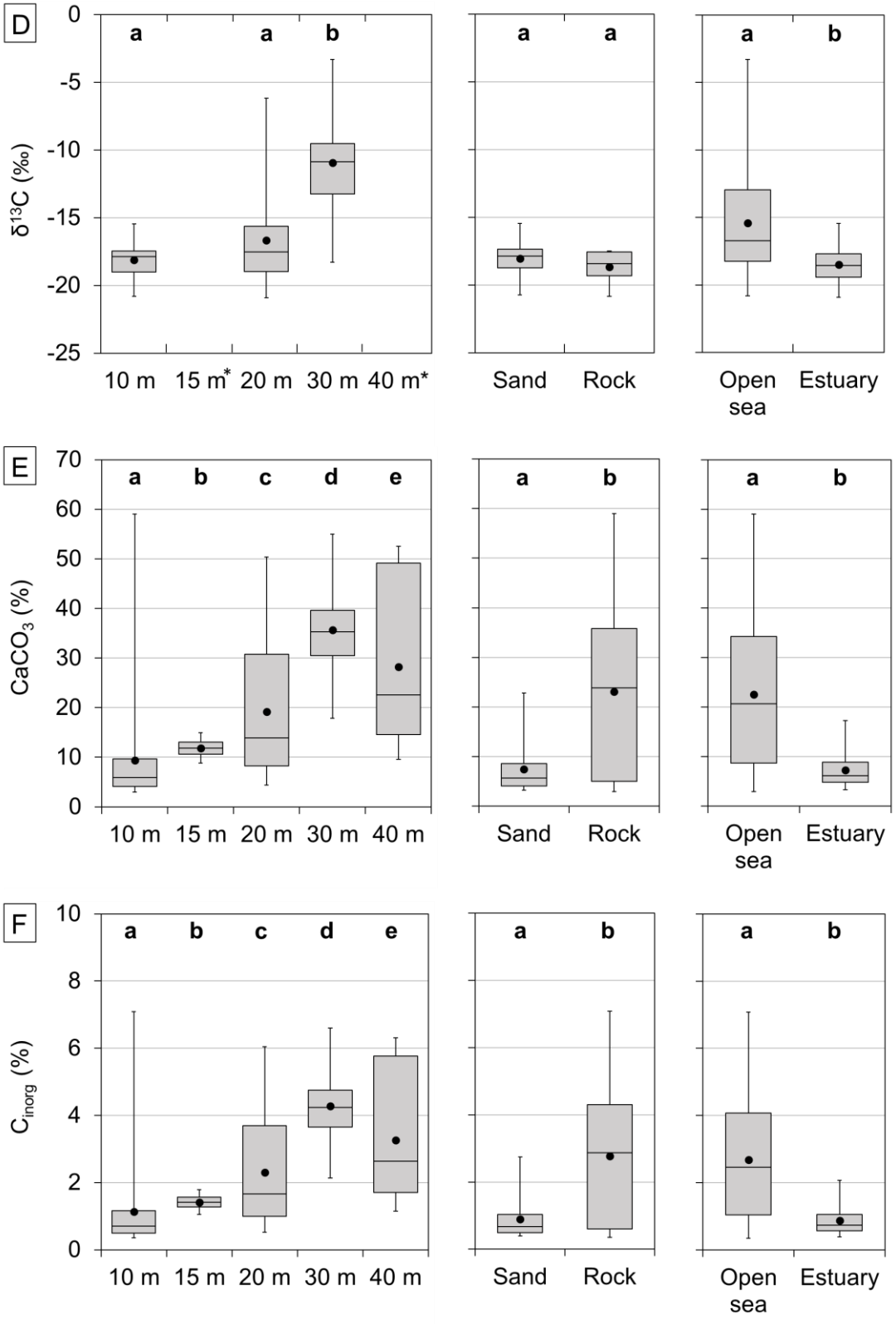

Figure 5.3. Box plots of (a) bulk density, (b) %TOM, (c) $\%C_{org}$, (d) $\delta^{13}C$ isotopic signatures of the sedimentary organic carbon (e) $\%CaCO_3$, and (f) $\%C_{inorg}$ at different depths, substrates and depositional environment from *Posidonia oceanica* meadow of east coast of Corsica (normalized for a top 100 cm thickness of matte). Black circles represent the mean value. Dissimilar letters denote significant differences between groups (ANOVA, p-value<0.05). *No isotopic signature was obtained.

Table 5.3. Pearson's correlation matrix between the environmental and the biogeosedimentological parameters analyzed in the *P. oceanica* matte cores. Level of significance: *P≤0.05, **P≤0.01, ***P≤0.001; NS, P≥0.05; Significant correlations in bold (r value).

	Depth	Level	Density	%TOM	$\%C_{org}$	$\delta^{13}C$	$\%CaCO_3$	$\%C_{inorg}$
Depth		0.095	0.122	**-0.358**	-0.156	**0.660**	**0.745**	**0.745**
Level	NS		**0.575**	**-0.418**	**-0.364**	**0.285**	0.017	0.017
Density	NS	***		**-0.541**	**-0.498**	**0.241**	-0.061	-0.061
%TOM	***	***	***		**0.913**	**-0.397**	**-0.169**	**-0.169**
$\%C_{org}$	NS	***	***	***		**-0.157**	0.007	0.007
$\delta^{13}C$	***	***	**	***	*		**0.666**	**0.666**
$\%CaCO_3$	***	NS	NS	*	NS	***		**1.000**
$\%C_{inorg}$	***	NS	NS	*	NS	***	***	

The contribution of the C_{org} sources in the sediment was calculated over 11 stations and varied significantly across sites, depth, level in the soil, and the depositional environment as shown by the carbon isotopic ratios of the top 100 cm of matte ($p<0.0001$; Fig. 5.2.d; Fig. 5.3.d; Table 5.3). The isotopic signature of C_{org} found in the matte ranged between -3.31 to -20.91‰ with an average value of -16.21 ± 0.31‰ (Fig. 5.2.d). Values increased between the surface layers (-18.13 ± 0.47‰) to the bottom end of the section (-14.55 ± 1.60‰; $r = 0.285$; $p<0.001$; Table 5.3; Fig. 5.4.b). Mattes from the shallow stations (10-20 m) were significantly more depleted in ^{13}C (-17.38 ± 0.04‰; $p<0.0001$) than sediments from deep stations (30 m; -10.95 ± 0.14‰; Table 5.3; Fig.5.3.d; Fig. 5.4.b). The estuary stations had significantly lower $\delta^{13}C$ values compared to open sea stations ($p<0.0001$; Fig. 5.3.d; Fig. 5.4.b) with -18.47 ± 0.37‰ and -15.41 ± 0.20‰, respectively. Inversely, sandy stations (-18.03 ± 0.02‰) and rocky stations (-18.66 ± 0.22‰) showed no significant differences (Fig. 5.3.d; Fig. 5.4.b).

Among the potential carbon sources, *P. oceanica* combined tissues showed the most ^{13}C-enriched values (-10.94‰ to -14.31‰; mean: -12.49 ± 1.27‰; Fig. 5.4), while SPOM had the most ^{13}C-depleted values (-20.26‰ to -24.28‰; mean: -23.09 ± 0.91‰) and macroalgae showed great variability (-12.43‰ for *C. bursa* to -28.01‰ for *F. petiolata*), with an average value estimated between the seagrass and SPOM sources (-18.69 ± 5.11‰; Fig. 5.4.a). Those results suggests that the inputs of allochthonous organic matter sources have a high contribution to sedimentary carbon stocks. The high contribution of allochthonous sources was also confirmed by the significant correlation observed between the ^{13}C isotopic signature and the organic carbon content of the sediment ($r = -0.157$; $p<0.05$; Table 5.3). Autochthonous

sources (*P. oceanica* tissues) have also a large contribution to sediment C_{org} of *P. oceanica* matte notably in deeper stations (r = 0.660; p<0.001; Table 5.3; Fig. 5.4.a; Fig. 5.4.b) and with increasing level in the matte (r = 0.285; p<0.001; Table 5.3; Fig. 5.4.a; Fig. 5.4.b).

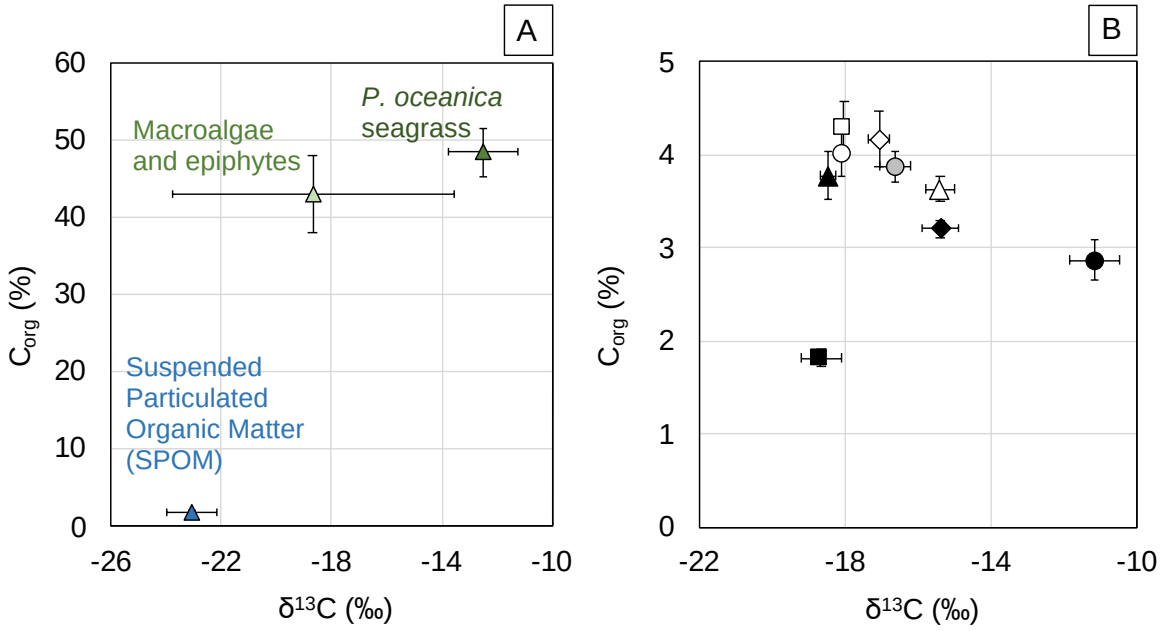

Figure 5.4. Mean (± S.E.) organic carbon content (%C_{org}) and $\delta^{13}C$ isotopic signature (‰) of potential sources of organic carbon in the matte (a) and found in *P. oceanica* matte sampled in the study site (b) according to different environmental parameters as depth (10 m: white circle; 20 m: grey circle; 30 m: black circle), sediment matrix (sand: white square; rock: black square), depositional environment (open sea: white triangle; estuary: black triangle) and soil depth considered (0-30 cm; white diamond; 30-100 cm: black diamond).

The first meter of matte was also compound by a high content in calcium carbonate (%$CaCO_3$) and consequently inorganic carbon (Fig. 5.2.e; Fig. 5.2.f.). In this section, the carbonate fraction was two- to three-fold higher than %TOM representing in average 18.86 ± 0.85% and reaching up to 59.04 ± 0.85% of the matte (Fig. 5.2.b). Thus, the C_{inorg} content of the matte accounted for 2.25 ± 0.10% and was estimated between 0.35 and 7.08%. Though *P. oceanica* meadows of the study site were mainly settled on calcareous biogenic sandy sediment (Table 5.1), no significant change in %$CaCO_3$ and %C_{inorg} was observed downcore (Table 5.3). However, these two parameters were declined significantly with depth (p<0.0001; Fig. 5.3.e; Fig. 5.3.f; Table 3). Indeed, shallow stations (10-20m) have a lower carbonate and inorganic carbon content (13.46 ± 0.95% $CaCO_3$ and 1.62 ± 0.11% C_{inorg}) than deep stations (31.96 ± 2.38% $CaCO_3$ and 3.77 ± 0.28% C_{inorg}). The highest and lowest $CaCO_3$ and C_{inorg} content

were recorded for the Golo delta station (GD-40; 47.71 ± 2.67% $CaCO_3$ and 5.67 ± 0.36 $\%C_{inorg}$) and for the shallowest stations in Urbino transect (UB-10; 4.57 ± 0.32 $\%CaCO_3$ and 0.55 ± 0.04 $\%C_{inorg}$), respectively. Similar trends were also highlighted between $CaCO_3$ and C_{inorg} with sediment matrix and depositional environment. Rocky and open sea stations showed significantly higher $\%CaCO_3$ and $\%C_{inorg}$ than sandy and estuary stations (<0.0001; Fig. 5.3.e; Fig. 5.3.f).

5.3.2. Accumulation rates of C_{org} and C_{inorg}

The linear chronostratigraphic age-depth models have contributed to determine the age and the mean sediment accretion rate (SAR) for the top 30 cm and 100 cm of matte for 11 cores throughout the study site (Table 5.4). For the first 30 cm of matte, the ages were ranged between 34 cal. yr BP (FT-10-α) and 1498 cal. yr BP (TM-20-β) with an average value estimated at 358 ± 123 cal. yr BP. For the standard top meter of matte, ages ranged between 350 cal. yr BP (FT-10-α) and 5277 cal. yr BP (TM-20-β) with an average age of 1649 ± 519 cal. yr BP. Whatever the soil depth considered, the mean SAR was estimated in average at 1.2 ± 0.2 mm yr^{-1} (Table 5.4). The SAR was higher for meadows growing on rocky substrate (2.8 ± 0.0 mm yr^{-1}) and meadows located both in shallow depth (10 m; 1.7 ± 0.3 mm yr^{-1}) and open sea areas (1.4 ± 0.3 mm yr^{-1}) compared to meadows located on sandy substrate, in deeper areas and influenced by higher fluvial inputs (Table 5.4).

The C_{org} accumulation rates of the *P. oceanica* meadows were ranged from 6.1 to 96.4 g C_{org} m^{-2} yr^{-1} (30 cm of matte) and 7.1 and 96.6 g C_{org} m^{-2} yr^{-1} (100 cm). The mean C_{org} accumulation rates were estimated at 46.1 ± 7.9 g C_{org} m^{-2} yr^{-1} (30 cm) and 43.2 ± 8.7 g C_{org} m^{-2} yr^{-1} (100 cm) (Table 5.4; Appendix A6). The effect of depth, sediment matrix and depositional environment on C_{org} accumulation rates for the two depth of soil were comparable (Fig. 5.5). For the first meter of soil, 10 m depth stations sequestered significantly more C_{org} than 20 m depth stations (p<0.0001; 65.8 ± 10.9 g C_{org} m^{-2} yr^{-1} and 24.3 ± 6.3 g C_{org} m^{-2} yr^{-1}, respectively). Parallelly, meadows located in open sea and settled on rocky substrates (53.2 ± 11.7 g C_{org} m^{-2} yr^{-1} and 78.7 ± 0.0 g C_{org} m^{-2} yr^{-1}, respectively) accumulated more C_{org} in their sediments compared to estuarine meadows and those growing on sandy substrate (p<0.0001; 25.6 ± 6.9 g C_{org} m^{-2} yr^{-1} and 39.6 ± 8.7 g C_{org} m^{-2} yr^{-1}, respectively).

In comparison with organic carbon, the mean C_{inorg} accumulation rates in the *P. oceanica* matte cores were approximately three to four-fold lower (Table 5.4). The C_{inorg} accumulation rates ranged from 5.1 to 24.0 g C_{inorg} m^{-2} yr^{-1} (30 cm of matte) and 5.6 and 27.2 g C_{inorg} m^{-2} yr^{-1} (100 cm). The mean C_{inorg} accumulation rates were estimated at 11.8 ± 1.7 g C_{inorg} m^{-2} yr^{-1} (30 cm) and 11.2 ± 1.8 g C_{inorg} m^{-2} yr^{-1} (100 cm) (Fig. 5.5). Considering the top 100 cm of soil, meadows located in shallow waters (10 m) and influenced by an open sea environment (12.9 ± 3.4 g C_{inorg} m^{-2} yr^{-1} and 14.0 ± 2.2 g C_{inorg} m^{-2} yr^{-1}, respectively) accumulated significantly more C_{inorg} in their sediments than intermediates meadows (20 m) and located near estuary ($p<0.0001$; 9.7 ± 1.4 g C_{inorg} m^{-2} yr^{-1} and 7.4 ± 1.4 g C_{inorg} m^{-2} yr^{-1}, respectively). Contrary to C_{org}, the C_{inorg} accumulated in the top 100 cm of soil showed no significant difference between sandy and rocky matrix (11.2 ± 2.0 g C_{inorg} m^{-2} yr^{-1} and 11.5 ± 0.0 g C_{inorg} m^{-2} yr^{-1}, respectively).

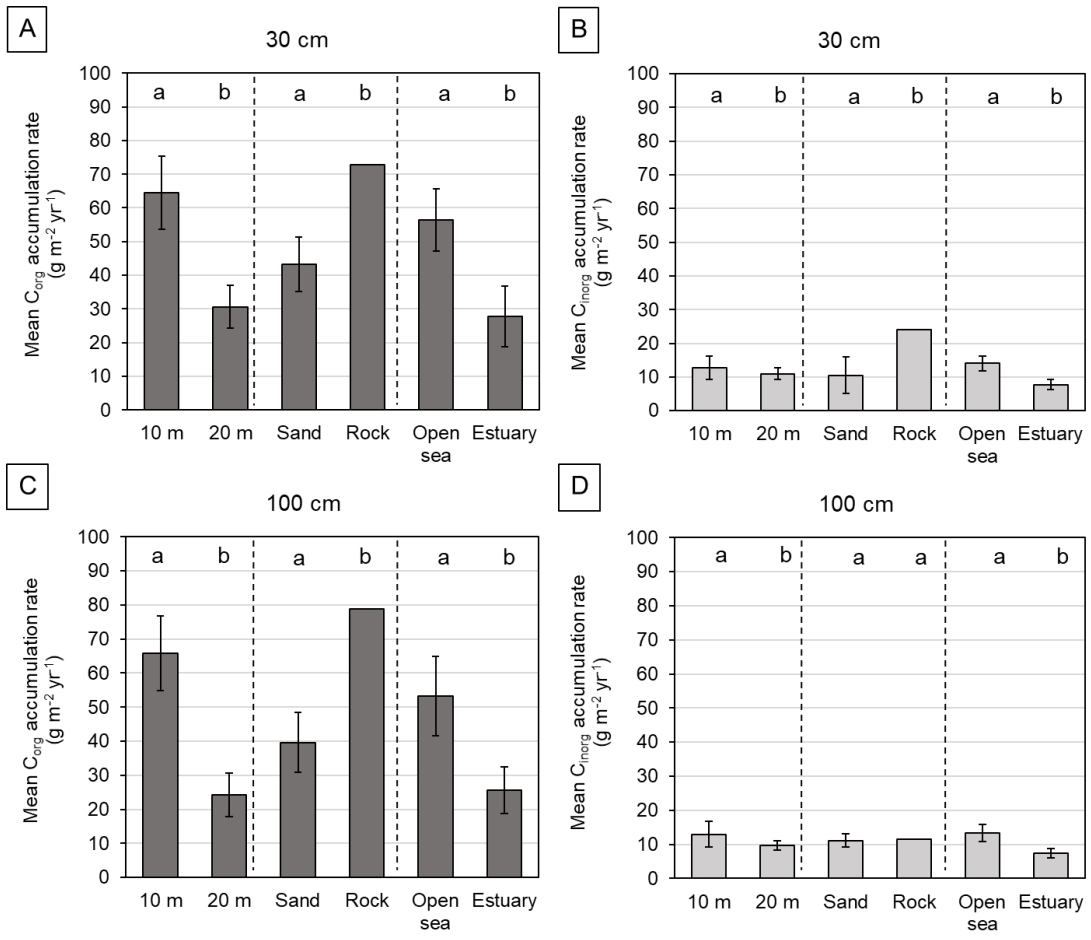

Figure 5.5. Average organic and inorganic carbon accumulation rates in the top 30 cm (a, b) and 100 cm (c, d) of *P. oceanica* matte according to depth, sediment matrix and depositional environment.

Table 5.4. Sediment accumulation rates, C_{org} and C_{inorg} accumulation rates in the *P. oceanica* matte. Estimates are normalized over 30 cm and 100 cm thick deposits. The corresponding age and sediment accretion rate are derived from ^{14}C dating.

30 cm				
Lab code	**Age (cal. yr BP)**	**Sediment accretion rate (mm yr^{-1})**	**C_{org} accumulation rate (g m^{-2} yr^{-1})**	**C_{inorg} accumulation rate (g m^{-2} yr^{-1})**
BG-10-γ	137	1.42	66.49	8.00
BG-20-γ	467	0.54	31.01	9.91
GM-10-α	347	0.70	29.54	5.13
TV-10-γ	84	1.90	96.38	16.31
TV-20-γ	495	0.51	26.11	18.06
TM-20-α	230	0.97	49.77	8.72
TM-20-β	1498	0.19	6.05	11.37
UB-10-γ	121	1.53	56.98	10.16
UB-20-α	192	1.12	45.08	11.85
SL-20-α	342	0.71	25.54	5.68
FT-10-α	34	2.83	72.75	24.02

100 cm				
Lab code	**Age (cal. yr BP)**	**Sediment accretion rate (mm yr^{-1})**	**C_{org} accumulation rate (g m^{-2} yr^{-1})**	**C_{inorg} accumulation rate (g m^{-2} yr^{-1})**
BG-10-γ	630	1.42	61.97	9.81
BG-20-γ	1881	0.54	19.70	15.19
GM-10-α	1348	0.70	31.03	5.64
TV-10-γ	436	2.00	96.63	27.22
TV-20-γ	4711	0.51	9.66	8.40
TM-20-α	950	0.97	39.64	11.40
TM-20-β	5277	0.19	7.12	6.61
UB-10-γ	474	1.53	60.73	10.57
UB-20-α	805	1.12	45.15	10.88
SL-20-α	1275	0.71	24.42	5.85
FT-10-α	350	2.83	78.71	11.46

5.3.3. Stocks of C_{org} and C_{inorg}

The mean standing C_{org} and C_{inorg} stocks per unit area were calculated for the 19 stations selected throughout the study site (Figs. 5.6). The carbon stocks showed significant difference between sites ($p<0.0001$). The C_{org} stock in shallow sediments (top 30 cm of soil) showed a homogeneous trend (10.7 ± 0.5 kg C_{org} m^{-2}; Fig. 5.6.a) and exhibited a continuously increasing pattern with sediment depth ($p<0.0001$). Indeed, the mean stocks were estimated at 32.7 ± 1.5 kg C_{org} m^{-2} and 72.3 ± 4.6 kg C_{org} m^{-2}, for 100 cm and 250 cm thick matte deposits,

respectively (Fig. 5.6.b; Fig. 5.6.c). For 100 cm-thick matte, the lowest and highest C_{org} stocks were recorded at UB-30 station (14.4 kg C_{org} m^{-2}) and BG-10 station (44.3 kg C_{org} m^{-2}), respectively (Fig. 5.6.b). The maximum values reached was observed for the 250 cm thick-matte deposit at BG-10 (111.3 kg C_{org} m^{-2}; Fig. 5.6.c).

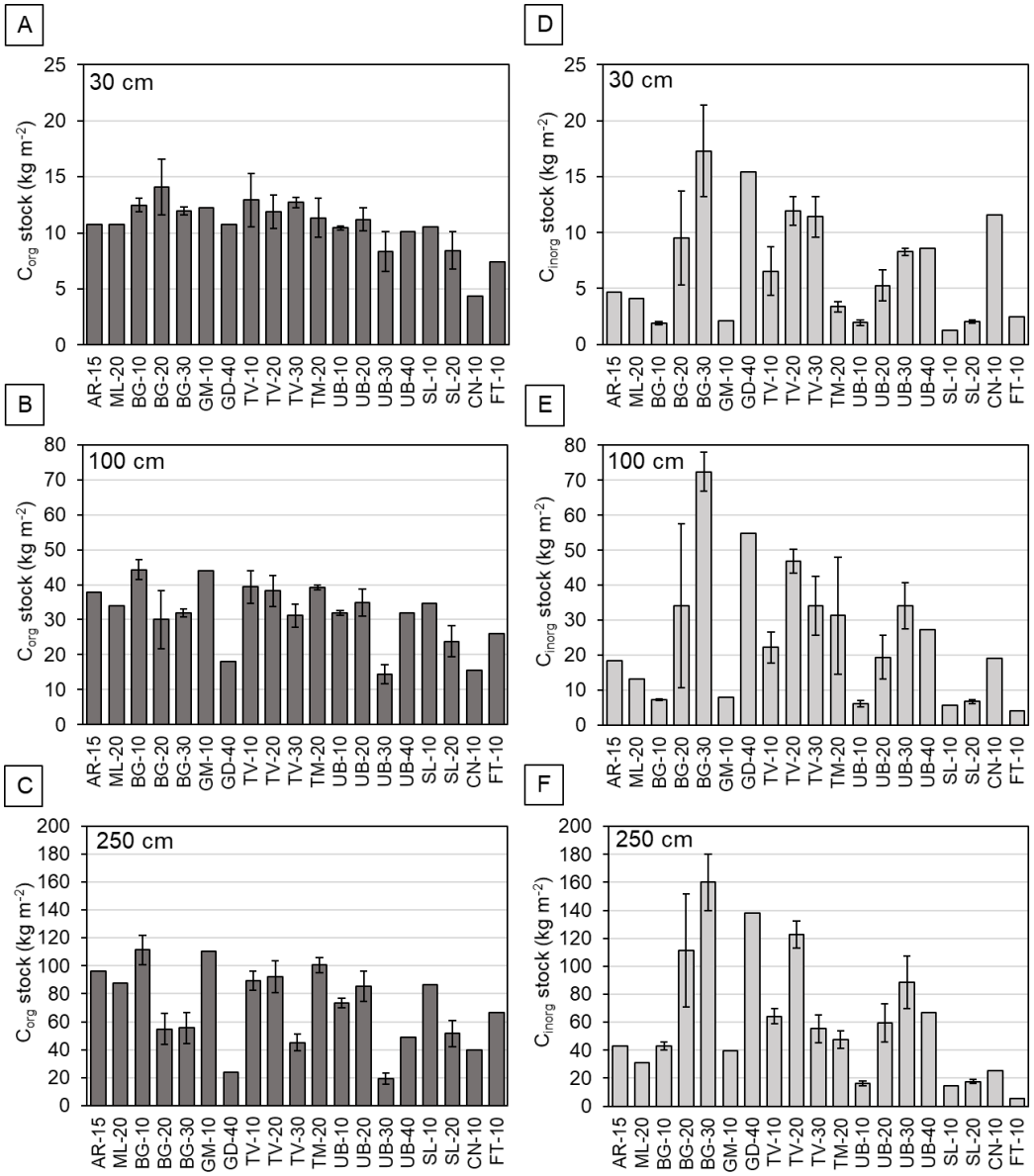

Fig. 5.6. Mean (± S.E.) organic (a, b, c) and inorganic (d, e, f) carbon stocks determined in 30 cm-, 100 cm- and, 250 cm-thick *P. oceanica* matte deposits through the different stations (from north to south).

In the studied site, the C_{inorg} stock occurring in *P. oceanica* matte deposits accounted for an important part of the total carbon stock, exceeding the C_{org} stock in some stations (Fig. 5.6.d; Fig. 5.6.e; Fig. 5.6.f). Compared to C_{org}, the C_{inorg} stock in first 30 cm of soil is more heterogeneous (Fig. 5.6.d) and was estimated between 1.3 and 17.3 kg C_{inorg} m^{-2}. The mean

stocks were estimated at 6.8 ± 1.1 kg C_{inorg} m^{-2}, 24.5 ± 4.5 kg C_{inorg} m^{-2} and, 60.5 ± 9.9 kg C_{inorg} m^{-2} for 30 cm, 100 cm and 250 cm thick matte deposits, respectively (Fig. 5.6.b; Fig.5.6.c). Over the first 100 cm of matte, an eighteen-fold difference was observed in the C_{inorg} stocks between FT-10 (4.0 kg C_{inorg} m^{-2}) and BG-30 (72.4 kg C_{inorg} m^{-2}). The maximum C_{inorg} stocks reached up to 160.1 kg C_{inorg} m^{-2} for the top 250 cm of soil at the station BG-30. Considering the total carbon stock accumulated, the lowest values were recorded at FT-10 station (30.1 kg C m^{-2} for 100 cm and 71.6 kg C m^{-2} for 250 cm) whereas the highest total carbon stock was observed for the deepest station of the Biguglia transect (BG-30; 104.3 kg C m^{-2} for 100 cm and 215.6 kg C m^{-2} for 250 cm).

Overall, the C_{org} and C_{inorg} stocks in the *P. oceanica* matte changed significantly with depth ($p<0.0001$; Figs. 5.7) except for C_{org} stock calculated in the first 30 cm of soil; Fig. 5.7.a). Over the 100 cm-thick matte deposits, the C_{org} stock decreased significantly through depth ($p<0.0001$) with 35.8 ± 1.3 kg C_{org} m^{-2} for shallow stations (10-20 m) to 26.1 ± 1.1 kg C_{org} m^{-2}. A similar trend was observed when considering a 250 cm-thick matte with 87.2 ± 4.9 kg C_{org} m^{-2} and 39.5 ± 3.2 kg C_{org} m^{-2} for shallow and deep stations, respectively.

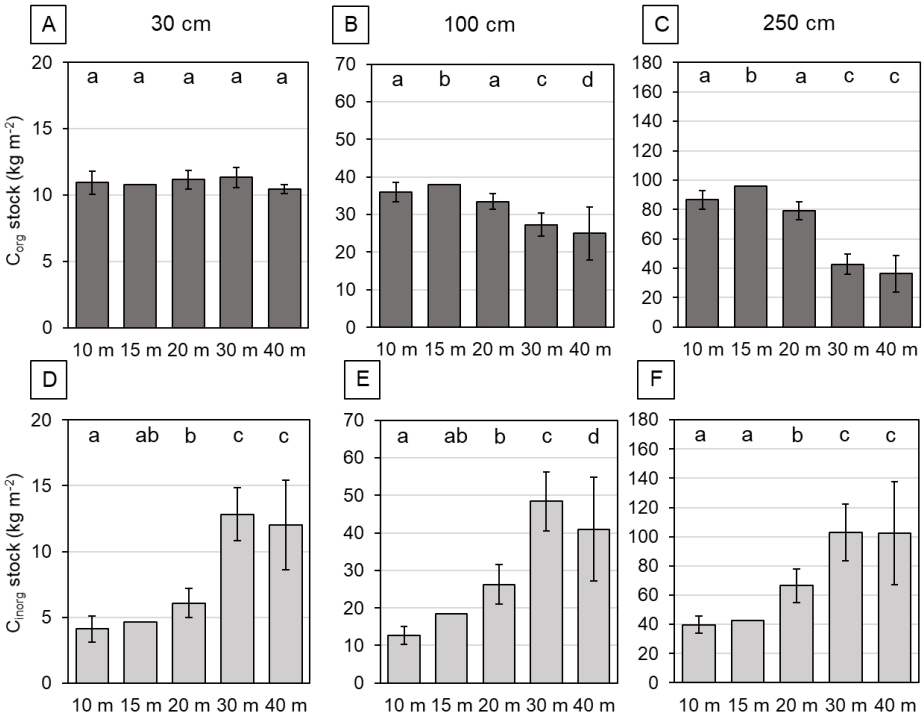

Fig. 5.7. Mean (± S.E.) organic (a, b, c) and inorganic (d, e, f) carbon stocks determined at different depths within 30 cm-, 100 cm- and, 250 cm-thick *P. oceanica* matte deposits.

The C_{inorg} stock showed an inverse pattern than C_{org} stock by globally increasing from shallowest to deepest meadows in the study site, whatever the soil depth considered (Fig. 5.6.d; Fig. 5.6.e; Fig. 5.6.f). Indeed, shallow meadows (10-20 m) contained 4.9 ± 0.7 kg C_{inorg} m^{-2}, 18.6 ± 4.4 kg C_{inorg} m^{-2} and 48.1 ± 9.4 kg C_{inorg} m^{-2}, for the first 30 cm, 100 cm, and 250 cm of matte, respectively. However, deep meadows (30-40 m) showed two- to three-fold higher C_{inorg} stock in their sediments with 12.4 ± 0.4 kg C_{inorg} m^{-2}, 44.7 ± 3.7 kg C_{inorg} m^{-2} and 102.6 ± 0.2 kg C_{inorg} m^{-2}, for the top 30 cm, 100 cm, and 250 cm of matte, respectively.

The C_{org} and C_{inorg} stocks of *P. oceanica* meadows changed with sediment matrix whatever the soil depth considered (Figs. 5.9). Seagrass meadows settled on sandy substrate showed substantially higher C_{org} stocks than meadows settled on rocky substrate ($p<0.0001$; Figs. 5.9). For instance, in the first meter of soil, the C_{org} stock in rocky and sandy areas were valued at 20.8 ± 5.3 kg C_{org} m^{-2} and 38.6 ± 2.1 kg C_{org} m^{-2}, respectively. Concerning the C_{inorg} stocks, significant differences were observed between sandy and rocky matrix ($p<0.0001$). The C_{inorg} stocks in sandy meadows exhibited a twelve-fold increase from 30 cm to 250 cm soil depth whereas in rocky areas, the C_{inorg} was mainly located in shallow sediments (two-fold increase between 30 cm and 250 cm soil depth; Fig. 5.8.d; Fig. 5.8.e; Fig. 5.8.f).

Contrary to sediment matrix, the C_{org} stock occurring in seagrass sediment showed no significant difference between the two depositional environments (Fig. 5.8.a; Fig. 5.8.b; Fig. 5.8.c). Indeed, taking into account the first 100 cm of soil, estuarine and open sea meadows stored 33.5 ± 3.3 kg C_{org} m^{-2} and 35.1 ± 1.9 kg C_{org} m^{-2}, respectively (Fig. 5.8.b). Inversely, the C_{inorg} stock of meadows influenced by estuarine environment was significantly different than open sea meadows ($p<0.0001$; Fig. 5.8.d; Fig. 5.8.e; Fig. 5.8.f). Depending on the soil depth, the C_{inorg} stock occurring in estuarine sediments of *P. oceanica* showed to be up to three-fold lower than in open sea environment. Estuarine seagrass meadows stored 15.9 ± 7.1 kg C_{inorg} m^{-2} (100 cm-thick matte) whereas open sea meadows accumulated up to 20.5 ± 3.8 kg C_{inorg} m^{-2} (Fig. 5.8.e).

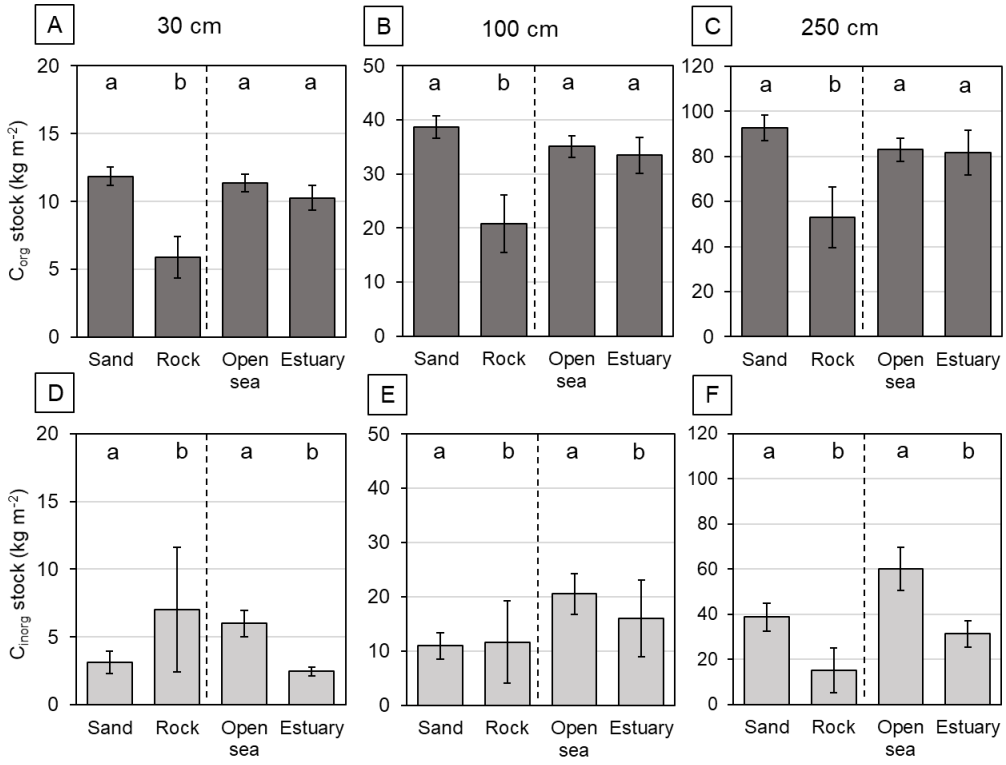

Fig. 5.8. Mean (± S.E.) organic (a, b, c) and inorganic (d, e, f) carbon stocks determined in different sediment matrix (sandy matrix or rocky matrix) and environmental influence (open sea or estuary) within 30 cm-, 100 cm- and, 250 cm-thick *P. oceanica* matte deposits.

5.3.4. Scaling of C_{org} and C_{inorg} stocks in the study site

The global estimates of C_{org} and C_{inorg} stocks associated to *P. oceanica* meadows on the eastern coast of Corsica island were based on the relationship between the carbon stock and depth gradient observed in this study (Figs. 5.7). Thus, the C_{org} and C_{inorg} stock values determined in the top 100 cm and 250 cm of *P. oceanica* matte (n = 19) coupled to the corresponding depth were used to fit logarithmic regression curve (Fig. 5.9). The C_{org} stocks estimated in the top 100 cm and 250 cm of sediment showed to be negatively correlated with depth, $r = -0.353$ ($p<0.05$) and $r = -0.591$ ($p<0.01$), respectively. Inversely, the C_{inorg} stocks exhibited a positive correlation with depth in the first 100 cm and 250 cm of sediment, $r = 0.712$ ($p<0.001$) and 0.651 ($p<0.01$), respectively.

Upscaling of C_{org} and C_{inorg} stocks were undertaken after integrating the respective functions describing the changes in stocks with depth into the morpho-bathymetric DTM raster mosaic of sea bottom (Figs. 5.10). The estimates were performed over an areal coverage

of 20425 ha (see above). For the first meter of matte, the C_{org} and C_{inorg} stocks ranged from 26.5 to 59.8 kg C_{org} m^{-2}, and from 0 to 47.5 kg C_{inorg} m^{-2} (mean: 30.5 ± 0.2 kg C_{org} m^{-2} and 28.9 ± 0.1 kg C_{inorg} m^{-2}; Fig. 5.10.a; Fig.5.10.b). The global carbon stock in the top meter of matte over the study site was estimated respectively at 6.2 million t C_{org} and 5.9 million t C_{inorg}, representing approximately 12.1 million t C. Considering the mean thickness of matte observed in the study site (250 cm), the C_{org} and C_{inorg} stock were ranged from 42.6 to 221.1 kg C_{org} m^{-2}, and from 0 to 109.5 kg C_{inorg} m^{-2} (mean: 64.5 ± 0.1 kg C_{org} m^{-2} and 70.7 ± 0.1 kg C_{inorg} m^{-2}; Fig. 5.10.c; Fig.5.10.d). Consequently, the global carbon quantity stored in the mean thickness of matte over the study site (250 cm-thick deposit) was assessed respectively at 13.2 million t C_{org} and 14.4 million t C_{inorg}, a total of approximately 27.6 million t C.

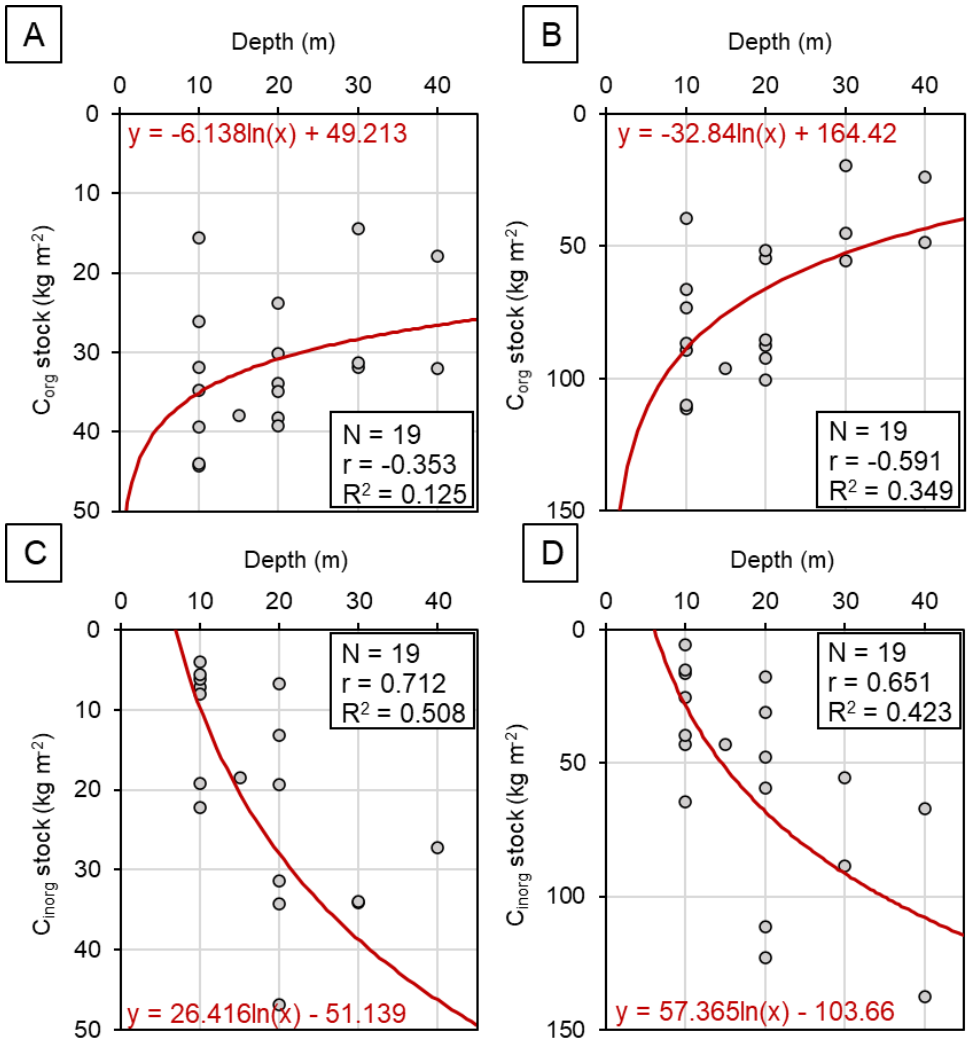

Figure 5.9. Multiple relationship between the organic and inorganic carbon stocks in 100 cm (a, b) and 250 cm (c, d) thick *P. oceanica* matte deposits and depth.

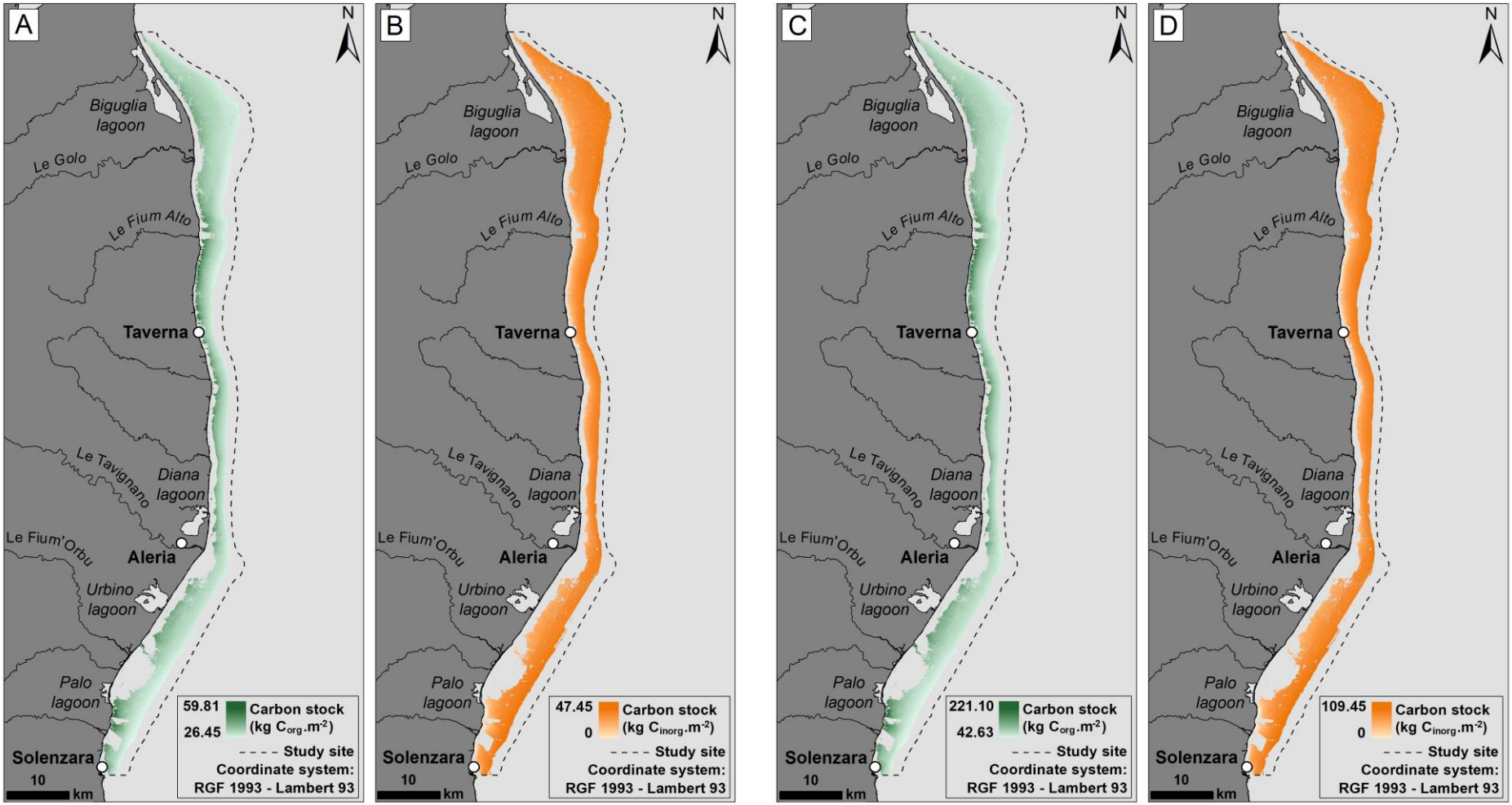

Figure 5.10. Predictive map of organic and inorganic carbon stored in the first 100 cm (a, b) and 250 cm (c, d) of *P. oceanica* matte deposits throughout the study site.

5.4. Discussion

5.4.1. Variability in C_{org} stocks and fluxes

The present study showed a significant variability in the C_{org} accumulated and stored in the sedimentary compartment found beneath *P. oceanica* meadows between the different sites, water depth, sediment matrix (sandy or rocky substrate) and depositional environment (open sea or estuary). At the site scale, the C_{org} stocks and fluxes in the first meter of *P. oceanica* sediment (14.4-44.3 kg C_{org} m^{-2} and 6.1-96.6 g C_{org} m^{-2} yr^{-1}; Fig. 5.6; Table 5.4) were coherent with other values determined throughout Mediterranean Sea (4.7-75.5 kg C_{org} m^{-2} and 9-249 g C_{org} m^{-2} yr^{-1}; Mateo *et al*., 1997, 2006; Romero *et al*., 1994; Serrano *et al*., 2012, 2014, 2016a). These values confirm that C_{org} stock per unit area in the *P. oceanica* matte deposits is an exception in seagrass ecosystems (Lavery *et al*., 2013; Rozaimi, 2015) and one of the highest ever recorded in coastal and marine ecosystems (Mcleod *et al*., 2011; Duarte *et al*., 2013; Laffoley and Grimsditch, 2009 and references therein; Alongi, 2018).

Along water depth gradients, C_{org} accumulated in sediments of *P. oceanica* and *Posidonia* spp. proved to decrease (Serrano *et al*., 2014, 2016a; 2016b). Here, the two- to three-fold difference observed in C_{org} accumulation with depth gradient (10 m and 20 m depth) confirms this trend both for the top 30 cm and 100 cm of sediment. Even though previous studies demonstrated significant reduction in C_{org} accumulation rates and stocks in shallow sediments (20 cm) of *P. oceanica* meadows along depth gradients (Romero *et al*., 1992; Mateo and Romero, 1997), here no significant change in C_{org} stock of shallow sediments (30 cm) was observed with depth (Fig. 5.7.a). Inversely, the C_{org} stored in the top 100 cm and 250 cm of matte deposits exhibited a two- to three-fold difference between 10 m and 40 m depth confirming the significant influence of depth in the storage of C_{org} in seagrass soils (Mateo and Romero, 1997; Serrano *et al*., 2014, 2016a; Samper-Villareal *et al*., 2016).

Mapping of benthic habitats undertaken along the Corsican shoreline demonstrated that depth distribution of seagrass meadows is very extensive at site-level (Valette-Sansevin *et al*., 2019) which correspond to depth range reported throughout the Mediterranean in literature (Duarte, 1991; Boudouresque et al., 2012). Although *P. oceanica* meadows occupy

areas down to 40 m water depth, light reduction associated with depth gradient have a significant effect in the plant primary production and canopy complexity which are key determinant factors influencing both the C_{org} sequestration and storage capacity of seagrass meadows (Alcoverro *et al*., 2001; Collier *et al*., 2007; Serrano *et al*., 2014). Thus, an increase in seagrass canopy complexity (*i.e.* density, cover and biomass) contributed generally to the reduction of hydrodynamic energy resulting in higher trapping and retention of fine-grained sediment particles (*i.e.* silt and clay) from the water column, and consequently leading to higher sediment accretion rate (SAR; Gacia and Duarte, 2001; Hendriks *et al*., 2008; Samper-Villareal *et al*., 2016; Serrano *et al*., 2016b). Concurrently, the higher deposition of fine sediment particles and SAR of seagrass soils may contribute to an increase in C_{org} burial rates and preservation (Keil and Hedges, 1993; Burdige, 2007) due to reduce oxygen exposure time occurring in fine sediments (Hedges and Keil, 1995; Mateo *et al*., 2006; Burdige, 2007; Pedersen *et al*., 2011). Recently, the study of *P. oceanica* characteristics, primary production, and sequestration of C_{org} along depth-related gradients of light availability has been performed within the study area (Pergent-Martini *et al*., 2020). This work reported a reduction from shallow (5m) to deep (30 m) areas of shoot densities (from 550.5 to 106.1 shoots m^{-2}), mean total C_{org} fixation (426.6 to 33.5 g C_{org} m^{-2}) and mean C_{org} sequestration (84.4 to 7.7 g C_{org} m^{-2}) of *P. oceanica* meadows. These overall changes in the canopy complexity and productivity observed with depth coincide with the findings from this study revealing a reduction in SAR, C_{org} accumulation and storage along depth gradient (Figs. 5.5; Figs. 5.7).

In the same way as water depth gradient, increased turbidity resulting from freshwater terrestrial inputs in estuarine environments appears to affect the C_{org} accumulation in *P. oceanica* seagrass sediments within the study area. Similar to the effects initiated by water depth, increasing light attenuation have confirmed to decrease meadow productivity and canopy complexity (Alcoverro *et al*., 2001; Ruiz and Romero, 2001; Collier *et al*., 2009). Thus, the two-fold lower SAR and C_{org} accumulation rates in estuarine sediments compared to open sea areas (Table 5.4; Fig. 5.5.a; Fig. 5.5.c) may be explained by a decrease in biomass productivity and shoot density of *P. oceanica* meadows participating to lower sequestration of autochthonous C_{org} (Keil and Hedges, 1993; Gacia and Duarte, 2001; Burdige, 2007). As regards to the two-fold differences in sedimentary C_{org} burial rates between the two depositional environments, the C_{org} stored in open sea sediments was expected to be two-

fold higher than in estuary areas. However, no significant difference was established between the sedimentary C_{org} stocks found within sediments of the two depositional environments. Consequently, while lower SAR and C_{org} accumulation rates were found in high turbidity environments, the deposition of fine-grained sediment particles may contribute to preserve autochthonous C_{org} after burial and reduce remineralization of organic compounds related to reduce oxygen concentrations in fine sediments (Keil and Hedges, 1993; Mateo *et al*., 2006; Burdige, 2007). This hypothesis seems to be confirmed by the lower isotopic signature of seagrass sediments organic matter in Golo and Tavignano estuarine environments (Fig. 5.3.d) suggesting a higher deposition of allochthonous particles in these sites which may increase the C_{org} preservation efficiency (see below). Higher deposition of C_{org} allochthonous particles from terrestrial- or sestonic inputs may also offset the reduction in autochthonous inputs due to light attenuation resulting in comparable C_{org} stocks in seagrass deposits (Samper-Villareal *et al.*, 2016; Ricart *et al*., 2020).

Although *P. oceanica* meadows have been described in historical literature as a species growing mainly on soft nutrient rich-substrates (Molinier and Picard, 1952; Boudouresque and Meinesz, 1982), the species can also colonize rocky substrates following the development of algal turf assemblages or penetration of roots through crevices (Pérès and Picard, 1964; De Falco *et al*., 2003, 2008; Boudouresque *et al*., 2012). The *P. oceanica* meadows settled on rocky substrate are generally influenced by higher exposure to hydrodynamic energy and lower particle deposition compared to sheltered areas defined by low wave amplitude and higher sediment deposition (Fonseca and Bell, 1998; Vacchi *et al.*, 2017a). In comparison with sheltered areas, the growth of exposed meadows (*i.e.* on rocky substrate) tends to be laterally-oriented contributing to the development of thin matte formation (<1 m; De Falco *et al*., 2008; Vacchi *et al*., 2017a). Indeed, in response to lower sediment deposition, meadows on rocky matrix exhibited a lower shoot density (222.27 shoots m^{-2}) than on sandy substrate (322.43 shoots m^{-2}) for comparable depths, a higher proportion of horizontal shoots than sheltered meadows (18% and 1.1-4.1%) but a lower rhizome growth rates (0.7 cm yr^{-1} and 1.1-1.2 cm yr^{-1}; respectively) as showed in Sardinia and Sicily (De Falco *et al*., 2008; Di Maida *et al.*, 2013). By influencing the deposition of allochthonous particles in exposed seagrass meadows, marine currents and waves may affect the C_{org} accumulation and storage in seagrass meadows (Samper-Villareal *et al.*, 2016; Mazarrasa *et al*., 2017, 2018 and references therein). Here, *P.*

oceanica meadows settled on rocky substrates exhibited significantly higher C_{org} content, SAR and C_{org} accumulation rate than meadows growing on sandy matrix. Yet, seagrass sediments in sandy sites showed two-fold higher C_{org} stocks compared to rocky areas, whatever the thickness of matte considered (Fig. 5.8.a; Fig. 5.8.b; Fig.5.8.c). This difference may be explained by the lower content of fine sediment particles found in exposed areas, the erosional patterns, and the high remineralization rates of already buried C_{org} in seagrass sediments found on rocky matrix likely related to hydrodynamic processes enhancing oxygen diffusion through the sediment (Gacia *et al*., 2002; Burdige, 2007; Samper-Villareal *et al*., 2016; Serrano *et al.*, 2016b, 2016c).

5.4.2. Variability in organic matter sources

The changes in $\delta^{13}C$ signature found in *P. oceanica* sediments (Fig. 5.2.d) confirmed that both seagrass-derived (autochthonous sources) and non-seagrass-derived materials (allochthonous sources) were preserved in seagrass meadow sediments (Gacia *et al*., 2002; Kennedy *et al*., 2010). In this study, the *P. oceanica* seagrass-derived organic matter showed to be more enriched in ^{13}C (-12.49 ± 1.27‰) compared to algal- and sestonic-derived organic matter (-18.69 ± 5.11‰ and -23.09 ± 0.91‰, respectively; Fig. 5.4) as reported by Kennedy *et al*. (2010). The isotopic signature of *P. oceanica* seagrass materials described in this study showed to be consistent with values observed in previous studies (-13.9 ± 1.0‰ to -11.9 ± 4.1‰; Hemminga and Mateo, 1996; Lepoint *et al*., 2000; Gacia *et al*., 2002; Kennedy *et al*., 2010). As in many other meadows, the $\delta^{13}C$ signature of *P. oceanica* seagrass sediments measured in the first meter of soil showed lower values relative to the seagrass tissues (Kennedy *et al*., 2010), likely due to a contribution of different carbon sources to the C_{org} accumulated in seagrass sediments (Kennedy *et al*., 2004; Papadimitriou *et al.*, 2005).

Over the first meter of sediment, $\delta^{13}C$ values increased continuously from the surface to the bottom end of section (-18.13 ± 0.47‰ to -14.55 ± 1.60‰). These differences in $\delta^{13}C$ values probably result from the different decomposition rates of the different organic matter sources accumulated within the sediment layers. Contrary to high-biomass and persistent seagrass species like *P. oceanica* containing relatively high amounts of refractory organic compounds (*e.g.* lignin, cellulose) which delays their mineralization (Duarte and Chiscano,

1999; Klap *et al*., 2000; Pedersen *et al*., 2011; Kaal *et al*., 2016, 2018), allochthonous organic matter sources deriving particularly from macroalgae and sestonic sources are richer in labile C_{org} compounds leading to early decomposition during diagenesis (Enriquez *et al*., 1993; Mateo and Romero, 1997; Klap *et al*., 2000; Cebrian *et al.*, 2002; Gacia *et al*., 2002). Consequently, the shifts in $\delta^{13}C$ values over the first meter of matte suggest that C_{org} from persistent seagrass-derived materials (*e.g.* rhizomes) are more preserved in sediments and exhibited no major change over time contrary to labile forms of C_{org} associated with algal and sestonic sources which are more vulnerable to remineralization (Henrichs, 1992, Enriquez *et al*., 1993; Burdige, 2007; Serrano *et al*., 2016b, 2016c).

Likewise, the significant changes of $\delta^{13}C$ values observed in the first meter of matte deposits along a water depth gradient and depositional environment confirm that abiotic factors influence contribution of allochthonous organic matter to the long-term carbon sinks (Kennedy *et al*., 2010). Shallower meadows are more depleted in ^{13}C than deep meadows (Fig. 5.3.d) except for Solenzara mouth transect where SM-10 station has higher $\delta^{13}C$ values than SM-20 station (-17.79 ± 0.19‰ and -19.50 ± 0.19‰, respectively; Fig. 5.2.d). This increasing trend in isotopic signature with depth gradient (from -18.10 ± 0.02‰ to -10.95 ± 0.13‰), suggests that larger amounts of allochthonous C_{org} (non-seagrass-derived C_{org}) are buried in the shallow seagrass sediments. Shallow seagrass meadows exhibit higher productivity and canopy complexity than deep meadows (Serrano *et al.*, 2014, 2016b) which likely result in enhanced epiphytic and algal assemblages contributing up to 50% of the aboveground biomass in seagrass meadows (Borowitzka *et al*., 2006) but equally in the trapping of a higher content of fine allochthonous sediment particles contributing both to C_{org} accumulation, as reported in recent studies (Samper-Villareal *et al*., 2016; Serrano *et al*., 2016b; Mazarrasa *et al*., 2018).

Parallelly, in estuarine ecosystems, seagrass meadows are generally submitted to higher deposition of fine sediment particles resulting from terrestrial freshwater inputs (*i.e.* runoff and river discharge) and accumulated up to four-fold higher amounts of fine grain-grained particles compared to coastal meadows (Kennedy *et al*., 2010; Serrano *et al*., 2016c). The deposition of allochthonous fine sediment resulting from sestonic or freshwater terrestrial inputs led to a greater accumulation of allochthonous C_{org} which is corroborated by

depleted values of $\delta^{13}C$ in sediments (Kennedy *et al*., 2010; Serrano *et al*., 2016c; Ricart *et al*., 2020). Therefore, the ^{13}C-depleted estuarine seagrass sediments found in this study could be explained by the significantly higher mud content (personal observation) resulting from the accumulation of allochthonous sources probably discharges from Golo and Tavignano rivers. Moreover, meadows settled on sandy substrate generally located in sheltered areas (*i.e*. lower exposure to hydrodynamic energy) are characterized by an enhanced sediment deposition and a higher content of fine sediment particles compared to rocky meadows located in more exposed areas (Fonseca and Bell, 1998; Samper-Villarreal *et al*., 2016). Due to the difference in sediment hydrodynamic exposure and sediment deposition between sandy and rocky meadows, the isotopic signature of rocky seagrass sediments was expected to be ^{13}C-enriched related to the low sediment deposition compared to sandy meadows. Yet, no significant changes in sedimentary $\delta^{13}C$ values were observed associated to matrix composition (Fig. 5.3.d) contrary to recent work (Ricart *et al.*, 2017). However, the isotopic signature of C_{org} accumulated in seagrass sediments are derived from the analysis of a limited number of samples in the FT-10 core (see above). Consequently, further analyses should be undertaken to precise the influence of sediment matrix in the accumulation and storage of C_{org} from allochthonous sources.

5.4.3. Variability in C_{inorg} stocks and fluxes

In coastal temperate areas, seagrass meadows have been recognized for their high trapping and retention capacity of sediment particles (Jeudy de Grissac and Boudouresque, 1985; Gacia and Duarte, 2001). Sediments accumulated in the *P. oceanica* meadows may be also composed by a high percentage of biogenic carbonate particles resulting from biota associated with seagrass meadows (Boudouresque and Jeudy de Grissac, 1983; De Falco *et al*., 2000; Serrano *et al*., 2012). Through their high calcium carbonate ($CaCO_3$) production, *P. oceanica* meadows have been considered as one of the main 'carbonate factory' of the Mediterranean coastal areas (Canals and Ballesteros, 1997; De Falco *et al*., 2008; Mateu-Vicens *et al*., 2012). Indeed, estimates of $CaCO_3$ production in *P. oceanica* meadows performed along the Balearic and Sardinian coastline show that values ranged between 68 to 1147 g $CaCO_3$ m^{-2} yr^{-1} (Canals and Ballesteros, 1997; De Falco *et al*., 2008). In this study, the mean $CaCO_3$ accumulation rates estimated in 10 m and 20 m depth meadows at 93.20 ± 15.15

g $CaCO_3$ m^{-2} yr^{-1} (Table 5.4) is in the range of the previous estimates but show lower values than algal communities (148.2-289.4 g $CaCO_3$ m^{-2} yr^{-1}), coralligenous habitats (169-6-464.6 g $CaCO_3$ m^{-2} yr^{-1}) and maërl beds (210.0 g $CaCO_3$ m^{-2} yr^{-1}; Canals and Ballesteros, 1997). After conversion, the mean inorganic carbon (C_{inorg}) accumulation rates estimated within the site (11.18 ± 1.82 g C_{inorg} m^{-2} yr^{-1}) show to be eleven-fold less important than in seagrass sediments worldwide (126 ± 31 to 182 ± 94 g C_{inorg} m^{-2} yr^{-1}; Mazarrasa *et al*., 2015; Saderne *et al*., 2019). Furthermore, the *P. oceanica* meadows investigated in this study exhibited a four- to five-fold lower C_{inorg} accumulation rates than in Portlligat bay (Spain; 452.9 ± 15.5 g $CaCO_3$ m^{-2} yr^{-1}; Serrano *et al*., 2012) and up to twelve-fold lower values than Cinorg burial estimates from seagrass sediments of Magalluf (Balearic islands, Spain; 226 g C_{inorg} m^{-2} yr^{-1}; Barrón *et al*., 2006). According to the lower C_{inorg} accumulation rates, the mean C_{inorg} stock found in the first meter of *P. oceanica* seagrass sediments showed lower values than previous studies. Indeed, the $CaCO_3$ accumulated led to an average C_{inorg} stock of 24.5 ± 4.5 kg C_{inorg} m^{-2}, half of that stored at Portlligat (41.7 ± 1.2 kg C_{inorg} m^{-2}; Serrano *et al*., 2012). Additionally, the mean C_{inorg} stock differed substantially from those found in *Posidonia* sp. meadows (40-60 kg C_{inorg} m^{-2}) and meadows located in the Mediterranean biogeographic region (65.44 ± 7.13 kg C_{inorg} m^{-2}; Mazarrasa *et al*., 2015 and references therein). Although mean C_{inorg} accumulation and stocks per unit of area were significantly lower than values reported in previous studies, a significant variability was observed within the site.

Along the water depth gradient, seagrass sediments showed a significant increase in $CaCO_3$ and C_{inorg} content (Fig. 5.3.e; Fig. 5.3.f; Table 5.3) but also in the C_{inorg} stock (Fig. 5.7). Seagrass habitats sheltered a rich community of organisms contributing to the production of biogenic $CaCO_3$ sediments (Jeudy de Grissac and Boudouresque, 1985; Fornos and Ahr, 1997; De Falco *et al*., 2008) but also imported significant amounts of $CaCO_3$ from adjacent sources like coral reefs or terrestrial lithogenic areas (Saderne *et al*., 2019). In this study, the approximately two-fold higher C_{inorg} stock found in deep meadows (30-40 m depth; 41.73 ± 3.72 kg C_{inorg} m^{-2} in the top meter of matte) compared to shallow meadows (10-20m depth; 18.60 ± 4.41 kg C_{inorg} m^{-2}) is likely related to the significant contribution of C_{inorg} allochthonous inputs in *P. oceanica* meadows. In the eastern coast of Corsica island, the lower limit of *P. oceanica* meadows is characterized by the occurrence and the wide distribution of both biocenosis of coastal detritic bottoms and rhodolith beds (Bonacorsi, 2012; Valette-Sansevin

et al., 2019). Through their high $CaCO_3$ content (~90-95%; Fornos and Ahr, 1997; Lecca *et al*., 2005; Brandano and Civitelli, 2007; Marengo, 2011; Bonacorsi *et al*., 2014) and their high production (210 g $CaCO_3$ m^{-2} yr^{-1}; Canals and Ballesteros, 1997), these calcareous habitats probably contribute to the C_{inorg} accumulation in seagrass sediments. Even though the distribution of biogenic carbonate production areas has been well identified in circalittoral zone along the Corsican coastline, some difficulties remain to clarify about the fate and the contribution of this production to the seagrass carbon sink at the site level. However, the hypothesis that high C_{inorg} stocks in deep meadows were related to the presence of these biocenosis seems confirmed by the high amounts of free-living calcareous red algae debris (*e.g. Lithothamnion corallioides*, *Phymatolithon calcareum* and *Spongites fruticulosa*) found in *P. oceanica* matte in the lower limit of seagrass meadows. Sedimentary analysis performed in lower limit of *P. oceanica* meadows located in the Cap Corse (Corsica, France) showed that biogenic sand matrix constituted by high $CaCO_3$ content (~60%) was also characterized by the presence of free-living calcareous organisms (*Lithothamnion valens*, *Lithophyllum racemus*) due to the interactions of rhodolith beds with seagrass meadows (Marengo, 2011; Bonacorsi, 2012). Thus, the concurrent export of $CaCO_3$ production from circalittoral coastal detritic bottoms and rhodoliths beds toward the coastline due to marine currents (Marengo, 2011) and the trapping of fine to coarse carbonate fragments and particles by the *P. oceanica* meadows likely explain the higher C_{inorg} stock found in the lower limit of seagrass meadows and probably confirm the role of seagrass meadows as major allochthonous C_{inorg} burial sites (Saderne *et al*., 2019). Furthermore, the high C_{inorg} stock reported in deep waters may be also related to the accumulation of C_{inorg} production resulting from the *P. oceanica* meadows which colonized lower bathymetric range before the sea level rise during the Pleistocene and Holocene periods (De Falco *et al*., 2011). Consequently, further studies should be achieved to better understand the processes leading to high amounts of C_{inorg} stocks in these areas.

P. oceanica meadows growing on a rocky matrix exhibited substantial higher C_{inorg} accumulation rates and stocks in the first 30 cm of matte than meadows growing on sandy bottom (Fig. 5.5.b; Fig. 5.8.d). The significantly higher $\%CaCO_3$ content found in meadows on rocky subtrate showed to be inconsistent with a previous work performed in Ponza (Pointinian Islands, Italy) by Mateu-Vicens *et al*. (2012) where $CaCO_3$ content in *P. oceanica* seagrass sediments was negatively correlated with rocky matrix. Indeed, the erosional pattern found

in exposed areas seemed to be responsible for the low content in $CaCO_3$ of temperate seagrass (Perry and Beavington-Penney, 2005). Here, the approximately two-fold difference in superficial C_{inorg} stocks (top 30 cm) between sandy and rocky matrix may be related to the presence of higher biogenic carbonate production associated with photophilic algal communities growing on rocky substrata enhancing C_{inorg} deposition in seagrass sediments for a short-term period. Photophilic algal communities exhibited one of the highest carbonate production rate among Mediterranean benthic ecosystems (34.73 g C_{inorg} m^{-2} yr^{-1}) while seagrass habitats displayed lower values (8.18-18.96 g C_{inorg} m^{-2} yr^{-1}; Romero, 1988; Canals and Ballesteros, 1997). Considering the first meter of matte, no significant difference was observed in C_{inorg} accumulation rates between sandy and rocky matrix (Fig. 5.5.d), and C_{inorg} stocks showed only a slight differences (Fig. 5.8.e). Finally, in a 250 cm-thick matte, the C_{inorg} stocks found in meadows settled on sandy substrate exceeded those found in rocky bottom. The higher deposition of fine particles and the lower erosion and exposure to hydrodynamic energy in sheltered meadows probably may have contributed to a higher preservation of the C_{inorg} over a longer period of time.

The carbonate production in the *P. oceanica* meadows is mainly due to heterotrophic (*i.e.* light-independent) organisms, well adapted to this ecosystem (*e.g.* Foraminifera, Bryozoa, Mollusca, Annelida, Arthropoda) but also to autotrophic and mixotrophic (*i.e.* light-dependent) organisms such Rhodophyta (*e.g. Pneophyllum* sp., *Hydrolithon* sp., *Titanoderma* sp.; Canals and Ballesteros, 1997; Mateu-Vicens *et al*., 2012). Yet, though photo-independent calcareous organisms are quantitatively more important, light remains a major factor controlling the carbonate production of these organisms within seagrass meadows. Heterotrophic organisms are significantly related to the presence of *P. oceanica* due to the formation of shelters and substrate for many carbonate producers (Mateu-Vicens *et al*., 2012). Consequently, lower shoot density and canopy complexity observed with decreasing light availability associated with a turbidity gradient may explained the lower $\%CaCO_3$, $\%C_{inorg}$, C_{inorg} accumulation rates and stocks observed in estuarine environments (Fig. 5.3.e; Fig. 5.3.f; Fig. 5.5; Fig. 5.8.).

5.4.4. Implications for climate change mitigation

The C_{org} and C_{inorg} stocks per unit area combined to the morpho-bathymetric DTM of sea bottoms modelled for the study site have contributed to estimate the global amount of carbon stored within the sedimentary pool beneath *P. oceanica* meadows ((Monnier *et al*., 2020; Fig. 5.10). In order to assess the global contribution of long-term carbon sinks to the climate change mitigation, values have been converted in CO_2 equivalent (CO_{2e}) multiplying C_{org} values by 3.67 (Howard *et al*., 2014a). Over the entire area studied, the amount of CO_{2e} stored have been estimated at 22.8 and 48.3 million t CO_{2e} for the top 100 cm and 250 cm of matte deposits, respectively (Table 5.5). Considering the annual CO_2 release per capita in France in 2018 (5.2 t CO_2 yr^{-1} $capita^{-1}$; Gilfillan *et al*., 2019; UNFCCC, 2019; BP, 2019) and the population estimated for Corsica (Pergent-Martini *et al*., 2020), the total amount of CO_2 emitted yearly at regional scale has been estimated at 1.8 million t CO_2. Thus, assuming that global CO_2 release was equivalent every year, the amount of CO_{2e} stored in the first 100 cm and 250 cm of long-term carbon sink associated with *P. oceanica* meadows is equivalent to 12.9 and 27.4 years of CO_2 emissions by the entire Corsican population, respectively.

At regional scale, the mapping of benthic habitats along the coastline performed by Valette-Sansevin *et al.* (2019) has contributed to estimate the area occupied by *P. oceanica* meadows which have been estimated at 53 735 ha. Based on this value and the mean C_{org} stocks per unit area (30.5 ± 0.2 kg C_{org} m^{-2} and 64.5 ± 0.1 kg C_{org} m^{-2} for the top 100 and 250 cm of matte, respectively), the global C_{org} stock beneath *P. oceanica* meadows have been estimated at 16.4 ± 0.1 million t C_{org} and 34.6 ± 0.1 million t C_{org} corresponding to 60.2 ± 0.4 million t CO_{2e} and 127.0 ± 0.2 million t CO_{2e}, respectively (Table 5.5). By dividing these regional CO_{2e} stocks estimates by the regional CO_2 emissions, the amount of CO_{2e} stored in the *P. oceanica* matte equals the CO_2 emissions of the population over 34.1 ± 0.2 and 72.0 ± 0.1 years, respectively (Table 5.5).

Table 5.5. Estimates of global C_{org} and CO_{2e} stocks in the first 100 cm and 250 cm of *P. oceanica* matte at site and regional scales. (1) Estimates performed within the site (Fig. 5.10.a; Fig. 5.10.c). (2) Calculated by multiplying the annual CO_2 release per capita in France in 2018 (5.2 t CO_2 yr^{-1} $capita^{-1}$) by the total population of Corsica. (3) Estimates performed within the site (see. Fig. 5.10.a and Fig. 5.10.c).

Study site				
Matte thickness	**Total C_{org} stock ($\times 10^6$ t C_{org})**	**Total CO_{2e} stock ($\times 10^6$ t CO_2)**	**Total CO_2 release per year in Corsica (2) ($\times 10^6$ t CO_2 yr^{-1})**	**Equivalent in years of CO_2 emissions**
100 cm	6.2 (1)	22.8	1.8	12.9
250 cm	13.2 (1)	48.3		27.4

Corsica					
Matte thickness	**Mean ± S.E. C_{org} stock (kg C_{org} m^{-2})**	**Total C_{org} stock ($\times 10^6$ t C_{org})**	**Total CO_{2e} stock ($\times 10^6$ t CO_2)**	**Total CO_2 release per year in Corsica (2) ($\times 10^6$ t CO_2 yr^{-1})**	**Equivalent in years of CO_2 emissions**
100 cm	30.5 ± 0.2 (3)	16.4 ± 0.1	60.2 ± 0.4	1.8	34.1 ± 0.2
250 cm	64.5 ± 0.1 (3)	34.6 ± 0.1	127.0 ± 0.2		72.0 ± 0.1

Most of global the Blue Carbon (BC) inventories performed in the last decades was focused mainly on C_{org}, neglecting C_{inorg} stock resulting from $CaCO_3$ production (Mcleod *et al*., 2011; Duarte *et al*., 2013). But given that the $CaCO_3$ fraction may contribute substantially to the C_{inorg} stocks in seagrass meadows (Mazarrasa *et al*., 2015; Saderne *et al*., 2019), several studies have recently emphasized the necessity to include $CaCO_3$ production to determine the balance 'carbon sink-carbon source' of these BC ecosystems (Pergent *et al*., 2012; Howard *et al*., 2014b; Macreadie *et al*., 2017; Gullström *et al*., 2018). Through the high C_{org} burial rate and storage, seagrass meadows are considered as long-term CO_2 sinks but this capacity should be considered in relation to C_{inorg} production and storage to evaluate the net exchange of CO_2 (Howard *et al*., 2014b). Indeed, if the calcification process leads to a net emission of CO_2 ('rule of the 0.6'; Ware *et al*., 1992; Frankignoulle *et al*., 1994), then the CO_2 emission resulting from this processes has to be subtracted from the C_{org} fluxes and stocks. For instance, a global estimate performed for the entire Mediterranean demonstrated that calcification in *P. oceanica* meadows could be responsible for the emission of 2.6 to 15.4 Tg CO_{2e} to the atmosphere (Mateo and Serrano, 2012). By associating these estimates with the organic sink, this study proved that *P. oceanica* ecosystems could also represent a significant net CO_2 source (-27.2 to +14.3 Tg CO_2 yr^{-1}; Mateo and Serrano, 2012).

However, one of the main difficulties to assess the role of BC ecosystems as carbon sink or source is to evaluate the net $CaCO_3$ production associated with these habitats and the allochthonous inputs resulting from adjacent sources (Kennedy *et al*., 2010; Saderne *et al*., 2019). Though calcification resulting from calcareous organisms showed to have an important contribution in the C_{inorg} accumulation rates and stock in BC ecosystems (Serrano *et al*., 2012; Mazarrasa *et al*., 2015), many benthic habitats (*e.g.* photophilic algal communities, coralligenous biocenosis, coastal detritic bottoms and rhodolith beds, coral reefs) with high $CaCO_3$ content (Canals and Ballesteros, 1997; Bonacorsi *et al*., 2014) may contributed to the deposition of C_{inorg} in seagrass ecosystems (Saderne *et al*., 2019) and notably *P. oceanica* which constituted one of their main habitats in the infralittoral zone along Mediterranean shorelines (Hemminga and Duarte, 2000; Boudouresque *et al*., 2012).

Assuming that all soil carbon stocks and fluxes in the *P. oceanica* meadows resulted from autochthonous sources (no export of autochthonous carbon and no import of allochthonous carbon) as reported by Howard *et al*. (2014), estimates of net CO_{2e} burial and net CO_{2e} stock were performed at the site scale (Table 5.6; Table 5.7) following the method established in Howard *et al*. (2014) and Macreadie *et al*. (2017). Thus, estimates of net CO_{2e} burial and net CO_{2e} stocks were calculated using the following equations:

$$\text{net } CO_{2e} \text{ burial} = [\ C_{org} \text{ burial} - \psi \times C_{inorg} \text{ burial}\ ] \times 3.67 \qquad (1)$$

$$\text{net } CO_{2e} \text{ stock} = [\ C_{org} \text{ stock} - \psi \times C_{inorg} \text{ stock}\ ] \times 3.67 \qquad (2)$$

where C_{org} and C_{inorg} burial are the C_{org} and C_{inorg} accumulated (g C_{org} m^{-2} yr^{-1} and g C_{inorg} m^{-2} yr^{-1}, respectively), ψ is the gas exchange : reaction ratio of CO_2 and $CaCO_3$ proposed by Smith (2013) (ψ =0.6, estimated for the shallow waters and used by Mazarrasa *et al*., 2015) and C_{org} and C_{inorg} stock are the C_{org} and C_{inorg} stored (kg C_{org} m^{-2} and kg C_{inorg} m^{-2}, respectively).

Thus, taking *P. oceanica* matte C_{org} and C_{inorg} accumulation rates into account, seagrass meadows seem to constitute net sinks of CO_2 (Table 5.6). Indeed, by applying the 'rule of the 0.6', a decrease of net C_{org} burial capacity was observed (estimated between 8.7 to 24.3%) but these results assume that *P. oceanica* meadows are net CO_2 sink along the eastern coast of

Corsica. The results highlighted also an average net CO_{2e} accumulation rate of 133.6 ± 29.4 g CO_{2e} m^{-2} yr^{-1} (1.3 t CO_{2e} ha^{-1} yr^{-1}) which appears to be coherent with the average value estimated along the Andalusian coast (Spain; 1.3 t CO_{2e} ha^{-1} yr^{-1}; Mateo *et al.*, 2018). However, it appears important to mention that C_{org} and C_{inorg} accumulation rates in this study have been calculated for shallow waters (10-20 m; Figs. 5.5), not taking into consideration the C_{inorg} accumulation rates in deeper areas (30-40 m) where high C_{inorg} stocks have been found in seagrass meadows sediments (Fig. 5.7.e).

Table 5.6. Estimates of net C_{org} and net CO_{2e} burial in the first 100 cm of *P. oceanica* sediments based on the balance between their C_{org} accumulation rates (CO_2 sink) and C_{inorg} accumulation rates (CO_2 source). (1) Calculated by multiplying the C_{inorg} accumulation rates by 0.6 to meet the assumption that 0.6 moles of CO_2 are released per mole of $CaCO_3$ precipitated, then deducting this adjusted C_{inorg} value from C_{org} accumulation rates to get the net C_{org} burial (in green: C_{org} and CO_2 net sink). (2) Calculated by multiplying net C_{org} burial by 3.67.

Top 100 cm		**C_{org} burial (g C_{org} m^{-2} yr^{-1})**	**C_{inorg} burial (g C_{inorg} m^{-2} yr^{-1})**	**net C_{org} burial (1) (g C_{org} m^{-2} yr^{-1})**	**net CO_{2e} burial (2) (g CO_{2e} m^{-2} yr^{-1})**
	n	**Mean ± S.E.**	**Mean ± S.E.**	**Mean ± S.E.**	**Mean ± S.E.**
Mean	11	43.2 ± 8.7	11.2 ± 1.8	36.4 ± 8.0	133.6 ± 29.4
Depth					
10 m	5	65.8 ± 10.9	12.9 ± 3.7	58.0 ± 9.0	212.9 ± 33.0
20 m	6	24.3 ± 6.3	9.7 ± 1.4	18.4 ± 6.1	67.5 ± 22.4
Substrate					
Sandy bottom	4	39.6 ± 8.7	11.2 ± 2.0	32.9 ± 7.9	102.7 ± 28.9
Rocky bottom	1	78.7 ± 0.0	11.5 ± 0.0	71.8 ± 0.0	263.5 ± 0.0
Depositional environment					
Open sea	7	53.2 ± 11.7	13.4 ± 2.4	45.2 ± 10.9	165.9 ± 40.0
Estuary	4	25.6 ± 6.9	7.4 ± 1.4	21.1 ± 6.5	77.4 ± 23.9

Considering the C_{org} and C_{inorg} stocks estimates over the top 100 cm of matte, *P. oceanica* meadows along the eastern coast of Corsica seem to constitute net CO_{2e} sinks, except for the 30 m depth where a negative net CO_{2e} stock has been revealed (-8.3 ± 24.6 kg CO_{2e} m^{-2}; Table 5.7) due to the high amount of C_{inorg} stored at this depth (Fig. 5.7.e). When considering the first 250 cm of *P. oceanica* matte, comparable results were obtained for the meadows located at 30 m (-75.9 ± 60.4 kg CO_{2e} m^{-2}) and 40 m depth (-92.3 ± 123.7 kg CO_{2e} m^{-2}) (Table 5.7). Thus, contrary to shallow areas, meadows located in deep areas within the study site seem to constitute net CO_2 sources related to the high C_{inorg} stock found in their sediments.

Table 5.7. Estimates of net C_{org} and net CO_2 stock in the first 100 cm (top) and 250 cm (bottom) of *P. oceanica* sediments based on the balance between the C_{org} stock (CO_2 sink) and the C_{inorg} stock (CO_2 source). (1) Calculated by multiplying the C_{inorg} stock by 0.6 to meet the assumption that 0.6 moles of CO_2 are released per mole of $CaCO_3$ precipitated, then deducting this adjusted C_{inorg} value from the C_{org} stock to get the net CO_2 stock (in green: net CO_2 sink, in red: net CO_2 source). (2) Calculated by multiplying the net C_{org} stock by 3.67.

Top 100 cm		**C_{org} stock (kg C_{org} m^{-2})**	**C_{inorg} stock (kg C_{inorg} m^{-2})**	**net C_{org} stock (1) (kg C_{org} m^{-2})**	**net CO_{2e} stock (2) (kg CO_{2e} m^{-2})**
	n	**Mean ± S.E.**	**Mean ± S.E.**	**Mean ± S.E.**	**Mean ± S.E.**
Mean	19	31.6 ± 2.0	24.5 ± 4.3	17.0 ± 3.6	62.3 ± 13.2
Depth					
10 m	7	33.7 ± 3.9	10.3 ± 2.7	27.5 ± 4.6	100.9 ± 16.8
15 m	1	37.9 ± 0.0	18.5 ± 0.0	26.8 ± 0.0	98.4 ± 0.0
20 m	6	33.2 ± 2.3	27.7 ± 6.1	16.6 ± 2.8	61.0 ± 10.2
30 m	3	25.8 ± 5.7	46.8 ± 12.8	-2.3 ± 6.7	-8.3 ± 24.6
40 m	2	25.0 ± 7.0	41.0 ± 13.8	0.4 ± 15.3	1.4 ± 56.3
Substrate					
Sandy bottom	5	38.8 ± 2.5	9.8 ± 3.1	33.0 ± 2.8	121.0 ± 10.4
Rocky bottom	2	20.8 ± 5.3	11.6 ± 7.6	13.8 ± 9.8	50.8 ± 36.1
Depositional environment					
Open sea	15	30.6 ± 2.3	27.6 ± 4.9	14.1 ± 4.1	51.8 ± 15.1
Estuary	4	35.4 ± 4.3	12.9 ± 6.2	27.7 ± 4.7	101.6 ± 17.1

Top 250 cm		**C_{org} stock (kg C_{org} m^{-2})**	**C_{inorg} stock (kg C_{inorg} m^{-2})**	**net C_{org} stock (1) (kg C_{org} m^{-2})**	**net CO_{2e} stock (2) (kg CO_{2e} m^{-2})**
	n	**Mean ± S.E.**	**Mean ± S.E.**	**Mean ± S.E.**	**Mean ± S.E.**
Mean	19	70.4 ± 6.4	60.5 ± 10.2	34.1 ± 10.2	125.1 ± 37.4
Depth					
10 m	7	82.4 ± 9.6	29.8 ± 7.7	64.5 ± 8.3	236.8 ± 30.4
15 m	1	96.0 ± 0.0	42.8 ± 0.0	70.3 ± 0.0	258.2 ± 0.0
20 m	6	76.9 ± 8.3	71.8 ± 17.5	33.9 ± 13.1	124.3 ± 47.9
30 m	3	40.1 ± 10.7	101.2 ± 30.9	-20.7 ± 16.4	-75.9 ± 60.4
40 m	2	36.3 ± 12.4	102.4 ± 35.4	-25.2 ± 33.7	-92.3 ± 123.7
Substrate					
Sandy bottom	5	94.2 ± 7.3	35.7 ± 9.2	72.8 ± 6.8	267.2 ± 25.1
Rocky bottom	2	53.0 ± 13.4	15.2 ± 9.9	43.8 ± 19.3	160.8 ± 70.8
Depositional environment					
Open sea	15	65.9 ± 7.1	68.7 ± 11.9	24.7 ± 11.6	90.7 ± 42.7
Estuary	4	87.3 ± 12.8	30.0 ± 8.1	69.3 ± 9.9	254.3 ± 36.2

By applying Eq. 2 to the global estimates of C_{org} and C_{inorg} stocks predicted by using morpho-bathymetric DTM raster mosaic of the sea bottom (Figs. 5.10), the contribution of the top 100 cm (Fig. 5.11.a) and the top 250 cm (Fig. 5.11.b) of *P. oceanica* matte deposits as carbon sink or carbon source have been estimated. Although global C_{org} stocks showed lower values compared to previous estimates (Fig. 5.10.a; Fig., 5.10.c; Table 5.5), *P. oceanica* meadows of the study site are assumed to be a net C_{org} and CO_{2e} sink. Indeed, the global amount of CO_{2e} stored in the top 100 cm and 250 cm of matte deposits have been estimated at 9.9 and 16.5 million t CO_{2e}, respectively (Table 5.8), which correspond to 5.6 and 9.4 years of CO_2 release by Corsican population, respectively (Table 5.8).

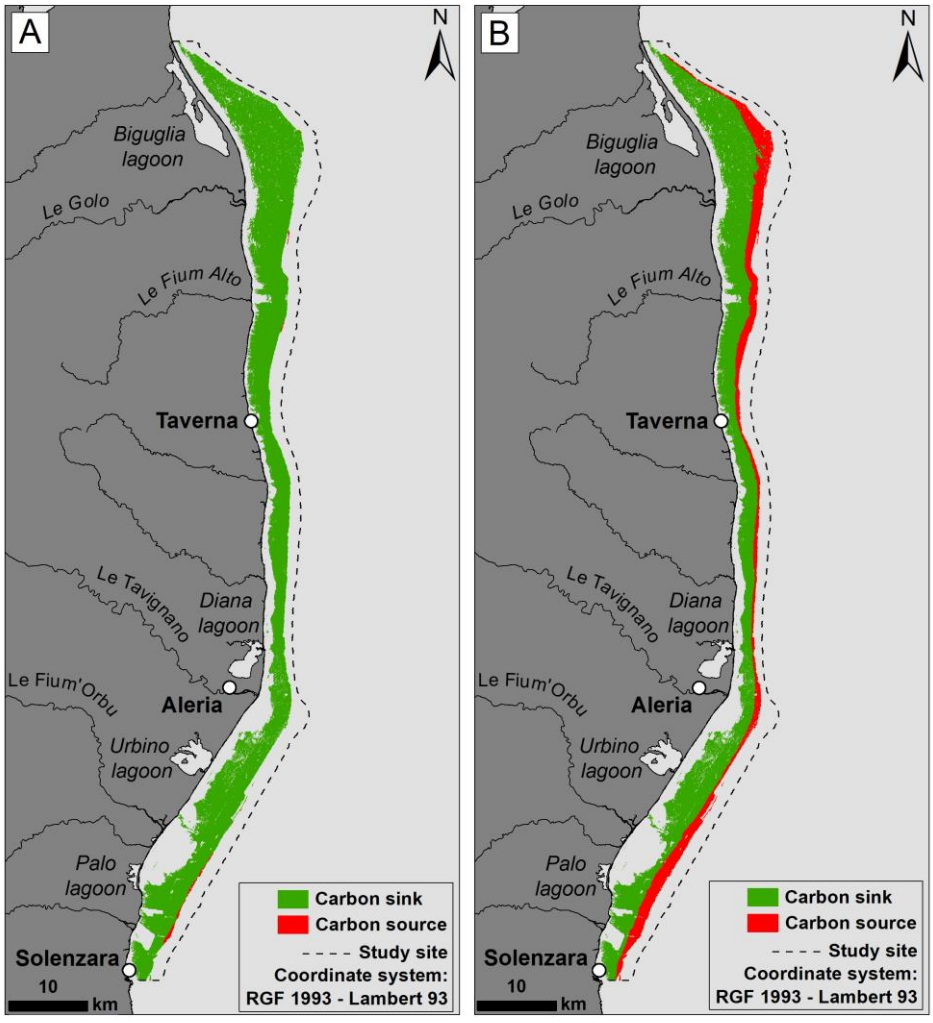

Figure 5.11. Contribution of the first 100 cm (a) and 250 cm (b) of *P. oceanica* matte deposits as CO_2 sink (in green) or CO_2 source (in red) based on the balance between C_{org} stock and C_{inorg} stock. Calculated by multiplying the C_{inorg} stock value in each DTM raster cell (Fig. 5.10.b and Fig. 5.10.d) by 0.6 to meet the assumption that 0.6 moles of CO_2 is released per mole of $CaCO_3$ precipitated, then deducting this adjusted C_{inorg} value from the C_{org} stock (Fig. 5.10.a and Fig. 5.10.c) to get the net CO_2 stock.

Table 5.8. Estimates of global C_{org} and CO_{2e} stocks in the first 100 cm and 250 cm of *P. oceanica* matte at site and regional scales by applying 'the rule of the 0.6' (Ware *et al*., 1992). (1) Estimates performed within the site (Fig. 5.11.a; Fig. 5.11b). (2) Calculated by multiplying the annual CO_2 release per capita in France in 2018 (5.2 t CO_2 yr^{-1} $capita^{-1}$) by the total population of Corsica. (3) Estimates performed within the site (see. Fig. 5.11.a and Fig. 5.11.b).

Study site				
Matte thickness	**Total C_{org} stock ($\times 10^6$ t C_{org})**	**Total CO_{2e} stock ($\times 10^6$ t CO_2)**	**Total CO_2 release per year in Corsica (2) ($\times 10^6$ t CO_2 yr^{-1})**	**Equivalent in years of CO_2 emissions**
100 cm	2.7 (1)	9.9	1.8	5.6
250 cm	4.5 (1)	16.5		9.4

Corsica					
Matte thickness	**Mean ± S.E. C_{org} stock (kg C_{org} m^{-2})**	**Total C_{org} stock ($\times 10^6$ t C_{org})**	**Total CO_{2e} stock ($\times 10^6$ t CO_2)**	**Total CO_2 release per year in Corsica (2) ($\times 10^6$ t CO_2 yr^{-1})**	**Equivalent in years of CO_2 emissions**
100 cm	13.2 ± 0.1 (3)	7.1 ± 0.1	26.0 ± 0.2	1.8	14.7 ± 0.1
250 cm	22.0 ± 0.1 (3)	11.8 ± 0.1	43.4 ± 0.2		26.6 ± 0.1

At regional scale, the global net CO_{2e} stock found in the sedimentary pool of *P. oceanica* meadows have been estimated at 26.0 ± 0.2 million t CO_{2e} (top 100 cm) and 43.4 ± 0.2 million t CO_{2e} (top 250 cm) which is equivalent to 14.7 ± 0.1 and 26.6 ± 0.1 years of CO_2 release of the entire population of Corsica island. The global estimates presented here show that *P. oceanica* meadows are significant net CO_2 reservoirs. However, this study has also underlined the necessity to account for biotic and abiotic factors leading to variability in C_{org} and C_{inorg} burial rates and stocks into *P. oceanica* sediments. Given the results obtained, this study confirms the crucial necessity to include both the soil C_{org} and C_{inorg} accumulation rates and stocks when assessing the carbon sink-source balance of these ecosystems in order to precise the contribution of these Blue Carbon ecosystems to the climate change mitigation.

Chapitre 6

Long-term dynamics of a *Cladocora caespitosa* bank as recorded by a *Posidonia oceanica* millenary archive

Abstract

Along most Mediterranean coasts, the endemic seagrass species *Posidonia oceanica* builds extensive meadows and complex peat-like bioconstructions known as 'matte'. These belowground deposits are recognized as a valuable long-term archive allowing the reconstruction and the study of palaeo-climatic and palaeo-ecological changes in the coastal environment over the Holocene period. One of the *P. oceanica* matte cores sampled during a coring survey along the eastern continental shelf of Corsica Island (France, NW Mediterranean) revealed the unprecedented finding of a dead bank of the scleratinian coral *Cladocora caespitosa* embedded in the matte. Measurement of the morphological and biometrical features of corallite fragments coupled to biogeosedimentological analysis and radiocarbon dating contributed to provide a basis for the reconstruction of the stratigraphic sequence since the mid-Holocene (last 4750 years). The study of the sediment core enabled identification of three major phases: (i) the settlement of the *C. caespitosa* colonies (~4750-3930 cal. yr BP), (ii) the coexistence of the *C. caespitosa* bank and the *P. oceanica* meadow (~3930-1410 cal. yr BP), followed by (iii) the death of the coral bank and the development of the *P. oceanica* meadow (~1410 cal. yr BP-present). The sclerochronological analysis completed on the well-preserved corallite fragments revealed that the mean annual growth rate of the coral ranged between 1.9-3.1 mm yr^{-1} with a mean value estimated at 2.3 ± 0.8 mm yr^{-1}. Trend analysis showed semi-millennial to millennial oscillations in annual growth rates which are probably related to environmental climatic changes during this period (Subatlantic Period, 2925-2200 cal. yr BP) to Dark Ages Cold Period (1500-1000 cal. yr BP). After ~1750 cal. yr BP, the decline and the death of the bank (~1410 cal. yr BP) was probably due to the combined effect of a prolonged increase in summer temperatures and an increase in the competition with the *P. oceanica* meadow during the Roman Warm Period (2200-1500 cal. yr BP).

6.1. Introduction

Palaeo-environmental reconstruction studies provide interesting local or regional broad-based information on natural fluctuations and ecosystem successions at millennial to centennial scales (Mateo *et al*., 2010). The reconstruction of long-term environmental changes requires adequate preservation of palaeo-records and proxies. In terrestrial ecosystems, peatlands and lacustrine sediments represent the best examples of palaeo-archives (Clymo, 1992, Reille *et al*., 1999). With a few exceptions (*i.e*. coral reefs, coastal swamps and marine phanerogams; Reille, 1984; Laborel *et al*., 1961; Mateo *et al*., 2002; Peirano *et al*., 2004; Montagna *et al*., 2007; Serrano *et al*., 2012; Currás *et al*., 2017), coastal and marine ecosystems rarely meet the appropriate conditions to ensure reliable palaeo-environmental reconstruction of the seabed due to high hydrodynamic energy and bioturbation at the marine-terrestrial interface (Mateo *et al*., 2002, 2010).

In the Mediterranean Sea, the endemic seagrass *Posidonia oceanica* (Linnaeus) Delile forms extensive and highly productive meadows all along the coast in the infralittoral area (Boudouresque *et al*., 2012). The development of the meadows results in the formation of a complex peat-like bioconstruction known as 'matte' (Molinier and Picard, 1952). This deposit, mainly composed by biogenic debris from the belowground organs of the plant (sheaths, rhizomes and roots), shows has a very low decay rate owing to the highly refractory nature of seagrass remains (Kaal *et al*., 2016). The accumulation of large quantities of *P. oceanica* debris and allochthonous particles associated with the anoxic condition prevailing in the matte results in the formation of structures up to 14 m in thickness (Miković, 1977; Boudouresque *et al*., 1980; Lo Iacono *et al*., 2008; Serrano *et al*., 2012). The high chronostratigraphic consistency and preservation of this organic-rich material accumulated over millennia constitutes an interesting biogeochemical sink and a unique palaeo-ecological archive for the study of the historical changes in the Mediterranean coastal environment during the Holocene. In the last decades, several palaeo-ecological applications have proven that *P. oceanica* matte is a valuable archive of environmental information for the reconstruction of vegetation and landscape dynamics, anthropogenic activities and changes in palaeo-climatic and meadow productivity over the last millennia (López-Saéz *et al*., 2009; Mateo *et al*., 2010;

Serrano *et al*., 2011, 2012, 2013; López-Merino *et al*., 2015, 2017; El Zrilli *et al*., 2017; Leiva-Dueñas *et al*., 2018).

This archive is also recognized for the unusually good preservation conditions of abundant carbonate and siliceous fossil remains from marine organisms inhabiting the microhabitats formed by the leaf canopy, the rhizome layer and the matte of *P. oceanica* (Harmelin *et al*., 1964; Russo *et al*., 1984, 1991a, 1991b; Scipione *et al*., 1996; Buia *et al*., 2000). To our knowledge, Boudouresque *et al*. (1980), were the first to describe a fossil biogenic reef formation built by calcifying Rhodophyceae embedded in the matte of *P. oceanica* in the bay of Calvi (France). Although marine bioconstructors and biogenic structures are common in the Mediterranean Sea (Laborel, 1987; Relini, 2009; Ingrosso *et al*., 2018), the discovery and description of the shift from biogenic reef formations from calcareous organisms to marine phanerogam soils are unprecedented and reflect significant environmental and climatic events.

One of the most widespread bioconstructional organisms is the zooxanthellate and colonial scleractinian coral *Cladocora caespitosa* (Linnaeus, 1767) (Zibrowius, 1980; Peirano *et al*., 2004). This species can develop from several meters below the sea surface down to 40 m depth (Morri *et al*., 1994; Peirano *et al*., 1998). It occurs in a wide range of habitats from rocky to sandy substrates, and from clear waters with high irradiance to exposed areas with strong marine currents and turbid waters (Zibrowius, 1982; Schiller, 1993a; Peirano *et al*., 1999; Kružić and Benković 2008, Kersting and Linares 2012). The *C. caespitosa* coral forms hemispherical and phaceloid colonies constituted by distinct tubular corallites growing in a continuous rectilinear way. The banding pattern of corallites studied by perfoming sclerochronological analysis, showed an annual growth rate ranging from 1.3 to 6.9 mm yr^{-1} (Peirano *et al*., 1999, 2005; Kružić and Požar-Domac, 2002). Several studies have reported that the variation in the skeletal growth is related to environmental factors (*i.e.* temperature, turbidity and irradiance) and proved that *C. caespitosa* coral represents a valid proxy for past climate fluctuations (Morri *et al*., 2001; Ferrier-Pagès *et al*., 2003; Peirano *et al*., 2004; Silenzi *et al*., 2005; Montagna *et al*., 2007).

The colonies of *C. caespitosa* live solitarily but can occur in three distinct formations know as (i) 'beds' (dense populations of several distinct colonies), (ii) 'banks' (formed of several large connected colonies) rising up to 1 m above the surrounding seafloor and covering several square meters), and (iii) free-living coral nodules or coralliths (Kersting *et al*., 2017, Ingrosso *et al*., 2018). These living banks or beds have been reported at several sites in the Mediterranean, but the largest structures have been recorded in the Adriatic Sea along the Croatian and Slovenian coasts (Schiller 1993a; Kružić and Požar-Domac, 2002, 2003; Kružić and Benković, 2008), along the coasts of Italy (Morri *et al*., 1994, 2000; Peirano *et al*., 2001, 2005; Rodolfo-Metalpa *et al*., 2008), Spain (Casado-Amezúa *et al*., 2011; 2014; Kersting and Linares 2012; Kersting *et al*., 2013), France (Laborel and Laborel-Deguen, 1978; Casado-Amezúa *et al*., 2015), in the Levantine basin along the coasts of Greece (Laborel, 1961, 1987), Turkey (Öztürk, 2004; Özalp and Alparslan, 2011), Cyprus (Jiménez *et al*., 2014), and in Tunisia (Zibrowius, 1980). The existence of major fossil deposits of *C. caespitosa* from the Holocene and Pleistocene have been mentioned from several localities (Fornós *et al*., 1996; Kühlmann, 1996; Bernasconi *et al*., 1997; Peirano *et al*., 1998, 2009), but the oldest have been described in Spain (Aguirre and Jiménez, 1998). Throughout the Mediterranean, well-preserved 'subfossil' formations of *C. caespitosa* covered by thick sediment layers or calcareous algae have been also described (Peirano *et al*., 1998 and references therein). In Corsica, similar dead banks dated back to 600-2400 years BP and reaching several meters diameter were reported by Laborel (1987).

This paper focuses on the description of well-preserved corallite fragments of a *C. caespitosa* bank found in a *P. oceanica* matte sequence on the eastern coast of Corsica. The analysis of the morphological features of coral fragments coupled to biogeosedimentological characterization and radiocarbon dating provided (i) a first evaluation of the past annual growth rate of *C. caespitosa* in this location, and (ii) the opportunity to describe a colonization event of the substrate by *C. caespitosa* followed by its gradual substitution by a *P. oceanica* meadow.

6.2. Material and methods

6.2.1. Study site

The shelf of the eastern continental margin of Corsica Island (France, NW Mediterranean) is characterized by a 5-25 km width range with a low gradient slope (~1-2°) (Gervais *et al*., 2006; Pluquet, 2006). The widest extension of this continental shelf is notably observed off the Golo fan system (Bellaiche *et al*., 1994; Mulder and Maneux, 1999; Gervais *et al*., 2004). The infralittoral zone of the underwater delta of the Golo river presents the largest *P. oceanica* meadow in Corsica (Fig. 6.1). The *C. caespitosa* studied occurs near the upper limit of the *P. oceanica* meadows. The marine currents on the east margin, represented by coastal drift oriented towards the south (Millot *et al*., 1987 *in* Pluquet, 2006), are moderate to strong and have generated several landscape discontinuities ('intermattes'; Abadie *et al*., 2015). The sea bottom is dominated by sand fractions with interspersed areas with larger grain sizes, from gravels to pebbles (Guennoc *et al*., 2001). Though concentrations of suspended matter have been lower over the last century, sediment deposits have been strongly influenced by the Mediterranean climate, extreme events (*e.g*. flash floods, shelf storms) and long-shore drift (Conchon, 1975; Orszag-Sperber and Pilot, 1976; Conchon and Gauthier, 1985). The mean monthly sea surface temperature (SST) recorded between 2014 and 2019 ranges from 14.21 ± 0.22°C (February) to 26.85 ± 0.96°C (August) (buoy WMO #6100295; http://www.emodnet-physics.eu/map).

6.2.2. Sampling of sediment

Sediment sampling was performed with a Kullenberg gravity corer during the oceanographic research survey Carbonsink (August 2018) aboard the R/V L'Europe (Ifremer). The core barrel consists of a stainless-steel tube 5 m long with a PVC tube (internal diameter 90 mm) inside it and surmounted by a lead weight of ~1 ton. The coring head is constituted of a sharp edge to cut the fibrous matte material and minimize the effects of compression during sediment sampling. Among the 12 cores taken in this sector, deposits of *C. caespitosa* fragments were only observed in one of them (BIG-10M-PO-A). The collection of this vertical core in the matte of *P. oceanica* was carried out at 10.0 ± 0.5 m (mean depth ± S.D.). The

corers were cut open longitudinally, the matte sliced at regular 5 cm intervals and the subsamples stored in polypropylene vials at 5°C before processing.

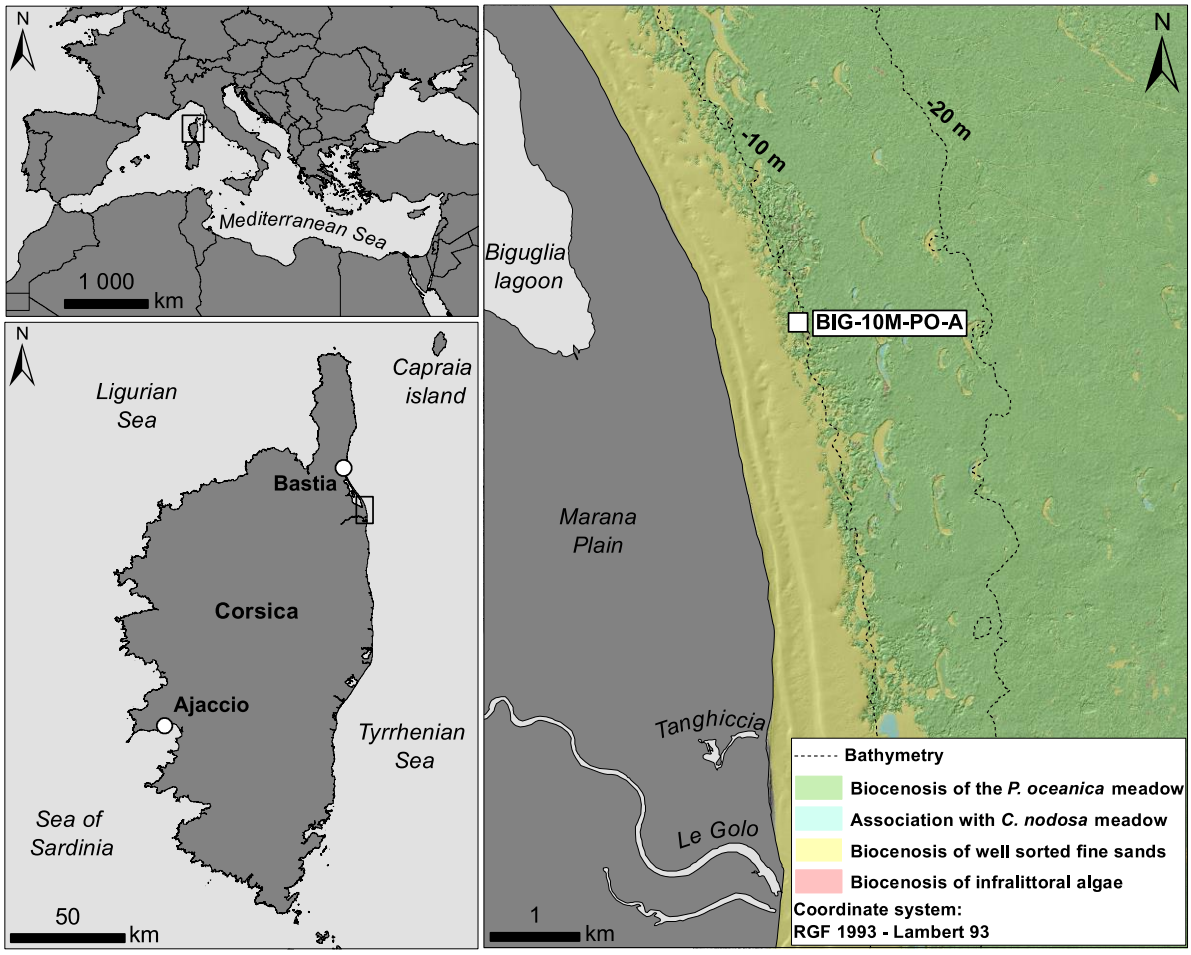

Figure 6.1. Location of the study site on the eastern continental shelf of Corsica.

6.2.3. Laboratory analysis of sediment core

Sediment bulk density and grain size were measured after drying the samples at 70 °C until constant weight (Howard *et al*., 2014a). The samples were sieved and weighed after drying and then separated into two fractions: the fine (<2 mm) and coarse fraction (>2 mm). The fine fraction is composed of the inorganic and organic matter of the sediment (SOM). The coarse fraction was sorted into different categories: (i) the coarse organic fraction (COM, fragments of *P. oceanica*), (ii) the coarse mineral fraction (gravel), and (iii) the coarse

carbonate fraction (shells and biogenic debris). After sorting, the COM was ground, homogenized and integrated into the fine fraction. The total organic matter (TOM) and calcium carbonate ($CaCO_3$) were determined by following loss on ignition method (Heiri *et al*., 2001). TOM represents the total amount of SOM (<2 mm) and COM (>2 mm). The analyses performed on sediment samples provided a basis for defining 6 main biogeosedimentological sections along the core (Fig. 6.3). Fragments of *C. caespitosa* from the coarse carbonate fraction were isolated from each sample for further analysis (Fig. 6.4).

6.2.4. Measurements on corallites of *C. caespitosa*

Samples of corallites were cleaned of epibionts and organic matter by immersion in 30% hydrogen peroxide (H_2O_2) solution for 24 hours. Corallites were carefully washed in an ultrasonic bath filled with ultrapure MilliQ™ water for 5 minutes to remove fine sediment particles. After drying at 70°C, all corallites were weighed to determine the concentration of coral fragments for each sample. High-quality images were taken by stereomicroscopy for morphological measurements (Leica EZ4D stereomicroscope with integrated HD numerical camera) with the LAS EZ Leica Application Suite 3.3.0. (Leica Microsystems, Switzerland). In a first approach, total length and corallite diameter were measured on stereomicroscopy images with the ImageJ software (http://imagej.nih.gov/ij/dowbload.html; Schneider *et al*., 2012). Annual growth rates of *C. caespitosa* were also computed by measuring, on the outer wall of unbored corallites, the distance between two adjacent thick lines indicating where the high-density bands (HD) start (Kružić and Požar-Domac, 2002) during the winter season (low temperature and low light intensity; Peirano *et al*., 1999, 2005; Silenzi *et al*., 2005). The mean annual growth rates were calculated for each sediment sample by compiling all measures. Statistical analyses were performed using the statistics software package XLSTAT (Addinsoft, 2019). Normality of parameter values was checked using a Shapiro-Wilk test. Inter-relationships between the biometrical parameters of coral fragments and biogeosedimentological parameters analyzed in the core were investigated by performing Pearson's correlation test. The correlation coefficient was calculated together with p-values to determine the significance and strength of each relationship. Differences between mean growth rates were analyzed through one-way ANOVA and post-hoc Tukey's HSD tests.

6.2.5. Radiocarbon dating

The chronostratigraphic reconstruction of the soil was performed from radiocarbon (^{14}C) measurements by Accelerator Mass Spectrometry at the DirectAMS laboratory (Accium BioSciences, Seattle, WA). Samples of *P. oceanica* (n = 2) and *C. caespitosa* debris (n = 3) were collected at ~1 m intervals along the core (Table 6.1). Before ^{14}C measurements, seagrass remains were first rinsed and placed in an ultrasonic bath of ultrapure MilliQ™ water for 5 minutes to remove sediment particles. Finally, samples were inspected under a stereomicroscope for any attached materials and placed in baths of hydrochloric acid (HCl 1M, 80 °C for 30 minutes) and sodium hydroxyde (NaOH 0.2M, 80 °C for 30 minutes) to eliminate the carbonates, the fulvic and humic acids and the atmospheric carbon dioxide, respectively (Brock *et al*., 2010). Fragments of *C. caespitosa* were mechanically cleaned in HCl solution to remove the superficial carbonate layer, reducing the mass by ~25-35%. The material was rinsed three times in ultrapure MilliQ™ water and dried at 60°C prior to crushing and further treatment before dating. Radiocarbon data, expressed as years before present (yr BP), were subsequently calibrated for the local marine reservoir effect (ΔR = 46 years, error ΔR = 40 years; Siani *et al*., 2000) using the CALIB 7.1.0 software (Stuiver and Reimer, 1993) in conjunction with the Marine 13.14C calibration curve (Reimer *et al*., 2013). After corrections, the calibrated ages before present (cal. yr BP) were used to produce age-depth models using the clam package in R software (Blaauw, 2010). The best-fitted chronostratigraphic model was obtained with the smooth-spline model to approximate the respective mean sediment accumulation rate (SAR; mm yr^{-1}) and resolution (yr cm^{-1}).

6.3. Results

6.3.1. Age-depth model and accretion rates

The radiocarbon dating performed along the core showed that the stratigraphic sequence encompassed the 4750 cal. yr BP (Table 6.1). The ages corrected for the marine reservoir effect (excluding one inconsistent dating; Table 6.1), coupled to one hypothetical date at the top of the sequence (present; *i.e.* AD 2018), were used to construct the age-depth model of the core (Fig. 6.2.a). According to this model, the accretion rates ranging from 0.4 to

4.0 mm yr^{-1} (mean: 1.2 ± 1.1 mm yr^{-1}; Fig. 6.2.b; Table 6.2) decreased linearly from the top to the bottom of the core (4.0 to 0.6 mm yr^{-1}; r = -0.808; p<0.05).

Table 6.1. Radiocarbon dating of the *Posidonia oceanica* debris and *Cladocora caespitosa* fragments collected along the core. *Sample not considered for the age-depth model.

Lab ID	Material	Depth (cm)	Radiocarbon age (yr BP)	Calibrated age (cal. yr BP - 2σ)	Mean calibrated age (cal. yr BP - 2σ)
D-AMS	*P. oceanica*	151	1476 ± 33	876-1126	1001 ± 125
D-AMS	*C. caespitosa*	170	1894 ± 22	1295-1507	1401 ± 106
D-AMS	*P. oceanica*	263	3917 ± 35	3673-3986	3860 ± 157
D-AMS	*C. caespitosa*	265	2460 ± 25	1904-2187	2046 ± 142*
D-AMS	*C. caespitosa*	320	4599 ± 27	4593-4860	4727 ± 134

The vertical trends showed that the resolution ranged from 2.5 to 27.5 yr cm^{-1} (mean: 15.1 ± 8.5 yr cm^{-1}; Fig. 6.2.b; Table 6.2) and followed an inverse pattern increasing from the bottom to the top of the core (r = 0.774; p<0.05). The 0-170 cm section (~1400 cal. yr BP-present) showed higher mean accretion rates (1.8 ± 1.1 mm yr^{-1}) than the 170-270 cm section (~2100-1400 cal. yr BP) with a mean SAR of 0.4 ± 1.1 mm yr^{-1} and the 270-320 cm section (~4600-2100 cal. yr BP) was defined by a mean accretion rate of 0.6 ± 0.1 mm yr^{-1}.

Table 6.2. Sediment accretion rates and resolution values calculated for different biogeosedimentological units of the core. No available data for U1 section.

Core section	Accretion rate (mm yr^{-1})			Resolution (yr cm^{-1})		
	Mean ± S.D.	Minimum	Maximum	Mean ±	Minimum	Maximum
U6 (0-170 cm)	1.8 ± 1.1	0.5	4.0	8.3 ± 5.3	2.5	20.1
U5b (170-225 cm)	0.4 ± 0.0	0.4	0.5	25.4 ± 2.2	20.4	27.5
U5a (225-270 cm)	0.4 ± 0.0	0.4	0.5	24.6 ± 2.2	20.3	27.3
U4 (270-285 cm)	0.5 ± 0.0	0.5	0.6	18.7 ± 0.8	17.5	20.1
U3 (285-310 cm)	0.6 ± 0.0	0.6	0.7	15.9 ± 0.7	15.0	17.3
U2 (310-320 cm)	0.7 ± 0.0	0.7	0.7	14.8 ± 0.1	14.7	14.9
U2-U6 (0-320 cm)	1.2 ± 1.1	0.4	4.0	15.1 ± 8.5	2.5	27.5

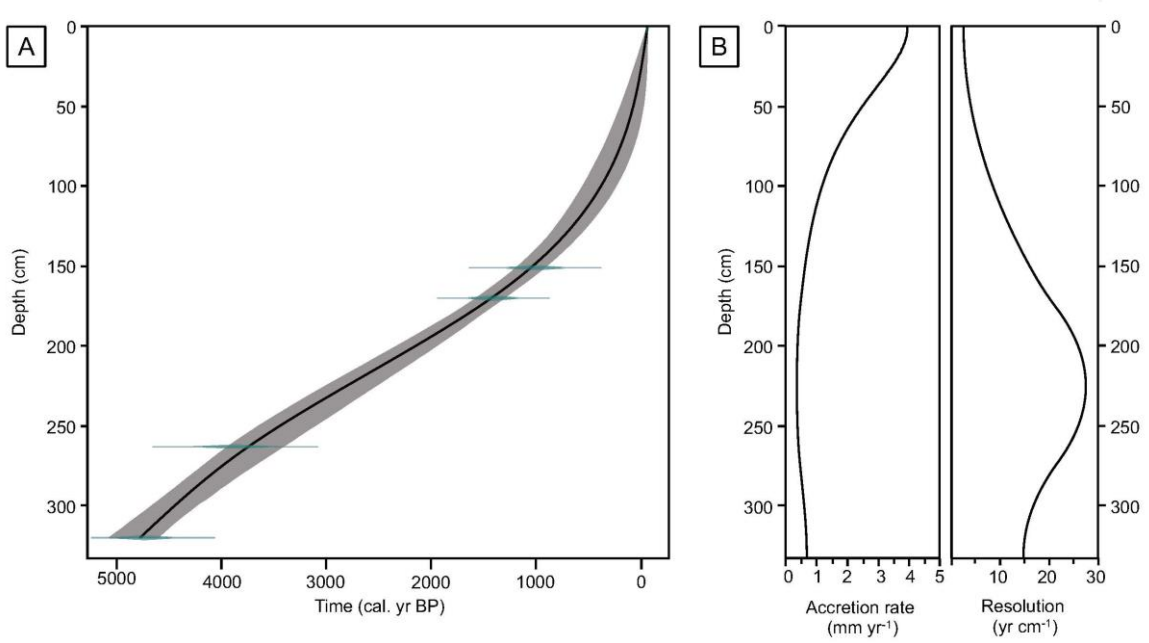

Figure 6.2. (a) Age-depth model (smooth spline) for the studied sedimentary core. Four radiocarbon dates were calibrated using the marine13.14C calibration curve and corrected for a local marine reservoir effect (ΔR = 46 ± 40). The blue and black lines represent radiocarbon dates and the "best" model based on the mean age for each depth, respectively. The grey areas include 2σ confidence range (95% CI) of calibrated dates. (b) SAR and resolution curves.

6.3.2. General stratigraphy of the sequence

Based on the biogeosedimentological analyses performed, 6 main units and 2 sub-units (Fig. 6.3) were identified along the core and are described as follows:

U1 (365-330 cm, before 4750 cal. yr BP) is mainly composed of pebbles with a medium to coarse grey sand matrix. On average, the sediment in this unit is poor in total carbonate (4.9 ± 2.7%) and organic content (2.2 ± 2.5%). Macro- and micro-fauna are rare but eroded. *C. caespitosa* fragments were identified together with several shell remains of marine molluscs (*e.g*. *Bittium reticulatum*, *Cerithium vulgatum*).

U2 (330-310 cm, 4750-4610 cal. yr BP) consists of coarse sand to gravel grey sediment with the sporadic occurrence of pebbles. The mean TOM and calcium carbonate are higher than in the U1 section, 5.5 ± 1.1% and 25.5 ± 10.9%, respectively. The marine mollusc assemblage is very well-preserved and largely composed of *B. reticulatum*, *Jujubinus*

exasperatus, *Tricolia speciosa* and *Venus verrucosa*, associated with *C. caespitosa* debris, that represent 6.0 ± 5.2% of the coarse calcium carbonate content.

U3 (310-285 cm, 4610-4210 cal. yr BP) is characterized by sandy sediment with fine pebbles (~4 cm) and some debris of *P. oceanica*. This unit exhibits a higher content of corallite fragments of *C. caespitosa* which increase continuously from the bottom to the top of the unit, from 11.4% to 41.4% (coarse calcium carbonate content). The mean TOM (5.6 ± 0.8%) and calcium carbonate (30.4 ± 3.7%) are similar that of the previous unit. In this case, the faunal assemblage was dominated by *Glans trapezia*, *Arca noae* and individuals of *Alvania* sp.

U4 (285-270 cm, 4210-3930 cal. yr BP) is mainly constituted by a sandy-muddy matrix (52.4 ± 2.2%) with a low content in coarse mineral fraction (8.6 ± 3.6%) corresponding to gravel. The presence of *C. caespitosa* debris in the coarse calcium carbonate fraction was lower than in section U3 (9.0 ± 5.0%) and mainly ascribed to a mollusc assemblage strongly similar to the U2-U3 sections. Furthermore, the sequence exhibits a constant content in TOM (5.3 ± 1.0%).

U5 (270-170 cm, 3930-1410 cal. yr BP) is composed by a brown to grey muddy sediment with intact rhizomes and root debris characteristic of the matte of *P. oceanica*. This deposit shows a high constant organic and mineral content (10.0 ± 2.1% and 61.1 ± 6.5%, respectively) associated with a significant accumulation of well-preserved *C. caespitosa* corallites in living position. These fragments represent on average 34.1 ± 29.3% of the coarse calcium carbonate content and increase continuously from the bottom (15.8%) to the top (100.0%) of the unit. The faunal assemblage of these two sub-units is overall similar that of the previous unit but differ by the occurrence of several individuals of *Haliotis tuberculata* and *Loripes lacteus*. The sequence is characterized notably by two sub-units:

Sub-unit U5a (270-225 cm, 3930-2830 cal. yr BP) is characterized by a 13.5 ± 9.4% content in *C. caespitosa* in the coarse calcium carbonate fraction and by a total carbonate content of 26.9 ± 8.5%. The mean mineral fraction (63.8 ± 6.8%) slowly decreased from the bottom to the top of the sub-unit (60.5 to 51.5%) whereas the organic content (9.3 ± 2.5%) doubled (from 4.2 to 8.5%).

Sub-unit U5b (225-170 cm, 2830-1410 cal. yr BP) recorded the highest content in *C. caespitosa* in the coarse calcium carbonate fraction (51.7 ± 28.1%) and the highest content in total carbonate (30.4 ± 6.3%). In comparison with the previous sub-unit, similar content in mineral and organic fraction was observed with 59.1 ± 5.7% and 10.6 ± 1.6%, respectively.

As for the previous section of the stratigraphic sequence, U6 (170-0 cm, 1410 cal. yr BP-present) is constituted by the matte of *P. oceanica* in which the TOM content increases from the bottom (12.4%) to the top (58.3%). The mineral fraction is almost entirely composed of the finer fraction and represents on average 81.5 ± 11.1% of the sediment. The total carbonate fraction decreases from the bottom (13.6%) to the top (4.8%). This lower content is notably due to the absence of *C. caespitosa* fragments. The faunal assemblage is rather well-preserved and is mainly characterized by the presence of *B. reticulatum*, *J. exasperatus*, *T. speciosa*, *G. trapezia* and *Alvania spp.*

6.3.3. Morphology and biometrical values of corallites

A total of 390 coral fragments were found in the coarse carbonate fraction of the sediment samples. These fragments were constituted exclusively of debris of *C. caespitosa* and were collected in all sediment samples of the core between 169 cm and 325 cm (Fig. 6.4.a) except for the 174-175 cm, 239-240 cm and 254-255 cm samples (Fig. 6.5.a). The well-preserved and abundant layer of fragments (Fig. 6.4.c; Fig. 6.4.d) was found in the upper part of section U5a (224-230 cm) and in the whole of section U5b (170-225 cm), both characterized by the presence of *P. oceanica* matte (Fig. 6.3). Inversely, a lower content in *C. caespitosa* and the most degraded fragments were observed in the lower part of the core (230-325 cm) defined by a higher content in coarse mineral fraction (Fig. 6.3; Table 6.3). These coral remains were characterized by traces of boring activity, often associated with coral dwellers, and by a high erosion of their external walls (Fig. 6.4.b; Fig. 6.4.e; Fig. 6.4.f).

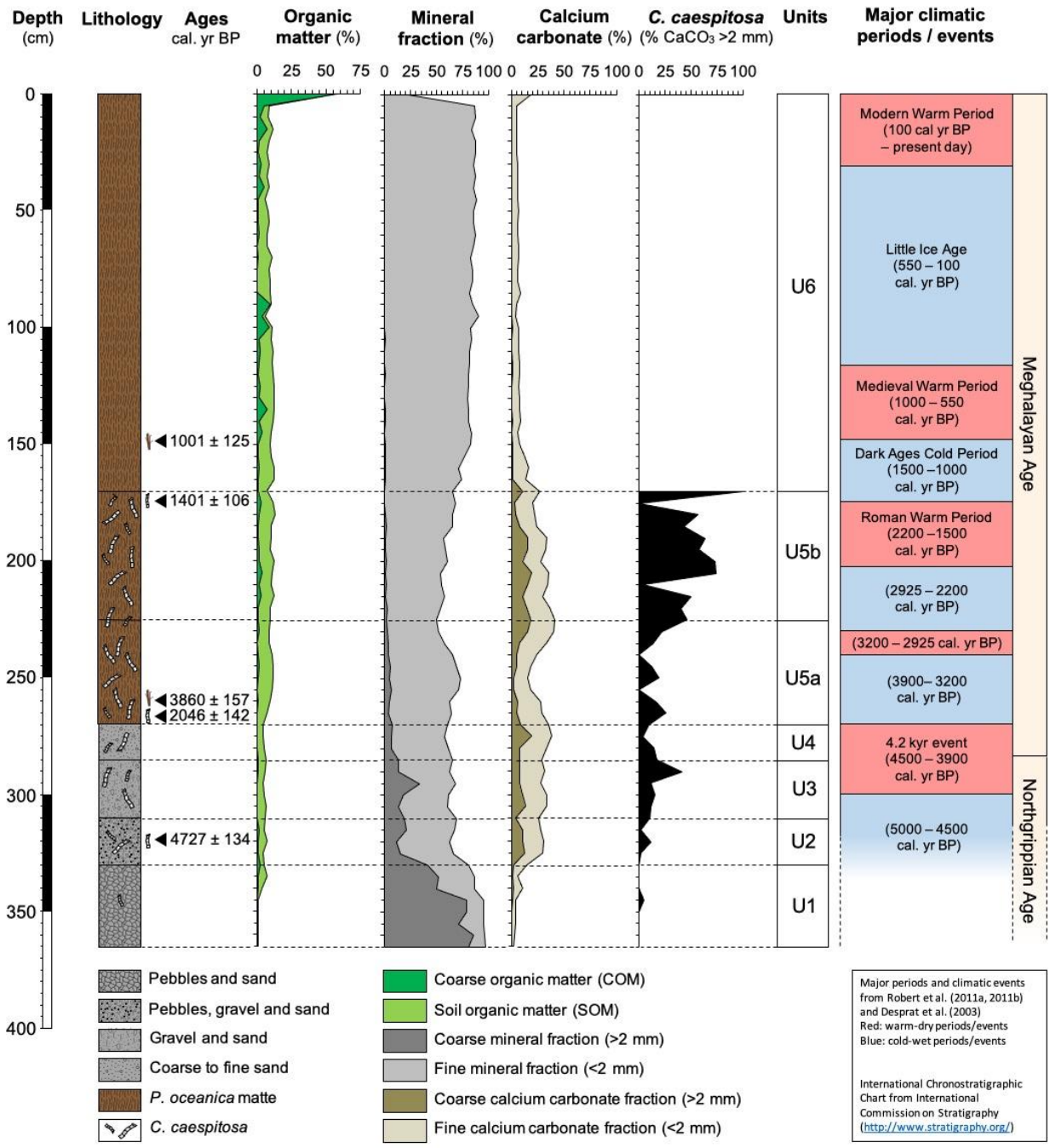

Figure 6.3. Lithology, calibrated radiocarbon dates, content in organic matter, mineral and calcium carbonate in the total fraction, content in *Cladocora caespitosa* in the coarse calcium carbonate fraction and biogeosedimentological units identified in the core.

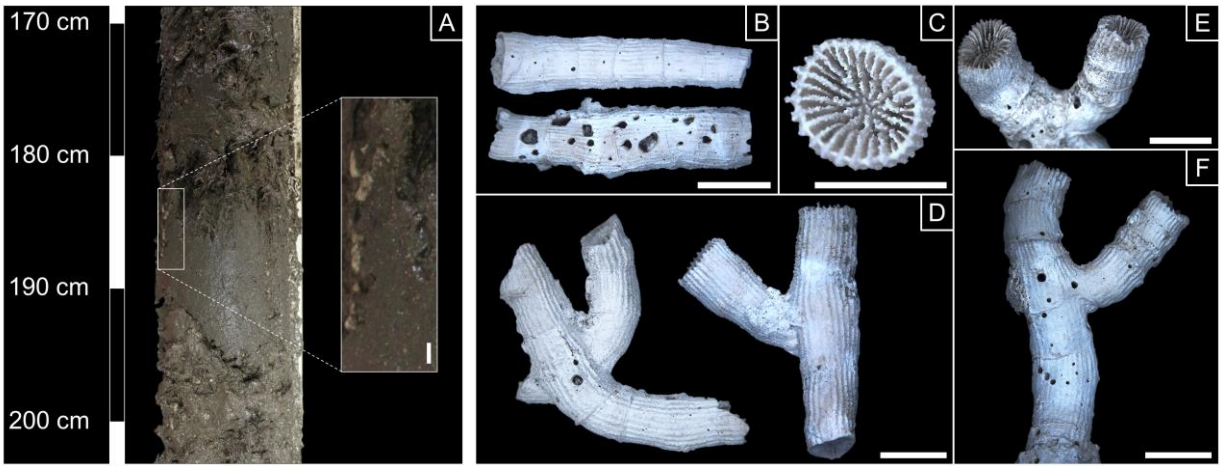

Figure 6.4. (a) *Cladocora caespitosa* fragments visible after the core opening, (b) well-preserved and bored coral fragments, (c) calice of *C. caespitosa*, (d) coral fragments with branches, (e, f) eroded corallite fragments characterized by traces of growth pattern on the external wall. Scale bars: 5 mm.

The individual length of coral fragments ranged between 1.0 and 55.0 mm (mean ± S.D., 11.4 ± 8.1 mm; n = 390; Fig. 6.5.b). The lowest and highest mean values were recorded at 314-315 cm (2.5 ± 0.7 mm) and at 184-185 cm (15.5 ± 7.7 mm), respectively. The total length of coral fragments showed an approximately two-fold decrease between the 170-230 cm and 230-325 cm section with 12.8 ± 8.5 mm and 6.7 ± 4.0 mm (Fig. 6.5.b), respectively. The minimum and maximum individual diameter of *C. caespitosa* debris ranged between 1.0 and 6.0 mm with a mean value of 3.0 ± 0.8 mm (± S.D.; n = 390; Fig. 6.5.c). The lowest average value was recorded at 314-315 cm (2.5 ± 0.7 mm) and the highest at 244-245 cm (4.0 ± 0.5 mm) and 259-260 cm (4.0 ± 0.4 mm; Fig. 6.5.c).

The colonies of *C. caespitosa* are generally phaceloid but in some cases the corallites build irregular coral branches. The total number of additional ramifications observed with the main corallites found was 104 branches. The highest cumulated number of branches was recorded at 189-190 cm (n = 16 branches) and the highest number of branches for a coral fragment was recorded at 224-225 cm (n = 3 branches on a coral fragment). The mean cumulated number of branches decreased from the top to the bottom of the core with ~6.3 ± 1.2 branches per sample (170-230 cm section) to 1.2 ± 0.2 branches per sample (230-325 cm section). Considering the accumulated number of branches and the number of coral fragments found in each sample, the highest branching rate was detected at 314-315 cm (1.0 ± 1.0 branches per fragment), with a mean value estimated at 0.3 ± 0.1 branches per coral fragment (Fig. 6.6.a).

A total of 36 calices were found among the 390 coral fragments of *C. caespitosa*. The highest accumulated number of branches was measured at 219-220 cm (n = 8) where the highest number of calices for a coral fragment was recorded (n = 2 calices on a coral fragment; Fig. 6.4.d; Fig. 6.4.e). Similarly to the branching pattern, the mean accumulated number of calices decreased from the top to the bottom of the core with approximately 2.2 ± 0.8 to 0.4 ± 0.2 (at 169-230 and 230-325 cm, respectively). Considering the accumulated number of calices and the number of coral fragments found in each sample, the highest number of calices per fragment and sample were measured recorded at 219-220 cm (0.3 ± 0.1) and 299-300 cm (0.3 ± 0.2), with a mean value estimated at 0.1 ± 0.0 (Fig. 6.6.b).

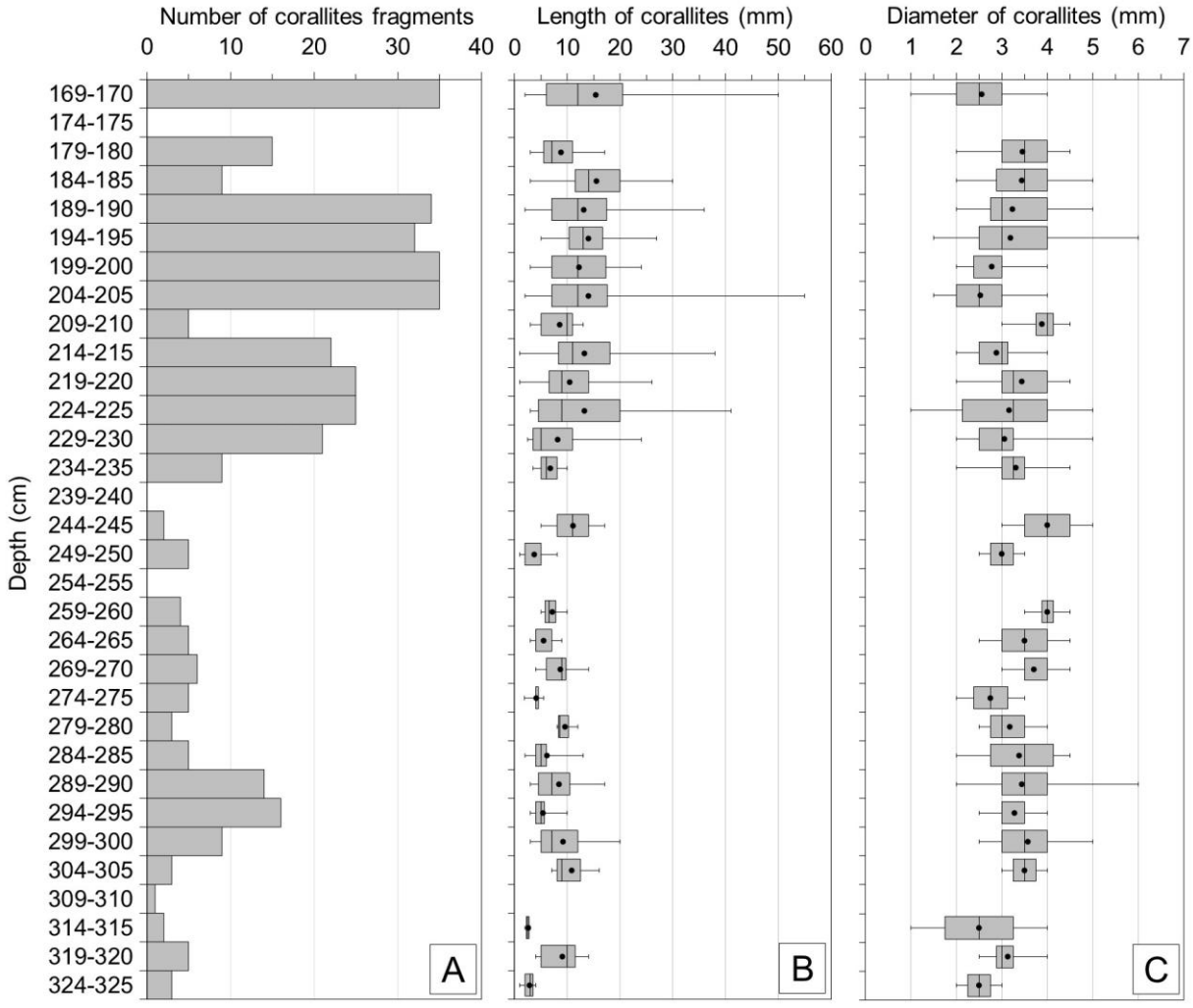

Figure 6.5. (a) Number of *Cladocora caespitosa* fragments, box plots of (b) length of coral fragments and (c) of the diameter of coral fragments collected along the core. The mean and median values are represented by the black dots and by the crossbar lines in the boxes, respectively. The minimum and maximum values are indicated by the external bars outside the boxes.

Table 6.3. Pearson's correlation matrix between the morphological and biometrical parameters measured on *Cladocora caespitosa* fragments and biogeosedimentological parameters analyzed in the core. Fragments: number of fragments; Content: *C. caespitosa* content measured in dry weight percentage of total sample dry weight (%); Length: mean length (mm); Diameter: mean diameter (mm); Branches: branches per fragment; Calices: calices per fragment; Depth: depth in soil; Min >2 mm and Min <2 mm: mineral fraction >2 mm and <2 mm. Level of significance: *P≤0.05, **P≤0.01, ***P≤0.001; NS, P≥0.05. Significant correlations in bold (r value).

	Fragments	**Content**	**Length**	**Diameter**	**Branches**	**Calices**	**Depth**	**COM**	**SOM**	**Min >2 mm**	**Min <2 mm**	**$CaCO_3$ >2 mm**	**$CaCO_3$ <2 mm**
Fragments		**0.929**	**0.677**	**-0.386**	-0.101	0.193	**-0.697**	**0.442**	0.338	**-0.424**	0.101	**0.456**	-0.203
Content	***		**0.756**	**-0.398**	-0.029	0.117	**-0.665**	**0.531**	0.294	**-0.500**	0.166	**0.531**	-0.259
Length	***	***		0.033	0.005	0.089	**-0.698**	**0.410**	**0.437**	**-0.557**	0.299	0.297	-0.170
Diameter	*	*	NS		-0.204	0.279	0.012	-0.265	0.246	-0.023	0.051	-0.371	0.326
Branches	NS	NS	NS	NS		-0.016	0.144	-0.050	-0.154	0.104	-0.131	0.108	0.014
Calices	NS	NS	NS	NS	NS		0.005	-0.213	0.060	0.064	-0.124	-0.007	0.132
Depth	***	***	***	NS	NS	NS		**-0.455**	**-0.744**	**0.785**	**-0.592**	-0.154	0.296
COM	*	**	*	NS	NS	NS	*		**0.416**	**-0.413**	0.222	0.307	**-0.453**
SOM	NS	NS	*	NS	NS	NS	***	*		**-0.681**	**0.702**	-0.238	**-0.392**
Min >2 mm	*	**	**	NS	NS	NS	***	*	***		**-0.732**	-0.177	0.099
Min <2 mm	NS	NS	NS	NS	NS	NS	***	NS	***	***		**-0.411**	**-0.428**
$CaCO_3$ >2 mm	*	**	NS	NS	NS	NS	NS	NS	NS	NS	*		0.004
$CaCO_3$ <2 mm	NS	NS	NS	NS	NS	NS	NS	*	*	NS	*	NS	

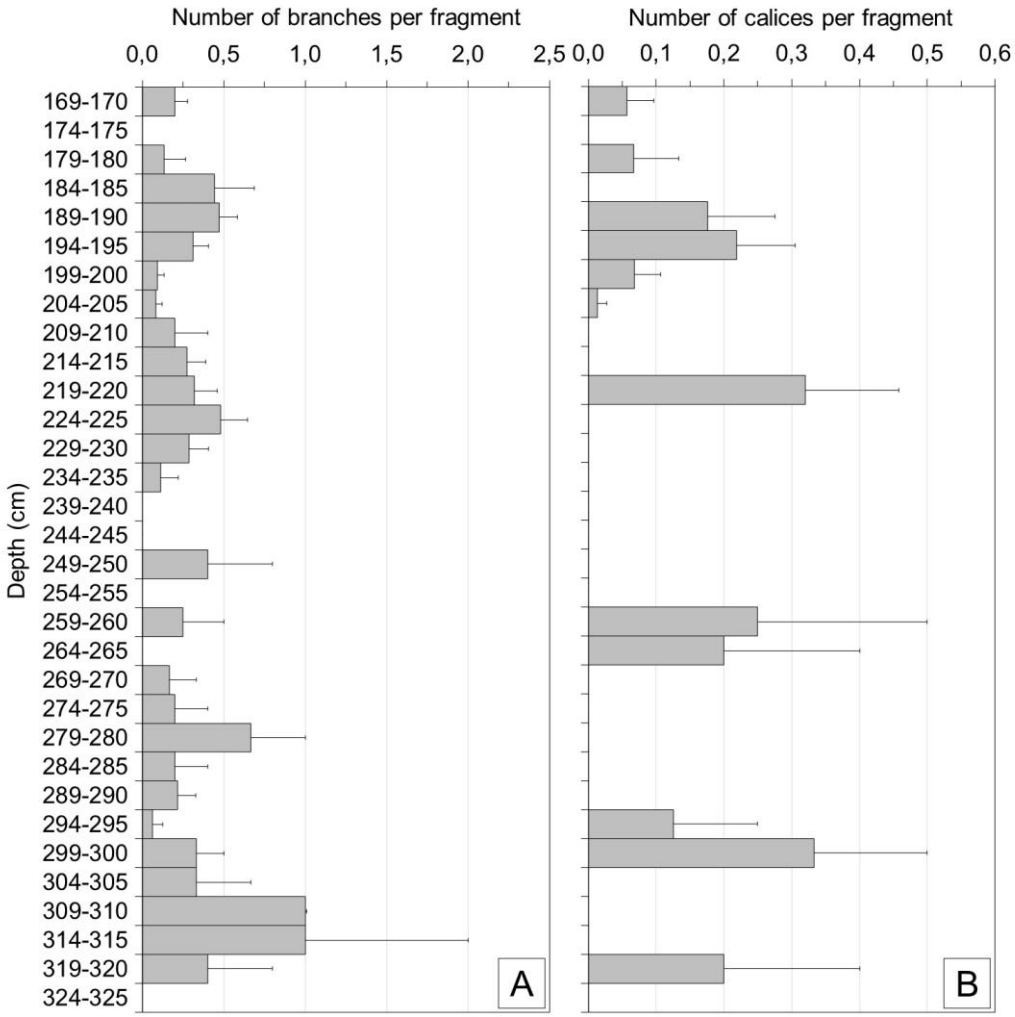

Figure 6.6. Mean values (± S.D.) observed along the core of (a) branches per coral fragment and (b) calices per coral fragment of *Cladocora caespitosa*.

6.3.4. Growth rates of *C. caespitosa*

The annual growth rates were determined by measuring the distance between two adjacent thick lines which occur on the outer wall of corallites (Fig. 6.4.a; Fig. 6.4.e). However, these thick lines deposited annually were not always clearly noticeable on external walls of coral fragments due to high bio-erosion and boring features associated with organisms inhabiting the coral (Fig. 6.4.a; Fig. 6.4.e). Consequently, a high number of corallites had to be discarded for coral growth rate measurements. Thus, the image analysis for growth patterns was performed on the corallite fragments occurring between 169 and 230 cm depth (Fig. 6.7). In total, 427 measurements were made on 83 coral skeleton images representing ~4.6 ± 1.2 measurements per corallite and 38.8 ± 12.0 measurements per sediment sample. The number

of measurements ranged between 6 and 114 (at samples 214-215 and 204-205 cm, respectively).

The individual minimum and maximum growth rates were 0.67 and 5.02 mm yr^{-1}, respectively (average of 2.32 ± 0.79 mm yr^{-1}; Fig. 6.8). The lowest and highest mean annual growth rates were 1.85 ± 0.78 and 3.09 ± 0.81 mm yr^{-1} (at 224-225 and 184-185 cm, respectively). Significant differences were found between growth rates in investigated sediments samples of the 169-230 cm core section (ANOVA $p<0.001$). Tukey HSD *post hoc* test contributed to identify three groups with high (A; 3.09 mm yr^{-1}), intermediate (AB; 2.26 to 2.62 mm yr^{-1}) and low growth rate (B; 1.85 to 2.15 mm yr^{-1}; Fig. 6.7).

The mean annual growth rate obtained between 169-170 cm (1408 cal. yr BP) and 229-230 cm (2963 cal. yr BP) was 2.30 ± 0.81 mm yr^{-1} (Fig. 6.7; Fig. 6.8). The mean annual growth rate appeared to decrease with depth in the soil (Fig. 6.7; Fig. 6.8) but no significant correlation was found ($r = -0.386$; $p>0.05$; Table 6.3). Similarly, although the mean annual growth rate of corallites and the SAR followed the same pattern with depth in the soil (Fig. 6.8), no significant correlation was highlighted between these two parameters ($r = 0.055$; $p>0.05$; Table 6.3). For the same core section (169-230 cm), the mean annual growth was higher than the mean accretion rate (0.39 ± 0.03 mm yr^{-1}; Fig. 6.8) highlighting no burial of coral colonies at this period.

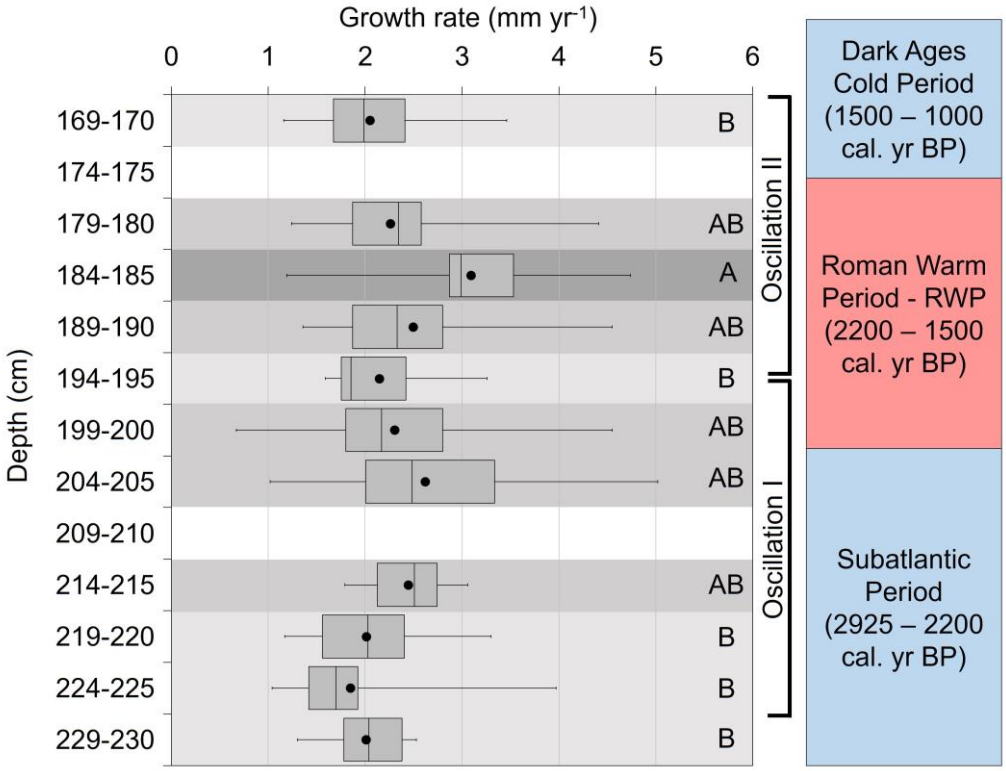

Figure 6.7. Box plot of growth rates measured on well-preserved *Cladocora caespitosa* corallites collected in the 169-230 cm core section (left). Dissimilar letters denote significant differences between groups (p-value<0.05). For major warm-dry and cold-wet climatic period, see Fig. 6.3.(right).

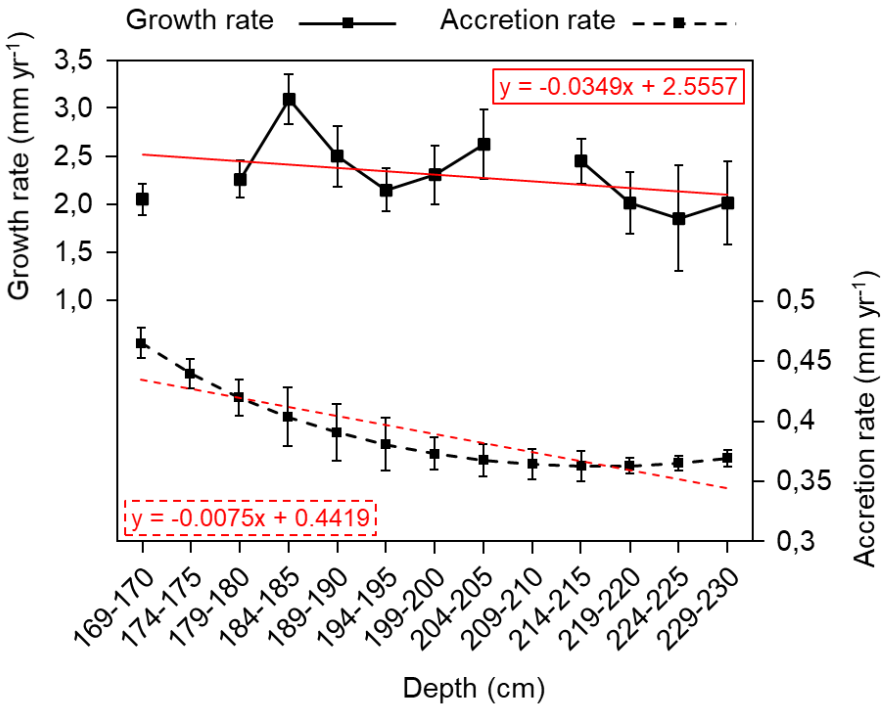

Figure 6.8. Relationship between the mean growth rate (mm yr^{-1}) measured on *C. caespitosa* corallites and sediment accretion rate (mm yr^{-1}) from the smooth spline age-depth model on the 169-230 cm core section.

6.4. Discussion

The sedimentary sequence analyzed from the core collected on the north-eastern continental margin of Corsica Island enabled us to provide a first palaeo-environmental reconstruction of the area over the last 5000 years. The biogeosedimentological analyses coupled to the chronostratigraphic model have shown that the sedimentary sequence was characterized by a succession of open-marine ecosystems since up to ~4750 cal. yr BP forming three major phases. The presence of well-preserved coral fragments in the matte reinforces the known role of P. oceanica as a unique palaeo-archive in the Mediterranean. The analysis of the *C. caespitosa* debris found in this organic deposit revealed that the mean annual growth rate is similar to other values recorded in the Mediterranean. The occurrence of this *C. caespitosa* bank in this area and its growth pattern appeared to be closely related to the past environmental conditions and climatic periods since the mid-Holocene.

6.4.1. The settlement phase: establishment of the *C. caespitosa* colonies following a major sediment alluvial input (~4750-3930 cal. yr BP)

The lower part of the core from U1 (365-330 cm, up to 4750 cal. yr BP) to U4 sections (285-270 cm, 3 930 cal. yr BP) was defined by a graded bedding of sedimentary layers which evidenced the variation in the marine depositional environment during the Chalcolithic period and the early Bronze Age (~5450-3950 cal. yr BP). The analysis of the mollusc assemblages performed at the base of the core (U1 section) revealed the presence of macro- and micro-shell debris assigned to the marine environment (mainly *B. reticulatum*, *J. exasperatus* and *T. speciosa*; Pérès and Picard, 1964; Pérès, 1982). However, these shell fragments may not have been produced locally but may have been imported from adjacent marine areas by hydrodynamic forces during high energy events. The coarse sedimentary deposit found at the bottom end of the core and characterized by well-rounded pebbles embedded in a sandy grey matrix may have resulted from littoral drift, shelf storms or high alluvial sediment input after major river floods (Orszag-Sperber and Pilot, 1976; Gauthier, 1981; Conchon and Gauthier, 1985; Gervais *et al*., 2004). In the east coast of Corsica, the Golo river is the largest drainage basin and has developed both a wide underwater delta (Ottman, 1958) and a large deltaic plain (Marana Plain; Fig. 6.1). This deltaic plain was mainly constituted of recent alluvial

terraces with grey soil (*Fy3*; Orofino *et al*., 2010) exhibiting similar geological properties than the sedimentary layer observed at the base of the studied core. The high sediment input identified here may perhaps be linked to the maximum of precipitation observed during the mid-Holocene period in the western parts of the Mediterranean (Roberts *et al*., 2011a, 2011b; Peyron *et al*., 2013). Thus, the exact origin of this pebble layer is difficult to determine but could be related to (i) massive alluvial deposits from the Golo river (Conchon and Gauthier, 1985; Mulder and Maneux, 1999) associated with (ii) a redistribution of sediments on the shelf by littoral drift generally oriented from south to north (Gauthier, 1981; Gaillot and Chavarot, 2001).

The setting up of pebble beds in this sector has most likely favored the formation of coral colonies of *C. caespitosa*. Similar fossil buildups settled on basal conglomerate with pebbles or boulders have been already found by D'Alessandro and Bromley (1994) and Schiller (1993a). This coral species preferentially grows on rocky substrates (Peirano *et al*., 1998; Kersting *et al*., 2012) even if it can also be found free on sedimentary or organic substrates (Laborel, 1987; Kružić and Benković, 2008). Though some coral debris of *C. caespitosa* was found in the 344-345 cm sample (Fig. 6.3), the most probable settlement of the *C. caespitosa* colonies at this site was situated at the basal part of the U2 section (320 cm) and dated back to ~4750 cal. yr BP. *Cladocora caespitosa* can colonize areas with a wide range of marine currents and turbid conditions (Laborel *et al*., 1961; Zibrowius, 1980; Peirano *et al*., 1998). In the Mediterranean, the occurrence of *C. caespitosa* banks were recorded in the vicinity of river mouths exposed to abundant sedimentary and alluvial inputs (Fornós *et al*., 1996; Aguirre, 1998, Drinia *et al*., 2010; Tremblay *et al*., 2011). Such a turbid environment is consistent with the observation of coral fragments in this study. Nevertheless, the development of this coral species in shallow waters remains strongly influenced by other parameters such as temperature, food supply and irradiance (Schiller, 1993a, 1993b; Peirano *et al*., 1998, 2005; Kružić and Benković 2008; Chefaoui *et al*., 2017). Considering the reconstruction of the Relative Sea Level (RSL) changes in Corsica performed by Vacchi *et al*. (2017b), the RSL at this period was placed ~2.0 m below the present mean sea level (MSL), allowing us to estimate the beginning of the *C. caespitosa* colonization at around 8.0 m below the MSL. At this depth, the light intensity was enough for the symbiotic zooxanthellae to perform photosynthesis efficiently, hence allowing coral calcification even if the growth

process is linked to a combination of autotrophy and heterotrophy (Schiller, 1993b; Peirano *et al*., 1999; Rodolfo-Metalpa *et al*., 2008). This capability gives *C. caespitosa* an advantage for undertaking the colonization of deeper areas or locations with higher sedimentation rates (Peirano *et al*., 1998; Morri *et al*., 2001). The particulate organic matter from turbid waters have proved to play directly or indirectly a role in coral metabolism (Schiller and Herndl, 1989; Rodolfo-Metalpa *et al*., 2008) to build large coral beds or banks (Laborel, 1961; Tur and Pere Godall, 1982; Peirano *et al*., 1998; Kružić and Benković 2008). Here, the mean TOM content revealed in the U2-U4 sections (~5%) could have been advantageous for the growth of *C. caespitosa*. The proximity with the *P. oceanica* meadow, evidenced by fine root debris in the U3 section, could have resulted in the increase in SOM content in the study area. The normal graded bedding observed between the U2-U4 sections suggests a slight progressive decrease in the transport energy. This hypothesis seems to be confirmed by the striking change in sedimentation from the predominantly coarse siliciclastic sediment deposit assigned to the presumed terrestrial inputs, to the calcareous and biogenic sediment associated with open-sea environment (Fig. 6.3). Overall, the increase of coral fragment content observed between the U2-U4 sections could be related to a development of *C. caespitosa* colonies which probably benefited from favorable environmental conditions (*i.e.* moderate fine sediment alluvial inputs, decrease in the bottom sea currents).

6.4.2. The transitional phase: coexistence between the *C. caespitosa* bed and the *P. oceanica* meadow (~3930-1410 cal. yr BP)

During the Bronze Age (3930 cal. yr BP), a major environmental change occurred with the settlement of the *P. oceanica* meadow, as suggested by a major increase in the SOM content (~5% to 10%) and also by the presence of COM remains from the seagrass species (root and rhizome debris). The colonization of the studied site was probably related to the progressive RSL rise rate of ~2 mm yr^{-1}, observed during the whole Chalcolithic period and the early Bronze Age (~5450-3950 cal. yr BP; Vacchi *et al*., 2017b). According to Vacchi *et al*. (2016, 2017b), the RSL has increased from ~2.7 m (4750 cal. yr BP) to ~1.5 m (3930 cal. yr BP) below the present MSL between the *C. caespitosa* settlement and the *P. oceanica* meadow colonization. Thus, the progression of the upper limit of the *P. oceanica* meadow towards the coast could be related to the RSL rise and coincides with the 4.2 kyr event (Fig. 6.3)

characterized by a global climatic shift and major drought through the Mediterranean region (Magny *et al*., 2013).

Sub-section U5a, ranging between the 269-270 cm (3930 cal. yr BP) and 224-225 cm samples (2830 cal. yr BP), is notably defined by a transitional phase characterized by the coexistence of *P. oceanica* meadow and the coral beds of *C. caespitosa*. During this phase, a decrease in the coral fragments content (Fig. 6.3) and in the accretion rate (Table 6.2) was observed. The radiocarbon dating performed on *P. oceanica* remains and *C. caespitosa* fragments at the basal part of sub-section U5a has contributed to highlighting a significant disruption in the SAR and probable erosion and re-deposition events during the colonization of the area by the *P. oceanica* meadow. The anomalous age of *C. caespitosa* of 2046 cal. yr BP found beneath the 3860 cal. yr BP date measured on the *P. oceanica* remains could be explained by major alluvial inputs or extreme storms. An alternative explanation is related to the collection of the sedimentary sequence with the Kullenberg corer. The displacement of coral fragments in the lower part of the core could probably be associated with the sampling method. Displacement of *P. oceanica* leaves was also noted during the same oceanographic survey with the Kullenberg corer. The occurrence of reworked material can be also identified during the chrono-stratigraphic reconstruction of a *P. oceanica* matte sequence obtained by performing successive coring operations (Serrano *et al*., 2012).

In the subsequent core sub-section U5b, delimited between the 224-225 cm (2 830 cal. yr BP) and the 164-165 cm (1300 cal. yr BP) samples, the *P. oceanica* meadow is already well-established and the matte is very dense. During this period, an increase in the *C. caespitosa* content was observed and appeared to be significantly and positively correlated with the content in organic matter ($r = 0.531$; $p<0.01$; Table 6.3). Similarly, the length of coral fragments was revealed to be negatively correlated to depth in the soil ($r = -0.698$; $p<0.001$; Table 6.3). The actual abundance and the lengthier coral debris in the upper part of the sequence could suggest good coexistence with the seagrass and enhanced preservation in the matte of *P. oceanica*, confirming the role played by this structure as a valuable archive of palaeo-environmental information in the Mediterranean (Romero *et al*., 1994; Mateo *et al*., 1997, 2002; Serrano *et al*., 2012). However, these findings must be considered with caution because

the actual abundance of debris does not necessarily reflect the palaeo-abundance of the coral during this period and can be affected by a post-depositional process (degradation).

In this sub-section, the mean annual growth rate measurements were determined by performing direct measurements on the external walls of corallites and were highly dependent on the coral fragments. This method was efficiently and easily implemented with minimal manipulation of the corallite fragments. However, further analyses should be performed by combining different methods (X-ray method, Alizarin method; Table 6.4) in order to assess the accuracy of the measurements, and also to estimate the annual growth rate on eroded or bored corallite fragments (Peirano *et al*., 1999, 2004). The mean annual growth rates obtained for *C. caespitosa* in this study are within the 1.3 to 6.9 mm yr^{-1} range obtained by different authors using either Alizarin staining or X-ray analysis on living or fossil colonies (Table 6.4).

Table 6.4. Annual mean growth rates of living or fossil *Cladocora caespitosa* and their standard deviations obtained in this study and as reported in the literature. Table modified from Kersting and Linares (2012).

Location	**Annual growth rate (mm yr^{-1})**	**Method**	**Authors**
Mallorca (Aquarium)	5.0	Direct measurement	Oliver Valls (1989)
Piran (Adriatic)	4.4 ± 0.6	Alizarin	Schiller (1993a)
La Spezia (NW Med.)	1.3 ± 0.6 – 4.3 ± 1.4	X-ray	Peirano *et al.* (1999)
La Spezia (NW Med.)	4.8 ± 1.7	Alizarin	Rodolfo-Metalpa *et al*. (1999)
Mljet (Adriatic)	4.7 ± 0.6 / 4.7 ± 0.6	Alizarin / X-ray	Kružić and Požar-Domac (2002)
Tuscany	6.3 ± 3.0	X-ray	Peirano *et al*. (2004)
Calabria	2.6 ± 0.8	X-ray	Peirano *et al*. (2004)
Sardinia	2.1 ± 0.7 – 4.1 ± 1.3	X-ray	Peirano *et al*. (2004)
Apulia	2.1 ± 0.9 – 6.9 ± 2.1	X-ray	Peirano *et al*. (2004)
La Spezia (NW Med.)	3.01	X-ray	Peirano *et al*. (2005)
Prvić (Adriatic)	3.2 ± 0.1	X-ray	Kružić and Benković (2008)
Pag (Adriatic)	3.1 ± 0.1	X-ray	Kružić and Benković (2008)
Mljet (Adriatic)	3.7 ± 1.3	X-ray	Kružić and Benković (2008)
N to S Adriatic	2.6 ± 0.2 – 4.1 ± 0.6	X-ray	Peirano *et al.* (2009)
Ligurian Sea	3.7 ± 0.5 – 3.3 ± 0.4	X-ray	Peirano *et al.* (2009)
South Italy	3.1 ± 0.3 – 3.2 ± 0.3	X-ray	Peirano *et al*. (2009)
Tunisia	2.3 ± 0.2	X-ray	Peirano *et al*. (2009)
Illa Grossa	2.5 ± 0.8 / 2.5 ± 0.8	Alizarin / X-ray	Kersting and Linares (2012)
Corsica (NW Med.)	1.9 ± 0.8 – 3.1 ± 0.8	Direct measurement	This study

The analysis of the mean annual growth rate in the U5b sub-section highlighted a steady increase and the occurrence of oscillations (Fig. 6.7; Fig. 6.8). Considering the chronostratigraphic model and the SAR curve (Fig. 6.2.a; Fig. 6.2.b), the wide oscillations on the growth pattern of *C. caespitosa* corallites can be related to major climatic periods (Fig. 6.7). While decadal growth rate oscillation has been already described in the Late Pleistocene bank of Santa Teresiola by Peirano *et al.* (2009), in this study, the growth pattern appears to follow semi-millennial to millennial oscillations.

The first oscillation ranged between the minimum growth rates observed at 224-225 cm (2830 cal. yr BP) and at 194-195 cm (2010 cal. yr BP) with a maximum at 204-205 cm (2280 cal. yr BP). This oscillation corresponds historically to the Late Bronze Age and Iron Age period in Corsica (Currás *et al*., 2017) and coincides with the Subatlantic period (2925-2200 cal. yr BP) and the Roman Warm Period - RWP (2200-1500 cal. yr BP; Desprat *et al*., 2003; Klimenko and Klimanov, 2003). Over the first oscillation, the annual mean growth rate was 2.2 ± 0.3 mm yr^{-1} and was characterized by intermediate and low mean growth rate (Fig. 6.7). Peirano *et al*. (1999) suggests that the coral growth rate of corallites cannot be interpreted just as SSTs effect alone, but also as a result of the light intensity that affects the photosynthetic efficiency of zooxanthellae. Kružić and Benković (2008) propose that the biometrical values are affected by sea currents, temperature and sedimentation. According to Vella *et al*. (2016), from 2650-2450 cal. yr BP, the mouth of the Golo river was located 1-2 km northwards of its modern position (Tanghiccia mouth; Fig. 6.1). Consequently, the influence of the alluvial inputs of fine sediments was probably higher due to the shift in the location of the mouth of the Golo river coupled to the cold Subatlantic period contributing to low light intensity and SSTs. The stratigraphic sequence mainly constituted by the matte of *P. oceanica* exhibited a lower SAR (0.4 ± 0.0 mm yr^{-1}) than other meadows in the Mediterranean (Serrano *et al*., 2012 and references therein). A decline in irradiance has been shown to have a significant impact on the physiology, morphology and structure of the meadow and also on its productivity (Serrano *et al*., 2011; Leiva-Dueñas *et al*., 2018). However, Peirano *et al*. (2005) showed that *C. caespitosa* exhibits enhanced growth in low light intensities and turbid waters during the winter when the energy and nutrient supply is high. Thus, low irradiance could have led both to a decrease in the productivity of the *P. oceanica meadow* and in its accretion helping indirectly the growth of *C. caespitosa*. Similar phenomena have been observed along the

Ligurian coast after heavy anthropogenic siltation causing the regression of the *P. oceanica* meadows (Bianchi and Peirano, 1990) which could have enhanced the development of the *C. caespitosa* bank (Peirano *et al*., 1998).

The second oscillation occurred between 194-195 cm (2010 cal. yr BP) and 169-170 cm (1410 cal. yr BP) with a peak at 184-185 cm (1750 cal. yr BP). This oscillation coincides with the historic and climatic Roman periods in Corsica (Currás *et al*., 2017; Desprat *et al*., 2003) and the Dark Ages Cold Period - DACP (1500-1000 cal. yr BP; Ljungqvist, 2010). This oscillation is characterized by a slightly higher mean growth rate of corallites and SAR than during the first oscillation, with 2.4 ± 0.4 mm yr^{-1} and 0.4 ± 0.0 mm yr^{-1}, respectively. Similarly, the content and the mean total length of coral fragments were the highest recorded in the core (Fig. 6.3; Fig. 6.5.a; Fig. 6.5.b). The warmer and dryer climatic epoch of the RWP was probably advantageous for the development of *C. caespitosa* colonies and the *P. oceanica* meadow. Although studies confirmed the good adaptation of this temperate coral to cold and turbid environmental conditions (Peirano *et al*., 2005, 2009; Kružić and Benković, 2008), the largest bank of *C. caespitosa* occurred in coastal environments characterized by alluvial inputs and warmer temperatures. Several analyses of growth patterns of corallites showed a sinusoidal trend in accordance with the air temperature (Peirano *et al*., 1999, 2004, 2005) and the SSTs (Morri *et al*., 2001; Kružić and Požar-Domac, 2002; Silenzi *et al*., 2005; Peirano *et al*., 2005). However, after the mean annual growth rate of 3.1 ± 0.4 mm yr^{-1} peaked at 184-185 cm, the growth pattern steadily decreased down to the 169-170 cm sample where the *C. caespitosa* bank abruptly disappeared (Fig. 6.3; Fig. 6.7).

6.4.3. The decline phase: death of the *C. caespitosa* bank and development of the *P. oceanica* meadow (~1410 cal. yr BP-present)

The disappearance of the *C. caespitosa* bank seems to be linked to a major and sudden environmental event. The analysis of the biogeosedimentological features of this period denotes no major phenomena related to a possible alluvial input. Nevertheless, another possible cause of the death of the bank was linked to the high sensitivity of *C. caespitosa* to elevated and prolonged SSTs (Peirano *et al*., 2005). While recent observations have shown that a rise in SSTs throughout the Mediterranean enhanced corallite growth, the increase of

SSTs up to 26-28°C during more than one month coupled to high irradiance may have caused extensive mortality events, as observed in the Ligurian Sea by Rodolfo-Metalpa *et al*. (2000, 2005, 2006) and in the Adriatic Sea by Kružić and Požar-Domac (2002). The death of this bank would probably be linked to thermal and irradiance stresses causing a major mortality event during the RWP (1750 cal. yr BP). This hypothesis seems to be confirmed by the estimations of decadal mean temperature variations over the two last millennia in the northern Hemisphere and (Ljungqvist, 2010).

Nevertheless, the presence of *C. caespitosa* and the continuous decrease in the growth pattern between 1700-1410 cal. yr BP suggest rather a progressive decline of the *C. caespitosa* bank. The dryer and warmer climate observed during the RWP could have resulted in enhanced development and productivity of the *P. oceanica* meadow. Peirano *et al*. (1998) suggest that the distribution, occurrence, and abundance of the *C. caespitosa* in the La Spezia region is mainly controlled by competition with soft and frondose algae. Here, the presence of a well-developed seagrass meadow could have led to an increase in the competition with *C. caespitosa* already weakened by the mortality events. The higher meadow coverage and leaf canopy could have involved an increase in the mechanical trapping of fine particles by the plants favoring silt and mud deposition on the sea bottom, and also an increase in bioclastic sediments linked to epiphyte and invertebrate production (De Falco *et al*., 2000). *Cladocora caespitosa* polyps are well-adapted to high sedimentation rates by removal of the sediment from the oral disc, hence sedimentation within a certain limit may have favored the accretion of the bank (Dodge *et al*., 1974; Schiller, 1993a). Excessive siltation can be considered as a limiting factor for *C. caespitosa* (Tins, 1978). Thus, the decline of the coral bank and the complete extinction of *C. caespitosa* at this site could be related to a major mortality events that occurred during the RWP coupled to higher competition with *the P. oceanica* meadow which experienced better development.

Section U6, (1410 cal. yr BP-present) is exclusively constituted by the *P. oceanica* matte. During this phase, the sequence remains relatively stable as evidenced by the biogeosedimentological analysis (Fig. 6.3) in spite of the succession of major climatic periods over the last millennia: the Medieval Warm Period - MWP (1000-700 cal. yr BP; Lamb, 1965; Bradley *et al*., 2003) and the Little Ice Age - LIA (550-100 cal. yr BP; Ljungqvist, 2010). The TOM

decreased from the top to bottom of the section linked to a degradation of the *P. oceanica* matte whereas the total carbonate fraction is relatively steady along the core section except between 150-170 cm where the content increased. Similarly, the mineral fraction is stable and totally composed of the finer fraction (Fig. 6.3). The major changes observed in the stratigraphic sequence concern SAR of the matte which increased following the death of the *C. caespitosa* bank. The SAR of the matte ranged between 0.5 and 4.0 mm yr^{-1} with a mean value estimated at 1.8 ± 1.1 mm yr^{-1} (Fig. 6.2.b), which is similar to values recorded in Mediterranean Sea (Serrano *et al*., 2012). The SAR exhibited values of 0.5 ± 0.4, 0.7 ± 0.5, and 1.5 ± 0.4 mm yr^{-1} for the DACP, MWP, and LIA periods, respectively.

6.5. Conclusion

The analysis of the stratigraphic sequence collected on the eastern coast of Corsica has contributed to revealing for the first time the presence of a fossil bank of *C. caespitosa* surrounded by the matte of the *P. oceanica* meadow. The well-preserved coral fragments found in the matte added to the known role of this bioconstruction as palaeo-archive in the Mediterranean coastal areas. The sedimentological analysis coupled to the biological measurements performed on the *C. caespitosa* corallites provided the opportunity to perform a palaeo-environmental reconstruction of the conditions at the site during the last 4750 years. At the study site, the presence and the abundance of the colonial coral *C. caespitosa* and also the fluctuations observed in its growth pattern were shown to be probably related to the abiotic parameters (*i.e.* marine currents, sedimentation, competition) and to past climate conditions (major events and climatic periods) since the mid-Holocene.

Chapitre 7

Synthèse générale et perspectives

Cette étude conduite au sein du site Natura 2000 « FR9402014 - Grand Herbier de la Côte orientale » (Corse, France) a permis d'établir un inventaire des stocks et flux de carbone piégés sous forme de matières organiques et de carbonates dans les sédiments des herbiers à *Posidonia oceanica*. À notre connaissance, les résultats réalisés dans ce travail de thèse constituent le premier inventaire majeur des stocks de carbone piégés au sein d'un puits de « Carbone Bleu » sur les côtes méditerranéennes françaises mais également l'une des principales estimations à l'échelon du bassin méditerranéen. Ces travaux se sont appuyés sur l'acquisition et le traitement d'un important jeu de données numériques (*i.e.* sismiques, optiques et acoustiques) couplé à la collecte de prélèvements sédimentaires et à leur analyse biogéochimique. Les résultats de ces travaux de thèse permettent au travers des différents chapitres de souligner l'importance des herbiers marins dans l'atténuation des changements climatiques, mais aussi le rôle joué par les mattes des herbiers à *P. oceanica* comme archives biologiques et environnementales.

7.1. Optimisation de la méthodologie de cartographie des puits de carbone.

La cartographie des communautés benthiques et des caractéristiques morphologiques des zones côtières et marines constitue une étape fondamentale pour les scientifiques et gestionnaires afin de suivre l'évolution des écosystèmes (MESH, 2008). En effet, la cartographie offre la possibilité de (i) constituer un état de référence et un suivi de la dynamique spatio-temporelle des habitats côtiers et marins, (ii) d'identifier l'origine des perturbations survenues, mais également (iii) de prédire avec précision l'évolution de ces écosystèmes soumis à des pressions croissantes (Fumagalli *et al*., 2014 ; Gissi *et al*., 2020).

Pour déterminer la contribution des écosystèmes à « Carbone Bleu » à l'atténuation des effets du changement climatique, l'évaluation de la distribution géographique des herbiers marins, des mangroves et des prés salés constitue l'une des principales étapes (Mateo et Serrano, 2012 ; Howard *et al*., 2014a). Alors que les écosystèmes à Carbone Bleu constituent des puits de carbone majeurs en zone côtière, ces derniers font cependant partis des habitats les plus menacés à la surface de la planète (Waycott *et al*., 2009 ; Gedan *et al*., 2009 ; Pendleton *et al*., 2012 ; Hamilton et Casey, 2016). Bien que leur distribution historique soit très difficile à déterminer en raison des pertes significatives survenues au cours des

dernières décennies, les évaluations globales, entreprises sur la base de cartographies, estiment que la surface occupée par ces écosystèmes aurait diminuée entre 25 % et 70 % (Alongi *et al*., 2002 ; Waycott *et al*., 2009 ; Pendleton *et al*., 2012 ; Howard *et al*., 2014a ; Mcowen *et al*., 2017). Parmi ces écosystèmes, le déclin des herbiers marins serait l'un des plus importants avec un taux de perte global annuel atteignant en moyenne 1,5 % depuis le début du XXe siècle (Waycott *et al*., 2009).

Les pertes, les dégradations et les conversions de ces écosystèmes au profit des activités anthropiques ont pour conséquence la perte d'un grand nombre de services écosystémiques nécessaires pour l'atténuation et d'adaptation aux changements climatiques, tels que la protection des littoraux face aux événements extrêmes, la régulation de la qualité de l'eau, la présence d'habitats pour de nombreuses espèces et le rôle de puits de carbone (Costanza *et al*., 1997 ; Duarte *et al*., 2013 ; Serrano *et al*., 2019). Alors que ces écosystèmes participent au cycle du carbone océanique, ces derniers sont cependant très sensibles et vulnérables aux effets du changement climatique, conduisant à des incertitudes quant à leur efficacité future (Lovelock et Reef, 2020). En effet, les pressions anthropiques associées aux changements globaux (*e.g.* hausse des précipitations et des températures, du niveau marin ; acidification des océans ; intensification des événements extrêmes) influenceront très probablement la composition et la distribution des écosystèmes présents en zone côtière (Duarte *et al*., 2013 ; Lovelock et Reef, 2020).

À l'échelle du bassin méditerranéen, la Corse constitue une région de référence soumise à de faibles pressions anthropiques (Lafabrie *et al*., 2008 ; Gobert *et al*., 2017 ; Marengo *et al*., 2018). Depuis les années 1990, le littoral de la Corse fait l'objet d'un important effort d'inventaire des habitats benthiques ayant permis de disposer d'une cartographie continue des écosystèmes marins (Pasqualini, 1997 ; Guennoc *et al*., 2001 ; Bonacorsi, 2012 ; Valette-Sansevin *et al*., 2019). Ces travaux ont permis d'identifier des zones d'intérêts majeurs caractérisées par la présence des écosystèmes à Carbone Bleu (*i.e.* herbiers marins) mais également la présence de zones de dégradation localisées liées aux activités anthropiques dont l'ampleur est loin d'être négligeable (*e.g.* ancrage, chalutage ; Alami *et al*., 2014 ; Pergent-Martini *et al*., 2015). Malgré cela, les récents résultats mettent en évidence une distribution significative des écosystèmes à « Carbone Bleu » autour de la Corse et notamment des

herbiers à *P. oceanica* qui couvrent 61 % des fonds marins entre 0 et 40 m de profondeur (Valette-Sansevin *et al*., 2019). La réalisation de cette cartographie des habitats côtiers s'est appuyée sur l'acquisition et le traitement d'un jeu de données conséquent issues de capteurs optiques (images aériennes et satellitaires) en partie superficielle et de données acoustiques (sondeurs multifaisceaux et sonars à balayage latéral) en partie profonde (Valette-Sansevin *et al*., 2019). La calibration de ces données grâce à l'acquisition de données terrain constitue généralement une étape indispensable dans le processus de validation des cartographies des habitats benthiques (MESH, 2008). Cependant, l'acquisition de ces données terrain est souvent sporadique (points ou transects) et s'avère généralement être un processus long et coûteux selon la méthode utilisée ainsi que la surface et la profondeur du site cartographié (Kenny *et al*., 2003).

C'est dans un objectif d'optimisation des techniques cartographiques que la méthodologie basée sur l'utilisation simultanée d'une caméra sous-marine et d'un sonar à balayage latéral a été développée (Chapitre 2; Pergent *et al*., 2017). La mise en œuvre de cette méthode au cours des campagnes océanographiques PosidCorse (2015) et Carbonsink (2018) a contribué à l'identification des habitats et types de fonds entre 10 et 50 mètres de profondeur (Chapitre 2) et s'est révélée être une stratégie performante pour acquérir des données terrain continues. Les avancées des moyens d'investigations mis à disposition de la communauté scientifique et des gestionnaires couplés à l'utilisation de techniques de validation de plus en plus sophistiquées permettront d'optimiser les méthodes de cartographie (Kenny *et al*., 2003 ; MESH, 2008). À l'image des résultats cartographiques obtenus à l'échelle de la Corse depuis les années 1990, l'optimisation des moyens technologiques a permis de préciser significativement la distribution et l'état de conservation des écosystèmes impliqués dans l'atténuation des effets du changement climatique (Valette-Sansevin *et al*., 2019). Les connaissances acquises au cours des dernières décennies sur la distribution de ces habitats a offert la possibilité d'estimer les quantités de carbone fixées, séquestrées et stockées par ces écosystèmes à l'échelle régionale ou globale (*e.g.* Howard *et al*., 2014a ; Fourqurean *et al*., 2012 ; Atwood *et al*., 2017 ; Mateo *et al*., 2018 ; Serrano *et al*., 2019 ; Pergent-Martini *et al*., 2020).

Les données LiDAR topographiques, topo-bathymétriques et bathymétriques aéroportés, acquises très récemment sur l'ensemble du littoral de la Corse dans le cadre de l'opération « Risques côtiers, Litto3D® » (SHOM-CDC-DREAL Corse, 2019) apportent de nouvelles connaissances sur la distribution des habitats côtiers et marins. La représentation tridimensionnelle des fonds marins issues de ces données aéroportées et les interprétations préliminaires menées sur ces relevés ont d'ores et déjà permis d'affiner l'extension géographique des herbiers à *P. oceanica* en limite supérieure (Galonnier, 2020) et confirment la présence significative de traces d'activités anthropiques (*i.e.* ancrage, chalutage, rejets d'eaux usées issues d'émissaires) identifiées sur le littoral orientale de la Corse lors de précédentes études (Alami *et al*., 2014 ; Pergent-Martini *et al*., 2015 ; Fig. 7.1). L'inventaire des zones caractérisées par des dégradations significatives des herbiers marins sur le littoral de la Corse permettra d'adapter les mesures de conservation et de gestion de ces écosystèmes alors même que ces derniers font déjà l'objet de mesures de protection sur le plan réglementaire (Boudouresque *et al*., 2012) mais aussi de cibler les zones susceptibles d'accueillir de futurs projets de renforcement de ces puits de carbone à travers des actions de restauration écologique.

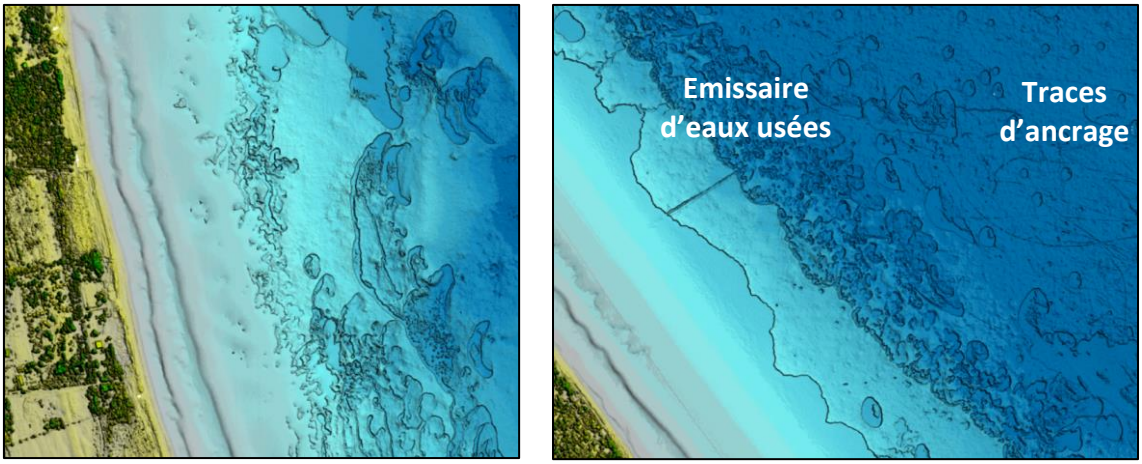

Figure 7.1. Représentations tridimensionnelles des fonds marins de la côte orientale de la Corse obtenues avec l'imagerie LiDAR (SHOM-CDC-Dreal Corse, 2019).

7.2. Apport des données de sismique réflexion pour la quantification des puits de carbone.

Depuis la fin des années 2000 et la parution d'ouvrages de portée internationale reconnaissant le rôle des écosystèmes côtiers dans l'atténuation des effets du changements climatiques (Nellemann *et al*., 2009 ; Laffoley et Grimsditch, 2009), un important effort de recherche a été entrepris pour quantifier les flux et stocks de carbone au sein des herbiers marins (Alongi, 2018). En Méditerranée, les herbiers à *P. oceanica* sont reconnus depuis plusieurs années pour leur contribution à l'atténuation du changement climatique grâce au stockage d'importantes quantités de C_{org} dans la matte (Mateo *et al*., 1997, 2006 ; Lo Iacono *et al*., 2008 ; Serrano *et al*., 2012, 2014, 2016a) et leur vaste distribution sur les côtes de Méditerranée (Telesca *et al*., 2015). Cependant, les estimations des stocks de carbone associés aux herbiers à *P. oceanica* reposent majoritairement sur la collecte et l'analyse d'un nombre limité de carottes de matte (Mateo *et al*., 1997 ; Serrano *et al*., 2012, 2014, 2016a). Plusieurs études ont ainsi souligné la nécessité de prendre en considération la variabilité environnementale en augmentant le nombre de prélèvements et analyses sédimentaires, ainsi qu'en fournissant des estimations des épaisseurs et volumes occupés par les mattes des herbiers à *P. oceanica* (Mateo et Serrano, 2012 ; Pergent *et al*., 2014).

Dans ce contexte, afin de préciser l'extension spatiale (épaisseurs et volumes) des puits de carbone associées aux herbiers à *P. oceanica* au sein du site du « Grand Herbier de la Côte Orientale », ces travaux se sont appuyés sur l'acquisition et l'analyse de données de sismique-réflexion haute-résolution acquises lors de trois missions océanographiques (Chapitre 3 et 4). L'application de cette méthode géophysique non-destructrice a permis d'obtenir une représentation détaillée des couches sédimentaires le long du littoral oriental de la Corse. À notre connaissance, cette acquisition (~1 380 km de profils sismique) constitue l'un des plus importants effort d'investigation mené dans le cadre d'un inventaire des stocks de Carbone Bleu à l'échelle de la Méditerranée (Lo Iacono *et al*., 2008 ; Tomasello *et al*., 2009). Au cours de ces travaux, le déploiement de quatre appareils aux fréquences d'émissions distinctes (Sparker – 1,0 kHz ; Manta EDO – 2,5 kHz ; PeskAvel – 3,5 kHz et Innomar SES-2000 – 8,0 kHz) a permis d'identifier l'appareil le plus adapté vis-à-vis des objectifs de l'étude. Ainsi, au vu des résultats obtenus et des précédents travaux (Lo Iacono *et al*., 2008 ; Tomasello *et al*., 2009 ;

Blouet *et al*., 2014), l'utilisation d'un échosondeur de type non-paramétrique tel que l'INNOMAR-SES 2000 générant des relevées sismiques avec une résolution verticale et horizontale très élevée (quelques centimètres) constitue l'outil le plus à même de contribuer efficacement à la quantification des épaisseurs de mattes des herbiers à *P. oceanica*.

Conventionnellement, l'interprétation des données de sismique réflexion est rendue possible suite à la conversion temps-profondeur des données sismiques en utilisant une vitesse moyenne de 1 500 m s^{-1}, estimée pour les sédiments meubles en domaine océanique (Hamilton, 1963, 1969, 1970 ; Hicks et Kibblewhite, 1976 ; Bourbié *et al*., 1986 ; Turgut et Yamamoto, 1990). Néanmoins, au regard de la complexité des mattes des herbiers à *P. oceanica* et au vue de la précision requise pour estimer l'épaisseur de ces formations naturels, un effort particulier a été focalisé sur la mise en place d'une méthodologie visant à déterminer la vitesse de l'onde acoustique au sein de ces structures (Chapitre 3). Cette approche s'est appuyée sur l'acquisition de mesures de hauteurs de tombants de matte issues (i) des données sismiques et (ii) de deux modèles numériques de terrains des fonds marins issus de données bathymétriques (sondeurs multifaisceaux) et optiques (LiDAR) qui ont été intercalibrés grâce à des relevés terrains.

Au regard des résultats obtenues, les vitesses de l'onde acoustique dans la matte (n = 367), estimées entre 1 631,9 et 1 696,8 m s^{-1} (moyenne : 1 664,4 m s^{-1}), se sont avérées être en cohérence avec les valeurs obtenues dans les sédiments marins (*e.g.* Hamilton, 1971 ; Schreiber, 1968 ; Kearey *et al*., 2002). Toutefois, la cartographie de prédiction établie par interpolation a permis de souligner une forte variabilité au sein de la zone d'étude. Les analyses biogéosédimentologiques menées sur les carottes horizontales prélevées au niveau des tombants de matte ont mis en évidence une corrélation significative de la vitesse de l'onde acoustique avec la teneur en sable et gravier au sein de la matte confirmant les relations établis entre la taille des sédiments et la vitesse de l'onde acoustique dans la littérature (Hamilton *et al*., 1956 ; Sutton *et al*., 1957 ; Orsi et Dunn, 1991) mais aussi avec certains facteurs environnementaux tels que la distance à la côte ou d'une embouchure de fleuve. L'analyse approfondie de carottes de matte en laboratoire à travers l'utilisation de banc Geotek (*e.g.* Satra *et al*., 2003 ; https://www.geotek.co.uk) pourrait permettre d'identifier

avec précision les relations existantes entre les paramètres biogéophysiques de la matte (densité, granulométrie) et la vitesse des ondes acoustiques.

A l'instar des études conduites à Portlligat (Gerone, Espagne ; Lo Iacano *et al*., 2008) et dans la baie d'Augusta (Sicile, Italie ; Tomasello *et al*., 2009), l'interprétation des profils sismiques a permis d'évaluer les épaisseurs et les volumes occupés par les mattes des herbiers à *P. oceanica.* L'interpolation par krigeage ordinaire des épaisseurs (n = 861 544) sur l'ensemble du site d'étude contribue significativement à l'amélioration des connaissances sur l'extension verticale de ces structures et permet de disposer d'une cartographie prédictive très précise. Les résultats ont montré que les épaisseurs de mattes, estimées en moyenne à 251,9 cm, étaient plus importantes en zone peu profonde (-10 m à -20 m), près de l'embouchure des fleuves côtiers (*e.g.* Golo, Tavignano et Travo-Solenzara) et des graus des lagunes (e.g. Diana et Urbino), où des mattes atteignant 867 cm d'épaisseur ont pu être relevées, et localement en partie profonde (entre -30 m et -40 m).

Les datations au ^{14}C témoignent de la présence de ces herbiers depuis le milieu de la période Holocène (~7000-9000 ans AP). Sur les 100 premiers centimètres de sol, l'âge de la matte était compris entre 440 et 5331 ans AP et l'âge moyen a été calculé à 1656 ± 528 ans AP. Le taux d'accrétion de la matte, estimé en moyenne à 1,02 ± 0,21 mm an^{-1}, montre une forte variabilité entraînant une interaction complexe de multiples facteurs biotiques et abiotiques (e.g. les caractéristiques des espèces, la profondeur, l'exposition à l'hydrodynamisme, la géomorphologie

En se basant sur la surface occupée par les herbiers marins et les épaisseurs relevées sur le site d'étude et les données issues de la littérature, le volume de matte et le stock total de C_{org} ont pu être estimés respectivement à 403,5 ± 49,4 millions de m^3 (ratio: 2,2 m^3 m^{-2}) et 15,6 ± 2,2 millions de tonnes. L'application de la sismique réflexion à haute résolution pour dimensionner l'épaisseur et le volume potentiel occupés par les mattes a souligné la nécessité d'effectuer une évaluation à grande échelle de l'étendue spatiale de ces puits de carbone afin de préciser les estimations des stocks de carbone sous les herbiers marins en Méditerranée et à travers le monde.

7.3. Contribution des herbiers à *P. oceanica* à l'atténuation du changement climatique

Au cours des dernières décennies, la nécessité croissante de réduire les concentrations atmosphériques de dioxyde de carbone (CO_2) a récemment intensifié l'intérêt pour la quantification de la capacité des écosystèmes côtiers à séquestrer le carbone. Parmi les écosystèmes côtiers dominés par la végétation, les herbiers marins sont considérés comme d'importants puits de carbone en raison de leur capacité à stocker une grande quantité de carbone sur de longues périodes dans leurs sédiments. Cependant, afin de préciser la contribution de ces écosystèmes à l'atténuation du changement climatique, il apparaît nécessaire de prendre en considération les variations des stocks et flux de carbone, en particulier lorsque la variabilité environnementale est élevée. Ainsi, afin de préciser la contribution des herbiers de *P. oceanica* à l'atténuation du changement climatique, ces travaux de recherche se sont interessés à fournir une estimation des stocks de carbone au sein du site d'étude.

Cet inventaire majeur s'est appuyé sur le prélèvement et l'analyse biogéochimiques de 39 carottes sédimentaires prélevées dans les herbiers à *P. oceanica*. Les résultats ont montré une grande variabilité des stocks et des flux de carbone organique et inorganique (C_{org} et C_{inorg}, respectivement) au sein du site d'étude. Les estimations des stocks de C_{org} et C_{inorg} (moyenne: 327 ± 150 t ha^{-1} et 245 ± 45 t ha^{-1}, respectivement), montrent une forte variabilité liée à la profondeur, à la matrice sédimentaire (substrat sableux *vs* rocheux) ou encore à la sédimentation (mer ouverte *vs* estuaire). La signature isotopique ($\delta^{13}C$) a permis de révéler une contribution substantielle des apports allochtones de matière organique (macroalgues et sources sestoniques) principalement en milieu estuarien et dans les zones peu profondes. Les estimations globales des quantités de carbone stockées sur les 250 premiers cm de matte (épaisseur moyenne au niveau du site) ont été estimées entre 4,5 et 13,2 millions de tonnes de C_{org}. La conversion de ces résultats en équivalent CO_2 (CO_{2e}) a permis d'estimer la quantité de CO_{2e} stockée au sein des mattes à 16,5 et 48,3 millions de tonnes, soit l'équivalent de 9,4 à 27,4 années d'émissions de CO_2 de l'ensemble de la population de la Corse. L'extrapolation

des données à l'échelon régionale montre que les herbiers marins auraient stocké l'équivalent de 26,6 à 72,0 années d'émissions de CO_2.

7.4. Les mattes des herbiers à *P. oceanica* : une paléo-archive unique en Corse

En Méditerranée, les mattes des herbiers à *P. oceanica* sont reconnues comme des archives uniques permettant l'étude des changements paléoclimatiques et paléoenvironnementaux survenues au cours des derniers millénaires. La grande cohérence chronostratigraphique de ces dépôts associé à la préservation des matériaux organiques sur de longues périodes au sein des mattes constitue des registres exceptionnels au vu des conditions environnementales régnant au sein des zones côtières.

L'analyse des carottes sédimentaires collectées au cour de la campagne Carbonsink a permis de réaliser une découverte sans précédente d'un ancien banc de *Cladocora caespitosa* enfoui dans la matte. L'analyse des caractéristiques morphologiques et biométriques des fragments de corallite couplée à l'analyse biogéosédimentologique et à aux radiodatations ont permis de reconstruire la dynamique temporelle de la séquence stratigraphique depuis le milieu de l'Holocène (4750 dernières années). L'étude de la carotte sédimentaire a permis d'identifier trois phases majeures: (i) le développement des colonies de *C. caespitosa* (~ 4750-3930 ans AP), (ii) la coexistence du banc de *C. caespitosa* et des herbiers à *P. oceanica* (~3930-1410 ans AP), et (iii) la disparition du banc de corail et le développement des herbiers à *P. oceanica* (~ 1410 ans AP-présent).

L'analyse sclérochronologique réalisée sur les fragments de corallite bien conservés a révélé que le taux de croissance annuel moyen du corail variait entre 1,9 et 3,1 mm an^{-1} avec une valeur moyenne estimée à 2,3 ± 0,8 mm an^{-1}. Les mesures relevées sur les fragments montrent des oscillations semi-millénaires à millénaires des taux de croissance annuels qui sont probablement liées aux changements climatiques et environnementaux entre la période Subatlantique (2925-2200 ans AP) et le Haut Moyen-Âge (1500-1000 ans AP). Les éléments fournis lors de l'analyse de la séquence sédimentaire montrent que le déclin et la disparition du banc de corail (~1410 ans AP) résulte très probablement de l'effet combiné d'une

augmentation prolongée des températures et d'une augmentation de la compétition avec l'herbier à *P. oceanica* durant la période romaine (2200-1500 ans AP).

Références

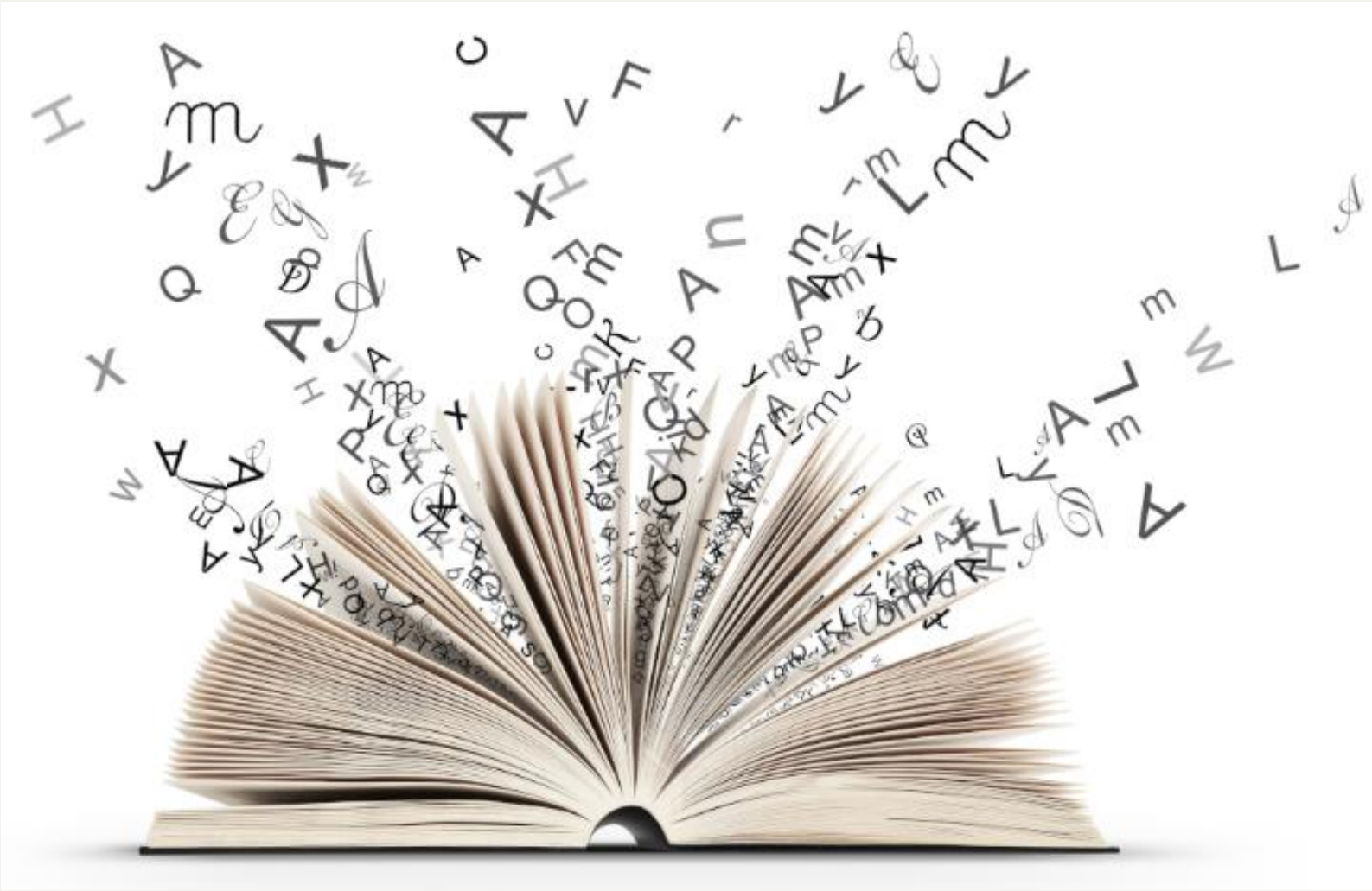

References

Références

Abadie, A., 2012. Evolution des herbiers à *Posidonia oceanica* (L.) Delile dans la baie de Calvi (Corse, France) et influence de l'ancrage dans la baie de l'Alga. Mémoire Master 2, Université Aix-Marseille, pp. 1-35.

Abadie, A., Gobert, S., Bonacorsi, M., Lejeune, P., Pergent, G., Pergent-Martini, C., 2015. Marine space ecology and seagrasses. Does patch type matter in *Posidonia oceanica* seascapes? Ecological Indicators 57, 435-446. http://dx.doi.org/10.1016/j.ecolind.2015.05.020.

Adame, M.F., Hermoso, V., Perhans, K., Lovelock, C.E., Herrera-Silveira, J.A., 2015. Selecting cost-effective areas for restoration of ecosystem services. Conservation Biology 29(2), 493-502. https://doi.org/10.1111/cobi.12391.

Adame, M.F., Wright, S.F., Grinham, A. Lobb, K., Reymond C. E., Lovelock C.E., 2012. Terrestrial–marine connectivity: Patterns of terrestrial soil carbon deposition in coastal sediments determined by analysis of glomalin related soil protein. Limnology and Oceanography 57, 1492-1502. https://doi.org/10.4319/lo.2012.57.5.1492.

Addinsoft, 2019. XLSTAT statistical and data analysis solution. Long Island, NY, USA. https://www.xlstat.com.

Aguirre, J., 1998. Bioconstrucciones de *Saccostrea cucullata* Born, 1778 en el Plioceno superior de Cádiz (SW de España) : implicaciones paleoambientales y paleoclimáticas. Revista Española de Paleontología 13, 27-36.

Aguirre, J., Jiménez, A.P., 1998. Fossil analogues of the present day ahermatypic *Cladocora caespitosa* coral banks: sedimentary setting, dwelling community, and taphonomy (Late Pliocene, W Mediterranean). Coral Reefs 17, 203-213. https://doi.org/10.1007/s003380050119.

Agus, F., Hairiah, K., Mulyani, A., 2011. Measuring carbon stock in peat soils: practical guidelines. Bogor, Indonesia: World Agroforestry Centre (ICRAF) Southeast Asia Regional Program, Indonesian Centre for Agricultural Land Resources Research and Development, pp. 1-60.

Akal, T., 1972. The relationship between the physical properties of underwater sediments that affect bottom reflection. Marine Geology 13(4), 251-266. https://doi.org/10.1016/0025-3227(72)90054-0.

Alami, S., Bonacorsi, M., Clabaut, P., Jouet, G., Pergent-Martini, C., Pergent, G., Sterckeman, A., 2014. Assessment and quantification of the anthropic impact on the *Posidonia oceanica* seagrass meadow. *In*: Langar, H., Bouafif, C., Ouerghi, A. (Eds.), Proceedings of the 5th Mediterranean Symposium on Marine Vegetation. UNEP/MAP-CAR/ASP publ., Tunis, 27-28 Oct. 2014, Portorož, Slovenia, 34-39.

Alcoverro, T., Cerbian, E., Ballesteros, E., 2001. The photosynthetic capacity of the seagrass *Posidonia oceanica*: Influence of nitrogen and light. Journal of Experimental Marine Biology and Ecology 261(1), 107-120. https://doi.org/10.1016/S0022-0981(01)00267-2.

Alcoverro, T., Duarte, C.M., Romero, J., 1995. Annual growth dynamics of *Posidonia oceanica*: contribution of large-scale versus local factors to seasonality. Marine Ecology Progress Series 120, 203-210. https://doi.org/10.3354/meps120203.

Alongi, D.M., 2002. Present state and future of the world's mangrove forests. Environmental Conservation 29(3), 331-349. https://doi.org/10.1017/S0376892902000231.

Alongi, D.M., 2018. Blue carbon: Coastal sequestration for climate change mitigation. Cham, Switzerland, Springer : Springer, pp. 1-88. https://doi.org/10.1007/978-3-319-91698-9.

Andromède Océanologie, Stareso, 2012. Inventaires biologiques et analyse écologique des habitats marins patrimoniaux du site Natura 2000 « Cap Rossu, Scandola, Pointe de la Revelatta, Canyon de Calvi » FR940201. Andromède Océanologie et Stareso / Agence Des Aires Marines Protégées, pp. 1-339.

Antonioli, F., Ferranti, L., Fontana, A., Amorosi, A., Bondesan, A., Braitenberg, C., Dutton, A., Fontolan, G., Furlani, S., Lambeck, K., Mastronuzzi, G., Monaco, C., Spada, G., Stocchi, P., 2009. Holocene relative sea-level changes and vertical movements along the Italian and Istrian coastlines.

Quaternary International 206(1-2), 102-133. https://doi.org/10.1016/j.quaint.2008.11.008.

Arrigo, K.R., 2005. Marine microorganisms and global nutrient cycles. Nature 437, 349-355. https://doi.org/10.1038/nature04159.

Assaad, F.A., LaMoreaux, J.W., Hughes, T., 2013. Field methods for geologists and hydrogeologists. Springer Science & Business Media. https://doi.org/10.1007/978-3-662-05438-3.

Atwood, T. B., Connolly, R. M., Almahasheer, H., Carnell, P. E., Duarte, C. M., Lewis, C.J.E., Irigoien, X., Kelleway, J.J., Lavery, P.S., Macreadie, P.I., Serrano, O., Sanders, C.J., Santos, I., Steven A.D.L., Lovelock, C.E., 2017. Global patterns in mangrove soil carbon stocks and losses. Nature Climate Change 7(7), 523-528. https://doi.org/10.1038/nclimate3326.

Barbier, E.B., Hacker, S.D., Kennedy, C., Koch, E.W., Stier, A.C., Silliman, B.R., 2011. The value of estuarine and coastal ecosystem services. Ecological Monographs, 81(2), 169-193. https://doi.org/10.1890/10-1510.1.

Barker, B.A., Helmond, I., Bax, N.J., Williams, A., Davenport, S., Wadley, V.A., 1999. A vessel-towed camera platform for surveying seafloor habitats of the continental shelf. Continental Shelf Research 19(9), 1161-1170. https://doi.org/10.1016/S0278-4343(99)00017-5.

Barrón, C., Duarte, C.M., Frankignoulle, M., Borges, A.V., 2006. Organic carbon metabolism and carbonate dynamics in a Mediterranean seagrass (*Posidonia oceanica*), meadow. Estuaries Coasts 29(3), 417-426. https://doi.org/10.1007/BF02784990.

Batjes, N.H., 1996. Total carbon and nitrogen in the soils of the world. European Journal of Soil Science 47(2), 151-163. https://doi.org/10.1111/j.1365-2389.1996.tb01386.x.

Beck, M.W., Heck, K.L., Able, K.W., Childers, D.L., Eggleston, D.B., Gillanders, B.M., Halpern, B., Hays, C.G., Hoshino, K, Minello, T.J., Orth, R.J., Sheridan, P.F., Weinstein, M.P., 2001. The Identification, Conservation, and Management of Estuarine and Marine Nurseries for Fish and Invertebrates A better understanding of the habitats that serve as nurseries for marine species and the factors that create site-specific variability in nursery quality will improve conservation and management of these areas. Bioscience, 51, 633-641. https://doi.org/10.1641/0006-3568(2001)051[0633:TICAMO]2.0.CO;2.

Beer, C., Reichstein, M., Tomelleri E., Ciais, P., Jung, M., Carvalhais, N., Rödenbeck, M., Arain, A., Baldocchi, D., Bonan, G.B., Bondeau, A., Cescatti, A., Lasslop, G., Lindroth, A., Lomas, M., Luyssaert, S., Margolis, H., Oleson, H.W., Roupsard, O., Veenendaal, E., Viovy, N., Williams, C., Woodward, F.I., Papale D., 2010. Terrestrial gross carbon dioxide uptake: Global distribution and covariation with climate. Science 329(5993), 834-838. https://doi.org/10.1126/science.1184984.

Bellaiche, G., Droz, L., Gaullier, V., Pautot, G., 1994. Small submarine fans on the eastern margin of Corsica: Sedimentary significance and tectonic implications. Marine Geology 117(1-4), 177-185. https://doi.org/10.1016/0025-3227(94)90013-2.

Bellan-Santini, D., Lacaze, J.C., Poizat, C., 1994. Les biocénoses marines et littorales de Méditerranée, synthèse, menaces et perspectives. Museum National d'Histoire Naturelle, Paris, pp. 1-246.

Belshe, E.F., Hoeijmakers, D., Herran N., Mtolera, M., Teichberg M., 2018. Seagrass community-level controls over organic carbon storage are constrained by geophysical attributes within meadows of Zanzibar, Tanzania. Biogeosciences 15(14), 4609-4626. https://doi.org/10.5194/bg-15-4609-2018.

Bernasconi, M.P., Corselli, C., Carobene, L., 1997. A bank of the scleractinian coral *Cladocora caespitosa* in the Pleistocene of the Crati valley (Calabria, Southern Italy): growth versus environmental conditions. Bolletino della Società Paleontologica Italiana 36(1-2), 53-61.

Bianchi, C.N., 2008. From bionomic mapping to territorial cartography, or from knowledge to management of marine protected areas. Biologia Marina Mediterranea 14, 22-51.

Bianchi, C.N., Peirano, A., 1990. Mappatura delle praterie di *Posidonia oceanica* in Mar Ligure. ENEA-CRAM S. Teresa, Rapporto tecnico interno, pp. 1-372.

Bianchi, T.S., Argyrou, M., Chippett, H.F., 1999. Contribution of vascular-plant carbon to surface sediments across the coastal margin of Cyprus (eastern Mediterranean). Organic Geochemistry 30, 287-297. https://doi.org/10.1016/S0146-6380(99)00016-9.

Bird, M.I., Fifield, L.K., Chua, S., Goh, B., 2004. Calculating sediment compaction for radiocarbon dating of intertidal sediments. Radiocarbon 46(1), 421-435. https://doi.org/10.1017/S0033822200039734.

Bitri A., Perrin J., Beauce A., 1996. La sismique réflexion haute résolution : principes et applications. Rapport BRGM, R 39220.

Blaauw, M., 2010. Methods and code for 'classical' age-modelling of radiocarbon sequences. Quaternary Geochronology 5, 512-518. https://doi.org/10.1016/j.quageo.2010.01.002.

Blanc, J.J., Jeudy de Grissac, A., 1978. Recherches de géologie sédimentaire sur les herbiers à Posidonies du littoral de la Provence. Centre National pour l'Exploitation des Océans, pp. 1-185.

Blanc, J.J., Jeudy de Grissac, A., 1984. Erosions sous-marines des herbiers à *Posidonia oceanica* (Méditerranée). *In:* Boudouresque, C.F., Jeudy de Grissac, A., Olivier, J. (Eds.), International Workshop on *Posidonia oceanica* beds. GIS Posidonie publ., France, 1, 23-28.

Blouet, S., Dupuy de la Grandrive, R., Chere, E., Noël, C., Viala, C., Marchetti, S., Bauer, E., Temmos, J.M., Boissery, P., 2014. Application de la sismique UHR pour le suivi de l'état de conservation des herbiers à *Posidonia oceanica. In:* Langar, H., Bouafif, C., Ouerghi, A. (Eds.), Proceedings of the 5th Mediterranean Symposium on Marine Vegetation. UNEP/MAP-CAR/ASP publ., Tunis, 27-28 Oct. 2014, Portorož, Slovenia, 46-51.

Boden, T., Marland, G., Andres, R., 2011. Global CO_2 emissions from fossil fuel burning, cement manufacture, and gas flaring: 1751-2008. Oak Ridge National Laboratory, U.S. Department of Energy,Carbon Dioxide Information Analysis Center, Oak Ridge, TN, USA., https://doi.org/10.3334/CDIAC/00001_V2011.

Bonacorsi, M., 2012. Caractérisation des peuplements benthiques du Cap Corse. Thèse de doctorat, Université de Corse, pp. 1-158.

Bonacorsi, M., Alami, S., Breand, N., Clabaut, P., Daniel, B., Pergent, G., Pergent-Martini, C., 2014. Cartography of main coastal ecosystems (coralligenous and rhodolith beds) along the Corsican coasts. *In*: Langar, H., Bouafif, C., Ouerghi, A. (Eds.), Proceedings of the 2nd Mediterranean Symposium on the conservation of Coralligenous & other Calcareous Bio-Concretions. UNEP/MAP-CAR/ASP publ., Tunis, 29-30 Oct. 2014, Portorož, Slovenia, 37-42.

Bonacorsi, M., Pergent-Martini, C., Bréand, N., Pergent, G., 2013. Is *Posidonia oceanica* regression a general feature in the Mediterranean Sea? Mediterranean Marine Science 14(1), 193-203. https://doi.org/10.12681/mms.334.

Bonacorsi, M., Pergent-Martini, C., Clabaut, P., Jouet, G., Pergent, G., 2013. Optimization and comparison of underwater mapping methods. *In:* Proceedings of the Global Congress on ICM: Lessons learned to Address New Challenges, EMECS 10 - MEDCOAST 2013 Joint Conference, 30 Oct - 03 Nov 2013, Marmaris, Turkey, Ozhan E. (Eds.), MEDCOAST Mediterranean Coastal Foundation, Dalyan, Mugla, Turkey, 2, 907-918.

Bonacorsi, M., Pergent-Martini, C., Clabaut, P., Pergent, G., 2012. Coralligenous ''atolls'': discovery of a new morphotype in the Western Mediterranean Sea. Comptes Rendus Biologies 335(10-11), 668-672. https://doi.org/10.1016/j.crvi.2012.10.005.

Borowitzka, M.A., Lavery, P.S., van Keulen, M., 2006. Epiphytes of seagrasses. *In:* Larkum, A.W.D., Orth, R.J., Duarte, C.M. (Eds.), Seagrasses: Biology, Ecology and Conservation. Springer, Netherlands, 441-461.

Botch, M S., Kobak, K.I., Vinson, T.S., Kolchugina, T.P., 1995. Carbon pools and accumulation in peatlands of the former Soviet Union, Global Biogeochemical Cycles 9(1), 37-46, https://doi.org/10.1029/94GB03156.

Boudouresque, C.F., Bernard, G., Bonhomme, P., Charbonnel, E., Diviacco, G., Meinesz, A., Pergent, G., Pergent-Martini, C., Ruitton, S., Tunesi, L., 2012. Préservation et conservation des herbiers à *Posidonia oceanica*. RAMOGE Publication, pp. 1-202.

Boudouresque, C.F., Bernard, G., Pergent, G., Shili, A., Verlaque, M., 2009. Regression of Mediterranean seagrasses caused by natural processes and anthropogenic disturbances and stress: a critical review. Botanica Marina 52(5), 395-418.

https://doi.org/10.1515/BOT.2009.057.

Boudouresque, C.F., Giraud, G., Thommeret, J., Thommeret, Y., 1980. First attempt at dating by ^{14}C the undersea beds of dead *Posidonia oceanica* in the bay of Port-Man (Port-Cros, Var, France). Travaux scientifiques du Parc national de Port-Cros 6, 239-242.

Boudouresque, C.F., Jeudy de Grissac, A., 1983. L'herbier à *Posidonia oceanica* en Méditerranée, les interactions entre la plante et le sédiment. Journal de recherche océanographique 8(2-3), 99-122.

Boudouresque, C.F., Jeudy de Grissac, A., Meinesz A., 1984. Relations entre la sédimentation et l'allongement des rhizomes orthotropes de *Posidonia oceanica* dans la baie d'Elbu (Corse). *In:* Boudouresque C.F., Jeudy de Grissac A., Olivier J. (Eds.), International Workshop on *Posidonia oceanica* beds, GIS Posidonie publication, 1, 185-191.

Boudouresque, C.F., Meinesz, A., 1982. Découverte de l'herbier de Posidonie. Cahier Parc National de Port-Cros, Hyères, pp. 1-79.

Bouguet, J.Y., 2010. Camera, Calibration. Toolbox for Matlab. Available online. https://vision.caltech.edu/bouguetj/calib_doc/index.html.

Bouillon, S., Borgess, A.V., Castañeda-Moya, E., Diele, K., Dittmar, T, Duke, N.C., Kristensen, E., Lee, S.Y., Marchand, C., Middelburg, J.J., Rivera-Monroy, V.H., Smith, T.J., Twilley, R.R., 2008. Mangrove production and carbon sinks: A revision of global budget estimates. Global Biogeochemical Cycles 22(2), GB2013. https://doi.org/10.1029/2007GB003052.

Bouillon, S., Dahdouh-Guebas, F., Rao, A., Koedam, N., Dehairs, F., 2003. Sources of organic carbon in mangrove sediments: variability and possible ecological implications. Hydrobiologia 495, 33-39. https://doi.org/10.1023/A:1025411506526.

Bourbié, T., Coussy, O., Zinszner, B., 1986. Acoustique des milieux poreux. Technip Ed., 27.

Bouysse, P., Lenotre, N., Martin, P., Scolari, G., 1981. La plateforme continentale de la Corse : résultats préliminaires d'une reconnaissance sédimentologique. Bulletin de la Société des Sciences historiques et naturelles de la Corse 641, 67-85.

Bowler, C., Karl, D.M., Colwell, R.R., 2009. Microbial oceanography in a sea of opportunity. Nature 459, 180-184. https://doi.org/10.1038/nature08056.

BP, 2019. Statistical Review of World Energy. Available at: https://www.bp.com/en/global/corporate/energy-economics/statistical-review-of-world-energy.html, last access June 2019.

Bradley, R.S., Hughes, M.K., Diaz, H.F., 2003. Climate in Medieval Time. Science 302, 404-405. https://doi.org/10.1126/science.1090372.

Brambilla, W., Conforti, A., Simeone, S., Carrara, P., Lanucara S., De Falco, G., 2019. Data set of submerged sand deposits organised in an interoperable spatial data infrastructure (Western Sardinia, Mediterranean Sea). Earth System Science Data 11(2), 515-527. https://doi.org/10.5194/essd-11-515-2019.

Brandano, M., Civitelli, G., 2007. Non-segrass meadow sedimentary facies of the Pontinian Islands, Tyrrhenean Sea : A modern example of mixed carbonate-siliciclastic sedimentation. Sedimentary Geology 201, 286-301. https://doi.org/10.1016/j.sedgeo.2007.05.012.

Breslau, L.R., Edgerton, H., 1968. The sub-bottom structure of the Gulf of La Spezia. NATO-SACLANTCEN Technical Report.

Brock F., Higham, T., Ditchfield, P., Ramsey C.B., 2010. Current pretreatment methods for AMS radiocarbon dating at the Oxford Radiocarbon Accelerator Unit (ORAU). Radiocarbon, 52(1), 103-112.

Brown, C.J., Smith, S.J., Lawton, P., Anderson, J.T., 2011. Benthic habitat mapping: A review of progress towards improved understanding of the spatial ecology of the seafloor using acoustic techniques. Estuarine, Coastal and Shelf Science 92(3), 502-520. https://doi.org/10.1016/j.ecss.2011.02.007.

Buia, M.C., Gambi, M.C., Zupo, V., 2000. Structure and functioning of Mediterranean seagrass ecosystems: an overview. Proceedings 4th International Seagrass Biology Workshop, Biologia Marina Mediterranea, Balagne, Corsica, France, pp. 167-190.

Burdige, D.J., 2007. Preservation of organic matter in marine sediments: controls, mechanisms, and an imbalance in sediment organic carbon budgets? Chemical Reviews 107(2), 467-485. http://dx.doi.org/10.1021/cr050347q.

Canals, M., Ballesteros, E., 1997. Production of carbonate particles by phytobenthic communities on the Mallorca–Menorca shelf, northwestern Mediterranean Sea. Deep Sea Research 44, 611-629. https://doi.org/10.1016/S0967-0645(96)00095-1.

Cannac-Padovani, M., 2014. Document d'objectifs Natura 2000 - FR 9402014 - Grand herbier de la côte orientale - Tome 1 : Etat des Lieux, Analyse Ecologique, Enjeux & Objectifs de Conservation. Rapport Office de l'Environnement de la Corse. Convention Etat / CTC, pp. 1-256.

Carruthers, T.J.B., Dennison, W.C., Kendrick, G.A., Waycott, M., Walker, D.I., Cambridge, M.L., 2007. Seagrasses of south-west Australia: A conceptual synthesis of the world's most diverse and extensive seagrass meadows. Journal of Experimental Marine Biology and Ecology 350(1-2), 21-45. https://doi.org/10.1016/j.jembe.2007.05.036.

Carver, R.E., 1971. Procedures in sedimentary petrology. Wiley-Interscience.

Casado-Amezúa, P., García-Jiménez, R., Kersting, D.K., Templado, J., Coffroth, M.A., Acevedo, I., Machordom, A., 2011. Development of microsatellite markers as a molecular tool for conservation studies of the Mediterranean reef builder coral *Cladocora caespitosa* (Anthozoa, Scleractinia). Journal of Heredity 102(5), 622-626. https://doi.org/10.1093/jhered/esr070.

Casado-Amezúa, P., Kersting, D., Linares, C.L., Bo, M., Caroselli, E., Garrabou, J., Cerrano, C., Ozalp, B., Terrón-Sigler, A., Betti, F., 2015. *Cladocora caespitosa*. The IUCN Red List of Threatened Species 2015: e.T133142A75872554.

Casado-Amezúa, P., Kersting, D.K., Templado, J., Machordom, A., 2014. Regional genetic differentiation among populations of *Cladocora caespitosa* in the Western Mediterranean. Coral Reefs 33, 1031-1040. https://doi.org/10.1007/s00338-014-1195-5.

Caye, G., 1980. Sur la morphogénèse et le cycle végétatif de *Posidonia oceanica* (L.) Delile. Thèse de doctorat, Université Aix-Marseille II, France, pp. 1-121.

Cebrian, J., 2002. Variability and control of carbon consumption, export, and accumulation in marine communities. Limnology and Oceanography 47, 11-22. https://doi.org/10.4319/lo.2002.47.1.0011.

Cebrian, J., Duarte, C.M., 1995. Plant growth-rate dependence of detrital carbon storage in ecosystems. Science 268(5217), 1606-1608. https://doi.org/10.1126/science.268.5217.1606.

Chabanet, P., Loiseau, N., Join, J.L., Ponton, D., 2012. VideoSolo, an autonomous video system for high-frequency monitoring of aquatic biota, applied to coral reef fishes in the Glorioso Islands (SWIO). Journal of Experimental Marine Biology and Ecology 430-431, 10-16. https://doi.org/10.1016/j.jembe.2012.06.024.

Chambers, J.Q., Higuchi, N., Tribuzy, E.S., Trumbore, S.R., 2001. Carbon sink for a century. Nature 410, 429. https://doi.org/10.1038/35068624.

Chapman, S.J., Bell, J.S., Campbell, C.D., Hudson, G., Lilly, A., Nolan, A.J., Robertson, A.H.J., Potts, J.M., Towers, W., 2013. Comparison of soil carbon stocks in Scottish soils between 1978 and 2009. European Journal of Soil Science 64(4), 455-465. https://doi.org/10.1111/ejss.12041.

Chassefière, B., Got, H., Leenhardt, O., 1974 . Comment aborder les travaux de reconnaissance des fonds sous-marins. Geologia tecnica 1, pp. 1-20.

Chavaillaz, Y., 2016. La vitesse du changement climatique et ses implications sur la perception des générations futures. Thèse de doctorat, Université Paris-Saclay, pp. 1-268.

Chefaoui, R.M., Casado-Amezúa, P., Templado J., 2017. Environmental drivers of distribution and reef development of the Mediterranean coral *Cladocora caespitosa*. Coral Reefs 36, 1195-1209. https://doi.org/10.1007/s00338-017-1611-8.

Chmura, G.L., Anisfeld, S., Cahoon, D., Lynch, J., 2003. Global carbon sequestration in tidal, saline wetland soils. Global Biogeochemical Cycles 17(4), 1-12. https://doi.org/10.1029/2002GB001917.

Ciais, P., Tagliabue, A., Cuntz, M., Bopp, L., Scholze, M., Hoffmann, G., Lourantou, A., Spencer Harrison S., Prentice, I.C., Kelley, D.I, Koven, C., Piao, S.L., 2012: Large inert carbon pool in the terrestrial

biosphere during the Last Glacial Maximum. Nature Geoscience 5, 74-79. https://doi.org/10.1038/ngeo1324.

Clabaut, P., Augris, C., 2014. Les fonds marins côtiers de Corse. Cartographie biomorphosédimentaire. Éd. Quae. 25 feuilles, échelle 1/20 000, livret d'accompagnement, pp. 1-80.

Clabaut, P., Augris, C., Pasqualini, V., Pergent G., Pergent-Martini, C., 2007. Identification et caractérisation des herbiers à *Posidonia oceanica* par sonar à balayage latéral : Vers une base de données méditerranéenne ? *In:* Proceedings of the 3rd Mediterranean Symposium on marine vegetation (Marseilles, France, 27-29 March 2007). Pergent-Martini, C., El Asmi, S., Le Ravallec, C. (Eds.), RAC/SPA publ., Tunis, 48-55.

Clymo, R.S. 1992 Productivity and decomposition of peaetland ecosystems. Peatland Ecosystems and Man: An Impact Assessment. Department of Biological Sciences, Dundee, U.K., 3-16.

Cogan, C., Todd, B., Lawton, P., Noji, T., 2009. The role of marine habitat mapping in ecosystem-based management. ICES Journal of Marine Science 66, 2033-2042. https://doi.org/10.1093/icesjms/fsp214.

Coggan, R., Populus, J., White, J., Sheehan, K., Fitzpatrick, F., Piel, S., 2007. Review of standards and protocols for seabed habitat mapping. Mapping European Seabed Habitats (MESH), pp. 1-210.

Colantoni, P., Gallignani, P., Fresi, E., Cinelli F., 1982. Patterns of *Posidonia oceanica* (L.) Delile Beds around the Island of Ischia (Gulf of Naples) and in Adjacent Waters. Marine Ecology 3(1), 53-74. https://doi.org/10.1111/j.1439-0485.1982.tb00105.x.

Colin, P.L., 2018. *Thalassodendron ciliatum* (Cymodoceaceae) in Palau: occurrence, typhoon impacts and changes over time. Botanica Marina 61(6), 537-546. https://doi.org/10.1515/bot-2017-0079.

Collier, C.J., Lavery, P., Ralph, P., Masini, R., 2009. Shade-induced response and recovery of the seagrass *Posidonia sinuosa*. Journal of Experimental Marine Biology and Ecology 370(1-2), 89-103. https://doi.org/10.1016/j.jembe.2008.12.003.

Collier, C.J., Lavery, P.S., Masini, R.J., Ralph, P.J., 2007. Morphological, growth and meadow characteristics of the seagrass *Posidonia sinuosa* along a depth- related gradient of light availability. Marine Ecology Progress Series 337, 103-115.

Commissariat général au développement durable, 2019. EFESE - La séquestration du carbone par les écosystèmes français. La Documentation Française (Ed.), Collection Théma Analyse, e-publication, pp. 1-102.

Conchon, O., 1975. Les formations quaternaires de type continental en Corse orientale. Thèse de doctorat, Université de Paris VI, pp. 1-514.

Conchon, O., Gauthier A., 1985. Phénomènes naturels exceptionnels en Corse : intérêt pour l'étude géologique de la période Quaternaire. Bulletin de la Société des Sciences Historiques et Naturelles Corse 648, 141-165.

Cordier, J.P., 1985. Velocities in reflection seismology. Springer, Dordrecht. https://doi.org/10.1007/978-94-017-3641-1.

Costanza, R., d'Arge, R., de Groot, R., Farber, S., Grasso, M., Hannon, B., Limburg, K., Naem, S., O'Neill, R.V., Paruelo, J., Raskin, R.G.,Sutton, P., van der Belt, M., 1997. The value of the world's ecosystem services and natural capital. Nature 387, 253-260. https://doi.org/10.1038/387253a0.

Crutchley, G.J., Kopp, H., 2018. Reflection and Refraction Seismic Methods. *In:* Micallef, A., Krastel, S., Savini, A. (Eds.), Submarine Geomorphology. Springer Geology. Springer, Cham, 43-62. https://doi.org/10.1007/978-3-319-57852-1_4.

Cullen-Unsworth, L., Unsworth, R., 2013. Seagrass meadows, ecosystem services, and sustainability. Environment: Science and Policy for Sustainable Development 55(3), 14-28. https://doi.org/10.1080/00139157.2013.785864.

Currás, A., Ghilardi, M., Peche-Quilichini, K., Fagel, N., Vacchi, M., Delanghe, D., Contreras, D., Vella, C., Ottaviani, J.C., 2017. Reconstructing past landscapes of the eastern plain of Corsica (NW Mediterranean) during the last 6000 years based on molluscan, sedimentological and palynological analyses. Journal of Archaeological Science : Reports 12, 755-769.

https://doi.org/10.1016/j.jasrep.2016.09.016.

Dahl, M., Deyanova, D., Lyimo, L.D., Näslund, J., Samuelsson, G.S., Mtolera, M.S.P., Björk, M., Gullström, M., 2016. Effects of shading and simulated grazing on carbon sequestration in a tropical seagrass meadow. Journal of Ecology 104(3), 654-664. https://doi.org/10.1111/1365-2745.12564.

D'Alessandro, A., Bromley, R., 1995. A new ichnospecies of Spongeliomorpha from the Pleistocene of Sicily. Journal of Paleontology 69(2), 393-398. https://doi.org/10.1017/S0022336000034727.

Danovaro, R., 1996. Detritus-Bacteria-Meiofauna interactions in a seagrass bed (*Posidonia oceanica*) of the NW Mediterranean. Marine Biology 127, 1-13. https://doi.org/10.1007/BF00993638.

De Falco, G., Baroli, M., Cucco, A., Simeone, S., 2008. Intrabasinal conditions promoting the development of a biogenic carbonate sedimentary facies associated with the seagrass *Posidonia oceanica*. Continental Shelf Research 28, 797-812. https://doi.org/10.1016/j.csr.2007.12.014.

De Falco, G., De Muro, S., Batzella T., Cucco A., 2011. Carbonate sedimentation and hydrodynamical pattern on a modern temperate shelf: the strait of Bonifacio (western Mediterranean). Estuarine, Coastal and Shelf Science 93(1), 14-26. https://doi.org/10.1016/j.ecss.2011.03.013.

De Falco, G., Ferrari, S., Cancemi, G., Baroli, M., 2000 Relationship between sediment distribution and *Posidonia oceanica* seagrass. Geo-Marine Letters 20, 50-57. https://doi.org/10.1007/s003670000030.

De Falco, G., Molinaroli, E., Baroli, M., Bellacicco, S., 2003. Grain size and compositional trends of sediment from *Posidonia oceanica* meadows to beach shore, Sardinia, Western Mediterranean. Estuarine, Coastal and Shelf Science 58(2), 299-309. https://doi.org/10.1016/S0272-7714(03)00082-9.

De Falco, S., Tonielli, R., Di Martino, G., Innangi, S., Simeone, S., Parnum, I. M., 2010. Relationships between multibeam backscatter, sediment grain size and *Posidonia oceanica* seagrass distribution. Continental Shelf Research 30(18), 1941-1950. https://doi.org/10.1016/j.csr.2010.09.006.

De'ath, G., Fabricius, K.E., Sweatman, H., Puotinen, M., 2012. The 27–year decline of coral cover on the Great Barrier Reef and its causes. Proceedings of the National Academy of Sciences of the United States of America, 109(44), 17995-17999. https://doi.org/10.1073/pnas.1208909109.

Deptuck, M.E., Piper, D.J., Savoye, B., Gervais, A., 2008. Dimensions and architecture of late Pleistocene submarine lobes off the northern margin of East Corsica. Sedimentology 55(4), 869-898. https://doi.org/10.1111/j.1365-3091.2007.00926.x.

Desprat, S., Sánchez Goñi, M.F., Loutre M.F., 2003. Revealing climatic variability of the last three millennia in northwestern Iberia using pollen influx data. Earth and Planetary Science Letters 213, 67-78. https://doi.org/10.1016/S0012-821X(03)00292-9.

Di Maida, G., Tomasello, A., Luzzu, F., Scannavino, A., Pirrotta, M., Orestano, C., Calvo, S., 2011. Discriminating between *Posidonia oceanica* meadows and sand substratum using multibeam sonar. ICES Journal of Marine Science 68(1), 12-19. https://doi.org/10.1093/icesjms/fsq130.

Di Maida, G., Tomasello, A., Sciandra, M., Pirrotta, M., Milazzo, M., Calvo, S., 2013. Effect of different substrata on rhizome growth, leaf biometry and shoot density of *Posidonia oceanica*. Marine Environmental Research 87-88, 96-102. https://doi.org/10.1016/j.marenvres.2013.04.001.

Dlugokencky, E., Tans, P.P., 2013. Globally averaged marine surface annual mean data, NOAA/ESRL. Accès le 28/08/2020, www.esrl.noaa.gov/gmd/ccgg/trends/.

Dodge, R.E., Aller, R.C., Thomson, J., 1974. Coral growth related to resuspension of bottom sediments. Nature 247, 574-576. https://doi.org/10.1038/247574a0.

Drexler, J.Z., 2011. Peat formation processes through the millennia in tidal marshes of the Sacramento-San Joaquin Delta, California, USA. Estuaries and Coasts 34(5), 900-911. https://doi.org/10.1007/s12237-011-9393-7.

Drinia, H., Koskeridou, E., Antonarakou, A., Tzortzaki, E., 2010. Benthic foraminifera associated with the zooxanthellate coral *Cladocora* in the Pleistocene of the Kos Island (Aegean Sea, Greece): Sea level changes and palaeoenvironmental conditions. Bulletin of the Geological Society of

Greece 43(2), 613-619. https://doi.org/10.12681/bgsg.11223.
Duarte, C.M., 1991. Seagrass depth limits. Aquatic Botany 40, 363-377. https://doi.org/10.1016/0304-3770(91)90081-F.
Duarte, C.M., 2017. Reviews and syntheses: hidden forests, the role of vegetated coastal habitats in the ocean carbon budget. Biogeosciences 14, 301-310. https://doi.org/10.5194/bg-14-301-2017.
Duarte, C.M., Cebrian, J., 1996. The fate of marine autotrophic production. Limnology and Oceanography 41(8), 1758-1766. https://doi.org/10.4319/lo.1996.41.8.1758.
Duarte, C.M., Chiscano, C.L., 1999. Seagrass biomass and production: a reassessment. Aquatic Botany 65(1-4), 159-174. https://doi.org/10.1016/S0304-3770(99)00038-8.
Duarte, C.M., Losada, I.J., Hendriks, I.E., Mazarrasa, I., Marbà, N., 2013. The role of coastal plant communities for climate change mitigation and adaptation. Nature Climate Change 3(11), 961-968. https://doi.org/10.1038/nclimate1970.
Duarte, C.M., Marba, N., Gacia, E., Fourqurean, J.W., Beggins, J., Barron, C., Apostolaki, E.T., 2010. Seagrass community metabolism: Assessing the carbon sink capacity of seagrass meadows. Global Biogeochemical Cycles 24(4), GB4032. https://doi.org/10.1029/2010GB003793.
Duarte, C.M., Merino, M., Agawin, N.S.R., Uri, J., Fortes, M.D., Gallegos, M.E., Marbá, N., Hemminga, M., 1998. Root production and belowground seagrass biomass. Marine Ecology Progress Series 171, 97-108. https://doi.org/10.3354/meps171097.
Duarte, C.M., Middelburg, J.J., Caraco, N., 2005. Major role of marine vegetation on the oceanic carbon cycle. Biogeosciences 2, 1-8. https://doi.org/10.5194/bg-2-1-2005.
Dupouy, M., 2011. Cartographie morpho-sédimentaire à l'embouchure du Golo (Est-Corse). Rapport École Ingénieur, Institut Polytechnique La Salle Beauvais, Brest.
Dupouy, M., 2011. Cartographie morpho-sédimentaire à l'embouchure du Golo (Est-Corse). Rapport École Ingénieur, Institut Polytechnique La Salle Beauvais, Brest, France.
Duschesne, M.J., Bellefleur, G., 2007. Processing of single-channel, high-resolution seismic data collected in the St. Lawrence estuary, Quebec. Technical Report, Geological Survey of Canada, Current Research 2007-D1. https://doi.org/10.4095/223483.
El Zrelli, R., Courjault-Radé, P., Rabaoui, L., Daghbouj, N., Mansour, L., Balti, R., Castet, S., Faouzi, A., Michel, S., Bejaoui, N., 2017. Biomonitoring of coastal pollution in the Gulf of Gabes (SE, Tunisia): use of *Posidonia oceanica* seagrass as a bioindicator and its mat as an archive of coastal metallic contamination. Environmental Science and Pollution Research, 24(28), 22214-22225. https://doi.org/10.1007/s11356-017-9856-x.
Elefteriou, A., McIntyre, A., (Ed.) 2005. Methods for the study of marine benthos. 3rd Edition. Blackwell Science Ltd., Oxford, UK, pp. 1-418.
Enríquez, S., Duarte, C.M., Sand-Jensen, K., 1993. Patterns in decomposition rates among photosynthetic organisms: The importance of detritus C:N:P content. Oecologia 94, 457-471. https://doi.org/10.1007/BF00566960.
Erftemeijer, P.L.A., Koch, E.W., 2001. Sediment geology methods for seagrass habitat, *In:* Short, F.T., Coles, R.G. (Eds.), Global Seagrass Research Methods. Elsevier Science, pp. 345-367. https://doi.org/10.1016/B978-0-444-50891-1.X5000-2.
ESRI, 2011. Environmental Systems Research Institute, ArcGIS Release 10.0. Redlands, CA, USA.
Falkowski, P.G., Katz, M.E., Knoll, A. H. Quigg, A., Raven, J.A. Schofield, O., Taylor, F.J.R., 2004. The evolution of modern eukaryotic phytoplankton. Science 305(5682), 354-360. https://doi.org/10.1126/science.1095964.
Ferranti, L., Antonioli, F., Mauz, B., Amorosi, A., Dai Pra, G., Mastronuzzi, G., Monaco, C., Orrù, P.E., Pappalardo, M., Radtke, U., Renda, P., Romano, P., Sansò, P., Verrubbi, V., 2006. Markers of the last interglacial sea-level high stand along the coast of Italy: tectonic implications. Quaternary International 145, 30-54. https://doi.org/10.1016/j.quaint.2005.07.009.
Ferrat, L., Bingert, A., Romeo, M., Gnassia-Barelli, M., Pergent-Martini, C., 2002. Mercury uptake and enzymatic response of *Posidonia oceanica* after an experimental exposure to organic and inorganic forms. Environmental Toxicology and Chemistry 21(11), 2365-2371.

https://doi.org/10.1126/science.1095964.

Ferrier-Pagès, C., Witting, J., Tambutté, E., Sebens, K., 2003. Effect of natural zooplankton feeding on the tissue and skeletal growth of the scleractinian coral *Stylophora pistillata*. Coral Reefs 22, 229-240. https://doi.org/10.1007/s00338-003-0312-7.

Fischer, H., Behrens, M., Bock, M., Richter, U., Schmitt, J., Loulergue, L., Chappellaz, J., Spahni, R., Blunier, T., Leuenberger, M., Stocker, T.F., 2008. Changing boreal methane sources and constant biomass burning during the last termination. Nature, 452, 864-867. https://doi.org/10.1038/nature06825.

Fonseca, M.S., Bell, S.S., 1998. Influence of physical setting on seagrass landscapes near Beaufort, North Carolina, USA. Marine Ecology Progress Series 171, 109-121.

Fornos, J.J., Ahr, W.M., 1997. Temperate carbonates on a modern, low-energy, isolated ramp: the Balearic Platform, Spain. Journal of Sedimentary Research 67(2), 364-373. https://doi.org/10.1306/D4268572-2B26-11D7-8648000102C1865D.

Fornós, J.J., Baron, A., Pons G.X., 1996. Arrecifes de corales hermatípicos (*Cladocora caespitosa*) en el relleno holoceno de la zona de Es Grau (Menorca, Mediterraneo Occidental). Geogaceta 20(2), 303-306.

Forster, P. *et al*., 2007. Changes in Atmospheric Constituents and in Radiative Forcing. *In:* IPCC, 2007. Climate Change 2007: The Physical Science Basis. Contribution of Working Group I to the Third Assessment Report of the Intergovernmental Panel on Climate Change, Solomon, S., Qin, D., Manning, M., Chen, Z., Marquis, M., Averyt, K.B., Tignor, M., Miller, H.L. (Eds.), Cambridge University Press, Cambridge, United Kingdom and New York, NY, USA, 129-234.

Fourqurean, J.W., Duarte, C.M., Kennedy, H., Marbà, N., Holmer, M., Mateo, M.Á., Apostolaki, E.T., Kendrick, G.A., Krause-Jensen, D., McGlathery, K.J., Serrano, O., 2012. Seagrass ecosystems as a significant global carbon stock. Nature Geoscience 5, 505-509. https://doi.org/10.1038/ngeo1477.

Frankignoulle, M., Canon, C., Gattuso, J.P., 1994. Marine calcification as a source of carbon dioxide: positive feedback of increasing atmospheric CO_2. Limnology and Oceanography 39(2), 458-462. https://doi.org/10.4319/lo.1994.39.2.0458.

Frost, H., 1969. The mortar wreck in Mellieha Bay. Gollcher Foundation, National museum of Malta.

Fumagalli, E., Bibuli, M., Caccia, M., Zereik, E., Del Bianco, F., Gasperini, L., Stanghellini, G., Bruzzone, G., 2014. Combined acoustic and video characterization of coastal environment by means of unmanned surface vehicles. IFAC Proceedings Volumes 47(3), 4240-4245. https://doi.org/10.3182/20140824-6-ZA-1003.02290.

Gacia, E., Duarte, C., 2001. Sediment retention by a Mediterranean *Posidonia oceanica* meadow: the balance between deposition and resuspension. Estuarine, Coastal and Shelf Science 52, 505-514. https://doi.org/10.1006/ecss.2000.0753.

Gacia, E., Duarte, C.M., Middelburg, J.J., 2002. Carbon and nutrient deposition in a Mediterranean seagrass (*Posidonia oceanica*) meadows. Limnology and Oceanography 47, 23-32. https://doi.org/doi:10.4319/lo.2002.47.1.0023.

Gaillot, S., Chavarot S., 2001. Méthode d'étude des littoraux à faible évolution. Cas du delta du Golo (Corse) et du littoral du Touquet (Pas-de-Calais) en France. Géomorphologie : relief, processus, environnement 1, 47-54. https://doi.org/10.3406/morfo.2001.1086.

Galonnier, C., 2020. Optimisation des outils de cartographie sous-marine pour estimer/évaluer les impacts des aménagements littoraux (Haute-Corse). Mémoire Master 2, Université de La Rochelle, pp. 1-69.

Garlan, 2004. Apports de la modélisation dans l'étude de la sédimentation marine récente. Mémoire d'Habilitation à Diriger des Recherches, Université de Lille, France, 1-190. https://doi.org/10.13140/RG.2.2.16289.81768.

Gattuso, J.P., Frankignoulle, M., Wollast, R., 1998. Carbon and carbonate metabolism in coastal aquatic ecosystems. Annual Review of Ecology and Systematics 29(1), 405-434. https://doi.org/10.1146/annurev.ecolsys.29.1.405.

Gauthier, A., 1981. Contribution à l'étude du débit solide et genèse des sédiments au cours de celui-

ci : Exemple du Fium'Orbo, fleuve de la Corse Orientale. Rapport BRGM 30, 163-172.

Gedan, K.B., Silliman, B., Bertness, M., 2009. Centuries of human-driven change in salt marsh ecosystems. Marine Science 1, 117-141. https://doi.org/10.1146/annurev.marine.010908.163930.

Gervais, A., 2002. Analyse multi-échelles de la morphologie, de la géométrie et de l'architecture d'un système turbiditique sableux profond (Système du Golo, Marge est-Corse, Mer Méditerranée) : implications pour la reconnaissance des processus de transport et de dépôt des sédiments et pour la construction des lobes sableux en domaine profond. Thèse de doctorat, Université de Bordeaux I, pp. 1-285.

Gervais, A., Mulder, T., Savoye, B., Gonthier, E., 2006. Sediment distribution and evolution of sedimentary processes in a small sandy turbidite system (Golo system, Mediterranean Sea): implications for various geometries based on core framework. Geo-Marine Letters 26(6), 373-395. https://doi.org/10.1007/s00367-006-0045-z.

Gervais, A., Savoye, B., Piper, D.J.W., Mulder, T., Cremer M., Pichevin L., 2004. Present morphology and depositional architecture of a sandy confined submarine system: the Golo turbidite system (eastern margin of Corsica). Geological Society, London, Special Publications 222(1), 59-89. https://doi.org/10.1144/GSL.SP.2004.222.01.05.

Gilfillan, D., Marland, G., Boden, T., Andres, R., 2019. Global, Regional, and National Fossil-Fuel CO_2 Emissions. Carbon Dioxide Information Analysis Center at Appalachian State University, Boone North Carolina. Available at: https://energy.appstate.edu/research/work-areas/cdiac-appstate, last access: 27 September 2019.

Gilman, E., 2002. Guidelines for coastal and marine site-planning and examples of planning and management intervention tools. Ocean & Coastal Management 45, 377-404. https://doi.org/10.1016/S0964-5691(02)00076-5.

Giraud, G., 1979. Sur une méthode de mesure et de comptage des structures foliaires de *Posidonia oceanica* (L.) Delile. Bulletin du Musée d'Histoire Naturelle, Marseille, 39, 33-39.

Gissi, E., Manea, E., Mazaris, A.D., Fraschetti, S., Almpanidou, V., Bevilacqua, S., Coll, M., Guarnieri, G., Lloret-Lloret, E., Pascual, M., Petza, D., Rilov, G., Schonwald, M., Stelzenmüller, V., Katsanevakis, S., 2020. A review of the combined effects of climate change and other local human stressors on the marine environment. Science of The Total Environment 755(1), 142564. https://doi.org/10.1016/j.scitotenv.2020.142564.

Glew, J.R., Smol, J.P., Last, W.M., 2001. Sediment core collection and extrusion. In: Last, W.M., Smol, J.P. (Eds.), Tracking environmental change using lake sediments. Kluwer Academic Publishers, Dordrecht, 73-105. https://doi.org/10.1007/0-306-47669-X_5.

Gobert, S., Pasqualini, V., Dijoux, J., Lejeune, P., Durieux, E., Marengo, M., 2017. Trace element concentrations in the apex predator swordfish (Xiphias gladius) from a Mediterranean fishery and risk assessment for consumers. Mar. Pollut. Bull. 120, 364-369. https://doi.org/10.1016/j.marpolbul.2017.05.029.

Godet, L., Fournier, J., Toupoint, N., Olivier, F., 2009. Mapping and monitoring intertidal benthic habitats: a review of techniques and a proposal for a new visual methodology for the European coasts. Progress in Physical Geography 33(3), 378-402. https://doi.org/10.1177/0309133309342650.

González, J.M., Fernandez-Gomez, B., Fendandez-Guerra, A., Gomez-Consarnau, L., Sanchez, O., Coll-Llado, M., Del Campo, J., Escudero, L., Rodriguez-Martinez, R., Alonso-Saez, L., Latasa, M., Paulsen, I., Nedashkovskyaya, O., Lekunberri, I., Pinhassi, J., Pedros-Alio, C., 2008. Genome analysis of the proteorhodopsin-containing marine bacterium *Polaribacter* sp. MED152 (Flavobacteria). Proceedings of the National Academy of Science of the United States of America 105(25), 8724-8729. https://doi.org/10.1073/pnas.0712027105.

Gorgas, T.J., Wilkens, R.H., Fu, S.S., Frazer, L.N., Richardson, M.D., Briggs, K.B., Lee, H., 2002. In situ acoustic and laboratory ultrasonic sound speed and attenuation measured in heterogeneous soft seabed sediments: Eel River shelf, California. Marine Geology 182(1-2), 103-119. https://doi.org/10.1016/S0025-3227(01)00230-4.

Grant, J.A., Schreiber, R., 1990. Modern swaths sounding and sub-bottom profiling technology for research applications: The Atlas Hydrosweep and Parasound system. Marine Geophysical Researches 12(1-2), 9-19. https://doi.org/10.1007/BF00310559.

Guennoc, P., Palvadeau, E., Pluquet, F., Morando, A., Vairon, J., 2001. LIMA, cartographie des plates-formes sous-marines de la Corse entre 0 et 100m de profondeur. Rapport BRGM, RP-51523-FR, pp. 1-53.

Gullström, M., Lyimo, L.D., Dahl, M., Samuelsson, G.S., Eggertsen, M., Anderberg, E., Rasmusson, L.M., Linderholm, H.W., Knudby, A., Bandeira, S., Nordlud, L.M., Björk, M., 2018. Blue Carbon Storage in Tropical Seagrass Meadows Relates to Carbonate Stock Dynamics, Plant–Sediment Processes, and Landscape Context: Insights from the Western Indian Ocean. Ecosystems 21, 551-566. https://doi.org/10.1007/s10021-017-0170-8.

Hamilton, E.L., 1956. Low sound velocities in high-porosity sediment. The Journal of the Acoustical Society of America 28(16), 16-19. https://doi.org/10.1121/1.1908208.

Hamilton, E.L., 1963. Sediment sound velocity measurements made in situ from bathyscaphe Trieste. Journal of Geophysical Research 68(21), 5991-5998. https://doi.org/10.1029/JZ068i021p05991.

Hamilton, E.L., 1969. Sound velocity, elasticity, and related properties of marine sediments, North Pacific, 3, Prediction of in situ properties. Naval Undersea Research and Development Center. Technical publication, 145.

Hamilton, E.L., 1970. Sound velocity and related properties of marine sediments, North Pacific. Journal of Geophysical Research 75(23), 4423-4446. https://doi.org/10.1029/JB075i023p04423.

Hamilton, E.L., 1971. Elastic properties of marine sediments. Journal of Geophysical Research 76(2), 579-604. https://doi.org/10.1029/JB076i002p00579.

Hamilton, E.L., Bachman, R.T., 1982. Sound velocity and related properties of marine sediments. The Journal of the Acoustical Society of America 72(6), 1891-1904. https://doi.org/10.1121/1.388539.

Hamilton, E.L., Shumway, G., Menard, H.W., Shipek, C.J., 1956. Acoustic and other physical properties of shallow-water sediments off San Diego. The Journal of the Acoustical Society of America 28(1), 1-15. https://doi.org/10.1121/1.1908210.

Hamilton, L.J., Parnum, I., 2011. Acoustic seabed segmentation from direct statistical clustering of entire multibeam sonar backscatter curves, Continental Shelf Research 31(2), 138-148. https://doi.org/10.1016/j.csr.2010.12.002.

Hamilton, M.F., Blackstock, D.T., 1998. Nonlinear Acoustics: Theory and Applications. Academic Press, San Diego, California.

Hamilton, S.E., Casey, D., 2016. Creation of a high spatio-temporal resolution global database of continuous mangrove forest cover for the 21st century (CGMFC-21). Gobal Ecology and Biogepgraphy 25(6), 729-738. https://doi.org/10.1111/geb.12449.

Haoliang, L., Chongling, Y., Jingchun, L., 2007. Low-molecular-weight organic acids exuded by Mangrove (*Kandelia candel* (L.) Druce) roots and their effect on cadmium species change in the rhizosphere. Environmental and Experimental Botany 61(2), 159-166. https://doi.org/10.1016/j.envexpbot.2007.05.007.

Harmelin, J.G., 1964. Etude de l'endofaune des "mattes" d'herbiers de *Posidonia oceanica* Delile. Recueil des Travaux de la Station Marine d'Endoume 35, 43-105.

Harrison, P.G., 1989. Detrital processing in seagrass systems: A review of factors affecting decay rates, remineralization and detritivory. Aquatic Botany 35, 263-288. https://doi.org/10.1016/0304-3770(89)90002-8.

Hedges, J.I., Keil, R.G., 1995. Sedimentary organic-matter preservation: an assessment and speculative synthesis. Marine Chemistry 49, 81-115. https://doi.org/10.1016/0304-4203(95)00008-F.

Heiri, O., Lotter, A.F., Lemcke, G., 2001. Loss on ignition as a method for estimating organic and carbonate content in sediments: Reproducibility and comparability of results. Journal of Paleolimnology 25, 101-110. https://doi.org/10.1023/A:1008119611481.

Hemminga, M.A., Duarte, C.M., 2000. Seagrass ecology. Cambridge University Press, pp. 1-298 pp.

https://doi.org/10.1017/CBO9780511525551.
Hemminga, M.A., Mateo, M.A., 1996. Stable carbon isotopes in seagrasses: variability in ratios and use in ecological studies. Marine Ecology Progress Series, 140, 285-298. https://doi.org/10.3354/meps140285.
Hendriks, I.E., Bouma, T.J., Morris E.P., Duarte C.M., 2010. Effects of seagrasses and algae of the *Caulerpa* family on hydrodynamics and particle-trapping rates. Marine Biology 157, 473-481. https://doi.org/10.1007/s00227-009-1333-8.
Hendriks, I.E., Sintes, T., Bouma, T.J., Duarte. C.M., 2008. Experimental assessment and modeling evaluation of the effects of the seagrass *Posidonia oceanica* on flow and particle trapping. Marine Ecology Progress Series 356, 163-173. https://doi.org/10.3354/meps07316.
Henrichs, S.M., 1992. Early diagenesis of organic matter in marine sediments: progress and perplexity. Marine Chemistry 39, 119-149. https://doi.org/10.1016/0304-4203(92)90098-U.
Herr, D., Von Unger, M., Laffoley, D., Mcgivern, A., 2017. Pathways for implementation of blue carbon initiatives. Aquatic Conservation: Marine and Freshwater Ecosystems 27(51), 116-129. http://dx.doi.org/10.1002/aqc.2793.
Hicks, S.R., Kibblewhite, A.C., 1976. Seismic reflection profiling in very shallow waters in the upper Waitemata Harbour, New Zealand. New Zealand Journal of Geology and Geophysics 19(2), 213-231. https://doi.org/10.1080/00288306.1976.10423518.
Hogarth, P., 1999. The Biology of Mangroves. Oxford University Press, Oxford, UK, pp. 1-228.
Holon, F., Mouquet, N., Boissery, P., Bouchoucha, M., Delaruelle, G., Tribot, A.S., Deter, J., 2015. Fine-scale cartography of human impacts along French Mediterranean coasts: a relevant map for the management of marine ecosystems. PLoS One 10(8), e0135473. https://doi.org/10.1371/journal.pone.0135473.
Hopkinson, C., Chasmer, L., Lim, K., Treitz, P., Creed, I., 2006. Towards a universal lidar canopy height indicator. Canadian Journal of Remote Sensing 32(2), 139-152. https://doi.org/10.5589/m06-006.
Hopkinson, C., Chasmer, L.E., Sass, G., Creed, I., Sitar, M., Kalbfleisch, W., Treitz, P., 2005. Vegetation class dependent errors in lidar ground elevation and canopy height estimates in a boreal wetland environment. Canadian Journal of Remote Sensing 31(2), 191-206. https://doi.org/10.5589/m05-007.
Horn, B.K.P., 1981. Hill shading and the reflectance map. Proceedings of the IEEE 69(1), 14-47. https://doi.org/10.1109/PROC.1981.11918.
Horn, D.R., Horn, B.M., Delach, M.N., 1968. Correlation between acoustical and other physical properties of deep-sea cores. Journal of Geophysical Research 73(6), 1939-1957. https://doi.org/10.1029/JB073i006p01939.
Houghton, R.A., 2007. Balancing the global carbon budget. Annual Review of Earth and Planetary Sciences 35, 313-347. https://doi.org/10.1146/annurev.earth.35.031306.140057.
Howard, J.L., Creed, J.C., Aguiar, M.V.P., Fourqurean J.W., 2014b. CO_2 released by carbonate sediment production in some coastal areas may offset the benefits of seagrass “Blue Carbon” storage. Limnology and Oceanography 63(1), 160-172. https://doi.org/10.1002/lno.10621.
Howard, J., Hoyt, S., Isensee, K., Telszewski, M., Pidgeon, E., 2014a. Coastal Blue Carbon: Methods for assessing carbon stocks and emissions factors in mangroves, tidal salt marshes, and seagrasses. CIOC-UNESCO, IUCN, Arlington, Virginia, USA., pp. 1-180.
Howard, J., Sutton-Grier, A., Herr, D., Kleypas, J., Landis, E., Mcleod, E., Pidgeon, E., Simpson, S., 2017. Clarifying the role of coastal and marine systems in climate mitigation. Frontiers in Ecology and the Environment 15(1), 42-50. https://doi.org/10.1002/fee.1451.
Hribljan, J.A., Suárez, E., Heckman, K.A., Lilleskov, E.A., Chimner R.A., 2016. Peatland carbon stocks and accumulation rates in the Ecuadorian páramo. Wetlands Ecology and Management 24, 113-127. https://doi.org/10.1007/s11273-016-9482-2.
Ierodiaconou, D., Monk, J., Rattray, A., Laurenson, L., Versace, V.L., 2011. Comparison of automated classification techniques for predicting benthic biological communities using hydroacoustics and video observations. Continental Shelf Research 31(2), 28-38.

https://doi.org/10.1016/j.csr.2010.01.012.

Ingrosso, G., Abbiati, M., Badalamenti, F., Bavestrello, G., Belmonte, G., Cannas, R., Benedetti-Cecchi, L., Bertolino, M., Bevilacqua, S., Bianchi, C.N., Bo, M., Boscari, E., Cardone, F., Cattaneo-Vietti, R., Cau, A., Cerrano, C., Chemello, R., Chimienti, G., Congiu, L., Corriero, G., Costantini, F., De Leo, F., Donnarumma, L., Falace, A., Fraschetti, S., Giangrande, A., Gravina, M.F., Guarnieri, G., Mastrototaro, F., Milazzo, M., Morri, C., Musco, L., Pezzolesi, L., Piraino, S., Prada, F., Ponti, M., Rindi, F., Russo, G.F., Sandulli, R., Villamor, A., Zane, L., Boero F., 2018. Mediterranean bioconstructions along the Italian coast. Advances in Marine Biology, 79, 61-136. https://doi.org/10.1016/bs.amb.2018.05.001.

IPCC, 2001. Climate Change 2001: The Scientific Basis. Contribution of Working Group I to the Third Assessment Report of the Intergovernmental Panel on Climate Change. Cambridge, UK, and New York, NY, USA, pp. 1-881.

IPCC, 2013. Climate Change 2013: The Physical Science Basis. Contribution of Working Group I to the Fifth Assessment Report of the Intergovernmental Panel on Climate Change. Stocker, T.F., Qin D., Plattner, G.K., Tignor, M., Allen, S.K., Boschung, J., Nauels, A., Xia, Y., Bex, V., Midgley, P.M. (Eds.), Cambridge University Press, Cambridge, United Kingdom and New York, NY, USA, pp. 1-1535.

IPCC, 2019. IPCC Special Report on the Ocean and Cryosphere in a Changing Climate. Pörtner, H.O., Roberts, D.C., Masson-Delmotte, V., Zhai, P., Tignor, M., Poloczanska, E., Mintenbeck, K., Alegría, A., Nicolai, M., Okem, A., Petzold, J., Rama, B., Weyer, N.M. (Eds.) (in press), pp. 1-755.

Jenks, G.F., 1967. The Data Model Concept in Statistical Mapping. International Yearbook of Cartography 7, 186-190.

Jeudy de Grissac, A., 1975. Sédimentologie dynamiques des rades d'Hyères et de Giens (Var). Problèmes d'Aménagements. Thèse de doctorat, Université Aix-Marseille II, pp. 1-86.

Jeudy de Grissac, A., Boudouresque, C.F, 1985. Rôles des herbiers de phanérogames marines dans les mouvements des sédiments côtiers : les herbiers *à Posidonia oceanica*. Colloque franco-japonais d'océanographie 1, 143-151.

Jiménez, C., Hadjioannou, L., Petrou, A., Nikolaidis, A., Evriviadou, M., Lange M.A., 2014. Mortality of the scleractinian coral *Cladocora caespitosa* during a warming event in the Levantine Sea (Cyprus). Regional Environmental Change 16, 1963-1973. https://doi.org/10.1007/s10113-014-0729-2.

Johnson, B.J., Moore, K.A., Lehmann, C., Bohlen, C. & Brown, T.A., 2007. Middle to late Holocene fluctuations of C_3 and C_4 vegetation in a Northern New England Salt Marsh, Sprague Marsh, Phippsburg Maine. Organic Geochemistry 38(3), 394-403. https://doi.org/10.1016/j.orggeochem.2006.06.006.

Joos, F., Roth, R., Fuglestvedt, J.S., Peters, G.P., Enting, I.G., von Bloh, W., Brovkin, V., Burke, E.J., Eby, M., Edwards, N.R., Friedrich, T., Frölicher, T.L., Halloran, P.R., Holden, P.B., Jones, C., Kleinen, T., Mackenzie, F.T., Matsumoto, K., Meinshausen, M., Plattner, G.K., Reisinger, A., Segschneider, J., Shaffer, G., Steinacher, M., Strassmann, K., Tanaka, K., Timmermann, A., Weaver, A.J., 2013. Carbon dioxide and climate impulse response functions for the computation of greenhouse gas metrics: A multi-model analysis. Atmospheric Chemistry and Physics 13, 2793-2825. https://doi.org/10.5194/acp-13-2793-2013.

Kaal, J., Serrano, O., José, C., Rencoret, J., 2018. Radically different lignin composition in *Posidonia* species may link to differences in organic carbon sequestration capacity. Organic Geochemistry 124, 247-256. https://doi.org/10.1016/j.orggeochem.2018.07.017.

Kaal, J., Serrano, O., Nierop, K., Schellekens, J., Martínez Cortizas, A. Mateo, M.Á., 2016. Molecular composition of plant parts and sediment organic matter in a Mediterranean seagrass (*Posidonia oceanica*) mat. Aquatic Botany 133, 50-61. https://doi.org/10.1016/j.aquabot.2016.05.009.

Kathiresan, K., Bingham, B.L., 2001. Biology of mangroves and mangrove Ecosystems. Advances in Marine Biology, 40, 81-251. https://doi.org/10.1016/S0065-2881(01)40003-4.

Kauffman, J.B., Heider, C., Norfolk, J. Payton, F., 2014. Carbon stocks of intact mangroves and carbon

emissions arising from their conversion in the Dominican Republic. Ecological Applications 24(3), 518-527. https://doi.org/10.1890/13-0640.1.

Kauffman, J.B., Hernandez Trejo, H., del Carmen Jesus Garcia, M., Heider C., Contreras W.M., 2016. Carbon stocks of mangroves and losses arising from their conversion to cattle pastures in the Pantanos de Centla, Mexico. Wetlands Ecology and Management 24, 203-216. https://doi.org/10.1007/s11273-015-9453-z.

Kearey, P., Brooks, M., Hill, I., 2013. An introduction to geophysical exploration, third edition. Wiley-Blackwell.

Keil, R., Hedges, J., 1993. Sorption of organic matter to mineral surfaces and the preservation of organic matter in coastal marine sediments. Chemical Geology, 107(3-4), 385-388. https://doi.org/10.1016/0009-2541(93)90215-5.

Kennedy, H., Beggins, J., Duarte, C.M., Fourqurean, J.W., Holmer, M., Marbà, N., Middelburg, J.J., 2010. Seagrass sediments as a global carbon sink: isotopic constraints. Global Biogeochemical Cycles 24(4), https://doi.org/10.1029/2010GB003848.

Kennedy, H., Gacia, E., Kennedy, D.P., Papadimitriou, S., Duarte, C.M., 2004. Organic carbon sources to SE Asian coastal sediments. Estuarine, Coastal and Shelf Science 60(1), 59-68. https://doi.org/10.1016/j.ecss.2003.11.019.

Kennedy, V.S., 1984. The estuary as a filter. Academic Press, New York, NY, USA, pp. 1-528. https://doi.org/10.1016/C2013-0-10968-3.

Kenny, A.J., Cato, I., Desprez, M., Fader, G., Schuttenhelm, R.T.E., Side, J., 2003. An overview of seabed-mapping technologies in the context of marine habitat classification. ICES Journal of Marine Science 60, 411-418. https://doi.org/10.1016/S1054-3139(03)00006-7.

Kermabon, A., Gehin, C., Blavier, P., 1969. Numerical Results of the Analysis of Sea-Bottom Cores (Naples and Ajaccio Zones). NATO/SACLANTCEN Technical Report, La Spezia.

Kersting, D.K., Bensoussan, N., Linares, C., 2013. Long-term responses of the endemic reef-builder *Cladocora caespitosa* to Mediterranean warming. PLoS One 8, e70820. https://doi.org/10.1371/journal.pone.0070820.

Kersting, D.K., Cebrián, E., Verdura, J., Ballesteros, E., 2017. A new *Cladocora caespitosa* population with unique ecological traits. Mediterranean Marine Science 18(1), 38-42. https://doi.org/10.12681/mms.1955.

Kersting, D.K., Linares, C., 2012. *Cladocora caespitosa* bioconstructions in the Columbretes Islands Marine Reserve (Spain, NW Mediterranean): distribution, size structure and growth. Marine Ecology 33, 427-436. https://doi.org/10.1111/j.1439-0485.2011.00508.x.

Kim, D.C., Kim, G.Y., Jung, J.H., Seo, Y.K., Wilkens, R.H., Yoo, D.G., Lee, G.H., Kim, J.C., Yi, H.I., Cifci, G., 2008. Laboratory/in situ sound velocities of shelf sediments in the South Sea of Korea. Fisheries and Aquatic Sciences 11(2), 103-112. https://doi.org/10.5657/FAS.2008.11.2.103.

Kim, D.C., Sung, J.Y., Park, S.C., Lee, G.H., Choi, J.H., Kim, G.Y., Seo, Y.K., Kim, J.C., 2001. Physical and acoustic properties of shelf sediments, the South Sea of Korea. Marine Geology 179(1), 39-50. https://doi.org/10.1016/S0025-3227(01)00200-6.

King, S.E., Lester, J.N., 1995. The value of salt marsh as a sea defence. Marine Pollution Bulletin 30(3), 180-189. https://doi.org/10.1016/0025-326X(94)00173-7.

Klap, V.A., Hemminga, M.A., Boon, J.J., 2000. Retention of lignin in seagrasses: angiosperms that returned to the sea. Marine Ecology Progress Series 194, 1-11. https://doi.org/10.3354/meps194001.

Klimenko, V.V., Klimanov, V.A., 2003. Cold Climate of the Early Subatlantic Age in the Northern Hemisphere. Doklady Earth Sciences 391(6), 845-849.

Komatsu, T., Igarashi, C., Tatsukawa, K., Sultana, S., Matsuoka, Y., Harada, S., 2003. Use of multi-beam sonar to map seagrass beds in Otsuchi Bay on the Sanriku Coast of Japan. Aquatic Living Resources 16(3), 223-230. https://doi.org/10.1016/S0990-7440(03)00045-7.

Krauss, K.W., Noe, G.B., Duberstein, J.A., Conner, W.H., Stagg, C.L., Cormier, N. Jones, M.C., Bernhardt, C.E., Lockaby, B.G., From, A.S., Doyle, T.W., Day, R.H., Ensign, S.H., Pierfelice, K.N., Hupp, C.R., Chow, A.T., Whitbeck, J.L., 2018. The role of the upper tidal estuary in wetland blue carbon

storage and flux. Global Biogeochemical Cycles 32, 817-839. https://doi.org/10.1029/2018GB005897.

Kružić, P., Benković, L., 2008. Bioconstructional features of the coral *Cladocora caespitosa* (Anthozoa, Scleractinia) in the Adriatic Sea (Croatia). Marine Ecology 29, 125-139. https://doi.org/10.1111/j.1439-0485.2008.00220.x.

Kružić, P., Požar-Domac, A., 2002. Skeleton growth rates of coral bank of *Cladocora caespitosa* (Anthozoa, Scleractinia) in lake Veliko jezero (Mljet National Park). Periodicum Biologorum 104(2), 123-129.

Kružić, P., Požar-Domac, A., 2003. Banks of the coral *Cladocora caespitosa* (Anthozoa, Scleractinia) in the Adriatic Sea. Coral Reefs 22(4), 536. https://doi.org/10.1007/s00338-003-0345-y.

Kühlmann, D.H.H., 1996. Preliminary report on Holocene submarine accumulations of *Cladocora caespitosa* (L., 1767) in the Mediterranean. Göttinger Arbeit Geologie Paläontologie 2, 65-69.

Laborel, J., 1961. Sur un cas particulier de concrétionnement animal. Concrétionnement à *Cladocora caespitosa* (L.) dans le Golfe de Talante. Rapports et Procès-verbaux du Conseil Internationale pour l'Exploration de la Mer 16(2), 429-432.

Laborel, J., 1987. Marine biogenic constructions in the Mediterranean: a review. Scientific Reports of the Port-Cros National Park, 13, 97-126.

Laborel, J., Laborel-Deguen, F., 1978. Abondance du madréporaire *Cladocora caespitosa* (Linné 1767) dans les herbiers de posidonies de la baie de Port-Cros. Travaux scientifiques du Parc national de Port-Cros 4, 273-274.

Lafabrie, C., Pergent, G., Pergent-Martini, C., Capiomont, A., 2007. *Posidonia oceanica*: a tracer of past mercury contamination. Environmental Pollution 148, 688-692. https://doi.org/10.1016/j.envpol.2006.11.015.

Laffoley, D., Grimsditch, G., 2009. The Management of Natural Coastal Carbon Sinks. IUCN, Gland, Switzerland.

Lam, K., Shin, P.K.S., Bradbeer, R., Randall, D., Ku, K.K.K., Hodgson, P., Cheung, S.G., 2006. A comparison of video and point intercept transect methods for monitoring subtropical coral communities. Journal of Experimental Marine Biology and Ecology 333, 115-128. https://doi.org/10.1016/j.jembe.2005.12.009.

Lamb, H.H., 1965. The early Medieval Warm Epoch and its sequel. Palaeogeography, Palaeoclimatology, Palaeoecology 1, 13-37. https://doi.org/10.1016/0031-0182(65)90004-0.

Lambeck, K., Purcell, A., 2005. Sea-level change in the Mediterranean Sea since the LGM: model predictions for tectonically stable areas. Quaternary Science Reviews 24(18-19), 1969-1988. https://doi.org/10.1016/j.quascirev.2004.06.025.

Laursen, A.K., Mayer, L., Townsend, D., 1996. Lability of proteinaceous material in estuarine seston and subcellular fractions of phytoplankton. Marine Ecology Progress Series 136, 227-234. https://doi.org/10.3354/meps136227.

Lavery, P.S., Mateo, M.Á., Serrano, O., Rozaimi, M., 2013. Variability in the carbon storage of seagrass habitats and its implications for global estimates of blue carbon ecosystem service. PLoS ONE 8, e73748. https://doi.org/10.1371/journal.pone.0073748.

Lecca, L., De Muro, S., Cossellu, M., Pau, M., 2005. Modern terrigenous-carbonate sediments of the continental shelf of the Gulf of Cagliari. Italian Journal of Quaternary Science, 18(2), 201-221.

Lefebvre, A., Thompson, C.E.L., Collins, K.J., Amos, C.L., 2009. Use of a high-resolution profiling sonar and a towed video camera to map a *Zostera marina* bed, Solent, UK. Estuarine, Coastal and Shelf Science 82(2), 323-334. https://doi.org/10.1016/j.ecss.2009.01.027.

Leighton, T.G., Robb, G.B.N., 2008. Preliminary mapping of void fractions and sound speeds in gassy marine sediments from subbottom profiles. The Journal of the Acoustical Society of America 124(5), 313-320. https://doi.org/10.1121/1.2993744.

Leiva-Dueñas, C., López-Merino, L., Serrano, O., Martínez Cortizas, A., Mateo, M.Á., 2018. Millennial-scale trends and controls in *Posidonia oceanica* (L. Delile) ecosystem productivity. Global and Planetary Change 169, 92-104. https://doi.org/10.1016/j.gloplacha.2018.07.011.

Lepoint, G., Nyssen, F., Gobert, S., Dauby, P., Bouquegneau, J.M., 2000. Relative impact of a seagrass

bed and its adjacent epilithic algal community in consumer diets. Marine Biology 136, 513-518. https://doi.org/10.1007/s002270050711.

Leriche, A., Pasqualini, V., Boudouresque, C.F., Bernard, G., Bonhomme, P., Clabaut, P., Denis, J., 2006. Spatial, temporal and structural variations of a *Posidonia oceanica* seagrass meadow facing human activities. Aquatic Botany 84, 287-293. https://doi.org/10.1016/j.aquabot.2005.10.001.

Lipkin, Y. 1979 Quantitative aspects of seagrass communities, particularly of those dominated by *Halophila stipulacea*, in Sinai (Northern Red Sea). Aquatic Botany 7, 119-128. https://doi.org/10.1016/0304-3770(79)90016-0.

Lirman, D., Gracias, N.R., Gintert, B.E., Gleason, A.C.R., Reid, R.P., Negahdaripour, S., Kramer, P., 2007. Development and application of a video-mosaic survey technology to document the status of coral reef communities. Environmental Monitoring and Assessment, 125(1-3), 59-73. https://doi.org/10.1007/s10661-006-9239-0.

Ljungqvist, F.C., 2010. A new reconstruction of temperature variability in the extra-tropical Northern Hemisphere during the last two millennia. Geografiska Annaler: Series A, Physical Geography 92(3), 339-351.

Lo Iacono, C., Mateo, M.Á., Gràcia, E., Guasch, L., Carbonell, R., Serrano, L., Serrano, O., Danõbeitia, J., 2008. Very high-resolution seismo-acoustic imaging of seagrass meadows (Mediterranean Sea): Implications for carbon sink estimates. Geophysical Research Letters 35(18), 1-5. https://doi.org/10.1029/2008GL034773.

Lopez y Royo, C., Pergent, G., Pergent-Martini, C., Casazza, G., 2010. Seagrass (*Posidonia oceanica*) monitoring in western Mediterranean: implications for management and conservation. Environmental Monitoring and Assessment 171, 365-380. https://doi.org/10.1007/s10661-009-1284-z.

López-Merino, L., Colás-Ruiz, N.R., Adame, M.F., Serrano, O., Martínez Cortizas, A., Mateo, M.Á., 2017. A six thousand-year record of climate and land-use change from Mediterranean seagrass mats. Journal of Ecology 105(5), 1267-1278. https://doi.org/10.1111/1365-2745.12741.

López-Merino, L., Serrano, O., Adame, M., Mateo M., Martínez Cortizas, A., 2015. Glomalin accumulated in seagrass sediments reveals past alterations in soil quality due to land-use change. Global and Planetary Change 133, 87-95. https://doi.org/10.1016/j.gloplacha.2015.08.004.

López-Sáez, J.A., López-Merino, L., Mateo, M.Á., Serrano, O., Pérez-Díaz, S., Serrano, L., 2009. Palaeoecological potential of the marine organic deposits of *Posidonia oceanica*: A case study in the NE Iberian Peninsula. Palaeogeography, Palaeoclimatology, Palaeoecology 271(3-4), 215-224. https://doi.org/10.1016/j.palaeo.2008.10.020.

Lovelock, C.E., Reef, R., 2020. Variable Impacts of Climate Change on Blue Carbon. One Earth 3(2), 195-211. https://doi.org/10.1016/j.oneear.2020.07.010.

Ludvigsen, M., Johnsen, G., Sørensen, A.J., Lågstad, P.A., Ødegård, Ø., 2014. Scientific operations combining ROV and AUV in the Trondheim Fjord. Marine Technology Society Journal 48(2), 59-71. https://doi.org/10.4031/MTSJ.48.2.3.

Ludvigsen, M., Sortland, B., Johnsen, G., Singh, H., 2007. Applications of georeferenced underwater photo mosaics in marine biology and archaeology. Oceanography 20(4), 140-149. https://doi.org/10.5670/oceanog.2007.14.

Lüthi, D., Le Floch, M., Bereiter, B., Blunier, T., Barnola, J.M., Siegenthaler, U., Raynaud, D., Jouzel, J., Fischer, H., Kawamura, K., Stocker, T.F., 2008: High-resolution carbon dioxide concentration record 650,000–800,000 years before present. Nature, 453, 379-382. https://doi.org/10.1038/nature06949.

Macreadie, P.I., Anton, A., Raven, J.A., Beaumont, N., Connolly, R.M., Friess, D.A., Kelleway, J.J., Kennedy, H., Kuwae, T., Lavery, P.S., Lovelock, C.E., Smale, D.A., Apostolaki, E.T., Atwood, T.B., Baldock, J., Bianchi, T.S., Chmura, G.L., Eyre, B.D., Fourqurean, J.W., Hall-Spencer, J.M., Huxham, M., Hendriks, I.E., Krause-Jensen, D., Laffoley, D., Luisetti T., Marbà, N., Masque, P., McGlathery, K.J., Megonigal, J.P., Murdiyarso, D., Russell, B.D., Santos, R., Serrano, O., Silliman,

B.R., Watanabe K., Duarte, C.M., 2019. The future of Blue Carbon science. Nature Communications 10, 3998. https://doi.org/10.1038/s41467-019-11693-w.

Macreadie, P.I., Baird, M.E., Trevathan-Tackett, S.M., Larkum, A.W.D., Ralph, P.J., 2014. Quantifying and modelling the carbon sequestration capacity of seagrass meadows – A critical assessment. Marine Pollution Bulletin 83(2), 430-439. https://doi.org/10.1016/j.marpolbul.2013.07.038.

Macreadie, P.I., Serrano, O., Maher, D.T., Duarte, C.M., Beardall, J., 2017. Addressing calcium carbonate cycling in blue carbon accounting. Limnology and Oceanography Letters 2(6), 195-201.

Macreadie, P.I., Serrano, O., Maher, D.T., Duarte, C.M., Beardall, J., 2017. Addressing calcium carbonate cycling in blue carbon accounting. Limnology and Oceanography Letters 2(6), 195-201. https://doi.org/10.1002/lol2.10052.

Maggi, P., Gruet, Y., Lassus, P., 1997. Influence de la pollution urbaine sus la vitalité des herbiers de Posidonies dans le golfe de Giens. Science et Pêche, Bulletin de l'Institute des Pêches Maritimes 269, 5-13.

Magny, M., Combourieu-Nebout, N., de Beaulieu, J.L., Bout-Roumazeilles, V., Colombaroli, D., Desprat, S., Francke, A., Joannin, D., Ortu, E., Peyron, O., Revel, M., Sadori, L., Siani, G., Sicre, M.A., Sanmartin, S., Simonneau, A., Tinner, W., Vannière, B., Wagner, B., Zanchetta, G., Anselmetti, F., Brugiapaglia, E., Chapron, E., Debret, M., Didier, J., Essallami, L., Galop, D., Gilli, A., Haas, J.N., Kallel, N., Millet, L., Stock, A., Turon, J.L., Wirth, S., 2013. North-south palaohydrological contrasts in the central Mediterranean during the Holocene: tentative synthesis and working hypothesis. Climate of the Past 9, 2043-2071. https://doi.org/10.5194/cpd-9-1901-2013.

Malik, M., 2019. Sources and impacts of bottom slope uncertainty on estimation of seafloor backscatter from swath sonars. Geosciences 9(4), 183. https://doi.org/10.3390/geosciences9040183.

Mapping European Seabed Habitats (MESH), 2008. The MESH Blue Book. The Joint Nature Conservation Committee, Peterborough, UK, pp. 1-23.

Marbá, N., Duarte, C.M., Cebrián, J., Gallegos, M.E., Olesen, B., Sand-Jensen, K., 1996. Growth and population dynamics of *Posidonia oceanica* on the Spanish Mediterranean coast: elucidating seagrass decline. Marine Ecology Progress Series 137, 203-213. https://doi.org/10.3354/meps137203.

Marengo, M., 2011. Contribution des sédiments biogènes au stock sédimentaire dans la zone littoral autour Cap Corse (Méditerranée, France). Mémoire Master 2, Université de Corse, pp. 1-25.

Marengo, M., Durieux, E.D., Ternengo, S., Lejeune, P., Degrange, E., Pasqualini, V., Gobert, S., 2018. Comparison of elemental composition in two wild and cultured marine fish and potential risks to human health. Ecotox. Environ. Safe. 158, 204-212. https://doi.org/10.1016/j.ecoenv.2018.04.034.

Mateo, M.Á., Cebrián, J., Dunton, K., Mutchler, T., 2006. Carbon flux in seagrass ecosystems. *In:* Larkum A.W.D., Orth, R.J., Duarte, C.M. (Eds.), Seagrass: Biology, Ecology and Conservation. Springer, New York, 159-192. https://doi.org/10.1007/978-1-4020-2983-7_7.

Mateo, M.Á., Díaz-Almela, E., Piñeiro-Juncal, N., Leiva-Dueñas, C., Giralt, S., Marco-Méndez, C., 2018. Carbon stocks and fluxes associated to Andalusian seagrass meadows. Deliverable C1: Results Report LIFE Blue Natura. Centre for Advanced Studies of Blanes, Spanish Council for Scientific Research, Blanes, pp. 1-94.

Mateo, M.Á., Julia, R., Romero, J., Michener, R., 2002. An unexplored sedimentary record for the study of environmental change in Mediterranean coastal environments: *Posidonia oceanica* (L.) Delile peats. International Atomic Energy Agency, January, 163-173.

Mateo, M.Á., Renom, P., Guallar, C., Garrido, D., 2005. *Posidonia oceanica* : un archivo orgánico milenario. Evolucion Paleoambiental de los Puertos y Fondeaderos Antiguos en el Mediterraneo Occidental, Rubettino Editore, Seminario El patrimonio arqueológico submarino y los puertos antiguos, 14-15 Noviembre 2003, Alicante, España, 219-229.

Mateo, M.Á., Renom, P. Michener, R.H., 2010. Long-term stability in the production of a NW Mediterranean *Posidonia oceanica* (L.) Delile meadow. Palaeogeography, Palaeoclimatology,

Palaeoecology 291(3-4): 286-296. https://doi.org/10.1016/j.palaeo.2010.03.001.

Mateo, M.Á., Romero, J., 1997. Detritus dynamics in the seagrass *Posidonia oceanica*: Elements for an ecosystem carbon and nutrient budget. Marine Ecology Progress Series 151, 43-53. https://doi.org/10.3354/meps151043.

Mateo, M.Á., Romero, J., Pérez, M., Littler, M.M., Littler, D.S., 1997. Dynamics of Millenary Organic Deposits Resulting from the Growth of the Mediterranean Seagrass *Posidonia oceanica*. Estuarine, Coastal and Shelf Science 44(1), 103-110. https://doi.org/10.1006/ecss.1996.0116.

Mateo, M.Á., Serrano, O., 2012. The carbon sink associated to *Posidonia oceanica*. In: Pergent, G., *et al.* (Eds.), Mediterranean Seagrass Meadows: Resilience and Contribution to Climate Change Mitigation. Gland, Switzerland and Málaga, Spain. IUCN.

Mateu-Vicens, G., Brandano, M., Gaglianone, G., Baldassarre, A., 2012. Seagrass-meadow sedimentary facies in a mixed siliciclastic-carbonate temperate system in the Tyrrhenian Sea (Pontinian Islands, Western Mediterranean). Journal of Sedimentary Research 82(7), 451-463. https://doi.org/10.2110/jsr.2012.42.

Mazarrasa, I., Marbà, N., Garcia-Orellana, J., Masqué, P., Arias-Ortiz, A., Duarte, C.M., 2017. Effect of environmental factors (wave exposure and depth) and anthropogenic pressure in the C sink capacity of *Posidonia oceanica* meadows. Limnology and Oceanography 62(4), 1436-1450. https://doi.org/10.1002/lno.10510.

Mazarrasa, I., Marbà, N., Lovelock, C.E., Serrano, O., Lavery, P.S., Fourqurean, J.W., Kennedy, H., Mateo, M.A., Krause-Jensen, D., Steven, A.D.L., Duarte, C.M., 2015. Seagrass meadows as a globally significant carbonate reservoir. Biogeosciences 12, 4993-5003. https://doi.org/10.5194/bg-12-4993-2015.

Mazarrasa, I., Samper-Villarreal, J., Serrano, O., Lavery, P. S., Lovelock, C. E., Marbà, N., Duarte, C.M., Cortés, J., 2018. Habitat characteristics provide insights of carbon storage in seagrass meadows. Marine Pollution Bulletin 134, 106-117. https://doi.org/10.1016/j.marpolbul.2018.01.059.

McKee, K.L., 2010. Spatial and temporal patterns of soil organic carbon in mangrove forest ecosystems. American Geophysical Union Fall Meeting Abstracts, 13-17 December 2010, San Francisco, California, B24A-07.

McKee, K.L., Cahoon, D.R., Feller, I.C., 2007. Caribbean mangroves adjust to rising sea level through biotic controls on change in soil elevation. Global Ecology and Biogeography 16(5), 545-556. https://doi.org/10.1111/j.1466-8238.2007.00317.x.

McKenzie, L.J., Nordlund L.M., Jones, B.L., Cullen-Unsworth, L.C., Roelfsema, C., Unsworth, R.K.F., 2020. The global distribution of seagrass meadows. Environmental Research Letters 15(7), 074041. https://doi.org/10.1088/1748-9326/ab7d06.

Mcleod, E., Chmura, G.L., Bouillon, S., Salm, R., Björk, M., Duarte, C.M., Lovelock C.E., Schlesinger W.H., Silliman, B.R., 2011. A blueprint for blue carbon: toward an improved understanding of the role of vegetated coastal habitats in sequestering CO_2. Frontiers in Ecology and the Environment 9(10), 552-560. https://doi.org/10.1890/110004.

Mcowen, C., Weatherdon, L.V., Bochove, J., Sullivan, E., Blyth, S., Zockler, C., Stanwell-Smith, D., Kingston, N., Martin, C.S., Spalding, M., et al., 2017. A global map of saltmarshes. Biodiversity Data Journal 5, e11764. https://doi.org/10.3897/BDJ.5.e11764.

Meinesz, A., Genet, I., Hesse, B., 1990. Données quantitatives sur les biocénoses littorales marines de la Corse et impact de l'aménagement du littoral. Rapport GIS Posidonie/DRAE Corse, pp. 1-22.

Micallef, A., LeBas, T.P., Huvenne, V.A.I., Blondel, P., Hühnerbach, V., Deidun, A., 2012. A multi-method approach for benthic habitat mapping of shallow coastal areas with high-resolution multibeam data. Continental Shelf Research 39-40, 14-26. https://doi.org/10.1016/j.csr.2012.03.008.

Middelburg, J.J., Nieuwenhuize, J., Lubberts, R.K., van de Plassche, O., 1997b. Organic carbon isotope systematics of coastal marshes. Estuarine, Coastal and Shelf Science 45, 681-687. https://doi.org/10.1006/ecss.1997.0247.

Middelburg, J.J., Soetaert, K., Herman, P.M.J., 1997a. Empirical relationships for use in global diagenetic models. Deep-Sea Research I 44, 327-344. https://doi.org/10.1016/S0967-

0637(96)00101-X.
Middleton, B., McKee, K., 2001. Degradation of mangrove tissues and implications for peat formation in Belizean island forests. Journal of Ecology 89(5), 818-828. https://doi.org/10.1046/j.0022-0477.2001.00602.x.
Miković, M., 1977. Istražni radovi u moru. Bagerovanje u zavisnosti od bioloških uslova. Izgradnja. 9.
Millot, C., 1987. Circulation in the western Mediterranean Sea. Oceanologica Acta 10(2), 143-149.
Miyajima, T., Hori, M., Hamaguchi, M., Shimabukuro, H., Adachi, H., Yamano, H., Nakaoka, M., 2015. Geographic variability in organic carbon stock and accumulation rate in sediments of East and Southeast Asian seagrass meadows. Global Biogeochemical Cycles 29(4), 397-415. https://doi.org/10.1002/2014GB004979.
Molinier, R., Picard, J., 1952. Recherches sur les herbiers de Phanérogames marines du littoral méditerranéen français. Annales de l'Institut Océanographique (Paris) 27(3), 157-234.
Monnier, B., Pergent, G., Mateo, M.Á., Clabaut, P., Pergent-Martini, C., 2020. Seismic interval velocity in the matte of *Posidonia oceanica* meadows: Towards a non-destructive approach for large-scale assessment of blue carbon stock. Marine Environmental Research 161, 105085. https://doi.org/10.1016/j.marenvres.2020.105085.
Montagna, P., McCulloch, M., Mazzoli, C., Silenzi, S., Odorico, R., 2007. The non-tropical coral *Cladocora caespitosa* as the new climate archive for the Mediterranean: high-resolution (~weekly) trace element systematics. Quaternary Science Reviews 26, 441-462. https://doi.org/10.1016/j.quascirev.2006.09.008.
Morgan, N., 1969. Physical properties of marine sediments as related to seismic velocities. Geophysics 34(4), 529-543. https://doi.org/10.1190/1.1440029.
Morri, C., Peirano, A., Bianchi, C.N., 2001. Is the Mediterranean coral *Cladocora caespitosa* an indicator of climatic change? Archivio di Oceanografia e Limnologia 22, 139-144.
Morri, C., Peirano, A., Bianchi, C.N., Rodolfo-Metalpa, R., 2000. *Cladocora caespitosa*: a colonial zooxanthellate Mediterranean coral showing constructional ability. Reef Encounter 27, 22-25.
Morri, C., Peirano, A., Bianchi, C.N., Sassarini, M., 1994. Present-day bioconstructions of the hard coral, *Cladocora caespitosa* (L.) (Anthozoa, Scleractinia), in the Eastern Ligurian Sea (NW Mediterranean). Biologia Marina Mediterranea 1(1), 371-372.
Mosher, D.C., Simpkin, P.G., 1999. Environmental marine Geoscience 1. Status and trends of marine high-resolution seismic reflection profiling: Data acquistion. Geoscience Canada 26(4), 174-188.
Mucha, A.P., Almeida, C.M.R., Bordalo, A.A., Vasconcelos, M.T.S.D., 2005. Exudation of organic acids by a marsh plant and implications on trace metal availability in the rhizosphere of estuarine sediments. Estuarine, Coastal and Shelf Science 65, 191-198. https://doi.org/10.1016/j.ecss.2005.06.007.
Mulder, T., Maneux, E., 1999. Flux et bilan sédimentaires. Impact des apports fluviatiles sur la construction des éventails sous-marins profonds de la marge Est-Corse, Université de Bordeaux I, Rapport, pp. 1-20.
Mumby, P.J., 2006. Connectivity of reef fish between mangroves and coral reefs: algorithms for the design of marine reserves at seascape scales. Biological Conservation 128(2), 215-222. https://doi.org/10.1016/j.biocon.2005.09.042.
Myhre, G., Shindell, D., Bréon, F.M., Collins, W., Fuglestvedt, J., Huang, J., Koch, D., Lamarque, J.F., Lee, D., Mendoza, D., Nakajima, T., Robock, A., Stephens, G., Takemura, T., Zhang, H., 2013. Anthropogenic and natural radiative forcing. *In:* IPCC, 2013. Climate Change 2013: The Physical Science Basis. Contribution of Working Group I to the Fifth Assessment Report of the Intergovernmental Panel on Climate Change, Stocker, T.F., Qin, D., Plattner, G.K., Tignor, M., Allen, S.K., Doschung, J., Nauels, A., Xia, Y., Bex, V., Midgley, P.M. (Eds.), Cambridge University Press, 659-740, https://doi.org/10.1017/CBO9781107415324.018.
Nafe, J.E., Drake, C.L., 1957. Variation with depth in shallow and deep-water marine sediment of porosity, density and the velocities of compressional and shear waves. Geophysics 22(3), 523-552. https://doi.org/10.1190/1.1438386.

Nafe, J.E., Drake, C.L., 1961. Physical properties of marine sediments. Technical Report 2, Lamont Geological Observatory Palisades, New York.

Nellemann, C., Corcoran, E., Duarte, C.M., Valdé, L., De Young, C., Fonseca, L., Grimsditch, G., 2009. Blue Carbon: The role of healthy oceans in binding carbon, Rapid Response Assessment. Report United Nations Environment Programme/GRID-Arendal, Norway.

Nesteroff, W., 1965. Recherches sur les sédiments marins actuels de la région d'Antibes. Annales de l'Institut Océanographique, France, 43, pp. 1-135.

Norgren, P., Skjetne, R., 2014. Using autonomous underwater vehicles as sensor platforms for ice-monitoring. Modeling, Identification and Control 35(4), 263-277. https://doi.org/10.4173/mic.2014.4.4.

Norgren, P., Skjetne, R., 2015. Line-of-sight iceberg edge-following using an AUV equipped with multibeam sonar. IFAC-PapersOnLine 48(16), 81-88. https://doi.org/10.1016/j.ifacol.2015.10.262.

Oliver Valls, J.A., 1989. Développement de *Cladocora caespitosa* (Linné, 1767) en aquarium. Bulletin de l'Institut Océanographique de Monaco, 5, 205-209.

Onajite, E., 2014. Seismic Data Analysis Techniques in Hydrocarbon Exploration, Elsevier, pp. 1-256. https://doi.org/10.1016/C2013-0-09969-0.

Orofino, S., Baltassat, J.M., Frissant, N., Lanini, S., Prognon, C., Winckel, A., 2010. Etude des interactions entre les eaux souterraines, les eaux de surface et l'étang de Biguglia. Rapport BRGM, RP59068-FR, pp. 1-150.

Orsi, T.H., Dunn, D.A., 1991, Correlations between sound velocity and related properties of glacio-marine sediments: Barents Sea. Geo-Marine Letters 11, 79-83. https://doi.org/10.1007/BF02431033.

Orszag-Sperber, F., Pilot, M.D., 1976. Grands traits Néogène de Corse. Bulletin de la Société Géologique de France 7(5), 1183-1187.

Ott, J.A., 1980. Growth and production of *Posidonia oceanica* (L.) Delile. Marine Ecology 1, 47-64. https://doi.org/10.1111/j.1439-0485.1980.tb00221.x.

Ottman, F., 1958. Les formations pliocènes et quaternaires sur le littoral corse. Mémoires de la Société Géologique de France 37(84), 176-181.

Özalp, H.B., Alparslan, M., 2011. The first record of *Cladocora caespitosa* (Linnaeus, 1767) (Anthozoa, Scleractinia) from the Marmara Sea. Turkish Journal of Zoology 35(5), 701-705. https://doi.org/10.3906/zoo-0907-80.

Öztürk, B., 2004. Marine Life of Turkey in the Aegean & Mediterranean Sea. *In:* Phylum Cnidaria, Turkish Marine Research Foundation, Turkey, pp. 1-48.

Papadimitriou, S., Kennedy, H., Kennedy, D.P., Duarte, C.M., Marba, N., 2005. Sources of organic matter in seagrass-colonized sediments: a stable isotope study of the silt and clay fraction from *Posidonia oceanica* meadows in the western Mediterranean. Organic Geochemistry 36, 949-961. https://doi.org/10.1016/j.orggeochem.2004.12.002.

Pasqualini, V., Clabaut, P., Pergent, G., Benyoussef, L., Pergent-Martini, C., 2000. Contribution of side scan sonar to the management of Mediterranean littoral ecosystems. International Journal of Remote Sensing 21(2), 367-378. https://doi.org/10.1080/014311600210885.

Pedersen, M.Ø., Serrano, O., Mateo, M.Á., Holmer, H., 2011. Decomposition of *Posidonia oceanica* matte in a climate change setting. Aquatic Microbial Ecology 65(2), 169-182. https://doi.org/10.3354/ame01543.

Peirano, A., Abbate, M., Cerrati, G., Difesca, V., Peroni, C., Rodolfo-Metalpa, R., 2005. Monthly variations in calyx growth, polyp tissue and density banding of the Mediterranean scleractinian *Cladocora caespitosa* (L.). Coral Reefs 24, 404-409. https://doi.org/10.1007/s00338-005-0020-6.

Peirano, A., Kružić, P., Mastronuzzi, G., 2009. Growth of Mediterranean reef of *Cladocora caespitosa* (L.) in the Late Quaternary and climate inferences. Facies 55(3), 325-333. https://doi.org/10.1007/s10347-008-0177-x.

Peirano, A., Morri, C., Bianchi, C.N., 1999. Skeleton growth and density pattern of the temperate,

zooxanthellate scleractinian *Cladocora caespitosa* from the Ligurian Sea (NW Mediterranean). Marine Ecology Progress Series 185, 195-201. https://doi.org/10.3354/meps185195.

Peirano, A., Morri, C., Bianchi, C. N., Aguirre, J., Antonioli, F., Calzetta, G., Carobene, L., Mastronuzzi, G., Orrù, P., 2004. The Mediterranean coral Cladocora caespitosa: a proxy for past climate fluctuations? Global and Planetary Change 40(1-2), 195-200. https://doi.org/10.1016/S0921-8181(03)00110-3.

Peirano, A., Morri, C., Bianchi, C.N., Rodolfo-Metalpa, R., 2001. Biomass, carbonate standing stock and production of the Mediterranean coral *Cladocora caespitosa* (L.). Facies 44, 75-80. https://doi.org/ https://doi.org/10.1007/BF02668168.

Peirano, A., Morri, C., Mastronuzzi, G., Bianchi, C.N., 1998. The coral *Cladocora caespitosa* (Anthozoa, Scleractinia) as a bioherm builder in the Mediterranean Sea. Memorie Descrittive Carta Geologica d'Italia, 52(1994), 59-74.

Pelletier, D., Leleu, K., Mallet, D., Mou-Tham, G., Hervé, G., Boureau, M., Guilpart, N., 2012. Remote high-definition rotating video enables fast spatial survey of marine underwater macrofauna and habitats. PLoS ONE 7(2), e30536. https://doi.org/10.1371/journal.pone.0030536

Pelletier, D., Leleu, K., Mou-Tham, G., Guillemot, N., Chabanet, P., 2011. Comparison of visual census and high definition video transects for monitoring coral reef fish assemblages. Fisheries Research 107, 84-93. https://doi.org/10.1016/j.fishres.2010.10.011.

Pendleton, L., Donato, D.C., Murray, B.C., Crooks, S., Jenkins, W.A., Sifleet, S., Craft, C., Fourqurean J.W., Kauffman J.B., Marbà, N., Megonigal, P., Pidgeon, E., Herr, D., Gordon D., Baldera, A., 2012. Estimating global "blue carbon" emissions from conversion and degradation of vegetated coastal ecosystems. PLoS ONE 7, e43542. https://doi.org/10.1371/journal.pone.0043542.

Pepin, L., 2012. Variations de la teneur en CO_2 de l'atmosphère au cours des 4 derniers cycles glaciaire-interglaciaires, à partir de l'analyse de la carotte de Vostok (Antarctique) : implications sur l'évolution du climat et du cycle du carbone. Thèse de doctorat, Université Joseph-Fourier Grenoble I, pp. 1-258.

Peralta, G., Van Duren, L. A., Morris, E. P., and Bouma, T. J., 2008. Consequences of shoot density and stiffness for ecosystem engineering by benthic marcrophytes in flow dominated areas: a hydrodynamic flume study. Marine Ecology Progress Series 368, 103-115. https://doi.org/10.3354/meps07574.

Péres, J.M., 1982. Major benthic assemblages. *In:* Kinne, O. (Ed.). Marine Ecology 5, Part 1. Wiley, Chichester, 373-522.

Pérès, J.M., Picard, J., 1964. Nouveau manuel de bionomie benthique de la mer Méditerranée. Recueil des Travaux de la Station Marine d'Endoume 31(47), 5-138.

Pergent, G., Bazairi, H., Bianchi, C.N., Boudouresque, C.F., Buia, M.C., Clabaut, P., Harmelin-Vivien, M., Mateo, M.Á., Montefalcone, M., Morri, C., Orfanidis, S., Pergent-Martini, C., Semroud, R., Serrano, O., Verlaque, M. 2012. Mediterranean seagrass meadows: Resilience and contribution to climate change mitigation. IUCN, Gland, Switzerland & Malaga, Spain. pp. 1-80.

Pergent, G., Bazairi, H., Bianchi, C.N., Boudouresque, C.F., Buia, M.C., Clabaut, P., Harmelin-Vivien, M., Mateo, M.Á., Montefalcone, M., Morri, C., Orfanidis, S., Pergent-Martini, C., Semroud, R., Serrano, O., Thibaut, T., Tomasello, A., Verlaque, M., 2014. Climate change and Mediterranean seagrass meadows: A synopsis for environmental managers. Mediterranean Marine Science 15(2), 462-473. https://doi.org/10.12681/mms.621.

Pergent, G., Pergent-Martini, C., 1991. Leaf renewal cycle and primary production of *Posidonia oceanica* in the Bay of Lacco Ameno (Ischia, Italy) using lepidochronological analysis. Aquatic Botany 42(1), 49-66. https://doi.org/10.1016/0304-3770(91)90105-E.

Pergent, G., Pergent-Martini, C., 1999. Mercury levels and fluxes in *Posidonia oceanica* meadows. Environmental Pollution 106(1), 33-37. https://doi.org/10.1016/S0269-7491(99)00064-0.

Pergent, G. Pergent-Martini, C., Bein, A., Dedeken, M., Oberti, P., Orsini, A., Santucci, J.F., Short, F., 2015. Dynamic of *Posidonia oceanica* seagrass meadows in the northwestern Mediterranean:

Could climate change be to blame? Comptes Rendus Biologies 338(7), 484-493. https://doi.org/10.1016/j.crvi.2015.04.011.

Pergent, G., Pergent-Martini C., Boudouresque, C.F., 1995. Utilisation de l'herbier à *Posidonia oceanica* comme indicateur biologique de la qualité du milieu littoral en Méditerranée : état des connaissances. Mésogée 54, 3-29.

Pergent, G., Rico-Raimondino, V., Pergent-Martini, C., 1997. Fate of primary production in *Posidonia oceanica* meadows of the Mediterranean. Aquatic Botany 59(3-4), 307-321. https://doi.org/10.1016/S0304-3770(97)00052-1.

Pergent, G., Romero, J., Pergent-Martini, C., Mateo, M.Á., Boudouresque, C.F., 1994. Primary production, stocks and fluxes in the Mediterranean seagrass *Posidonia oceanica*. Marine Ecology Progress Series 106(1-2), 139-146. https://doi.org/10.3354/meps106139.

Pergent-Martini, C., Pergent G., 2000. Marine phanerogams as a tool in the evaluation of marine trace-metal contamination: an example from the Mediterranean. International Journal of Environmental Pollution 13(1-6), 126-147. https://doi.org/10.1504/IJEP.2000.002313.

Pergent-Martini, C., Pergent, G., Monnier, B., Boudouresque, C.F., Mori, C., Valette-Sansevin, A., 2020. Contribution of *Posidonia oceanica* meadows in the context of climate change mitigation in the Mediterranean Sea. Marine Environmental Research 165, 105236.

Pergent-Martini, C., Valette-Sansevin, A., Pergent, G., 2015. Cartographie continue des habitats marins en Corse / Résultats cartographiques - Programme CARTHAMED. AAMP-UCPP (Equipe Ecosystèmes Littoraux), Corte, pp. 1-60.

Perry, C.T., Beavington-Penney, S.J., 2005, Epiphytic calcium carbonate production and facies development within sub-tropical seagrass beds, Inhaca Island, Mozambique: Sedimentary Geology 174, 161-176.

Peyron, O., Magny, M., Goring, S., Joannin, S., de Baulieu J.L., Brugiapaglia, E., Sadori, L., Garfi, G., K. Kouli, K., Ioakim, C., Combourieu-Nebout, N., 2013. Contrasting patterns of climatic changes during the Holocene across the Italian Peninsula reconstructed from pollen data. Climate of the Past 9, 1233-1252. https://doi.org/10.5194/cp-9-1233-2013.

Picard, J., 1953. Les herbiers de posidonies important facteur de l'élévation des fonds littoraux. Revue Gémorphodynamique 2, 83-84.

Piñeiro-Juncal, N., Leiva-Dueñas, C., Serrano, O., Mateo, M.Á., Martínez-Cortízas, A., 2020. Pedogenic Processes in a *Posidonia oceanica* Mat. Soil Systems 4, 18. https://doi.org/10.3390/soilsystems4020018.

Pirc, H., 1985. Growth dynamics in *Posidonia oceanica* (L.) Delile. Marine Ecology 6, 141-165. https://doi.org/10.1111/j.1439-0485.1985.tb00135.x.

Pluquet, F., 2006. Évolution récente et sédimentation des plates-formes continentales de la Corse. Thèse de doctorat, Université de Corse, pp. 1-300.

Pongratz, J., Reick, C.H., Raddatz, T., Claussen, M., 2009. Effects of anthropogenic land cover change on the carbon cycle of the last millennium. Global Biogeochemical Cycles, 23(4). https://doi.org/10.1029/2009GB003488.

Ponti, M., Perlini, R.A., Ventra, V., Grech, D., Abbiati, M., Cerrano, C., 2014. Ecological shifts in Mediterranean coralligenous assemblages related to gorgonian forest loss. PLoS ONE 9(7), e102782. https://doi.org/10.1371/journal.pone.0102782.

Prather, M.J., Holmes, C.D., Hsu, J., 2012. Reactive greenhouse gas scenarios: Systematic exploration of uncertainties and the role of atmospheric chemistry. Geophysical Research Letters 39(9), L09803. https://doi.org/10.1029/2012GL051440.

Prentice, I.C., *et al*., 2001. The carbon cycle and atmospheric carbon dioxide. *In:* IPCC, 2001. Climate Change 2001: The Scientific Basis. Contribution of Working Group I to the Third Assessment Report of the Intergovernmental Panel on Climate Change, Houghton, J.T., Ding, Y., Griggs, D.J., Noquer, M., van der Linden, P.J., Dai, X., Maskell, K., Johnson, C.A. (Eds.), Cambridge University Press, Cambridge, United Kingdom and New York, NY, USA, 183-237.

Reille, M., 1984. Origine de la végétation actuelle de la Corse sud-orientale ; analyse pollinique de cinq marais côtiers. Pollen et Spores 26(1), 43-60.

Reille, M.J., Gamisans, V., Andrieu-Ponel, V., De Balieu, J.L., 1999. The Holocene at Lac de Creno, Corsica, France: a key site for the whole island. The New Phytologist 141, 291-307. https://doi.org/10.1046/j.1469-8137.1999.00343.x.

Reimer, P., Bard, E., Bayliss, A., Beck, J.W., Blackwel, P.G., Bronk Ramsey, C., Buck, C.E., Cheng, H., Edwards, R.L., Friedrich, M., Grootes, P.M., Guilderson, T.P., Haflidason, H., Hajdas, I., Hatte, C., Heaton, T.J., Hoffmann, D.L., Hogg, A.G., Hughen, K.A., Kaiser, K.F., Kromer,B., Manning, S.W., Niu, M., Reimer,R.W., Richards, D.A., Scott, E.M., Southon, J.R., Staff, R.A., Turney, C.S.M., van der Plicht, J., 2013. Intcal13 and Marine13 radiocarbon age calibration curves 0-50,000 years cal BP. Radiocarbon 55(4), 1869-1887. https://doi.org/10.2458/azu_js_rc.55.16947.

Relini, G., 2009. Italian Habitats. Marine Bioconstructions. Nature's Architectural Seascapes. Italian Ministry of the Environment and Territorial Protection. Friuli Museum of Natural History, Udine, pp. 1-159.

Rende, S.F., Irving, A.D., Bacci, T., Parlagreco, L., Bruno, F., De Filippo, F., Montefalcone, M., Penna, M., Trabucco, B., Di Mento, R., Cicero, A.M., 2015. Advances in micro-cartography: a two-dimensional photo mosaicing technique for seagrass monitoring. Estuarine, Coastal and Shelf Science 167, 475-486. https://doi.org/10.1016/j.ecss.2015.10.029.

Rey, J., Diaz del Rio, V., 1989. Cartografía de los fondos marinos de la bahía de Palma (Baleares, España) : Distribución de las praderas vegetales y sedimentos superficiales. International Workshop *Posidonia oceanica* Beds, GIS Posidonie, Marseille, France, 28-41.

Reynolds, J.M., 2011. An Introduction to Applied and Environmental Geophysics. second ed. Wiley-Blackwell.

Ribera, G., Coloreu, M., Rodriguez-Prieto, C., Ballesteros, E., 1997. Phytobenthic assemblages of Addaia Bay (Menorca, Western Mediterranean): composition and distribution. Botanica Marina 40, 523-532. https://doi.org/10.1515/botm.1997.40.1-6.523.

Ricart, A.M., Pérez, M., Romero, J., 2017. Landscape configuration modulates carbon storage in seagrass sediments. Estuarine, Coastal and Shelf Science 185, 69-76. http://dx.doi.org/10.1016/j.ecss.2016.12.011.

Ricart, A.M., York, P.H., Bryant, C.V., Rasheed, M.A., Ierodiaconou, D., Macreadie, P.I., 2020. High variability of Blue carbon storage in seagrass meadows at the estuary scale. Scientific Reports 10, 5865. https://doi.org/10.1038/s41598-020-62639-y.

Ricart, A.M., York, P.H., Rasheed, M.A., Pérez, M., Romero, J., Bryant, C.V., Macreadie, P.I., 2015. Variability of sedimentary organic carbon in patchy seagrass landscapes. Marine Pollution Bulletin 100(1), 476-482. https://doi.org/10.1016/j.marpolbul.2015.09.032.

Roberts, N., Brayshaw, D., Kuzucuoğlu, C., Pérez, R., Sadori, L., 2011a. The mid-Holocene climatic transition in the Mediterranean: causes and consequences. The Holocene 21(1), 3-13. https://doi.org/10.1177/0959683610388058.

Roberts, N., Eastwood, W.J., Kuzucuoğlu, C., Fiorentino, G., Caracuta, V., 2011b. Climatic, vegetation and cultural change in the eastern Mediterranean during the mid-Holocene transition. The Holocene 21(1), 147-162. https://doi.org/10.1177/0959683610386819.

Robertson, A.I., Alongi, D.M., 1992. Tropical mangrove ecosystems. American Geophysical Union, Washington DC, USA, pp. 1-329.

Rodolfo-Metalpa, R., Bianchi, C.N., Peirano, A., 2000. Coral mortality in NM Mediterranean. Coral Reefs 19, 24.

Rodolfo-Metalpa, R., Bianchi, C.N., Peirano, A., Morri, C., 2005. Tissue necrosis and mortality of the temperate coral *Cladocora caespitosa*. Italian Journal of Zoology 72, 271-276. https://doi.org/10.1080/11250000509356685.

Rodolfo-Metalpa, R., Peirano, A., Houlbrèque, F, Abbate, M, Ferrier-Pagès, C., 2008. Effects of temperature, light and heterotrophy on the growth rate and budding of the temperate coral *Cladocora caespitosa*. Coral Reefs 27, 17-25. https://doi.org/10.1007/s00338-007-0283-1.

Rodolfo-Metalpa, R., Peirano, A., Morri, C., Bianchi, C.N., 1999. Coral calcification rates in the Mediterranean Scleractinian coral *Cladocora caespitosa* (L., 1767). Atti Associazione Italiana

Oceanologia Limnologia 13(1), 291-299.

Rodolfo-Metalpa, R., Richard, C., Allemand, D., Ferrier-Pagès, C., 2006. Growth and photosynthesis of two Mediterranean corals, *Cladocora caespitosa* and *Oculina patagonica*, under normal and elevated temperatures. The Journal of Experimental Biology 209, 4546-4556. https://doi.org/10.1242/jeb.02550.

Romero, J., 1988. Epifitos de las hojas de *Posidonia oceanica*: variaciones estacionales y batimetricas de biomasa en la pradera de las islas Medes (Girona). Oecologica Aquatica 9, 19-25.

Romero, J., Pérez, M., Mateo, M.Á., Sala, E., 1994. The belowground organs of the Mediterranean seagrass *Posidonia oceanica* as a biogeochemical sink. Aquatic Botany 47(1), 13-19. https://doi.org/10.1016/0304-3770(94)90044-2.

Romero, J., Pergent, G., Pergent-Martini, C., Mateo, M.Á., Regnier, C., 1992. The detritic compartment in a *Posidonia oceanica* meadow: litter features, decomposition rates and mineral stocks. Marine Ecology 13(1), 69-83. https://doi.org/10.1111/j.1439-0485.1992.tb00341.x.

Rooper, C.N., 2008. Underwater video sleds: Versatile and cost-effective tools for habitat mapping. Marine Habitat Mapping Technology for Alaska. Alaska Sea Grant College Program, University of Alaska Fairbanks. https://doi.org/10.4027/mhmta.2008.07.

Rosentreter, J.A., Maher, D.T., Erler, D.V., Murray, R., Eyre, B.D., 2018. Methane emissions partially offset "blue carbon" burial in mangroves. Science Adavnces 4(6), eaao4985. https://doi.org/10.1126/sciadv.aao4985.

Rotty, R.M., 1983. Distribution of and changes in industrial carbon-cycle production. Journal of Geophysical Research: Oceans 88(C2), 1301-1308. https://doi.org/10.1029/JC088iC02p01301.

Rozaimi, M., 2015. Carbon storage and preservation in seagrass meadows. Ph.D. Thesis. Edith Cowan University, Australia, pp. 1-174.

Rozaimi, M., Lavery, P.S., Serrano, O., Kyrwood, D., 2016. Long-term carbon storage and its recent loss in an estuarine *Posidonia australis* meadow (Albany, Western Australia). Estuarine, Coastal and Shelf Science 171, 58-65. https://doi.org/10.1016/j.ecss.2016.01.001.

Ruiz, J.M., Romero, J., 2001. Effects of in situ experimental shading on the Mediterranean seagrass *Posidonia oceanica*. Marine Ecology Progress Series 215, 107-120. http://dx.doi.org/10.3354/meps215107.

Russo, G.F., Chessa, L.A., Vinci, D., Fresi, E., 1991a. Molluscs of *Posidonia oceanica* beds in the bay of Porto Conte (North-Western Sardinia): Zonation pattern, seasonal variability and geographical comparison. Posidonia Newsletter 4(1), 5-14.

Russo, G.F., Fresi, E., Vinci, D., Chessa, L.A., 1984. Mollusk syntaxon of foliar stratum along a depth gradient in *Posidonia oceanica* (L.) Delile meadows: seasonal variability. *In:* Boudouresque, C.F., Jeudy de Grissac, A., Olivier, J. (Eds.), First International Workshop on *Posidonia oceanica* Beds, 1, GIS Posidonie Publication, 311-318.

Russo, G.F., Vinci, D., Scadri, M., Fresi, E., 1991b. Mollusc syntaxon of foliar stratum along a depth gradient in a *Posidonia oceanica* bed: 3 a year's cycle at Ischia Island. Posidonia Newsletter 4, 15-25.

Sabine C.L., Feely R.A., 2007. The oceanic sink for carbon dioxide. *In:* Reay, D., Hewitt, N., Grace J., Smith K. (Eds.), Greenhouse Gas Sinks, CABI Publishing, Oxfordshire, UK, 31-49.

Saderne, V., Cusack, M., Almahasheer, H., Serrano, O., Masqué, P., Arias-Ortiz, A., Krishnakumar, P.K., Rabaoui, L., Qurban, M.A., & Duarte, C.M., 2018. Accumulation of carbonates contributes to coastal vegetated ecosystems keeping pace with sea level rise in an arid region (Arabian Peninsula). Journal of Geophysical Research: Biogeosciences 123(5), 1498-1510. https://doi.org/10.1029/2017JG004288.

Saderne, V., Geraldi, N.R., Macreadie, P.I. Maher, D.T., Middelburg, J.J., Serrano, O., Almahasheer, H., Arias-Ortiz, A., Cusack, M., Eyre, B.D., Fourqurean, J.W., Kennedy, H., Krause-Jensen, D., Kuwae, T., Lavery, P.S., Lovelock, C.E., Marba, N., Masqué, P., Mateo, M.Á., Mazarrasa, I., McGlathery, K.J., Oreska, M.P.J., Sanders, C.J., Santos, I.R., Smoak, J.M., Tanaya, T., Watanabe, K., Duarte, C.M., 2019. Role of carbonate burial in Blue Carbon budgets. Nature Communications 10, 1106. https://doi.org/10.1038/s41467-019-08842-6.

Saenger, P., 2002. Mangrove Ecology, Silviculture and Conservation. Springer, pp. 1-360. https://doi.org/10.1007/978-94-015-9962-7.

Samper-Villarreal, J., Lovelock, C.E., Saunders, M.I., Roelfsema, C., Mumby, P.J., 2016. Organic carbon in seagrass sediments is influenced by seagrass canopy complexity, turbidity, wave height, and water depth. Limnology and Oceanography 61, 938-952. https://doi.org/10.1002/lno.10262.

Sanders, C.J., Maher, D.T., Tait, D.R., Williams, D., Holloway, C., Sippo, J.Z., Santos, I.R., 2016. Are global mangrove carbon stocks driven by rainfall? Journal of Geophysical Research: Biogeosciences 121(10), 2600-2609. https://doi.org/10.1002/2016JG003510.

Sañé, E., Chiocci, F.L., Basso, D., Martorelli, E., 2016. Environmental factors controlling the distribution of rhodoliths: an integrated study based on seafloor sampling, ROV and side scan sonar data, offshore the W-Pontine Archipelago. Continental Shelf Research 129, 10-22. https://doi.org/10.1016/j.csr.2016.09.003.

Sarmiento, J.L., Gruber, N., 2002. Sinks for Anthropogenic Carbon. Physics Today 55(8), 30. https://doi.org/10.1063/1.1510279.

Satra, C., Duval, F., Le Drezen, E., Berné, S., 2003. Le SIG du Golfe du Lion au département Géosciences Marines, de l'acquisition des données à la synthèse géologique. Rapport Ifremer, pp. 1-45.

Schiller, C., 1993a. Ecology of the symbiotic coral *Cladocora caespitosa* (L.) (Faviidae, Scleractinia) in the Bay of Piran (Adriatic Sea): I Distribution and biometry. P.S.Z.N.: Marine Ecology 14(3), 205-219. https://doi.org/10.1111/j.1439-0485.1993.tb00480.x.

Schiller, C., 1993b. Ecology of the symbiotic coral *Cladocora caespitosa* (L.) (Faviidae, Scleractinia) in the Bay of Piran (Adriatic Sea): II. Energy budget. P.S.Z.N.: Marine Ecology 14(3), 221-238. https://doi.org/10.1111/j.1439-0485.1993.tb00481.x.

Schiller, C., Herndl, G.J., 1989. Evidence of enhanced microbial activity in the interstitial space of branched corals: possible implications for coral metabolism. Coral Reefs 7, 179-184. https://doi.org/10.1007/BF00301596.

Schimmelmann, A., Qi, H., Coplen, T. B., Brand, W. A., Fong, J., Meier-Augenstein, W., Kemp, H. F., Toman, B., Ackermann, A., Assonov, S., Aerts-Bijma, A. T., Brejcha, R., Chikaraishi, Y., Darwish, T., Elsner, M., Gehre, M., Geilmann, H., Gröning, M., Hélie, J-F., Herrero-Martín, S., Meijer, H. A. J., Sauer, P. E., Sessions, A. L., and Werner, R. A., 2016, New organic reference materials for hydrogen, carbon, and nitrogen stable isotope-ratio measurements: caffeines, nalkanes, fatty acid methyl esters, glycines, L-valines, polyethylenes, and oils, Analytical Chemistry 88, 4294-4302. https://doi.org/10.1021/acs.analchem.5b04392.

Schlesinger, W.H., 1997. Biogeochemistry: an analysis of global change, 2nd Edition, San Diego, CA, Academic Press, pp. 1-588.

Schlesinger, W.H., Lichter, J., 2001. Limited carbon storage in soil and litter of experimental forest plots under increased atmospheric CO_2. Nature 411(6836), 466-9. https://doi.org/10.1038/35078060.

Schneider, C.A., Rasband, W.S., Eliceiri, K.W., 2012. NIH Image to ImageJ: 25 years of image analysis. Nature Methods 9, 671-675. https://doi.org/10.1038/nmeth.2089.

Schreiber, B.C., 1967. Sound velocity in the deep-sea sediments. Transactions of the American Geophysical Union 48, 144. https://doi.org/10.1029/JB073i004p01259.

Schreiber, B.C., 1968. Sound velocity in deep sea sediments. Journal of Geophysical Research 73(4), 1259-1268. https://doi.org/10.1029/JB073i004p01259.

Scipione, M.B., Gambi, M.C., Lorenti, M., Russo, G.F., Zupo, V., 1996. Vagile fauna of the leaf stratum of *Posidonia oceanica* and *Cymodocea nodosa* in the Mediterranean Sea. Seagrass Biology: Proceeding of an International Workshop, Rottnest Island, Australia, 249-260.

Scott, D.B., Greenberg, D.A., 1983. Relative sea level rise and tidal development in the Fundy tidal system. Canadian Journal of Earth Sciences 20(10), 1554-1564. https://doi.org/10.1139/e83-145.

Sengbush, R.L., 1983. Seismic Exploration Methods. Springer Science & Business Media. https://doi.org/10.1007/978-94-011-6397-2.

Serrano, O., Kelleway, J. J., Lovelock, C., Lavery, P.S., 2019. Conservation of blue carbon ecosystems for

climate change mitigation and adaptation. *In:* Perillo, G.M.E., Wolanski, E., Cahoon, D.R., Hopkinson C.S. (Eds.), Coastal wetlands: an integrated ecosystem approach, 2nd Edition, Elsevier, Amsterdam, 965-996. https://doi.org/10.1016/B978-0-444-63893-9.00028-9.

Serrano, O., Lavery, P.S., Duarte, C.M., Kendrick, G.A., Calafat, A., York, P.H., Steven, A., Macreadie, P.I., 2016c. Can mud (silt and clay) concentration be used to predict soil organic carbon content within seagrass ecosystems? Biogeosciences 13, 4915-4926. https://doi.org/10.5194/bg-13-4915-2016.

Serrano, O., Lavery, P.S., López-Merino, L., Ballesteros, E., Mateo, M.Á., 2016a. Location and associated associated carbon storage of erosional escarpments of seagrass *Posidonia* mats. Frontiers in Marine Science 3(42). https://doi.org/10.3389/fmars.2016.00042.

Serrano, O., Lavery, P.S., Rozaimi, M., Mateo, M.Á., 2014. Influence of water depth on the carbon sequestration capacity of seagrass. Global Biochemical Cycles 28, 950-961. https://doi.org/10.1002/2014GB004872.

Serrano, O., Martínez-Cortizas, A., Mateo, M.Á., Biester, H. Bindler, R., 2013. Millennial scale impact on the marine biogeochemical cycle of mercury from early mining on the Iberian Peninsula. Global Biogeochemical Cycles 27(1), 21-30. https://doi.org/10.1029/2012GB004296.

Serrano, O., Mateo, M.Á., Dueñas-Bohórquez, A., Renom, P., López-Sáez, J.A., Martínez Cortizas, A., 2011. The *Posidonia oceanica* marine sedimentary record: A Holocene archive of heavy metal pollution. Science of The Total Environment 409(22), 4831-4840. https://doi.org/10.1016/j.scitotenv.2011.08.001.

Serrano, O., Mateo, M.Á., Renom, P., Julià, R., 2012. Characterization of soils beneath a *Posidonia oceanica* meadow. Geoderma 185, 26-36. https://doi.org/10.1016/j.geoderma.2012.03.020.

Serrano, O., Ricart, A.M., Lavery, P.S., Mateo, M.Á., Arias-Ortiz, A., Masque, P., Steven, A., Duarte, C.M., 2016b. Key biogeochemical factors affecting soil carbon storage in *Posidonia* meadows. Biogeosciences 13, 4581-4594. https://doi.org/10.5194/bg-13-4581-2016.

Shepherd, S.A., Sprigg, R.C., 1976. Substrate, sediments and subtidal ecology of Gulf St. Vincent and Investigator strait. Natural History of the Adelaide Region Twidale, Royal Society of South Australia, Adelaide, 161-174.

Sheriff, R.E., Geldart, L.P., 1995. Exploration Seismology. Cambridge University Press, Cambridge.

SHOM-CDC-DREAL Corse, 2019. Open license (version 2.0). https://doi.org/10.17183/L3D_MAR_CORSE_2017_2018.

Short, F.T., Short, C.A., Novak, A.B., 2016. Seagrasses. *In:* Finlayson, C.M., Milton, G.R., Prentice, R.C., Davidson, N. (Eds.), The Wetland Book II: Distribution, Description and Conservation. Springer Science, pp. 1-19. https://doi.org/10.1007/978-94-007-6173-5_262-1.

Shumchenia, E.J., King, J.W., 2010. Comparison of methods for integrating biological and physical data for marine habitat mapping and classification. Continental Shelf Research 30(16), 1717-1729. https://doi.org/10.1016/j.csr.2010.07.007.

Shumway, G., 1960a. Sound speed and absorption studies of marine sediments by a resonance method. Part 1. Geophysics 25(2), 385-519. https://doi.org/10.1190/1.1438717.

Shumway, G., 1960b. Sound speed and absorption studies of marine sediments by a resonance method. Part 2. Geophysics 25(3), 659-682. https://doi.org/10.1190/1.1438749.

Siani, G., Paterne, M., Arnold, M., Bard, E., Métivier, B., Tisnerat, N. Bassinot, F., 2000. Radiocarbon reservoir ages in the Mediterranean Sea and Black Sea. Radiocarbon 42, 271-280. https://doi.org/10.1017/S0033822200059075.

Siegenthaler, U., Sarmiento, J.L., 1993. Atmospheric carbon dioxide and the ocean. Nature, 365, 119-125. https://doi.org/10.1038/365119a0.

Silenzi, S., Bard, E., Montagna, P., Antonioli, F., 2005. Isotopic records in a non-tropical coral (*Cladocora caespitosa*) from the Mediterranean Sea: evidence of a new high-resolution climate archive. Global and Planetary Change 49, 94-120. https://doi.org/10.1016/j.gloplacha.2005.05.005.

Silva, T.S.F., Costa, M.P.F., Melack, J.M., Novo, E.M.L.M., 2008. Remote sensing of aquatic vegetation: theory and applications. Environmental Monitoring and Assessment 140(1-3), 131-145. https://doi.org/10.1007/s10661-007-9855-3.

Silvestri, S., Knight, R., Viezzoli, A., Richardson, C., Anshari, G. Z., Dewar, N., Flanagan, N., Comas, X., 2019. Quantification of peat thickness and stored carbon at the landscape scale in tropical peatlands: A comparison of airborne geophysics and an empirical topographic method. Journal of Geophysical Research: Earth Surface 124(12), 3107-3123. https://doi.org/10.1029/2019JF005273.

Simon, N., Cras, A.L., Foulon, E., Lemée, R., 2009. Diversity and evolution of marine phytoplankton. Comptes Rendus Biologies 332, 159-170. https://doi.org/10.1016/j.crvi.2008.09.009.

Smith, C.J., Banks, A.C., Papadopoulou, K.N., 2007. Improving the quantitative estimation of trawling impacts from sidescan-sonar and underwater-video imagery. ICES Journal of Marine Science 64, 1692-1701. https://doi.org/10.1093/icesjms/fsm165.

Smith, J., O'Brien, P.E., Stark, J.S., Johnstone, G.J., Riddle, M.J., 2015. Integrating multibeam sonar and underwater video data to map benthic habitats in an East Antarctic nearshore environment. Estuarine, Coastal and Shelf Science 164, 520-536. https://doi.org/10.1016/j.ecss.2015.07.036.

Smith, L.C., MacDonald, G.M., Velichko, A.A., Beilman, D.W., Borisova, O.K., Frey, K.E., Kremenetski, K.V., Sheng, Y., 2004. Siberian peatlands a net carbon sink and global methane source since the early Holocene. Science 303(5656), 353-356. https://doi.org/10.1126/science.1090553.

Smith, S.V., 1981. Marine macrophytes as a global carbon sink. Science 211, 838-840. https://doi.org/10.1126/science.211.4484.838.

Smith, S.V., 2013. Parsing the oceanic calcium carbonate cycle: A net atmospheric carbon dioxide source or a sink?. Limnology and Oceanography e-Books. Association for the Sciences of Limnology and Oceanography (ASLO) Waco, TX, pp. 1-42. https://doi.org/10.4319/svsmith.2013.978-0-9845591-2-1.

Sousa, A.I., Lillebø, A.I., Risgaard-Petersen, N., Pardal, M.A., Caçador, I., 2012. Denitrification: an ecosystem service provided by salt marshes. Marine Ecology Progress Series 448, 79-92. https://doi.org/10.3354/meps09526.

Souza Filho, P.W.M., Cohen, M.C.L., Lara, R.J., Lessa, G.C., Koch, B., Behling, H., 2006. Holocene coastal evolution and facies model of the Braganca macrotidal flat on the Amazon mangrove coast, northern Brazil. Journal of Coastal Research 39, 306-331. https://www.jstor.org/stable/25741585.

Spieß, V., 1993. Digitale Sedimentechographie - Neue Wege zu einer hochauflösenden Akustostratigraphie. Berichte, Fachbereich Geowissenschaften, Universität Bremen 35, 1-199.

STARESO, 1991. Etude du milieu marin en vue de l'implantation d'un émissaire de rejet en mer par le syndicat intercommunal d'Aregno-Île Rousse. Paramètres biologiques, pp. 1-107.

Stuiver, M., Reimer, P.J., 1993. Extended ^{14}C database and revised CALIB radiocarbon calibration program. Radiocarbon 35, 215-230. https://doi.org/10.1017/S0033822200013904.

Sundquist, E.T., 1986. Geologic analogs: Their value and limitations in carbon dioxide research. *In:* Trabalka, J.R., Reichle, D.E. (Eds.), The Changing Carbon Cycle, Springer-Verlag, New York, 371-402. https://doi.org/10.1007/978-1-4757-1915-4_19.

Sutton, G.H., Berchemer, H., Nafe, J.E., 1957. Physical analysis of deep-sea sediments. Geophysics 22(4), 779-812. https://doi.org/10.1190/1.1438417.

Tchernia, A., Pomey, P., Hesnard, A., Couvert, M., Giacobbi, M.F., Girard, M., Hamon, E., Laubenheimer, F., Lecaille, F., 1978. L'épave romaine de la Madrague de Giens (Var) (Campagnes 1972–1975). Fouilles de l'Institut d'Archéologie Méditerranéenne. Galila 24, pp. 1-122.

Telesca, L., Belluscio, A., Criscoli, A., Ardizzone, G., Apostolaki, E.T., Fraschetti, S., Gristina, M., Knittweis, L., Martin, C.S., Pergent, G., Alagna, A., Badalamenti, F., Garofalo, G., Gerakaris, V., Pace, M.L., Pergent-Martini, C., Salomidi, M., 2015. Seagrass meadows (*Posidonia oceanica*) distribution and trajectories of change. Scientific Reports 5, 12505. https://doi.org/10.1038/srep12505.

Tins, W., 1978. Biotische und abiotische Limitierung bei der Koralle *Cladocora caespitosa* (Madreporaria). Verhandlung der Gesellschaft für Ökologie 7(1977), 79-87.

Tomasello, A., Luzzu, F., Di Maida, G., Orestano, C., Pirrotta, M., Scannavino, A., Calvo, S., 2009.

Detection and mapping of *Posidonia oceanica* dead matte by high-resolution acoustic imaging. Italian Journal of Remote Sensing 41(2), 139-146. https://doi.org/10.5721/ItJRS200941210.

Torbatinejad, N.M., Annison, G., Kay, R.M., Sabine, J.R., 2007. Structural constituents of the seagrass *Posidonia australis*. Journal of the Science of Food and Agriculture 55, 4021-4026.

Tremblay, P., Peirano, A., Ferrier-Pagès, C., 2011. Heterotrophy in the Mediterranean symbiotic coral *Cladocora caespitosa*: comparison with two other scleractinian species. Marine Ecology Progress Series 422, 165-177. https://doi.org/10.3354/meps08902.

Trumper, K., Bertzky, M., Dickson, B., van der Heijden, G., Jenkins, M., Manning, P., 2009. The Natural Fix? The role of ecosystems in climate mitigation. A UNEP rapid response assessment. UNEP-WCMC, Cambridge, UK, pp. 1-65.

Tur, J.M., Pere Godall, 1982. Consideraciones preliminaries sobre la ecología de los antozoos del litoral sur de la Costa Brava. Oecologia aquatica 6, 175-183.

Turgut, A., Yamamoto, T., 1990. Measurements of acoustic wave velocities and attenuation in marine sediments. The Journal of the Acoustical Society of America 87, 2376-2383. https://doi.org/10.1121/1.399084.

Tyne, J., Loneragen, N., Krutzen, M., Allen, S., Bejder, L., 2010. An integrated data management and video system for sampling aquatic benthos. Marine Freshwater Research 61(9), 1023-1028. https://doi.org/10.1071/MF09240.

UICN, 2016. Des solutions fondées sur la nature pour lutter contre les changements climatiques, Paris, France, pp. 1-16. www.uicn.fr/solutions-fondees-sur-la-nature.html.

UNEP-MAP-RAC/SPA, 2009. State of knowledge on the geographical distribution of marine magnoliophyta meadows in the Mediterranean. Information Document for the Ninth meeting of the Focal Points for SPAs, prepared by Leonardini, R., Pergent, G., Boudouresque, C.F., Floriana Malta, 3-6 June 2009. RAC/SPA publ., UNEP(DEPI)/MED WG 331/Inf 5, pp. 1-374.

UNEP-MAP-RAC/SPA, 2011. Draft guidelines for the standardization of mapping and monitoring methods of marine magnoliophyta in the Mediterranean. Working document, prepared by Pergent-Martini, C., for the tenth meeting of Focal Points for SPAs, Marseilles, France, 17-20 May 2011. RAC/SPA publ., UNEP(DEPI)/MED WG 359/9, pp. 1-59.

UNFCCC, 2016. Report of the Conference of the Parties on its 21st session, held in Paris from 30 Nov.-13 Dec. 2015. Addendum. Part two: Action taken by the Conference of the Parties at its 21st session, FCCC/CP/2015/10/Add.1, UNFCCC Secretariat, Bonn, pp. 1-40.

UNFCCC, 2019. National Inventory Submissions 2019. United Nations Framework Convention on Climate Change. Available at: https://unfccc.int/process-and-meetings/transparency-andreporting/reporting-and-review-under-the-convention/greenhouse-gas-inventories-annex-i-parties/national-inventory-submissions-2019, accessed June 2019.

Upadhyay, S.K., 2004. Seismic reflection processing: with special reference to anisotropy. Springer Science & Business Media. https://doi.org/10.1007/978-3-662-09843-1.

Vacchi, M., De Falco, G., Simeone, S., Montefalcone, M., Morri, C., Ferrari, M., Bianchi, C.N., 2017a. Biogeomorphology of the Mediterranean *Posidonia oceanica* seagrass meadows. Earth Surface Processes and Landforms 42(1), 42-54. https://doi.org/10.1002/esp.3932.

Vacchi, M., Ghilardi, M., Spada, G., Currás, A., Robresco, S., 2017b. New insights into the sea-level evolution in Corsica (NW Mediterranean) since the late Neolithic. Journal of Archaeological Science: Reports 12, 782-793. https://doi.org/10.1016/j.jasrep.2016.07.006.

Vacchi, M., Marriner, N., Morhange, C., Spada, G., Fontana, A., Rovere, A., 2016. Multiproxy assessment of Holocene relative sea-level changes in the western Mediterranean: Sea-level variability and improvements in the definition of the isostatic signal. Earth-Science Reviews 155, 172-197. https://doi.org/10.1016/j.earscirev.2016.02.002.

Valette-Sansevin, A., Pergent, G., Buron, K., Pergent-Martini, C., Damier, E., 2019. Continuous mapping of benthic habitats along the coast of Corsica: A tool for the inventory and monitoring of blue carbon ecosystems. Mediterranean Marine Science 20(3), 585-593. https://doi.org/10.12681/mms.19772.

Van de Broek, M., Vandendriessche, C., Poppelmonde, D., Merckx, R., Temmerman, S., Govers, G.,

2018. Long-term organic carbon sequestration in tidal marsh sediments is dominated by old-aged allochthonous inputs in a macrotidal estuary. Global Change Biology 24(6), 2498-2512. https://doi.org/10.1111/gcb.14089.

van Overmeeren, R., Craeymeersch, J., van Dalfsen, J., Fey, F., van Heteren, S., Meesters, E., 2009. Acoustic habitat and shellfish mapping and monitoring in shallow coastal water – Sidescan sonar experiences in The Netherlands. Estuarine, Coastal and Shelf Science 85(3), 437-448. https://doi.org/10.1016/j.ecss.2009.07.016.

Van Rein, H.B., Brown, C.J., Quinn, R., Breen, J., 2009. A review of sublittoral monitoring methods in temperate waters: a focus on scale. Underwater Technology: The International Journal of the Society for Underwater 28(3), 99-113. https://doi.org/10.3723/ut.28.099.

Varda, D., 2015. Some historical records of *Posidonia oceanica* matte in surrounding of Bar, Montenegro. *In:* Guala, I., Fais M. (Eds.), 4th Mediterranean Seagrass Workshop Sardinia 2015, 18-22 May 2015, Oristano, 125 (Poster).

Vassallo, P., Paoli, C., Rovere, A., Montefalcone M., Morri, C., Bianchi, C.N., 2013. The value of the seagrass *Posidonia oceanica*: A natural capital assessment. Marine Pollution Bulletin 75(1), 157-167. https://doi.org/10.1016/j.marpolbul.2013.07.044.

Vela, A., Garrido-Maestracci, M., 2008. Recensement des formations récifales superficielles bioconstruites sur le littoral corse. Rapport Sintinelle & DIREN Corse, pp. 1-154.

Vela A., Lafabrie C., Gobin C., 2010. Recensement et caractérisation des formations récifales superficielles hors Natura 2000 en Corse et propositions de gestion. Rapport Sintinelle & DREAL Corse, pp. 1-53.

Vela, A., Pasqualini, V., Leoni, V. Djelouli, A., Langar, H., Pergent, G., Pergent-Martini, C., Ferrat, L., Ridha, M., Djabou, H., 2008. Use of SPOT 5 and IKONOS imagery for mapping biocenoses in a Tunisian coastal lagoon (Mediterranean Sea). Estuarine, Coastal and Shelf Science 79(4), 591-598. https://doi.org/10.1016/j.ecss.2008.05.014.

Vella, C., Costa, K., Istria, D., Dussouillez, P., Ghilardi,M., Fleury, J., Delanghe, D., Demory, F., Cibecchini, F., Moreau, J., Jouët, G., 2016. Evolution du fleuve Golo autour des sites antique et médiéval de Mariana (Corse, France). La géoarchéologie des îles de Méditerranée, Actes du colloque GEOMEDISLANDS (30 juin-2 juillet 2015, Cargèse). CNRS éditions, 229-244.

Votruba, G.F., Artzy, M., Erkanal, H., 2016. A set Archaic anchor arm exposed within *P. oceanica* matte at Klazomenai/Liman Tepe, Turkey: A contribution for understanding marine stratigraphy. Journal of Field Archaeology 41(6), 671-683. https://doi.org/10.1080/00934690.2016.1211473.

Wang, C.K., Philpot, W.D., 2007. Using airborne bathymetric lidar to detect bottom type variation in shallow waters. Remote Sensing of Environment 106(1), 123-135. https://doi.org/10.1016/j.rse.2006.08.003.

Ward, L.G., Zaprowski, B.J., Trainer, K.D., Davis, P.T., 2008. Stratigraphy, pollen history and geochronology of tidal marshes in a Gulf of Maine estuarine system: Climatic and relative sea level impacts. Marine Ecology 256(1-4), 1-17. https://doi.org/10.1016/j.margeo.2008.08.004.

Ware, J.R., Smith, S.V., Reaka-Kudla, M.L., 1992. Coral reefs: Sources or sinks of atmospheric CO_2? Coral Reefs 11, 127-130. https://doi.org/10.1007/BF00255465.

Waycott, M., Duarte, C.M., Carruthers, T.J.B., Orth, R.J., Dennison, W.C., Olyarnik, S., Calladine, A., Fourqurean, J.W., Heck Jr., K.L., Hughes, A.R., Kendrick, G.A., Kenworthy, W.J., Short, F.T., Williams, S.L., 2009. Accelerating loss of seagrasses across the globe threatens coastal ecosystems. Proceedings of the National Academy of Sciences of the United States of America 106(30), 12377-12381. https://doi.org/10.1073/pnas.0905620106.

Wentworth, C.K., 1922. A scale of grade and class terms for clastic sediments. The Journal of Geology 30(5), 377-392. https://doi.org/10.1086/622910.

Wood, M., 1991. Maine salt marshes and sediment accumulation. Master Thesis. University of Maine, Orono, pp. 1-434.

Woodroffe, C.D., Mulrennan, M.E., Chappell, J., 1993. Estuarine infill and coastal progradation, southern van Diemen Gulf, northern Australia, Sedimentary Geology 83(3-4), 257-275.

https://doi.org/10.1016/0037-0738(93)90016-X.

Yilmaz, Ö., 2001. Seismic data analysis processing, inversion and interpretation of seismic data. Society of Exploration Geophysicists, Investigations in Geophysics, Tulsa, Oklahoma. https://doi.org/10.1190/1.9781560801580.

Zehetner, F., 2010. Does organic carbon sequestration in volcanic soils offset volcanic CO_2 emissions? Quaternary Science Reviews 29(11-12), 1313-1316. https://doi.org/10.1016/j.quascirev.2010.03.003.

Zibrowius, H., 1980. Les Scléractiniaires de la Méditerranée et de l'Atlantique nord-oriental. Mémoires de l'Institut Océanographique 11, 1-284.

Zibrowius, H., 1982. Taxonomy in a hermatypic scleractinian corals. Paleontographica Americana 54, 80-85.

Zimov, S.A., Davydov, S.P., Zimova, G.M., Davydova, A.I., Schuur, E.A.G., Dutta, K., Chapin, F.S., 2006. Permafrost carbon: Stock and decomposability of a globally significant carbon pool, Geophysical Research Letters 33, L20502. https://doi.org/10.1029/2006GL027484.

Zwolsman, J.J.G., Berger, G.W., Van Eck, G.T.M., 1993. Sediment accumulation rates, historical input, postdepositional mobility and retention of major elements and trace metals in salt marsh sediments of the Scheldt estuary, SW Netherlands. Marine Chemistry 44(1), 73-94. https://doi.org/10.1016/0304-4203(93)90007-B.

Annexes

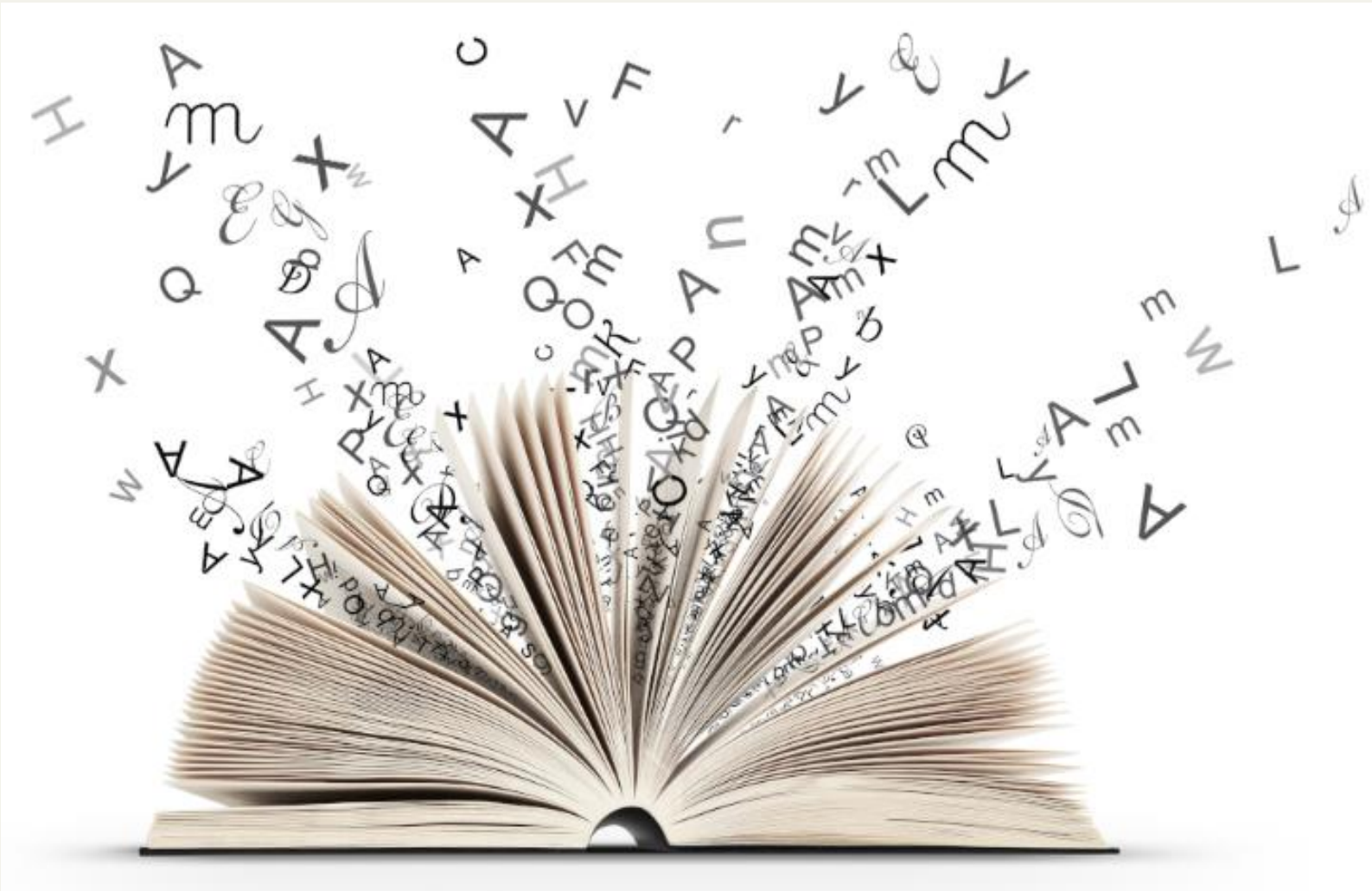

Appendices

Appendix A1. Taxonomic authorities of species mentionned in the manuscript.

Species	Phylum	Taxonomic authorities
Arca noae	Mollusca	Linnaeus, 1758
Bittium reticulatum	Mollusca	da Costa, 1778
Blysmopsis rufa	Tracheophyta	(Hudson) Oteng-Yeb, 1974
Cerithium vulgatum	Mollusca	Bruguière, 1792
Cladocora caespitosa	Cnidaria	Linnaeus, 1767
Cladophora prolifera	Chlorophyta	(Roth) Kützing, 1843
Codium bursa	Chlorophyta	(Olivi) C. Agardh, 1817
Cymodocea nodosa	Tracheophyta	(Ucria) Ascherson, 1870
Dictyota implexa	Phaeophyceae	(Desfontaines) J.V.Lamouroux, 1809
Eleocharis uniglumis	Tracheophyta	(Link) Schult, 1824
Flabellia petiolata	Chlorophyta	(Turra) Nizamuddin, 1987
Glans trapezia	Mollusca	Linnaeus, 1767
Haliotis tuberculata	Mollusca	Linnaeus, 1758
Jujubinus exasperatus	Mollusca	(Pennant, 1777)
Lithothamnion corallioides	Rhodophyta	P.Crouan & H.Crouan, 1867
Lithophyllum racemus	Rhodophyta	(Lamarck) Foslie, 1901
Lithothamnion valens	Rhodophyta	Foslie, 1909
Osmundaria volubilis	Rhodophyta	(Linnaeus) R.E.Norris, 1991
Padina pavonica	Phaeophyceae	(Linnaeus) Thivy, 1960
*Pestarella tyrrhena**	Arthropoda	Petagna, 1792
Peysonnelia squamaria	Rhodophyta	(S.G.Gmelin) Decaisne ex J.Agardh, 1842
Posidonia australis	Tracheophyta	J.D.Hooker, 1858
Posidonia oceanica	Tracheophyta	(Linnaeus) Delile, 1813
Posidonia sinuosa	Tracheophyta	Cambridge & Kuo, 1979
Phymatolithon calcareum	Rhodophyta	(Pallas) W.H.Adey & D.L.McKibbin ex Woelkering & L.M.Irvine, 1986
Rytiphlaea tinctoria	Rhodophyta	(Clemente) C.Agardh, 1824
Thalassodendron ciliatum	Tracheophyta	(Forsskål) Hartog, 1970
Spongites fruticulosa	Rhodophyta	Kützing, 1841
Tricolia speciosa	Mollusca	Megerle von Mühlfeld, 1824
Upogebia pusilla	Arthropoda	Petagna, 1792
Venus verrucosa	Mollusca	Linnaeus, 1758
Arca noae	Mollusca	Linnaeus, 1758
Bittium reticulatum	Mollusca	da Costa, 1778

*The species name *Pestarella tyrrhena* mentionned in this manuscript has been recently modified in *Gilvossius tyrrhenus* (Petagna, 1792) following the World Register of Marine Species (2020) http://www.marinespecies.org/aphia.php?p=taxdetails&id=1398927.

Appendix A2. Gravity corer (Kullenberg) used during the oceanographic survey Carbonsink (2018), water column collection with the Niskin bottle and 'wet' laboratory on the R/V 'L'Europe' (Ifremer) where the sedimentary sequences were subsampled (© Monnier B.).

Appendix A3. Chronostratigraphic linear age-depth models of cores computed in the program clam.R.

BG-10M

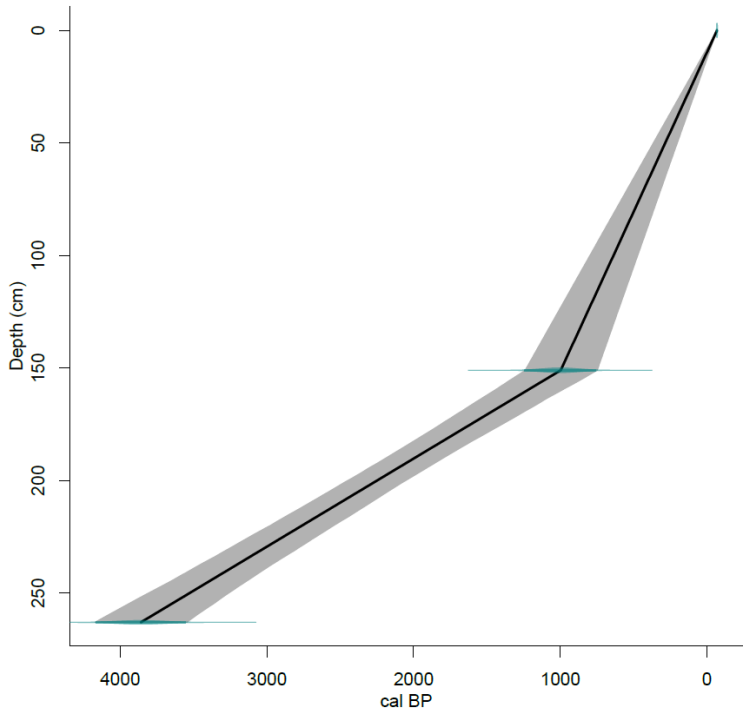

BG-20M

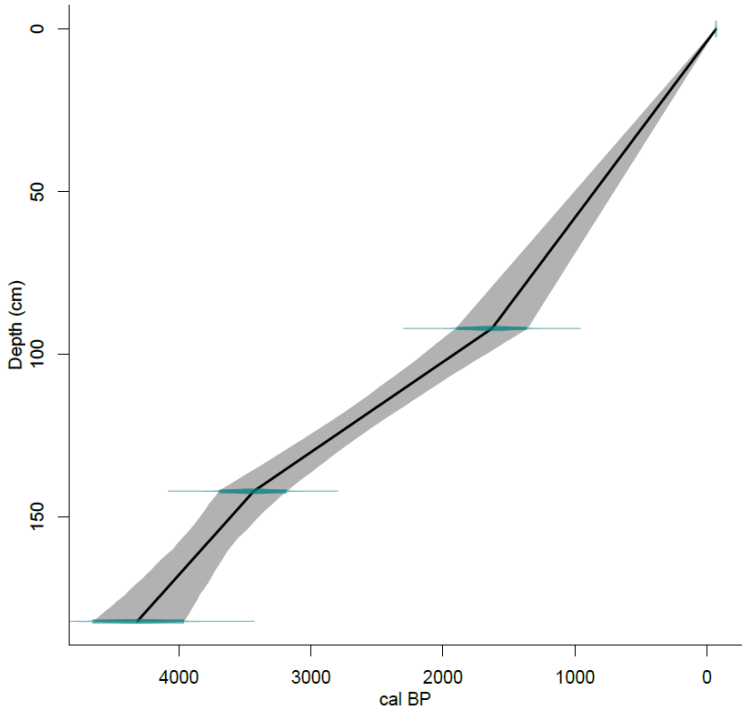

GM-10M

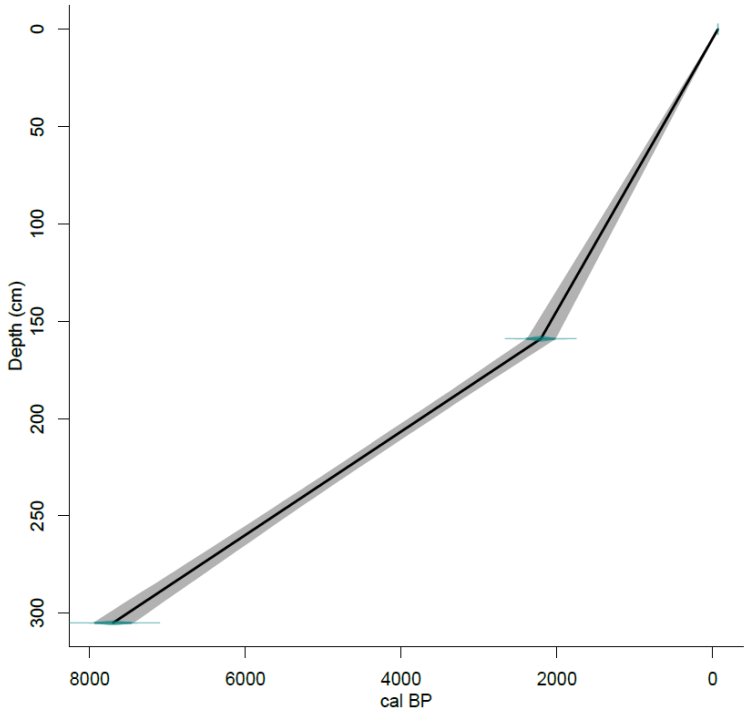
Depth (cm)
0
50
100
150
200
250
300
8000
6000
4000
2000
0
cal BP

TV-10M

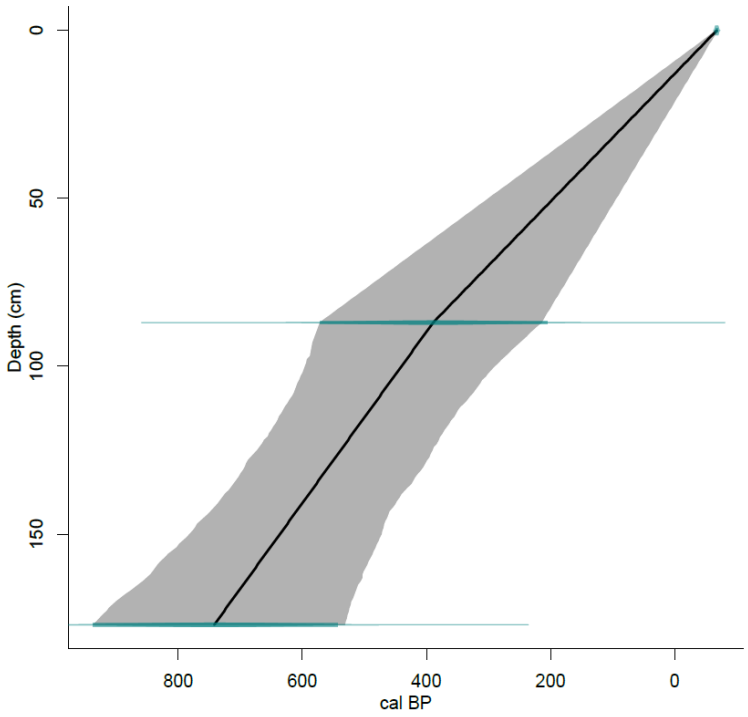
Depth (cm)
0
50
100
150
800
600
400
200
0
cal BP

TV-20M

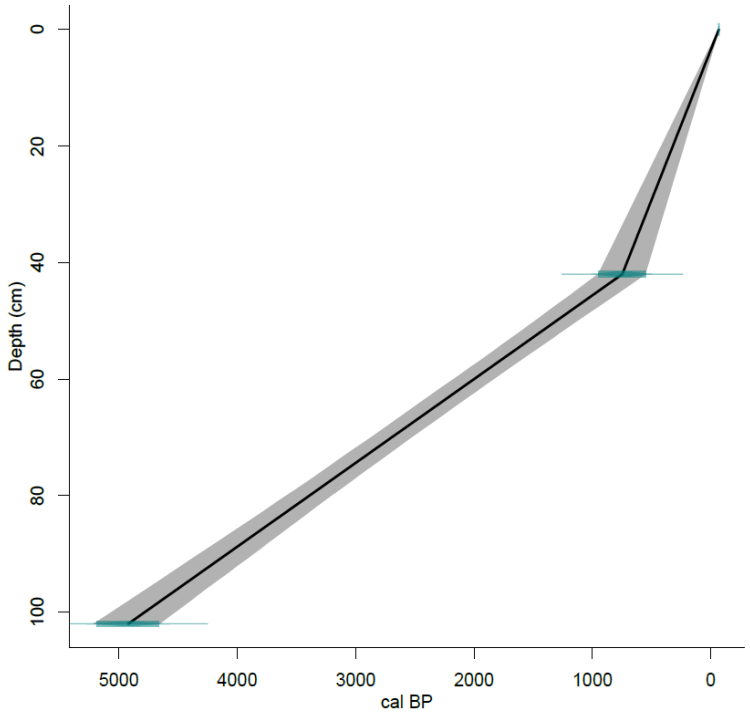
Depth (cm)
0
20
40
60
80
100
5000
4000
3000
2000
1000
0
cal BP

TM-20M

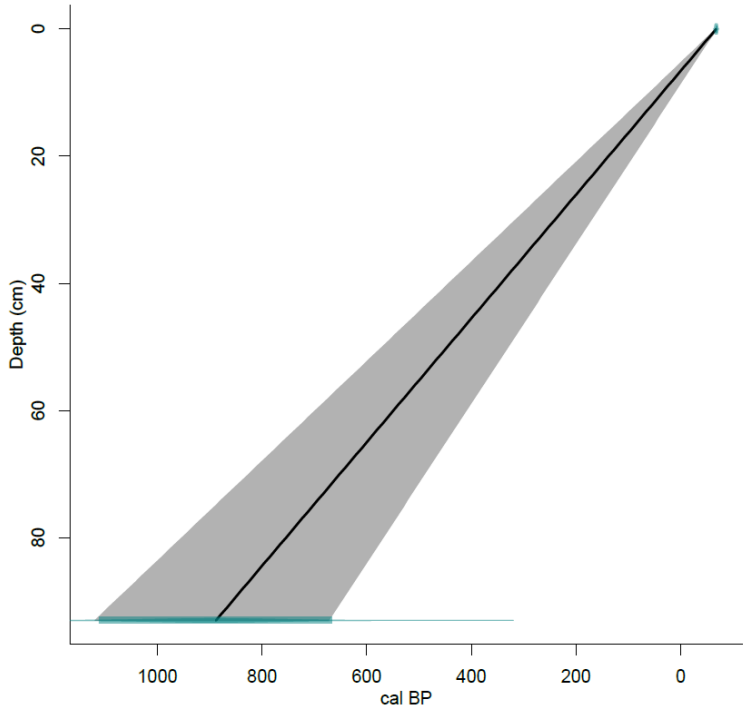
Depth (cm)
0
20
40
60
80
1000
800
600
400
200
0
cal BP

TM-20M

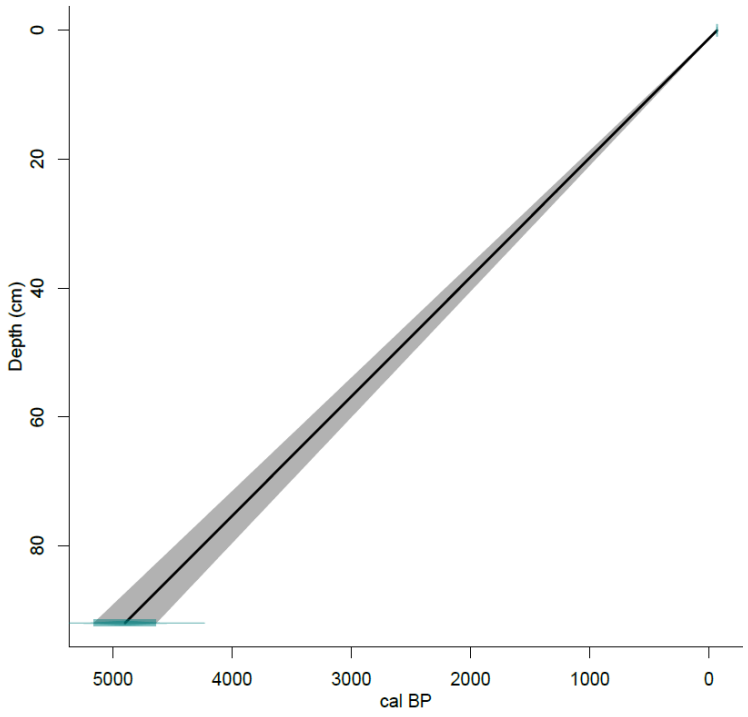
Depth (cm)
0
20
40
60
80
5000
4000
3000
2000
1000
0
cal BP

UB-10M

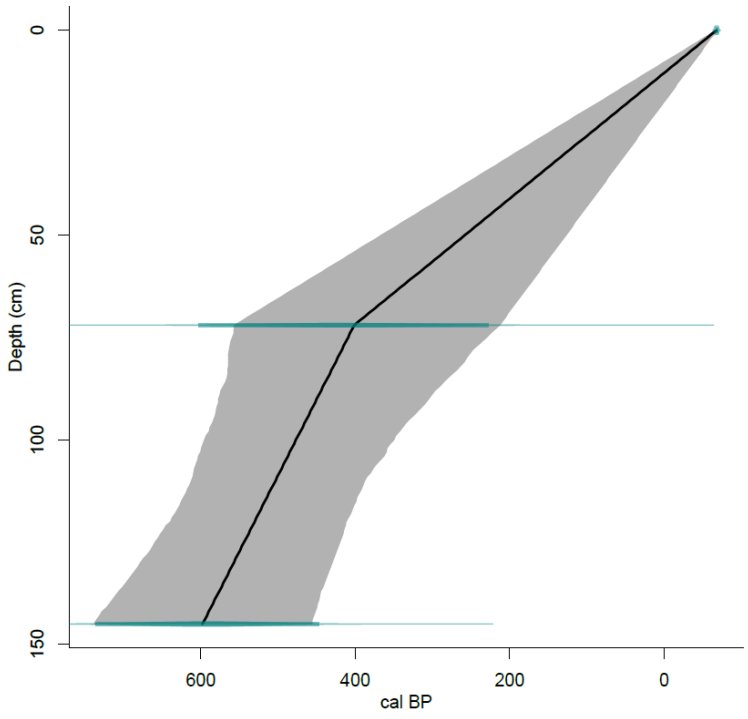
Depth (cm)
0
50
100
150
600
400
200
0
cal BP

UB-20M

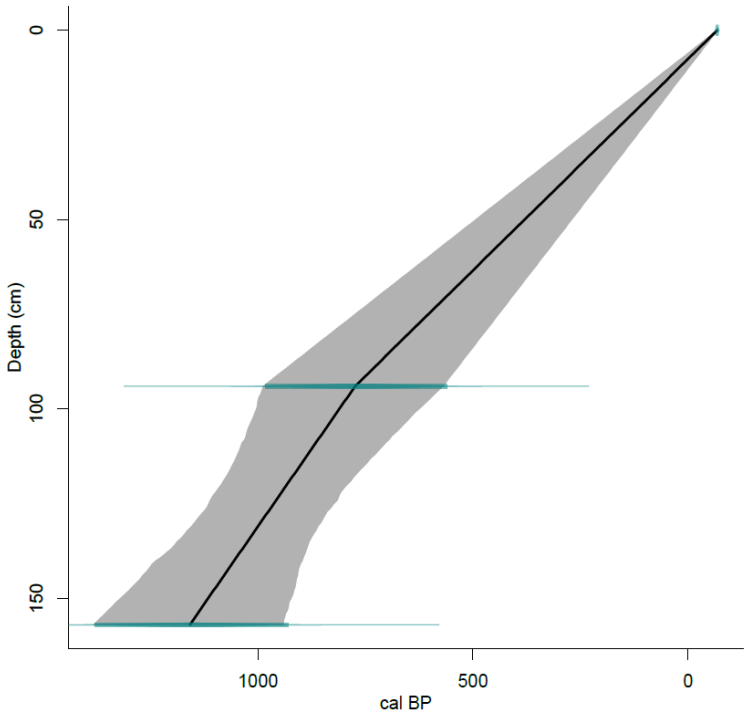
0
50
100
150
Depth (cm)
1000
500
0
cal BP

SL-20M

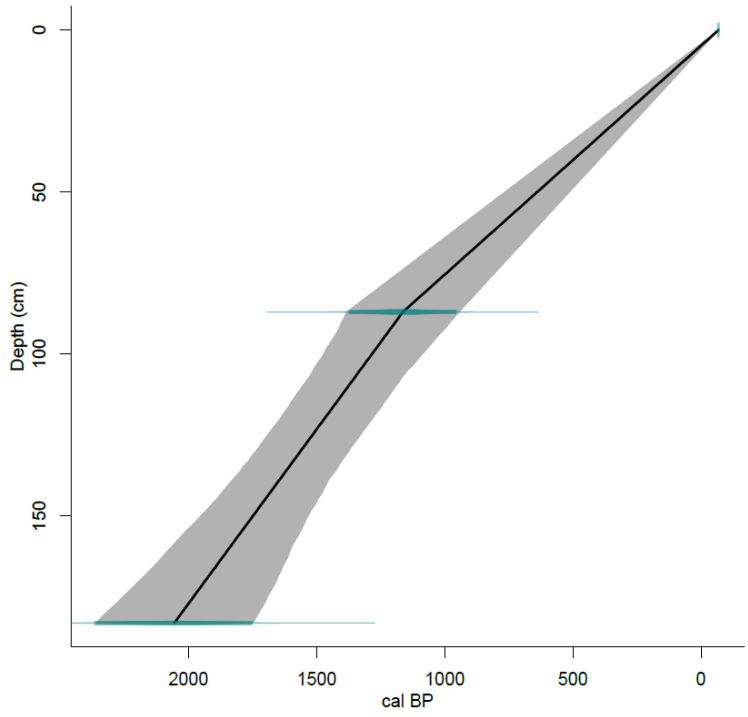
0
50
100
150
Depth (cm)
2000
1500
1000
500
0
cal BP

FT-10M

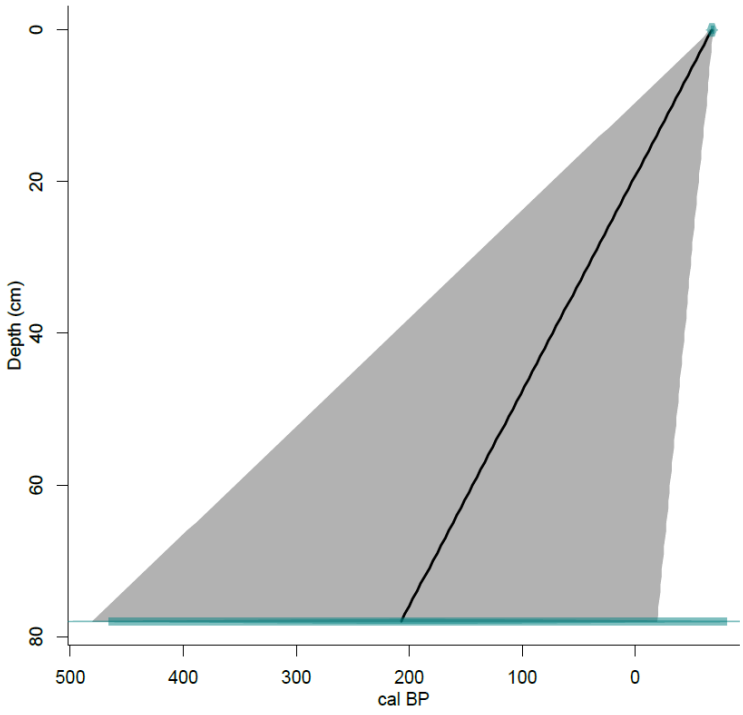

Appendix A4. Surface area and minimum, maximum and mean (± S.E.) volume of matte estimated for each categories of matte thickness within the different sectors of the study site.

Sector 2A					
Matte thickness (m)	**Surface (km^2)**	**Min. Volume ($\times 10^6$ m^3)**	**Max. Volume ($\times 10^6$ m^3)**	**Mean Volume ($\times 10^6$ m^3)**	**± S.E. ($\times 10^6$ m^3)**
0 - 0.5	0.0	0.0	0.0	0.0	0.0
0.5 - 1.0	0.0	0.0	0.0	0.0	0.0
1.0 - 1.5	1.4	1.4	2.1	1.8	0.4
1.5 - 2.0	8.2	4.1	16.5	10.3	6.2
2.0 - 2.5	23.1	11.5	57.7	34.6	23.1
2.5 - 3.0	13.7	6.9	41.1	24.0	17.1
3.0 - 3.5	7.5	3.8	26.3	15.0	11.3
3.5 - 4.0	3.0	1.5	12.0	6.7	5.2
4.0 - 4.5	1.6	0.8	7.4	4.1	3.3
4.5 - 5.0	0.7	0.4	3.5	1.9	1.6
5.0 - 5.5	0.4	0.2	2.3	1.3	1.1
5.5 - 6.0	0.1	0.1	0.9	0.5	0.4
6.0 - 6.5	0.1	0.1	0.7	0.4	0.3
6.5 - 7.0	0.1	0.0	0.4	0.2	0.2
7.0 - 7.5	0.0	0.0	0.0	0.0	0.0
7.5 - 8.0	0.0	0.0	0.0	0.0	0.0
Total	60.0	30.7	170.9	100.8	70.1

Sector 2B					
Matte thickness (m)	**Surface (km^2)**	**Min. Volume ($\times 10^6$ m^3)**	**Max. Volume ($\times 10^6$ m^3)**	**Mean Volume ($\times 10^6$ m^3)**	**± S.E. ($\times 10^6$ m^3)**
0 - 0.5	0.0	0.0	0.0	0.0	0.0
0.5 - 1.0	0.4	0.2	0.4	0.3	0.1
1.0 - 1.5	4.5	4.5	6.8	5.6	1.1
1.5 - 2.0	12.4	18.6	24.7	21.6	3.1
2.0 - 2.5	11.4	22.7	28.4	25.6	2.8
2.5 - 3.0	5.7	14.2	17.0	15.6	1.4
3.0 - 3.5	3.0	9.1	10.6	9.8	0.8
3.5 - 4.0	0.9	3.3	3.8	3.5	0.2
4.0 - 4.5	0.3	1.4	1.6	1.5	0.1
4.5 - 5.0	0.2	0.8	0.9	0.8	0.0
5.0 - 5.5	0.0	0.1	0.1	0.1	0.0
5.5 - 6.0	0.0	0.0	0.0	0.0	0.0
6.0 - 6.5	0.0	0.0	0.0	0.0	0.0
6.5 - 7.0	0.0	0.0	0.0	0.0	0.0
7.0 - 7.5	0.0	0.0	0.0	0.0	0.0
7.5 - 8.0	0.0	0.0	0.0	0.0	0.0
Total	38.8	74.8	94.2	84.5	9.7

Sector 2C					
Matte thickness (m)	**Surface (km^2)**	**Min. Volume ($\times 10^6$ m^3)**	**Max. Volume ($\times 10^6$ m^3)**	**Mean Volume ($\times 10^6$ m^3)**	**± S.E. ($\times 10^6$ m^3)**
0 - 0.5	0.3	0.0	0.2	0.1	0.1
0.5 - 1.0	0.2	0.1	0.2	0.1	0.0
1.0 - 1.5	0.7	0.7	1.1	0.9	0.2
1.5 - 2.0	3.1	4.6	6.2	5.4	0.8
2.0 - 2.5	8.6	17.2	21.5	19.4	2.2
2.5 - 3.0	8.8	22.1	26.5	24.3	2.2
3.0 - 3.5	3.8	11.3	13.2	12.3	0.9
3.5 - 4.0	0.7	2.3	2.6	2.5	0.2
4.0 - 4.5	0.3	1.1	1.3	1.2	0.1
4.5 - 5.0	0.0	0.0	0.0	0.0	0.0
5.0 - 5.5	0.0	0.0	0.0	0.0	0.0
5.5 - 6.0	0.0	0.0	0.0	0.0	0.0
6.0 - 6.5	0.0	0.0	0.0	0.0	0.0
6.5 - 7.0	0.0	0.0	0.0	0.0	0.0
7.0 - 7.5	0.0	0.0	0.0	0.0	0.0
7.5 - 8.0	0.0	0.0	0.0	0.0	0.0
Total	26.5	59.5	72.8	66.2	6.6

Sector 2D					
Matte thickness (m)	**Surface (km^2)**	**Min. Volume ($\times 10^6$ m^3)**	**Max. Volume ($\times 10^6$ m^3)**	**Mean Volume ($\times 10^6$ m^3)**	**± S.E. ($\times 10^6$ m^3)**
0 - 0.5	0.0	0.0	0.0	0.0	0.0
0.5 - 1.0	0.0	0.0	0.0	0.0	0.0
1.0 - 1.5	0.3	0.3	0.4	0.4	0.1
1.5 - 2.0	8.5	12.7	16.9	14.8	2.1
2.0 - 2.5	12.8	25.6	32.0	28.8	3.2
2.5 - 3.0	10.3	25.8	30.9	28.4	2.6
3.0 - 3.5	4.7	14.2	16.5	15.3	1.2
3.5 - 4.0	2.1	7.2	8.2	7.7	0.5
4.0 - 4.5	0.9	3.6	4.1	3.9	0.2
4.5 - 5.0	0.4	2.0	2.2	2.1	0.1
5.0 - 5.5	0.2	0.9	1.0	1.0	0.0
5.5 - 6.0	0.1	0.7	0.8	0.8	0.0
6.0 - 6.5	0.1	0.6	0.7	0.7	0.0
6.5 - 7.0	0.1	0.5	0.5	0.5	0.0
7.0 - 7.5	0.1	0.4	0.4	0.4	0.0
7.5 - 8.0	0.0	0.3	0.3	0.3	0.0
Total	40.6	94.8	115.1	104.9	10.1

Sector 2E					
Matte thickness (m)	**Surface (km^2)**	**Min. Volume ($\times 10^6 m^3$)**	**Max. Volume ($\times 10^6 m^3$)**	**Mean Volume ($\times 10^6 m^3$)**	**± S.E. ($\times 10^6 m^3$)**
0 - 0.5	0.0	0.0	0.0	0.0	0.0
0.5 - 1.0	0.1	0.0	0.1	0.0	0.0
1.0 - 1.5	3.9	3.9	5.9	4.9	1.0
1.5 - 2.0	8.2	12.3	16.4	14.4	2.1
2.0 - 2.5	5.9	11.8	14.7	13.3	1.5
2.5 - 3.0	6.4	16.0	19.2	17.6	1.6
3.0 - 3.5	6.8	20.3	23.7	22.0	1.7
3.5 - 4.0	2.9	10.1	11.6	10.8	0.7
4.0 - 4.5	1.3	5.2	5.9	5.6	0.3
4.5 - 5.0	1.0	4.7	5.2	4.9	0.3
5.0 - 5.5	1.1	5.5	6.1	5.8	0.3
5.5 - 6.0	0.6	3.6	3.9	3.7	0.2
6.0 - 6.5	0.1	0.8	0.8	0.8	0.0
6.5 - 7.0	0.0	0.1	0.1	0.1	0.0
7.0 - 7.5	0.0	0.0	0.0	0.0	0.0
7.5 - 8.0	0.0	0.0	0.0	0.0	0.0
Total	38.3	94.2	113.4	103.8	9.6

Appendix A5. Mean (± S.E.) content of the parameters and isotopic signatures in the cores.

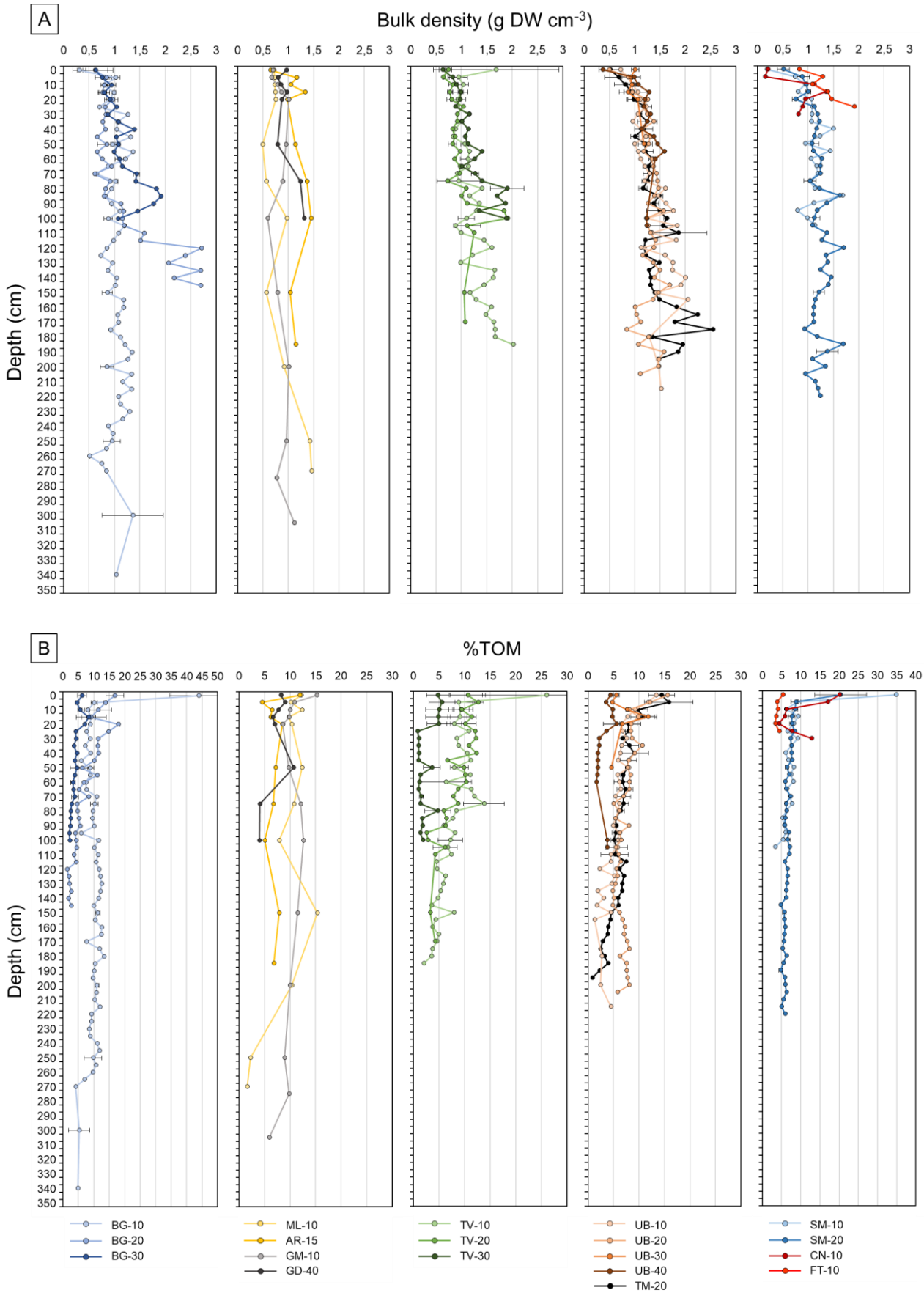

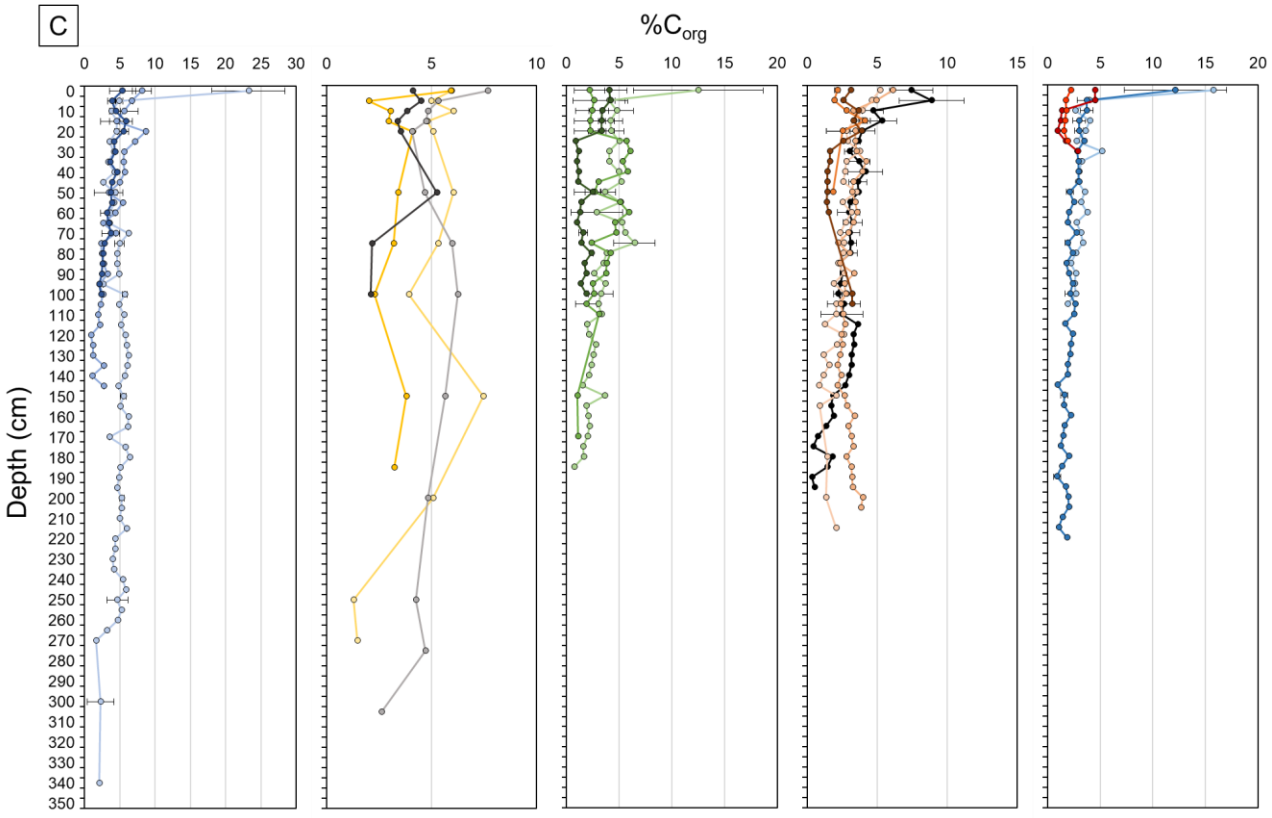
C
%Corg
Depth (cm)

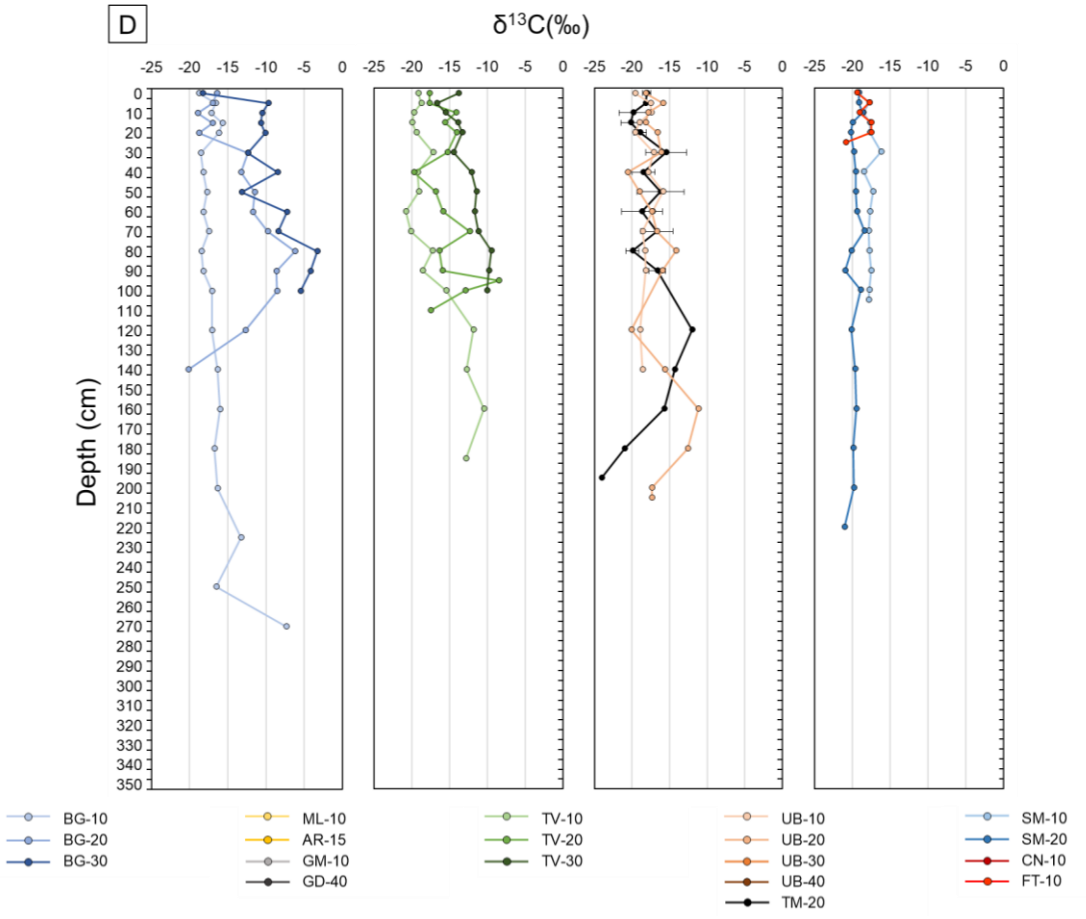
D
δ13C(‰)
Depth (cm)
BG-10
BG-20
BG-30
ML-10
AR-15
GM-10
GD-40
TV-10
TV-20
TV-30
UB-10
UB-20
UB-30
UB-40
TM-20
SM-10
SM-20
CN-10
FT-10

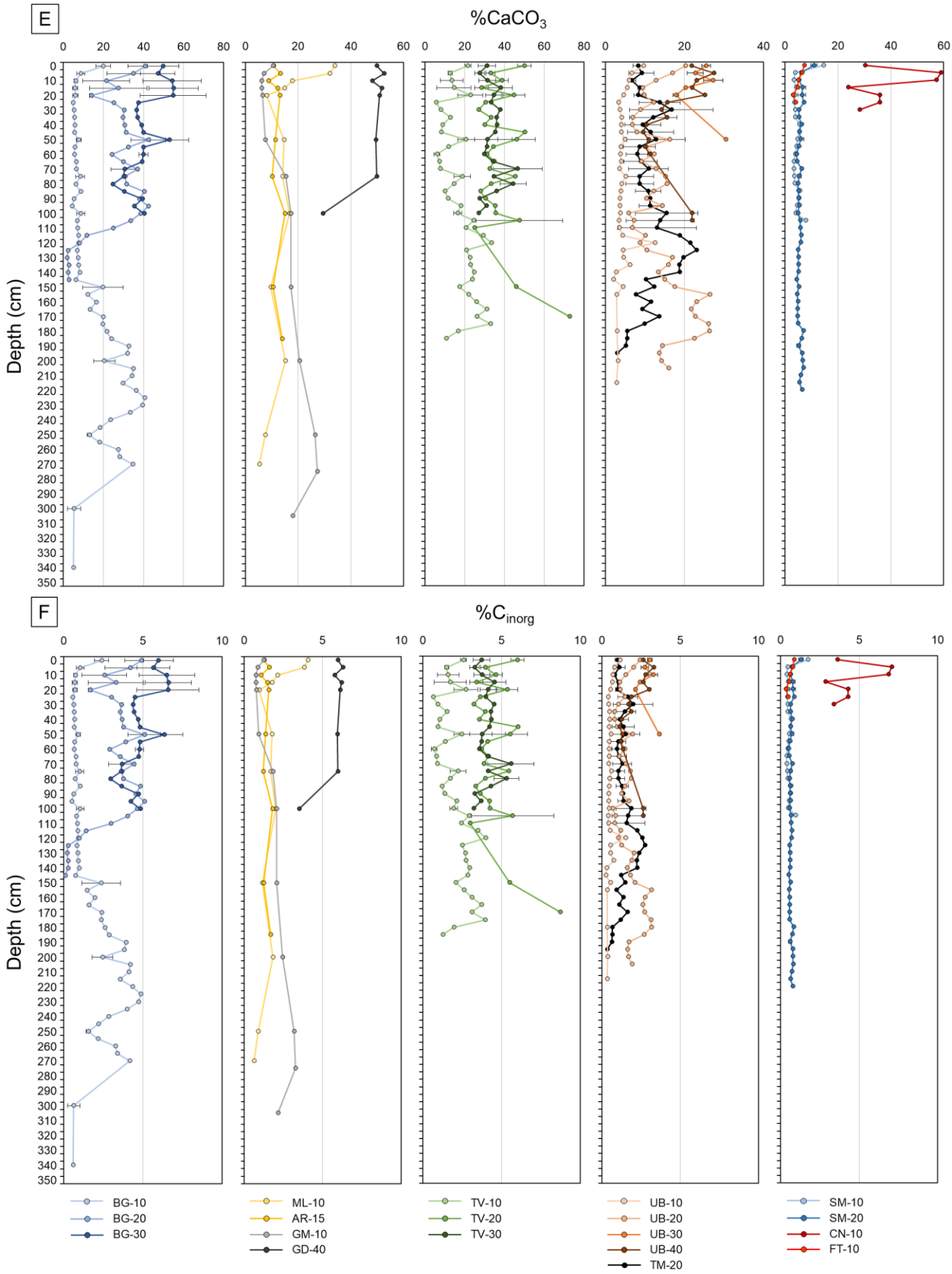
E
%CaCO3
Depth (cm)
F
%Cinorg
Depth (cm)
BG-10
BG-20
BG-30
ML-10
AR-15
GM-10
GD-40
TV-10
TV-20
TV-30
UB-10
UB-20
UB-30
UB-40
TM-20
SM-10
SM-20
CN-10
FT-10

Appendix A6. Sediment accumulation rates, C_{org} (top) and C_{inorg} (bottom) accumulation rates and stocks in the seagrass cores studied. Estimates are performed over 30 cm and 100 cm thick deposits. The corresponding age are derived from ^{14}C dating.

	30 cm				100 cm			
Lab code	**Age (cal. yr BP)**	**Sediment accretion rate (mm yr^{-1})**	**C_{org} accumulation rate (g m^{-2} yr^{-1})**	**C_{org} stock (kg m^{-2})**	**Age (cal. yr BP)**	**Sediment accretion rate (mm yr^{-1})**	**C_{org} accumulation rate (g m^{-2} yr^{-1})**	**C_{org}stock (kg m^{-2})**
BG-10-γ	137	1.42	66.49	13.63	630	1.42	61.97	43.25
BG-20-γ	467	0.54	31.01	16.59	1881	0.54	19.70	38.39
GM-10-α	347	0.70	29.54	12.26	1348	0.70	31.03	43.95
TV-10-γ	84	1.90	96.38	14.65	436	1.90	96.63	48.70
TV-20-γ	495	0.51	26.11	14.70	4711	0.51	9.66	46.16
TM-20-α	230	0.97	49.77	14.83	950	0.97	39.64	40.36
TM-20-β	1498	0.19	6.05	9.47	5277	0.19	7.12	38.05
UB-10-γ	121	1.53	56.98	10.77	474	1.53	60.73	32.92
UB-20-α	192	1.12	45.08	11.72	805	1.12	45.15	39.42
SL-20-α	342	0.71	25.54	11.29	1275	0.71	24.42	32.79
FT-10-α	34	2.83	72.75	7.42	350	2.83	78.71	27.55

	30 cm				100 cm			
Lab code	**Age (cal. yr BP)**	**Sediment accretion rate (mm yr^{-1})**	**C_{inorg} accumulation rate (g m^{-2} yr^{-1})**	**C_{inorg} stock (kg m^{-2})**	**Age (cal. yr BP)**	**Sediment accretion rate (mm yr^{-1})**	**C_{inorg} accumulation rate (g m^{-2} yr^{-1})**	**C_{inorg} stock (kg m^{-2})**
BG-10-γ	137	1.42	8.00	1.64	630	1.42	9.81	6.85
BG-20-γ	467	0.54	9.91	5.30	1881	0.54	15.19	29.60
GM-10-α	347	0.70	5.13	2.13	1348	0.70	5.64	7.98
TV-10-γ	84	1.90	16.31	2.48	436	1.90	27.22	13.72
TV-20-γ	495	0.51	18.06	10.17	4711	0.51	8.40	40.15
TM-20-α	230	0.97	8.72	2.60	950	0.97	11.40	11.61
TM-20-β	1498	0.19	11.37	17.81	5277	0.19	6.61	35.32
UB-10-γ	121	1.53	10.16	1.92	474	1.53	10.57	5.73
UB-20-α	192	1.12	11.85	3.08	805	1.12	10.88	9.50
SL-20-α	342	0.71	5.68	2.33	1275	0.71	5.85	7.86
FT-10-α	34	2.83	24.02	2.45	350	2.83	11.46	4.01